NUREG/CR-5214
EGG-2547

Analyses of Natural Circulation During a Surry Station Blackout Using SCDAP/RELAP5

Prepared by P.D. Bayless

EG&G Idaho, Inc.

Prepared for
U.S. Nuclear Regulatory
Commission

NUREG/CR-5214
EGG-2547
R3

Analyses of Natural Circulation During a Surry Station Blackout Using SCDAP/RELAP5

Manuscript Completed: September 1988
Date Published: October 1988

Prepared by
P.D. Bayless

EG&G Idaho, Inc.
Idaho Falls, ID 83415

Prepared for
Division of Systems Research
Office of Nuclear Regulatory Research
U.S. Nuclear Regulatory Commission
Washington, DC 20555
NRC FIN A6360

ABSTRACT

The effects of reactor coolant system natural circulation on the response of the Surry nuclear power plant during a station blackout transient were investigated. A TMLB' sequence (loss of all ac power, immediate loss of auxiliary feedwater) was simulated from transient initiation until after fuel rod relocation had begun. Integral analyses of the system thermal-hydraulics and the core damage behavior were performed using the SCDAP/RELAP5 computer code and several different models of the plant. Three scoping calculations were performed in which the complexity of the plant model was progressively increased to determine the overall effects of in-vessel and hot leg natural circulation flows on the plant response. The natural circulation flows extended the transient, slowing the core heatup and delaying core damage by transferring energy from the core to structures in the upper plenum and coolant loops. Increased temperatures in the ex-core structures indicated that they may fail, however. Nine sensitivity calculations were then performed to investigate the effects of modeling uncertainties on the multidimensional natural circulation flows and the system response. Creep rupture failure of the pressurizer surge line was predicted to occur in eight of the calculations, with the hot leg failing in the ninth. The failure time was fairly insensitive to the parameters varied. The failures occurred near the time that fuel rod relocation began, well before failure of the reactor vessel would be expected. A calculation was also performed in which creep rupture failure of the surge line was modeled. The subsequent blowdown led to rapid accumulator injection and quenching of the entire core.

EXECUTIVE SUMMARY

An increased awareness of severe accidents has been reflected in the U.S. Nuclear Regulatory Commission's research after the accident at Three Mile Island. A parallel experimental and analytical effort formed the basis of understanding of severe accidents. This research effort culminated in NUREG-0956, the "Reassessment of the Technical Bases for Estimating Source Terms," which described the current state of knowledge in the severe accident area and identified eight major areas of uncertainty. The draft "Reactor Risk Reference Document," NUREG-1150, used the source term methodology in NUREG-0956 to provide a basis for new estimates of reactor risk.

Natural circulation in the reactor coolant system was one of the major severe accident uncertainties identified in NUREG-0956. Three types of natural circulation that may occur during a high pressure boiloff transient in a pressurized water reactor were investigated for the Nuclear Regulatory Commission: in-vessel, hot leg countercurrent flow, and flow through the coolant loops. The objective of the analyses was to investigate the effects of various types of natural circulation on the transient, severe accident response of the plant. Sensitivity studies were also performed to investigate the effects of multidimensional natural circulation modeling uncertainties on the plant transient response. Of particular interest were changes in the events that occur, in event timing, and in the extent of core damage. A transient was also analyzed in which the surge line failure and subsequent blowdown of the reactor coolant system were modeled.

In meeting the objective of the analyses, insight into the phenomena controlling the plant response and the natural circulation flows have been developed. The importance of mechanistic integral analyses of severe accidents has been demonstrated. The results of the analyses have also helped to identify particular areas of research that could provide a better understanding of the natural circulation flows and their effects on the plant response.

The transient selected for the analyses was the TMLB' sequence in the Surry nuclear power plant. The TMLB' sequence involves the loss of all ac power and auxiliary feedwater, and was selected because all three types of natural circulation may occur during the transient. Surry is a three-loop Westinghouse pressurized water reactor with U-tube steam generators. It has a rated core thermal power of 2441 MW. Surry was selected because it is one of the reference plants used in source term and risk analyses.

The analyses were performed using the SCDAP/RELAP5 computer code. This code performs integral calculations of the system thermal-hydraulics and the core behavior. The model for the hot leg countercurrent flow was developed using work performed at Argonne National Laboratory with the COMMIX computer code.

In-vessel natural circulation occurs between the uncovered part of the core and the upper plenum. Vapor rises from the center of the core to the upper plenum, where it is cooled by the internal structures before returning to the core through the peripheral fuel assemblies. Hot leg countercurrent flow transfers energy to the hot leg piping and steam generators. Hot vapor flows from the reactor vessel to the steam generators along the top of the hot leg, while an opposing flow of cooler vapor proceeds from the steam generators to the reactor vessel along the bottom of the hot leg. Loop natural circulation involves superheated vapor flowing through the coolant loops, and it only occurs if the loop seals are cleared of liquid. This did not occur in any of these calculations for the Surry plant.

The major influence of these flows is to transfer energy from the core to other structures in the reactor coolant system, thereby reducing the heatup rate of the core. Besides extending the transient, a slower core heatup may alter the amount of cladding that is oxidized while still in fuel rod geometry, thereby changing the composition of the molten core. The energy removed from the core will heat other structures in the reactor coolant system. Higher temperatures will tend to reduce fission product retention, and sufficiently high temperatures may result in failure of the pressure boundary prior to breach of the reactor vessel by the molten core. Should this failure occur in the steam generator tubes, containment bypass through the steam lines may occur. If the failure occurs early enough, the system may depressurize sufficiently to avoid direct containment heating when the core debris is ejected following vessel failure.

The natural circulation flows did not change the core damage progression, only the times that various stages of damage occurred up to fuel rod relocation. Fuel rod relocation began at about 161 min with no multidimensional natural circulation flows modeled. In-vessel natural circulation delayed this event by 7 min. The modeling of both

in-vessel and hot leg natural circulation resulted in a further delay of 11 min. This difference in timing was not as significant as the difference in ex-vessel structure temperatures.

With no natural circulation flows modeled, the vapor leaving the reactor vessel was near the saturation temperature throughout the transient. With in-vessel circulation modeled, the vapor leaving the vessel was superheated. As a result, the hot leg and surge line piping heated up, so much so that creep rupture failure of at least the surge line pipe would be expected before the vessel is breached by the molten core. Such a failure would alter the course of the transient, compared to the calculation without in-vessel natural circulation. The extent of the change depends on the size of the failure and the resultant depressurization. With hot leg countercurrent flow also modeled, the steam generator tubes also heated up, but they were several hundred degrees below the surge line temperature. Therefore, steam generator tube rupture and the associated containment bypass would not be expected to occur during the transient.

Ballooning occurred in the scoping calculations with in-vessel natural circulation, resulting in a flow area reduction of 20-60% in the inner part of the core. Although some flow was diverted around the ballooned region, the recirculating flow between the core and the upper plenum was maintained. Ballooning of the cladding affected the amount of fuel dissolved by molten Zircaloy. Oxidation of the inner cladding surface in the ballooned regions prevented the molten Zircaloy from coming into contact with the fuel pellets, preventing fuel dissolution in those regions.

The TMLB' transient was also analyzed as part of the draft Reactor Risk Reference Document (NUREG-1150) effort. A significant difference in timing of events exists between that analysis and the scoping analyses performed here. In the draft NUREG-1150 calculation, vessel failure was predicted to occur 155 min into the transient. In the SCDAP/RELAP5 scoping calculation with no natural circulation, fuel rod relocation did not begin until 161 min, and vessel failure would not occur until some time well after 200 min. Even larger delays occurred when the in-vessel and hot leg natural circulation flows were modeled. Fuel rod relocation did not begin until 248 min in the best-estimate sensitivity calculation. More significantly, the likelihood of ex-vessel structural failure was illustrated in the calculations with multidimensional natural circulation, but was not explicitly considered in the draft NUREG-1150 analyses. These differences in timing and events demonstrate the importance of mechanistic modeling of severe accidents.

Sensitivity calculations were performed to investigate four areas of modeling uncertainty: axial power profile, steam generator inlet plenum mixing, heat loss from the piping, and radial flow resistance in the upper plenum and core. In all of these calculations, both in-vessel and hot leg natural circulation were modeled.

A base case was first performed that differed from the scoping calculations primarily in that a lower decay power was used. Creep rupture failure of the surge line was predicted to occur at about 246 min after the beginning of the transient, shortly before the onset of fuel rod relocation, and about 50 min later than in the comparable scoping calculation. Changing the axial power profile from a relatively flat to a chopped cosine shape had very little effect on the transient, with surge line failure occurring about 1 min earlier than in the base case.

Reducing the amount of flow that mixed in the steam generator inlet plena increased the hot leg flow and the heat transfer to the coolant loops. A 25% flow increase delayed the surge line failure by about 9 min. A bounding calculation that maximized the hot leg flow was also performed, in which there was no mixing in the steam generators. This led to a more uniform heatup of all the loop structures, and failure of the hot leg occurred nearly 45 min later than the surge line failure in the base case.

Heat loss through the hot leg and surge line pipes was modeled with radiative and/or convective heat transfer coefficients. While the heat loss increased the temperature difference across the pipes, the surge line was still predicted to fail. Delays in the failure of 6 to 13 min compared to the base case were realized.

Changing the radial flow resistances in the core and upper plenum had little effect on the predicted surge line failure. Decreasing the resistances in either location led to failures less than 2 min earlier than in the base case. Increasing the resistances in both locations resulted in surge line failure about 12 min sooner than in the base case. The faster heatup of the core in this last case was the result of ballooning in the core. The ballooning occurred when the cladding temperature was about 1400 K, and the resultant surface area increase and double-sided cladding oxidation accelerated the core heatup.

The magnitude of the hot leg flow was sensitive only to the amount of mixing in the steam generator inlet plena and the hot leg inlet vapor

temperature. Changes in the reactor vessel upper plenum flow affected the hot leg only in that they altered the hot leg inlet vapor temperature. Conversely, the upper plenum flow was affected by the hot leg flow. The flow recirculating within the upper plenum increased as the loop heat transfer increased, because cooler vapor was being returned to the plenum. This higher density fluid increased the buoyant driving force, and hence the flow.

A 0.15-m diameter hole in the pressurizer surge line was modeled at the time of the surge line failure in the final calculation. The system pressure rapidly decreased, allowing the accumulators to inject liquid into the reactor coolant system. This water entered the reactor vessel, where it quenched the entire core before any fuel rod relocation occurred. Fragmentation of the fuel rods was predicted, although debris formation was not permitted in the calculation. At the end of the calculation, the system pressure was below 1.0 MPa, the accumulators were empty, and the two-phase liquid level in the core was decreasing, although the core structures were still at the saturation temperature.

Further work is recommended in the natural circulation area. The size of the reactor coolant system failure needs to be determined, as does the ensuing system behavior until the time of reactor vessel failure. The effects of the natural circulation flows on the fission product transport and retention need to be quantified. Interactions between the natural circulation flows and noncondensible gases should be investigated further.

CONTENTS

FIGURES

TABLES

ACKNOWLEDGMENTS

I would like to thank Dr. James Han of the U.S. Nuclear Regulatory Commission, the sponsor of this work, for his guidance and reviews of the models and analyses. The staff at Argonne National Laboratory, particularly Drs. Hank Domanus and William Sha, were most helpful in providing and discussing the results of the COMMIX calculations.

ANALYSES OF NATURAL CIRCULATION DURING A SURRY STATION BLACKOUT USING SCDAP/RELAP5

1. INTRODUCTION

An increased awareness of severe accidents was reflected in the U.S. Nuclear Regulatory Commission's research after the accident at Three Mile Island. A parallel experimental and analytical effort formed the basis of understanding of severe accidents. This research effort culminated in the "Reassessment of the Technical Bases for Estimating Source Terms," NUREG-0956,[1] which described the current state of knowledge in the severe accident area and identified eight major areas of uncertainty. The draft "Reactor Risk Reference Document," NUREG-1150,[2] used the source term methodology in NUREG-0956 to provide a basis for new estimates of reactor risk.

Natural circulation in the reactor coolant system, one of the areas of major uncertainty identified in NUREG-0956, was discussed in the associated uncertainty papers[3]. However, phenomenological analyses in support of draft NUREG-1150 did not account for the natural circulation flows. Analyses have been performed for the U.S. Nuclear Regulatory Commission to mechanistically investigate the effects of various types of natural circulation on the transient, severe accident response of the Surry nuclear power plant. Of particular interest were changes in the events that occur, in event timings, and in the extent of core damage. Sensitivity studies have also been performed to investigate areas of major uncertainty in the modeling of multidimensional natural circulation flows. Blowdown of the plant following a postulated surge line failure has also been simulated.

The transient used to investigate the natural circulation flows was the TMLB' sequence, which is a loss of both onsite and offsite ac power, with early (immediate) failure of the steam-driven auxiliary feedwater pump. A high-pressure boiloff ensues. This transient was selected because it presents the potential for natural circulation flow in several regions of the reactor coolant system (RCS). It is also a useful transient in that it has been analyzed by modeling different plants with various computer codes.

The Surry nuclear power plant was used in these analyses. Surry is a Westinghouse-designed pressurized water reactor with three coolant loops and a rated core thermal power of 2441 MW. Surry is one of the reference plants used in source term and risk analyses. Therefore, calculations of the TMLB' sequence are available in which other computer codes and modeling assumptions were used. Comparing the results of those calculations with the current analyses may provide insight into how the codes and models used affect the calculated plant behavior.

The SCDAP/RELAP5 computer code[4] was used to perform the calculations of the plant response. This code provides best-estimate integral calculations of the system thermal-hydraulic and core damage response. Therefore, effects of the various natural circulation flows on the core damage progression could be explicitly determined.

There are three natural circulation flows in the RCS that are of interest in severe accidents. They are in-vessel circulation, hot leg countercurrent flow, and flow through the coolant loops. Figure 1 illustrates these natural circulation flows. In-vessel natural circulation is characterized by a hot plume of vapor rising from the center of the core into the upper plenum. Heat is transferred to the upper plenum structures, thereby cooling the vapor. The flow turns radially outward in the upper plenum, then returns to the core through the lower powered, and hence cooler, peripheral fuel assemblies. The flow continues downward into the core, slowly turning toward the center, where it again rises to the upper plenum. Hot leg natural circulation is characterized by single-phase, countercurrent flow in the hot leg between the upper plenum and U-tube steam generators. Hot vapor flows out the top of the hot leg to the steam generator inlet plenum. Some of the flow mixes with the fluid in the inlet plenum, while some continues into the steam generator tubes. The hot vapor cools as it flows to the outlet plenum through about 35% of the steam generator tubes.[5] The cooler vapor returns through the tubes to the inlet plenum. Again, some of this flow mixes in the inlet plenum, and some continues directly into the bottom of the hot leg. The cooler

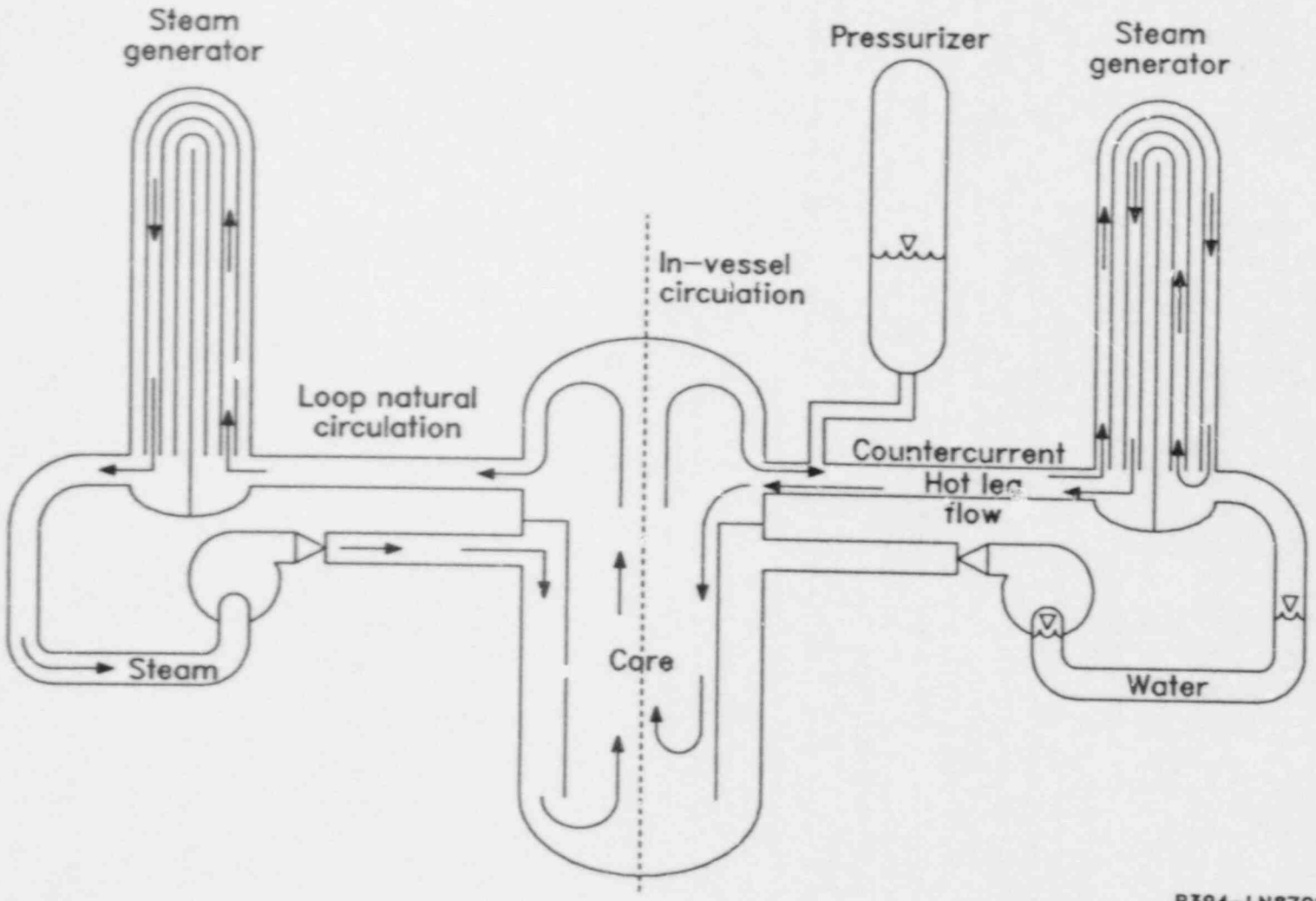

Figure 1. Severe accident natural circulation flows.

vapor then returns to the reactor vessel along the bottom of the hot leg. Superheated vapor flow through the coolant loops will occur only if the loop seals are cleared of liquid. If this flow occurs, the in-vessel and hot leg natural circulation flows will no longer exist, because the loop flow rate is high enough to preclude them.

The most important effect of the natural circulation flows is to transfer energy from the core to other parts of the RCS. This energy transfer reduces the heatup rate of the core, and delays the various stages of core damage. The heatup of the other structures will also affect the fission product deposition and retention, because higher structure temperatures will provide an impetus for driving the fission products further along the flow path. Higher temperatures in the ex-vessel structures also present the possibility of failure of the RCS before failure of the reactor vessel lower head. The possibility of such a failure is very important in the consideration of direct containment heating, because a large enough failure may allow the RCS to depressurize sufficiently by the time the vessel fails to preclude early containment failure by direct containment heating. Failure of the steam generator tubes may also provide a path for containment bypass, in that fission products could be transported through the ruptured steam generator tubes into the secondary side of the steam generators and from there, through the relief valves to the atmosphere.

A scoping study of the effects of the natural circulation flows was performed by systematically increasing the complexity of the Surry plant model. First, the transient was calculated using a once-through model of the reactor vessel. Second, the core and upper plenum model were changed to allow in-vessel natural circulation. Finally, the hot leg model was changed to allow hot leg countercurrent flow. By comparing the results of each calculation with those of the previous one, the changes effected by each natural circulation flow could be determined. The coolant loops were modeled so that loop natural circulation could occur if the loop seals cleared of liquid in any of the calculations. However, the loop seals did not clear in any of the calculations.

A series of sensitivity studies was then performed to investigate the effects of major phenomenological and modeling uncertainties on the RCS behavior until the time of RCS pressure boundary failure. Of particular interest were changes in the timing or location of the RCS failure. Parameters that were varied in the calculations included the axial power profile, the amount of mixing in the steam generator inlet plena, radial flow resistances in the core and upper plenum, and heat loss through the hot leg and pressurizer surge line piping. Finally, the failure of the surge line and the ensuing blowdown were analyzed.

Chapter 2 discusses the three natural circulation flows in greater detail. The results of the scoping and sensitivity analyses are presented in Chapters 3 and 4, respectively, followed by conclusions drawn from the analyses in Chapter 5 and references in Chapter 6. Appendix A briefly describes the Surry plant and the SCDAP/RELAP5 models of the plant. Appendix B provides a description of the SCDAP/RELAP5 computer code. Appendix C contains a paper addressing the applicability of the crossflow junction model in RELAP5 to the flow situations that might be encountered during a severe accident.

2. NATURAL CIRCULATION FLOWS

Three natural circulation flows that can be important during severe accidents are in-vessel circulation, hot leg countercurrent flow, and flow through the coolant loops. Each of these flows may be present during a high pressure boiloff transient such as the TMLB' sequence

The primary effect of natural circulation flows is to redistribute the energy being generated in the core. This energy redistribution will slow the heatup of the core, which in turn may affect the damage progression or the extent of the core damage. Slowing the core damage would allow more time for systems to be recovered to mitigate or terminate the accident. However, energy removed from the core will affect the structures to which it is transferred, in both the upper plenum and the coolant loops. The discussions below address the basic phenomena associated with the three types of natural circulation being considered, together with how the transient progression may be affected by the coolant flow. Appendix A provides information on how the multidimensional flows were modeled in these analyses.

2.1 In-Vessel Natural Circulation

In-vessel natural circulation begins when the core heatup begins. Because the center part of the core is at a higher power than the periphery, the superheated steam in the center is hotter and less dense, and a radial density gradient is established. The denser vapor in the outer part of the core tends to flow toward the center, replacing the hot vapor that rises into the upper plenum. This vapor plume rises to the top of the upper plenum, where it is turned radially outward to the core barrel, and then back down toward the top of the core. Heat transfer to the structures in the upper plenum cools the vapor, reinforcing the density gradient between the center of the vessel and the periphery. The cooler steam reenters the core through the top of the peripheral fuel assemblies. As core uncovering continues and the liquid level drops, the recirculating flow extends farther into the core. Depending on the axial power profile, the flow may eventually extend to the bottom of the core. The density gradient in the upper plenum also establishes a recirculating flow within the upper plenum.

In reality, many natural circulation cells will be established in the core, especially during the core damage portion of the transient. These cells will exist between fuel assemblies, between parts of fuel assemblies, and even between subchannels. Wherever a radial temperature gradient exists, a natural convection flow may be established. Rapid increases in local temperature associated with the accelerated oxidation of the Zircaloy fuel rod cladding, at a temperature around 1850 K, will result in the establishment of these relatively small natural circulation cells. These smaller flow cells are believed (assumed) to exist within larger overall natural convection cells involving the entire core. These analyses investigate and discuss such core-wide patterns.

In-vessel natural circulation flow may affect the cladding oxidation. Because steam is being recirculated from the upper plenum back into the core, it is less likely that the oxidation reaction will become steam-starved. The slower cladding heatup caused by the removal of some of the core energy to the upper plenum structures, combined with a steam-rich environment, may result in more extensive oxidation of the cladding at lower temperatures. More extensive oxidation of the cladding, in turn, may result in smaller amounts of unoxidized Zircaloy melting as the temperature increases, which could delay relocation of molten material and reduce dissolution of the fuel pellets.

The heating of the upper plenum structures could also result in their oxidation or melting, which could add to the hydrogen generated in the RCS before vessel failure and add more material to the melt that flows from the vessel at the time of lower head failure.

Both the smaller amount of fuel dissolved by liquid Zircaloy and the higher temperature of the upper plenum structures affect fission product behavior. The smaller amount of dissolved fuel may delay the release of many of the fission products until the fuel melts. At that later time, which will be closer to the time of vessel failure, there will be less time for the fission products to be retained on surfaces in the RCS, which may result in more fission products in the containment. The higher structure temperatures would tend to reduce the amount of fission products retained in the upper plenum, causing them to be deposited elsewhere or released to the containment.

Higher vapor temperatures in the upper plenum will also make hotter vapor available to the hot legs. Flow through the hot leg and surge line to the pressurizer power-operated relief valves (PORVs)

will heat the piping. If the pipe temperatures are high enough, creep rupture failure of these pipes may become a concern. Failure of the RCS piping before vessel failure could allow the system to depressurize, initiating accumulator injection. If the depressurization continues far and fast enough, the RCS pressure at the time of vessel failure may be low enough to preclude direct containment heating.

2.2 Hot Leg Countercurrent Flow

Single-phase countercurrent flow in the hot leg is the least well characterized of the three natural circulation flows being investigated. A general discussion of the basic considerations of the flow is presented below.

Superheated vapor enters the top of the hot leg, displacing saturated vapor, which then flows back to the reactor vessel along the bottom of the hot leg. When the hotter vapor enters the steam generator inlet plenum, it will rise toward the steam generator tubes. Vapor enters some of the tubes, displacing the cooler steam that was in the tubes. The displaced vapor enters the outlet plenum, then reenters other steam generator tubes, forcing vapor into the inlet plenum. A density gradient is thus established between tubes. This density gradient then pulls more hot vapor into the tubes, displacing cooler steam. The process continues until a steady flow is established, with hot vapor flowing from the inlet plenum to the outlet plenum through some of the steam generator tubes, and cooler vapor returning to the inlet plenum through the remaining tubes.

Now consider the flow streams shown in Figure 2. The hot (T_h) and cold (T_c) fluid temperatures at three locations will be examined: the hot leg nozzle (1), the steam generator end of the hot leg (2), and the inlet to the steam generator tubes (3). At each of the locations, hotter fluid is flowing from the reactor vessel toward the steam generator outlet plenum, and cooler fluid is flowing toward the reactor vessel.

The hot vapor entering the hot leg from the reactor vessel flows toward the steam generator along the top of the pipe. As it flows, heat is transferred to both the hot leg piping and the returning cooler fluid stream. This heat transfer occurs in both the Westinghouse natural circulation experiments[5] and calculations performed with the COMMIX computer code in which no hot leg structures were modeled.[6] There may also be some mass transfer between the two fluid streams. The result is that $T_{h,1} > T_{h,2}$. As the flow enters the steam generator inlet plenum, some of it mixes with the fluid in the plenum and with the cold flow exiting from some of the steam generator tubes. The mixing reduces the temperature of the steam entering the steam generator tubes, and $T_{h,3} < T_{h,2}$. Heat is transferred to the tubes as the steam flows through the steam generators. When the flow returns to the inlet plenum, some of it mixes with the hot leg flow. This mixing raises the temperature of the steam returning through the hot leg, so that $T_{c,2} > T_{c,3}$. As the flow proceeds along the bottom of the hot leg to the reactor vessel, heat is being transferred from the hotter fluid above to this cooler steam, and from this cooler steam to the hot leg pipe. Whether these energy transfers result in a net heating or cooling of the return flow has not been quantified, but the vapor temperature will probably not change significantly along the bottom of the hot leg. Also unaccounted for in this discussion is the effect of circumferential heat transfer in the hot leg piping, in which heat would be conducted from the hot upper part of the hot leg to the cool lower part.

Assuming a steady flow, the total energy transfer in the coolant loop is the product of the hot leg mass flow rate, the average heat capacity of the flowing vapor, and the temperature difference between the opposing flows at the hot leg nozzle. Analyses associated with the Westinghouse experiments showed that the hot leg mass flow rate is a function of geometric parameters, the fluid density, and the square root of the temperature difference ($T_{h,1}$-$T_{c,1}$). Thus, the heat transferred by the hot leg natural circulation flow depends on the temperature difference at the nozzle, and any interactions that tend to increase the cooler vapor temperature will reduce the flow rate and the heat transfer. Both the mixing in the steam generator inlet plenum and heat transfer from the hotter vapor above act to increase the temperature of the returning vapor.

Similarly, the heat transfer in the steam generator tubes is the product of the mass flow rate through the tubes, the average vapor heat capacity, and the temperature difference ($T_{h,3}$-$T_{c,3}$). Heat transfer in the tubes will be affected by interactions that alter either of these temperatures. Again, the mixing in the inlet plenum tends to reduce $T_{h,3}$, thereby limiting the heat transfer in the steam generators.

Now consider the case in which there is no mixing in the steam generator inlet plenum. The hot vapor temperatures in the hot leg will change little; a lower temperature in the cooler vapor will

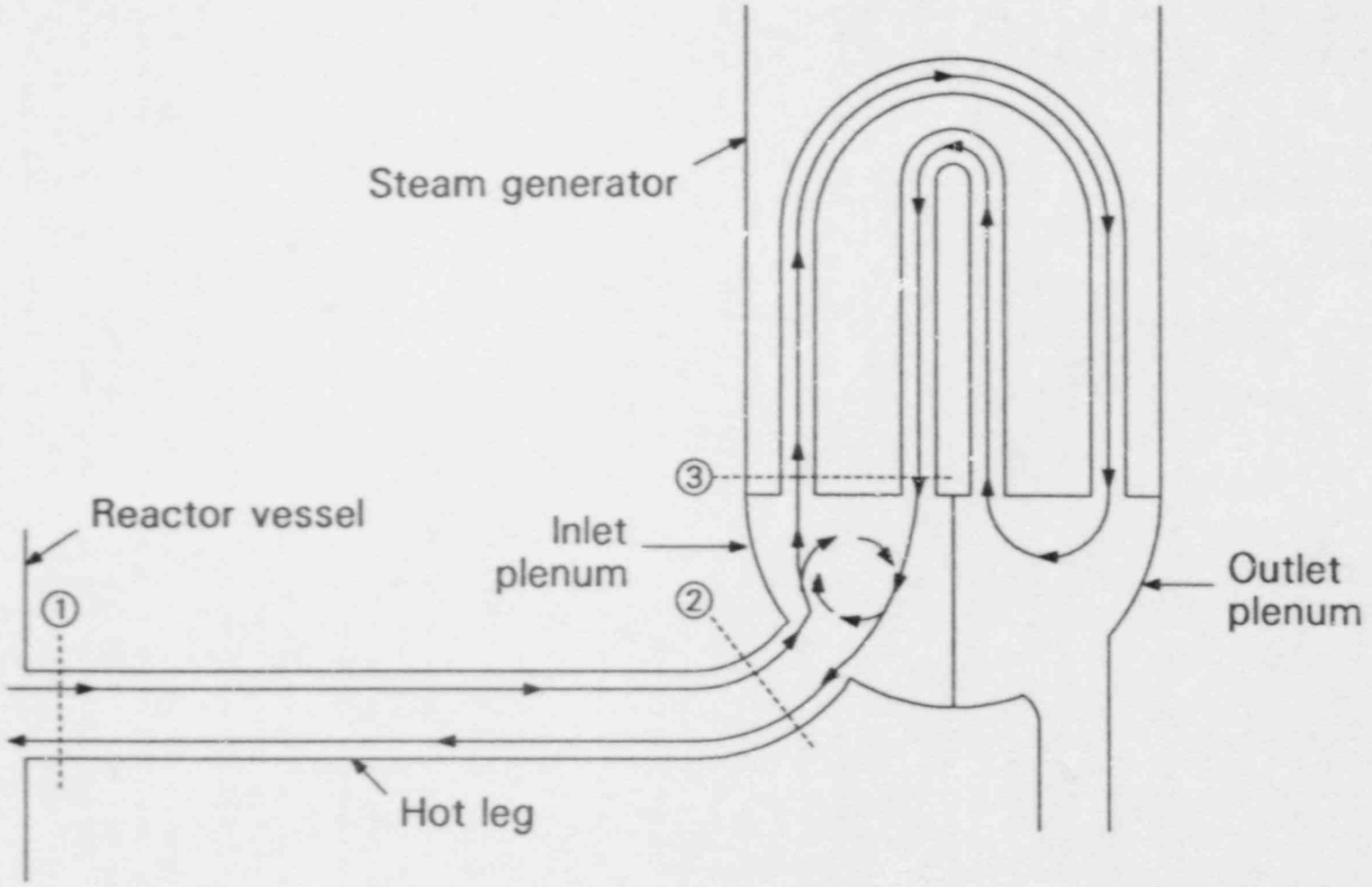

Figure 2. Hot leg natural circulation stream flows.

increase the amount of heat transferred between the opposing flow streams slightly. However, $T_{h,3} = T_{h,2}$. The higher temperature fluid entering the steam generator tubes will result in increased heat transfer to the tubes. The absence of mixing also means that $T_{c,2} = T_{c,3}$, so that the flow returning through the hot leg is colder. Since the flow is driven by the temperature difference between the hot and cold fluid streams in the hot leg, the mass flow will increase. The higher mass flow rate will increase the heat transfer in the loop, slowing the core heatup. Higher temperatures in the steam generator tubes will also change the relative energy deposition between the hot leg and the tubes, with more energy being transferred to the tubes.

Mixing in the steam generator plenum is a controlling parameter for the hot leg natural circulation flow. It limits the mass flow in the hot leg by increasing the temperature (and lowering the density) of the vapor returning from the steam generator along the bottom of the hot leg. It limits the heat transfer in the steam generator by reducing the temperature of the hot vapor entering the tubes. While accurate modeling of the mixing is important in providing a realistic simulation of the hot leg flow behavior, it is also clear that neglecting the mixing in the steam generator inlet plenum in the analyses will yield steam generator tube temperatures and hot leg mass flow rates that are higher than would be expected in an actual transient.

The primary structural consideration associated with the hot leg countercurrent flow is the integrity of the steam generator tubes. Steam generator tubes are very thin compared to the loop or surge line piping, and therefore, are quickly heated if exposed to high temperature vapor. Should the tubes fail, a direct path outside of containment (through the steam line relief valves) becomes available to any fission products carried in the coolant.

Fission product behavior may also be affected by the flow to the steam generators. An extremely large surface area is available on the steam generator tubes for deposition of fission products. If the tubes remain cool, deposited species may remain there and not be released to the containment. If the tubes continue to heat up so that revolatilization occurs, the flow may simply carry the resuspended fission products to cooler parts of the tubes, where they would again be deposited. The mixing in the steam generator inlet plenum may also play a part in the fission product behavior. If gaseous fission products are carried with the hot vapor along the top of the pipe, the sudden cooling associated with interaction with the cooler fluid in the inlet plenum may result in the condensation of the vapors, either on existing aerosols or as newly generated aerosols. In liquid form, these fission products would be deposited more quickly, and probably in the inlet plenum rather than in the tubes. The countercurrent flow in the hot leg itself may also affect the fission product transport. If gravitational settling is an important mechanism for fission product deposition in the hot leg, fission products falling from the flow heading toward the steam generators would enter the return vapor stream, where they would be carried back toward the reactor vessel rather than away from it. This phenomenon is beyond the capability of current analytical methods, since the flow in the hot legs is considered to be one-dimensional. However, the magnitude of the effect should be calculable since the amount of deposition that is caused by gravitational settling should be known from the fission product transport calculation.

2.3 Loop Flow

Should the loop seals clear of liquid during the transient, loop natural circulation would be reestablished. In contrast to the natural circulation that occurs following the initial reactor coolant pump coastdown, the fluid flowing through the coolant loops would be superheated vapor. Loop natural circulation flow is a buoyancy-driven one-dimensional flow with heat addition in the core and heat rejection primarily in the steam generators. However, in this situation, heat would be transferred to the piping throughout the coolant loops. Because of the resulting large vapor density differences and the height of the steam generators, this flow is generally large enough that it disrupts any multidimensional natural circulation flows that might exist.

The high flow rate and large amount of metal structures available as heat sinks result in a much slower core heatup. The slower heatup rate could result in complete oxidation of the cladding before any of the Zircaloy melts. Fuel rod relocation would be delayed for several hours. Failure of the piping anywhere in the RCS is possible, although the steam generator tubes would be particularly susceptible because they are much thinner than the hot or cold legs. Heating of all the piping will also tend to reduce the extent of fission product retention in the RCS.

3. SCOPING ANALYSES

Several scoping calculations were performed as the first part of the natural circulation analyses. While these were best-estimate simulations of the plant response, they are referred to as scoping calculations because the overall system effects of the in-vessel and hot leg natural circulation flows were being investigated, and to distinguish them from the sensitivity analyses presented in the next chapter. The analysis began with a single-channel, once-through model of the core and upper plenum. This model provided a basis for determining the effects of the natural circulation flows. Next, the core and upper plenum model was changed to investigate the effects of in-vessel natural circulation on the transient response of the plant. For the hot leg countercurrent flow analysis, a model was prepared which allowed both in-vessel and hot leg natural circulation flows. Thus, the approach was to use increasingly detailed models of the Surry plant to determine the incremental effects of the various natural circulation flows. In each case, the pump suction loop seal piping was modeled, so that clearing of the loop seals could occur. All three of the coolant loops were modeled separately, with one containing the pressurizer. Appendix A provides information on the various models used.

The sections below describe results of the scoping analyses. The single-channel analysis (no multidimensional natural circulation) will be described first, followed by the in-vessel, in-vessel and hot leg, and loop natural circulation flow analyses. This latter section briefly discusses the results from a prior analysis of the Bellefonte nuclear power plant, since the loop seals did not clear in any of the Surry calculations. Finally, the results of these Surry analyses are compared to one another and to the Surry analyses used in draft NUREG-1150, in order to provide insight into the impact of the natural circulation flows on the transient behavior.

3.1 Once-Through Model

A once-through model of the core and upper plenum was used in scoping Case 1 to provide a basis for evaluating the effects of the various natural circulation flows on the plant transient response. This has been the traditional modeling approach for analyzing plant behavior, and was used in the source term analyses presented in draft NUREG-1150.

The sequence of events for the transient is contained in Table 1. After the transient was initiated, decay heat was removed from the core to the steam generators by a natural circulation flow through the loops. When sufficient water had been boiled in the secondary side of the steam generators so that the remaining liquid was unable to remove the decay heat, the RCS began to heat up and pressurize. The pressurizer PORVs relieved the pressure by cycling between their open and close setpoints of 16.2 and 15.7 MPa, respectively. When the saturation temperature was reached at 101 min, boiling began in the core. As the boiling continued, the liquid inventory in the RCS decreased until the core began to uncover and heat up at 130 min. With no source of water, the heatup continued unmitigated until fuel rod relocation began at about 161 min. The calculation was terminated at 200 min.

Figure 3 presents the RCS pressure during the transient. The pressure decreased from the steady state value shortly after the transient began, as the steam generators were able to remove more energy from the reactor coolant than was being added in the core. After the reactor coolant pumps coasted down, natural circulation through the coolant loops transferred the decay heat from the core to the steam generators, and the RCS pressure remained relatively constant. The small oscillations in the pressure between 3 and 72 min reflected the cycling of the relief valves on the secondary side of the steam generator. As the steam generator pressure decreased, so did the saturation temperature, increasing the heat transfer from the primary system and consequently lowering the RCS pressure. After the steam generators dried out, the pressure increased until the PORVs opened. The pressure then cycled between the opening and closing setpoints of the PORVs for the remainder of the transient. For these analyses, it was assumed that the PORVs could cycle throughout the transient without failing.

The collapsed liquid level in the pressurizer is shown in Figure 4. The level decreased as the transient began because heat removal in the steam generators cooled the RCS liquid, causing it to contract, thereby reducing the level. When the RCS began to heat as the steam generators dried out, the level increased. The level continued to increase until all of the steam in the pressurizer had been relieved through the PORVs, at about 90 min. The pressurizer remained liquid-full until after boiling began in

Table 1. Sequence of events for scoping Case 1

Event	Time (min)
Transient initiation	0
PORV cycling begins	71.8
Steam generators dry	75.4-77.2
Hot legs reach saturation	100.6
Loop natural circulation flow ends	109.7
Core heatup begins	129.6
Cladding oxidation begins	144.1
Control rod relocation begins	157.2
Accelerated oxidation begins	157.9
Fuel rod relocation begins	160.5
Calculation ends	200.0

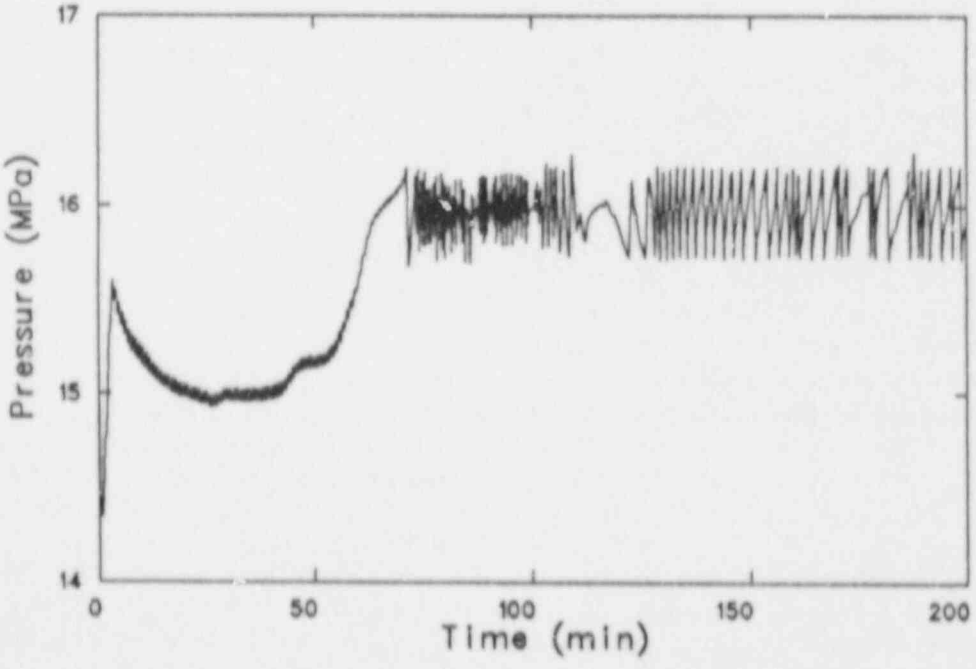

Figure 3. Pressurizer pressure for scoping Case 1.

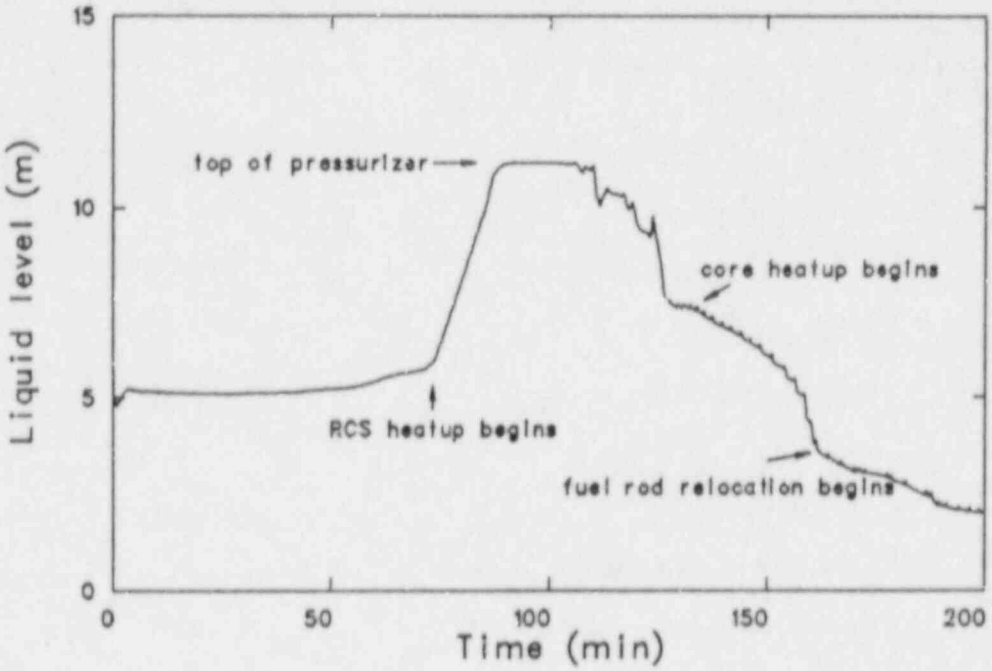

Figure 4. Pressurizer collapsed liquid level for scoping Case 1.

the core. Steam then entered the pressurizer, reestablishing the liquid level. The level decreased through the rest of the transient, but some liquid remained in the pressurizer as the core damage occurred.

Figure 5 shows fuel rod cladding surface temperatures at four of the ten axial nodes, including the top and bottom nodes, from 127 to 200 min. The top of the core began to heat up shortly before 130 min, and a top-down dryout of the core followed. The temperatures increased more rapidly as the cladding began to oxidize, and continued to increase until the temperature reached 2500 K. When that temperature was attained, the oxide shell on the cladding was assumed to rupture, initiating the relocation of molten material that had been contained within the cladding. This material flowed down the outside of the fuel rods until it froze at lower elevations. It should be noted that when fuel rod relocation began in the top part of the core at about 161 min, the bottom part of the core contained enough water so that the cladding was still at the saturation temperature. All of the material froze in the two axial nodes in the middle of the core, forming a cohesive debris at about 162 min. The cohesive debris caused the flow area to be reduced to less than 1% of the original axial flow area, nearly stopping steam flow through the core. Steam that was being generated in the lower plenum by heat transfer from relocated molten control rod material then flowed through the core bypass rather than through the core. The cladding temperatures in the top half of the core dropped to nearly 1000 K after relocation began for several reasons. Cladding oxidation stopped at elevations from which material relocated because all of the unoxidized Zircaloy flowed to lower elevations. Besides the lack of heat generation from oxidation, heat was being convected to the core baffle plates and core bypass region. Also, because of the flow blockage, little superheated steam was rising from the lower part of the core to heat the cladding in the upper part. Temperatures in the bottom of the core continued to increase because oxidation was still taking place. At about 192 min, the upper part of the core began to heat up again, the result of higher temperatures in the core bypass region, which reduced the heat transfer from the upper part of the core so that the decay heat was not being removed. The changes in the transient behavior associated with the cohesive debris formation demonstrate the limitations of analyses that model the core as a single channel; had more than one channel been modeled, flow could have proceeded through the core around a cohesive debris in one region of the core.

The cohesive debris was composed of Zircaloy and dissolved fuel from upper parts of the core,

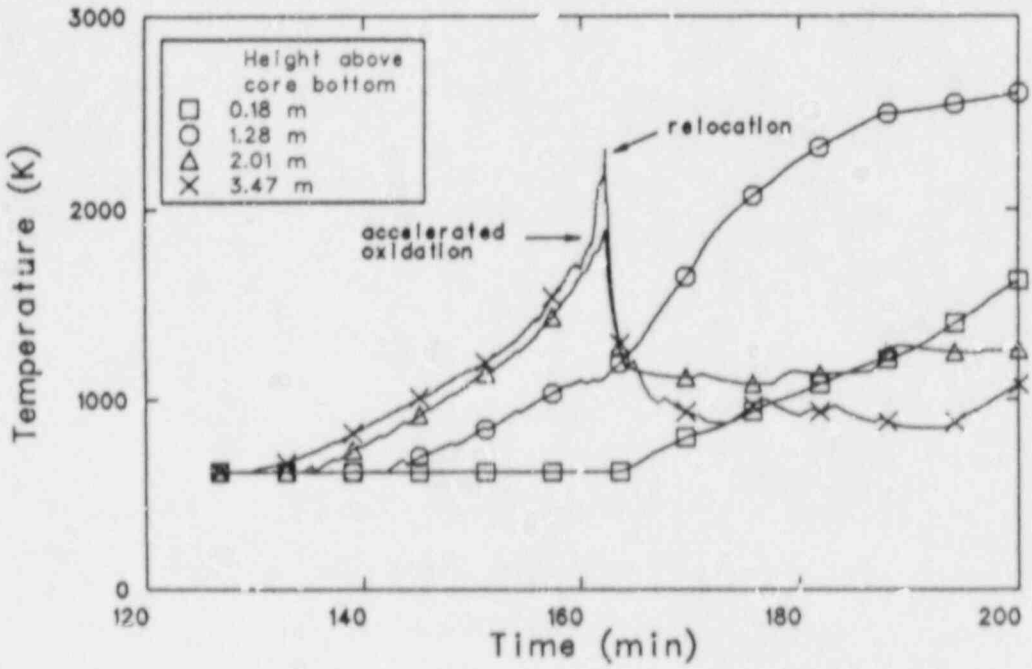

Figure 5. Fuel rod cladding surface temperatures at 0.18, 1.28, 2.01, and 3.47 m above the core bottom for scoping Case 1.

and contained 27.9% of the zirconium and 2.5% of the fuel initially in the core. At the end of the calculation, 90% of the control rods had relocated, as had 35.7% of the cladding and 7.2% of the fuel.

The total hydrogen generation rate in the core during the transient is shown in Figure 6. The rate of hydrogen production steadily increased as more of the cladding was being oxidized. After fuel rod relocation began, the cohesive debris formation and associated low core flow reduced the cladding oxidation. The increased generation rates at about 177 and 186 min reflected higher steam flows entering the core, which were caused by relocated core material boiling water in the lower plenum. At the time of fuel rod relocation, about 97 kg of hydrogen had been produced, corresponding to oxidation of about 14% of the Zircaloy in the core. The hydrogen generated after relocation began would probably be greater than that calculated by SCDAP/RELAP5 because the code does not calculate the oxidation of material while it is relocating. There was sufficient steam in the core to allow oxidation throughout the transient. The maximum hydrogen mole fraction in the vapor of 0.94 occurred in the top of the core just before cladding relocation began.

Fission product release to the coolant began when the cladding oxide shell was breached at about 161 min. At the end of the calculation, more than 15% of the xenon and krypton, 13% of the cesium, 11% of the iodine, and 17% of the tellurium that was originally in the fuel had been released.

The mass flow rate through the core bypass is presented in Figure 7. As the core uncovered, the density difference between the fluid in the core and that in the bypass caused a natural convection flow to be established. Steam flowed up through the core to the upper plenum, and a small amount of steam returned to the lower plenum through the core bypass. This flow pattern was maintained until the cohesive debris was formed in the core. After that, flow through the bypass was from the lower plenum to the upper plenum. Increases in flow occurred when molten material from the control rods and fuel rods relocated to the lower plenum. This material boiled some of the liquid remaining in the lower plenum, and the resulting steam flowed through the bypass to the upper plenum and hot leg.

Figure 8 presents the collapsed liquid level in the reactor vessel, which decreased throughout the transient. The level decrease slowed as less water

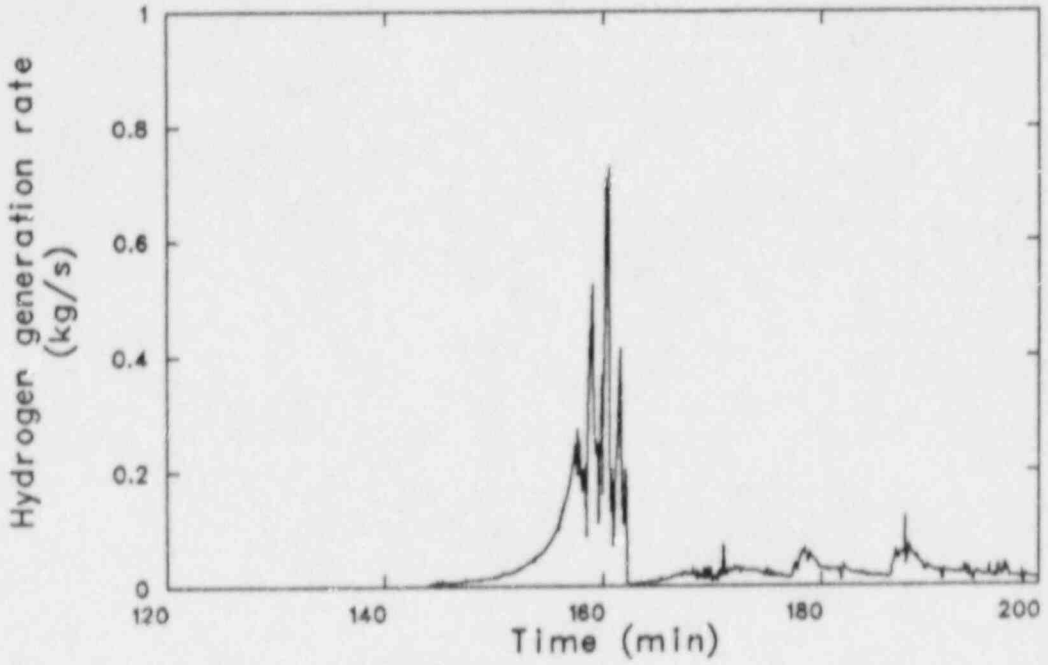

Figure 6. Total hydrogen generation rate for scoping Case 1.

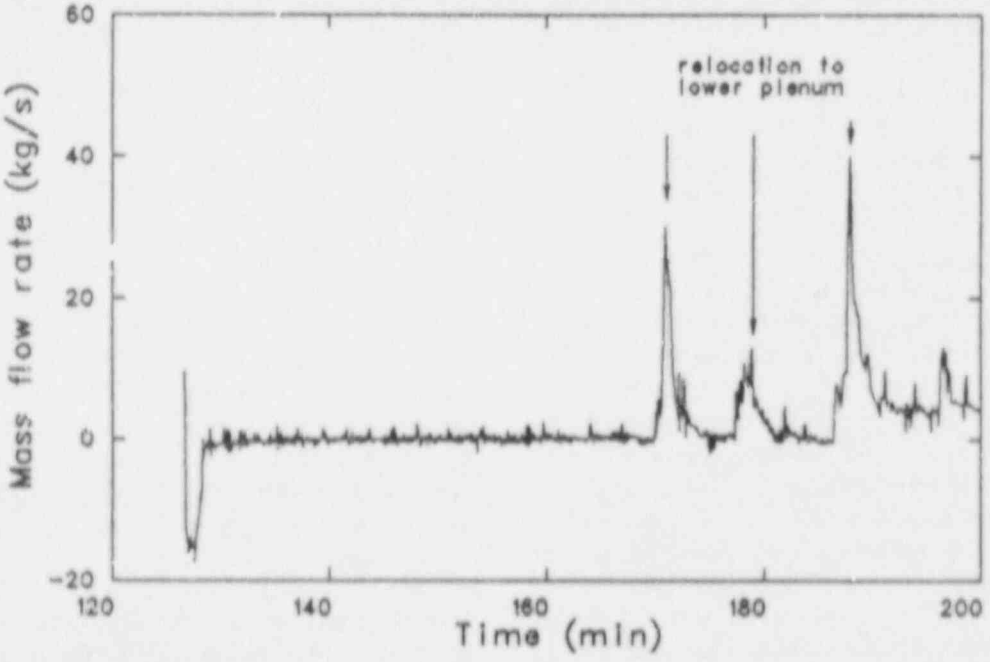

Figure 7. Mass flow rate through the core bypass for scoping Case 1.

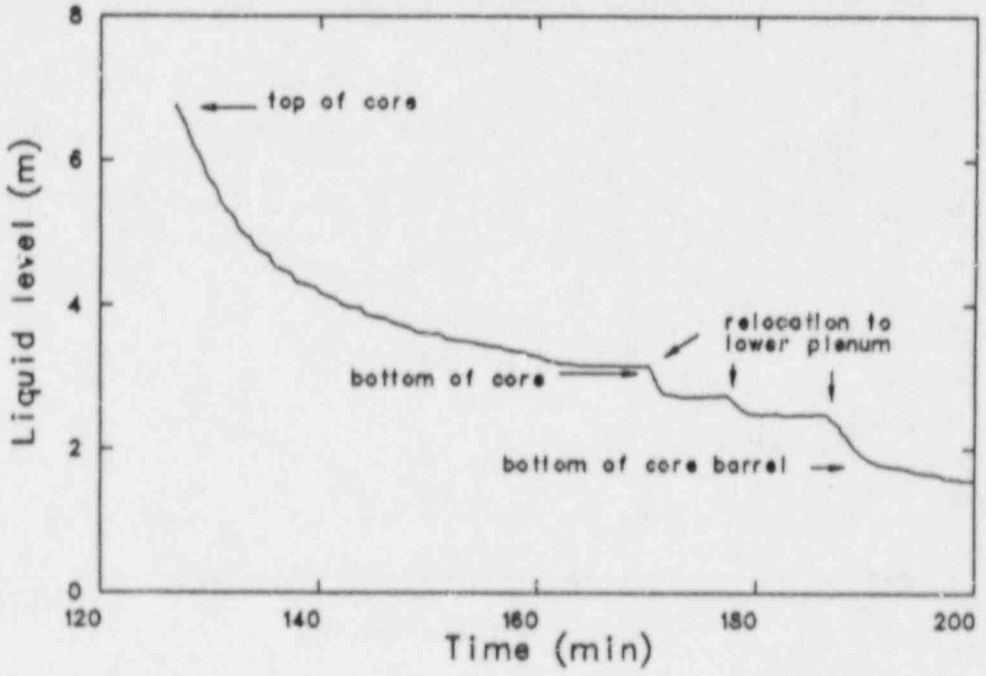

Figure 8. Reactor vessel collapsed liquid level for scoping Case 1.

remained in the core, nearly stopping after the core dried out. The incremental level decreases after 167 min occurred when molten material dropped from the core to the lower plenum, causing some of the remaining water to boil. At the end of the calculation, the lower plenum was completely filled with steam, and both the two-phase and the collapsed liquid levels were in the lower head.

The temperature of the hottest structure in the upper plenum is shown in Figure 9. This stainless steel structure is located just above the core. The temperature steadily increased until the fuel rod relocation began. The temperature then decreased from its maximum value of about 1200 K because virtually no vapor was flowing through the core. Cooler vapor flowed to the upper plenum through the core bypass, reducing the upper plenum structure temperature. The cooling continued until near the end of the calculation, when the vapor flowing through the bypass was hot enough to again cause the structure to heat up. The other structures in the upper plenum remained at or near the saturation temperature throughout the transient.

Figure 10 shows the highest structure-average temperatures of the piping in the pressurizer loop hot leg, surge line, and steam generator tubes. The temperatures of all three structures remained near the saturation temperature throughout the core heatup. None of these structures would be expected to fail before the bottom head of the vessel is breached. These results are typical of calculations that neglect natural circulation flows.

3.2 In-Vessel Circulation

In-vessel natural circulation is simulated with SCDAP/RELAP5 by modeling parallel flow channels in the core and upper plenum, connected radially by crossflow junctions. The crossflow junctions neglect certain momentum flux terms in the momentum equations. Neglect of these terms has been shown to have a second-order effect on calculated results for applications such as natural circulation. A discussion of these terms is included in Appendix C. Three parallel channels were used to model the core and upper plenum. In the following discussions, the center core channel refers to a grouping of 25 fuel assemblies in the center of the core, the outer core channel refers to the 36 fuel assemblies on the core periphery, the middle channel refers to the 96 fuel assemblies located between the center and outer channels, and the inner channels refers to the center and middle channels

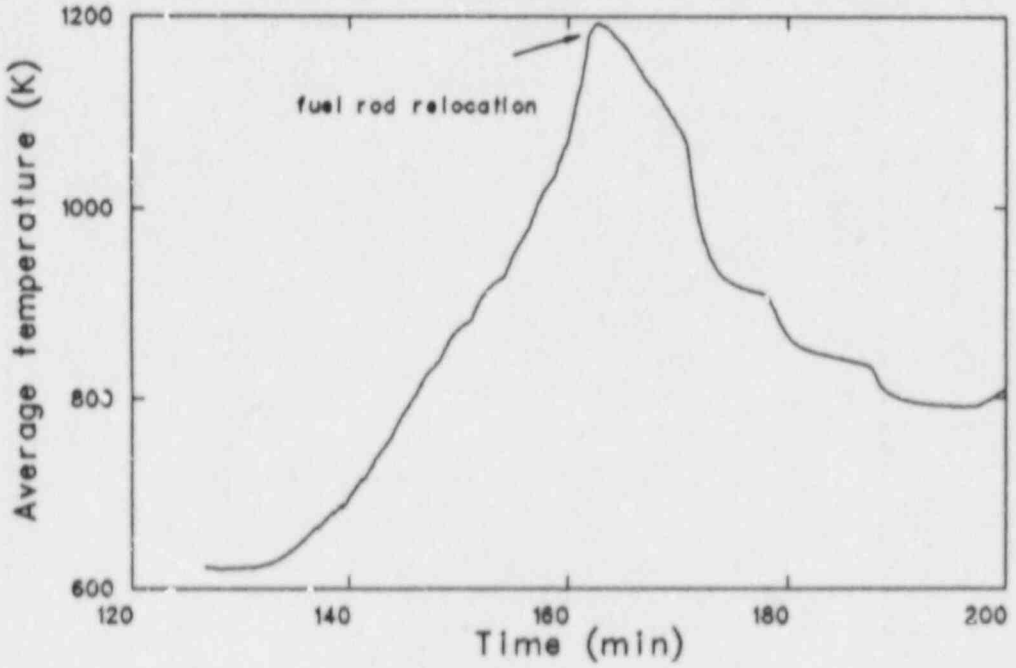

Figure 9. Volume-average temperature of the hottest upper plenum structure for scoping Case 1.

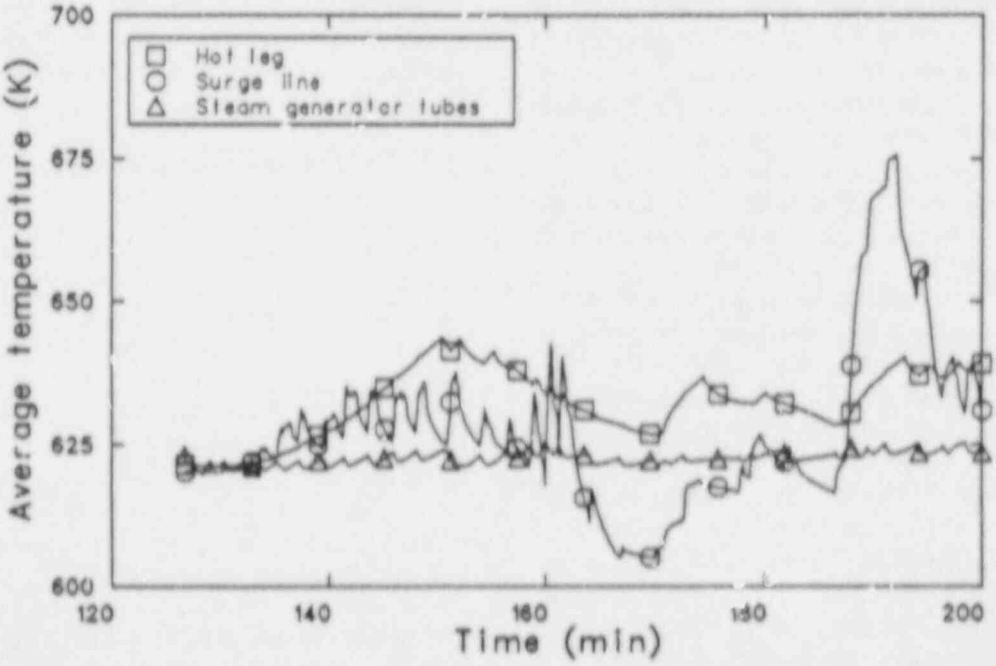

Figure 10. Volume-average temperatures of the hottest part of the hot leg pipe, surge line, and steam generator tubes for scoping Case 1.

together. More detail on the modeling of the channels is presented in Appendix A.

The scoping Case 2 calculation was initiated at about 127 min, shortly before the core began to uncover. The initial conditions for the calculation were taken from the Case 1 calculation at 127 min. The sequence of events, presented in Table 2, was nearly the same with in-vessel natural circulation modeled as without, but the damage progressed at a slower rate. The core heated up at a slower rate because energy was being transferred by the natural convection flow from the core to the structures in the upper plenum. Higher vapor temperatures in the upper plenum also led to heating of the hot leg and surge line piping in the pressurizer loop.

Figure 11 shows the flow velocity vectors in the core and upper plenum at about 167 min, shortly before fuel rod relocation began. There are four circulating flows. There is a flow from the center of the core rising into the upper plenum, where it turns toward the outer part of the plenum before descending back into the core through the peripheral fuel assemblies. A second flow exists in the upper plenum, with vapor recirculating from the periphery of the plenum toward the center, above the top of the core. This flow is not obvious in the figure because the large radial flow areas in the upper plenum result in very low radial velocities. A small amount of vapor flows across the top of the core from the middle to the outer channel because the fuel assembly upper end boxes present a large axial flow resistance at the core exit. The fourth flow recirculates vapor from the upper plenum to the lower plenum through the core bypass region. A maximum velocity of about 1.2 m/s occurs in the upper plenum. Although the velocities are nearly equal, the recirculating mass is higher in the upper plenum than in the core because of the larger flow area. About 15 kg/s is leaving the top of the core in the center and middle channels, and about 10 kg/s is returning to the core through the outer channel. The flow through the bypass is just over 2 kg/s. The flow recirculating in the upper plenum is over 32 kg/s, approximately three times greater than the flow recirculating between the core and upper plenum.

Fuel rod cladding surface temperatures from four elevations in the center (high power) channel are presented in Figure 12. Similar trends to those of scoping Case 1 are present. A top-down dryout of the core led to a heatup of the entire core. The core was completely uncovered by about 157 min. The temperatures increased at a rate of about 0.6 K/s until the temperature reached 1850 K. At that temperature, a change in the calculated oxidation kinetics resulted in a much more rapid rate of cladding oxidation and a more rapid heatup. The temperature then increased quickly to 2500 K, and relocation of molten cladding began at about 167 min at the top of the core. When the molten Zircaloy relocated, no unoxidized material was left in the upper part of the bundle. With no additional heat being generated from the oxidation reaction, the cladding temperatures decreased, eventually increasing again when the vapor flowing past was too hot to remove the decay heat. The cladding temperatures at the top of the core in all three channels are shown in Figure 13. The rates at which the three regions of the core heated up reflected the radial power distribution. The temperature increase from 1850 to 2500 K was slower in the outer channel than in the two inner channels because the oxide shell was thicker. This was the result of the slow heatup, which allowed oxidation to occur for about 17 min longer in the outer channel before the oxidation kinetics changed. The center channel was the first to relocate at approximately 167 min, followed by the middle channel at 171 min and the outer channel at about 173 min. The relocation in the middle and outer channels occurred at lower elevations than those shown in Figure 13. Relocation at the top of the core in these channels did not occur because the cladding was completely oxidized before the temperature reached 2500 K. The decrease in temperature at the bottom of the core at 183 min (seen in Figure 12) was caused by relocation of molten material to the lower plenum. Liquid was boiled by the relocated material, and the resulting steam flow cooled the lower part of the core.

The effects of the in-vessel natural circulation flow on the temperature distribution are evident in Figure 14, which presents the cladding surface temperatures in the outer (low power) channel at the same elevations as presented in Figure 12 for the center channel. Unlike the two inner channels, in which the temperature increased with increasing elevation in the core, the outer channel temperature increased from both the bottom and top of the core toward the middle. The flow returning to the core from the upper plenum was heated as it flowed down, and the flow entering from the bottom of the core was heated as it flowed up, resulting in a maximum cladding temperature just above the middle of the core. The cladding at this elevation relocated at 173 min, shortly after the cladding at the top of the middle channel relocated. This was the only elevation at which cladding relocation occurred in the

Table 2. Sequence of events for scoping Case 2

Event	Time (min)
Transient initiation	0
Calculation begins	126.7
Core heatup begins	129.8
Cladding oxidation begins	146.3
Control rod relocation begins	166.2
Fuel rod cladding balloons	166.7-170.0+
Fuel rod cladding fails	167.0,170.0+
Accelerated oxidation begins	167.2
Fuel rod relocation begins	167.3
Calculation ends	200.0

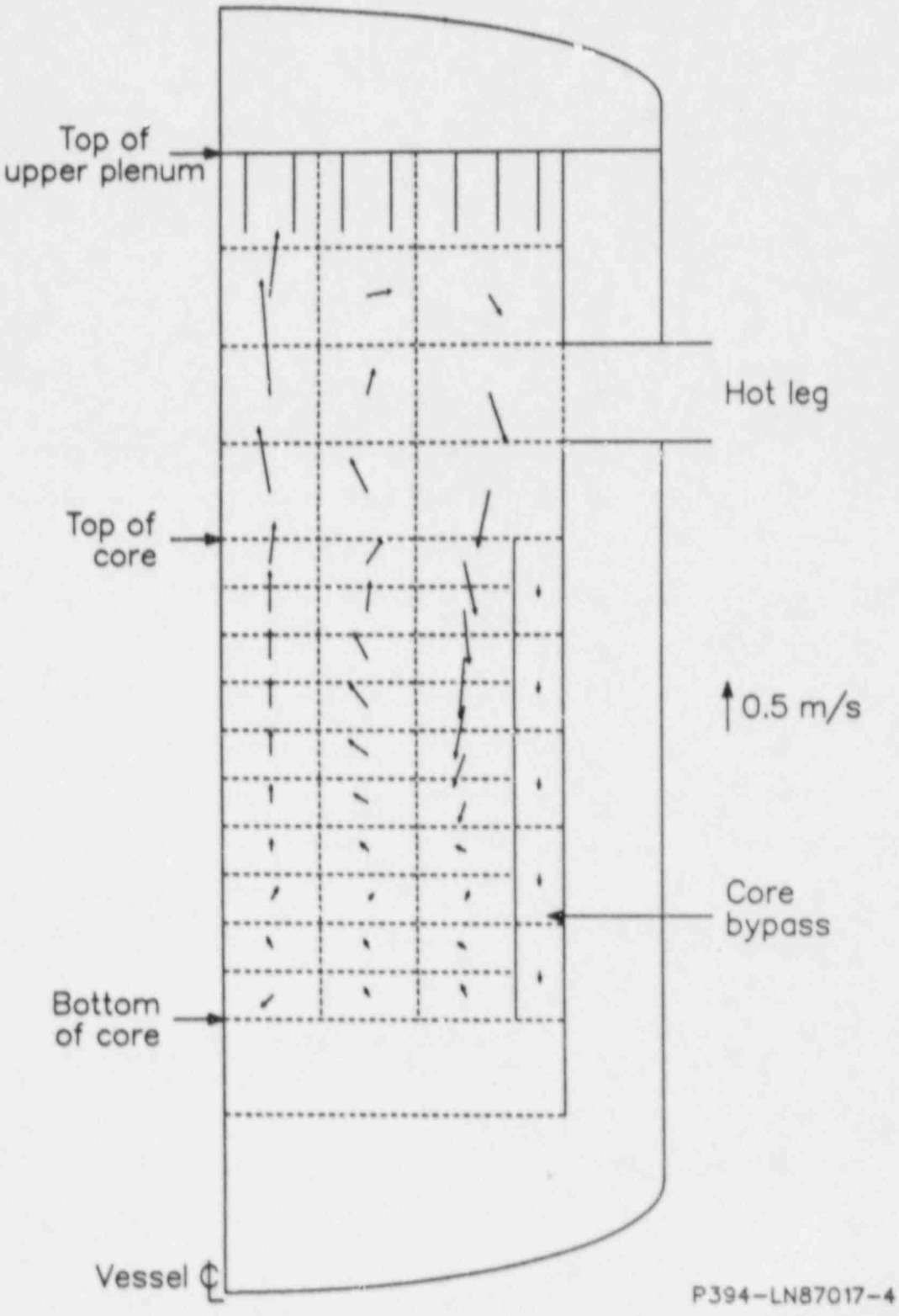

Figure 11. Vapor velocity vectors in the core and upper plenum at 167 min in scoping Case 2.

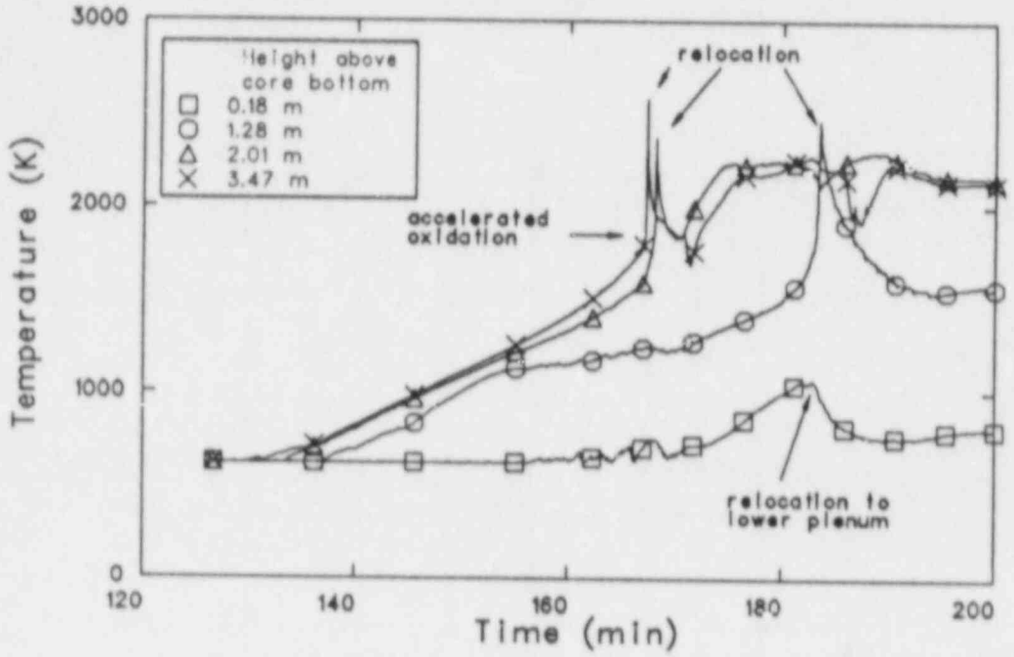

Figure 12. Center channel fuel rod cladding surface temperatures at 0.18, 1.28, 2.01, and 3.47 m above the bottom of the core for scoping Case 2.

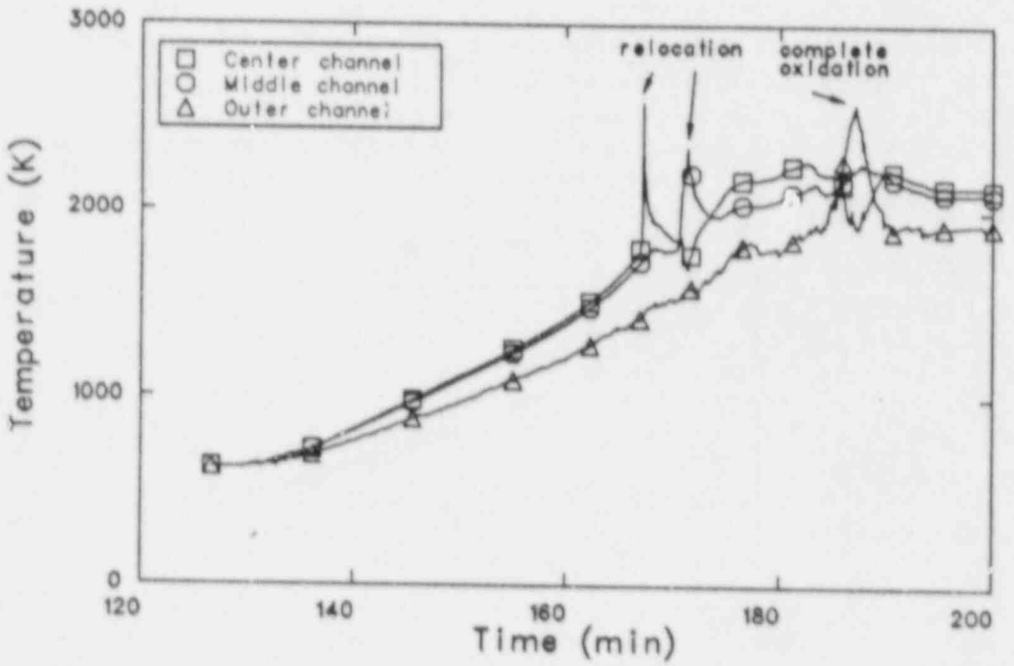

Figure 13. Fuel rod cladding surface temperatures at the top (3.47 m above the core bottom) of the three core channels for scoping Case 2.

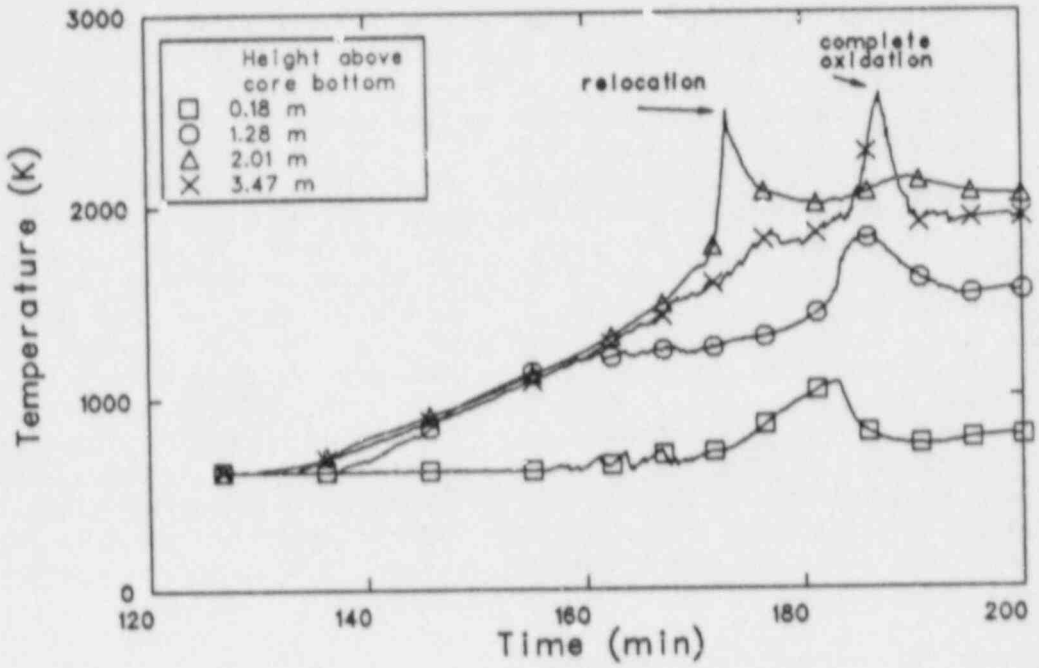

Figure 14. Outer channel fuel rod cladding surface temperatures at 0.18, 1.28, 2.01, and 3.47 m above the bottom of the core for scoping Case 2.

outer channel; the cladding at the other elevations was completely oxidized before the temperature reached 2500 K. This was the result of the lower power in the outer channel, which led to a slower heatup with more time to oxidize the cladding.

Some ballooning of the fuel rod cladding was predicted to occur. The fuel rods in the center channel ballooned and ruptured at about 167 min. The balloon extended over the upper 70% of the fuel rod length, and caused a flow area reduction of about 15%. The ballooning occurred with the cladding temperature varying from 1475 to 1775 K over the length of the affected cladding. The cladding rupture occurred at a temperature of 1481 K. The rupture occurred at this lower temperature because the higher temperature regions of the cladding had been oxidized more. (The cladding at the top of the core had more than twice as much oxide as that in the middle of the core, where the rupture occurred.) Although it was at a higher temperature, the more heavily oxidized cladding was stronger and did not rupture. Similar behavior was observed in the middle channel, in which the fuel rod cladding ballooned and ruptured shortly after 170 min. Again, the balloon extended over the upper 70% of the cladding, with a flow area reduction of about 20%. However, in this case, the ballooned cladding temperature ranged between 1560 and 1800 K, and the rupture occurred at a temperature of 1864 K. Ballooning did not occur in the outer channel because the fuel rods were at a lower average temperature than those in the inner channels, resulting in a lower gap pressure. No changes in the flow patterns were observed as a result of the ballooning because of the relatively small flow blockages.

It is questionable whether cladding ballooning would occur at these elevated temperatures because of interactions between the Zircaloy cladding and the Inconel grid spacers. Zirconium forms eutectics with both iron and nickel that, depending on the composition, melt at various temperatures well below 1800 K.[7] Experiments at KfK have shown pinhole cladding failures at grid spacers, generally by the time the temperature reaches 1500 K.[8,9] If a eutectic is formed, a hole in the cladding may result, allowing the gap and coolant pressures to equalize. With no pressure difference across the cladding, ballooning would not occur. Formation of a cladding/grid spacer eutectic would also be influenced by other factors, such as the heatup rate and the thickness of the oxide shell on the cladding. Time is required for the eutectic composition to

form and fail the cladding. The presence of an oxide shell inhibits the chemical interdiffusion required to form the eutectic composition.

Over 400 kg of hydrogen was generated over the course of the transient, corresponding to oxidation of 57% of the Zircaloy in the core. The maximum hydrogen mole fraction in the core was about 0.80, so that the oxidation reaction was never steam-starved. The top 60% of the fuel rod cladding in the outer channel was completely oxidized at the end of the calculation. Zircaloy had melted and relocated from nodes 4-10 in the center channel and from nodes 4-8 in the middle channel, but only from the sixth axial node in the outer channel. However, fuel liquefaction occurred only in the outer channel, where the cladding did not balloon. Since the cladding did not balloon, the molten Zircaloy on the inside of the cladding was able to make contact with and dissolve some of the fuel pellets. This mixture (52% zirconium, 48% uranium dioxide by mass) then flowed down the fuel rod when the zirconium dioxide shell on the cladding breached. In the inner channels, molten Zircaloy only existed in regions where the cladding had ballooned. The failure of the cladding after ballooning introduced steam to the gap, allowing the Zircaloy on the inside surface of the cladding to oxidize. In the calculation, this inner oxide layer prevented dissolution of the uranium dioxide by the molten Zircaloy.

The highest piping temperatures in the pressurizer loop hot leg, surge line, and steam generator tubes are shown in Figure 15. The temperatures in the other loops were lower than those in the pressurizer loop because the cycling PORVs drew flow from the reactor vessel to the pressurizer. Based on creep rupture considerations, which indicate that structural failure becomes a concern at temperatures above about 1000 K,[10] both the hot leg nozzle and the surge line piping would be candidates for failure. This failure would probably occur before the reactor vessel bottom head fails, and would not be predicted by once-through calculations. However, the steam generator tubes were still near the saturation temperature, so that failure of the tubes would not be expected.

Figure 16 shows the collapsed liquid level in the pressurizer, which illustrates that the liquid did not drain quickly into the hot leg. When the PORVs were open, the vapor velocity through the surge line was high enough to prevent the liquid in the pressurizer from draining into the surge line. The hot fluid also heated the piping. When the PORVs were closed, liquid did begin to drain into the surge line. Heat transfer from the hot surge line piping boiled some of the liquid and cooled the pipe. The liquid did not reach the hot leg before the PORVs opened again, drawing the liquid back into the pressurizer. The liquid was slowly boiled from the pressurizer as the PORVs cycled and as it interacted with the hot vapor entering through the surge line. All of the liquid was gone at about 198 min.

During the time that liquid remained in the pressurizer, it may have helped to scrub fission products from the effluent entering the containment through the PORVs. However, few fission products were released during this part of the transient. The release of fission products began when the cladding first ruptured, at about 167 min in the center channel. At the end of the calculation, less than 4% of the xenon and krypton, 3% of the cesium and iodine, and 5% of the tellurium that was originally in the core had been released from the fuel rods to the coolant.

3.3 Hot Leg Countercurrent Flow

A scoping calculation was performed in which hot leg countercurrent flow was modeled (Case 3). The results of COMMIX analyses[11] were used to guide the modeling of the flow. How this was done is discussed in Appendix A.

As in the Case 2 calculation, conditions gleaned from Case 1 at 127 min were used as initial conditions. The transient calculation began at 127 min as the core began to uncover, and continued until 180 min, shortly after fuel rod relocation had begun. The pressure during this part of the transient was controlled by the pressurizer PORVs, cycling between 15.7 and 16.2 MPa. The core began to heat up at 130 min, and was completely uncovered by 157 min.

Figure 17 presents the mass flow rate in the top of the hot leg in one of the non-pressurizer loops. A fairly steady natural circulation flow was established by about 133 min, and the magnitude decreased slowly as the transient progressed. The flow through the hot leg was interrupted by the opening of the PORVs. When the PORVs opened, vapor was drawn toward the pressurizer surge line from throughout the RCS. This temporarily reduced the flow proceeding from the reactor vessel toward the steam generators, and increased the flow from the steam generators to the vessel in the loops without the pressurizer. In the pressurizer loop, the flow was drawn toward the surge line from both the reactor vessel and the steam generator. The flow through the steam generators was also

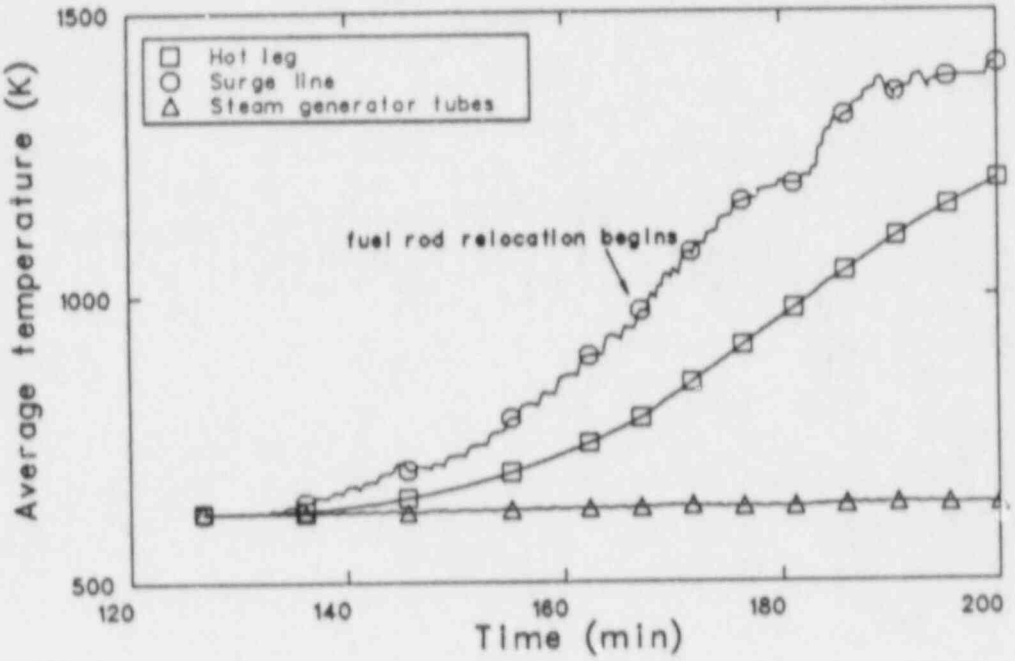

Figure 15. Volume-average temperatures of the hottest part of the hot leg pipe, surge line, and steam generator tubes for scoping Case 2.

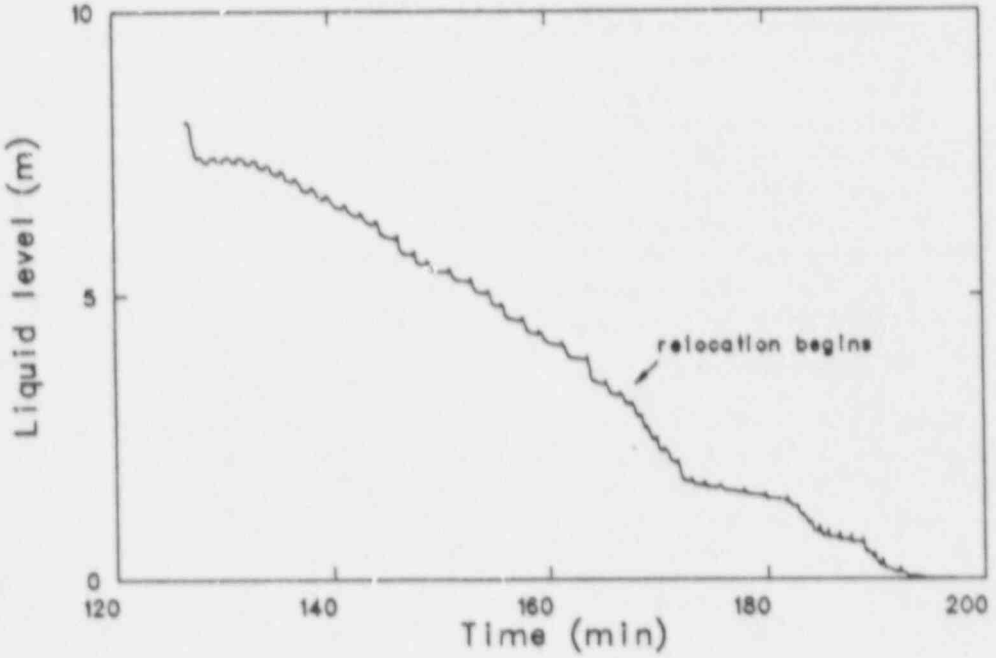

Figure 16. Pressurizer collapsed liquid level for scoping Case 2.

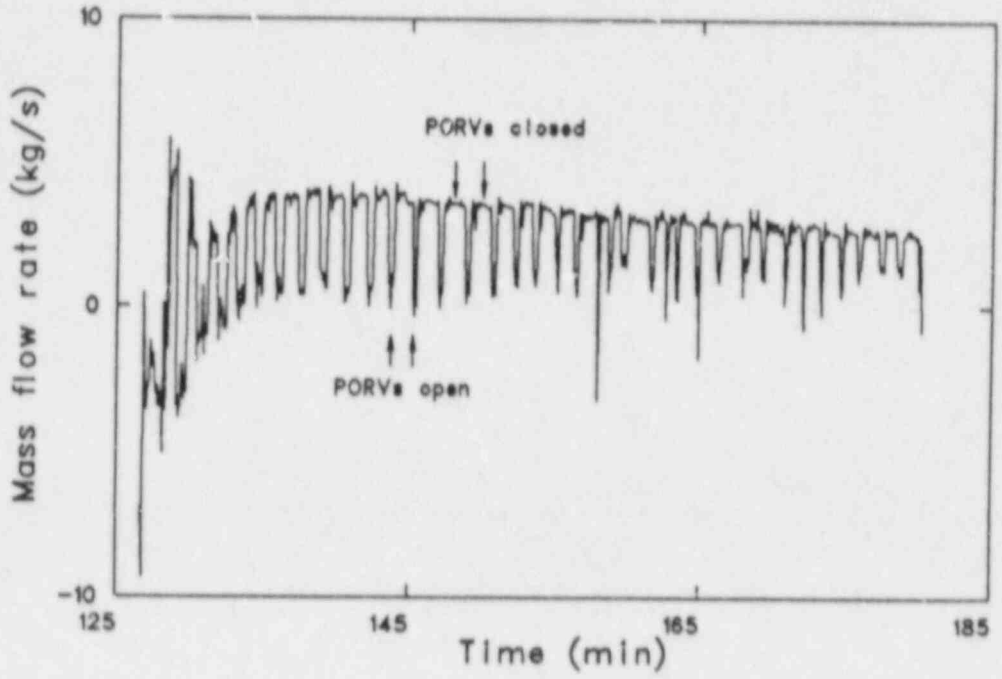

Figure 17. Mass flow rate in the top of a non-pressurizer loop hot leg for scoping Case 3.

affected by the PORV opening, although there was always some flow proceeding from the inlet plenum to the outlet plenum. When the PORVs closed, the natural circulation flows in the hot leg and steam generator tubes were quickly reestablished.

Figure 18 shows the fuel rod cladding surface temperatures at four of the ten axial nodes in the center channel. The temperatures steadily increased from saturation to about 1500 K, when the heatup rate increased as the rate of cladding oxidation increased. When the temperature reached 1850 K, the oxidation kinetics changed, and the temperature increased rapidly to 2500 K. At that point, the cladding oxide shell was assumed to be breached, allowing molten unoxidized Zircaloy to flow from inside the cladding down the outside of the fuel rods; no fuel liquefaction occurred because the cladding had ballooned. The ballooning and rupture allowed the inside surface of the cladding to develop an oxide shell, which prevented molten Zircaloy from coming into contact with and dissolving the fuel. With no further material to oxidize, the heat generation at these elevations decreased, as did the temperature. Relocation began at 178 min in the center channel; no relocation had occurred in the other channels by the end of the calculation. Figure 19 presents cladding temperatures from the highest temperature regions of each of the three core channels. The temperature differences reflected power differences between the three core regions. The maximum temperature in the outer channel was near the center of the core because of the in-vessel natural circulation flow. The vapor was heated by fuel rods as it flowed down the outer core channel.

Oxidation of the Zircaloy cladding began at 148 min. The oxidation rate gradually increased as the temperature increased. When cladding relocation began, nearly 34 kg of hydrogen had been generated. At the end of the calculation, 52 kg had been produced. The oxidation reaction was at no time steam-starved.

During the first part of the heatup, the cladding was collapsed onto the fuel pellets. However, the continued heatup of the fuel rods allowed the gap pressure to increase above the coolant pressure, and the cladding ballooned and ruptured. Ballooning began in the center channel at about 176 min. The balloon extended over the top 70% of the fuel rod length, and caused a flow area reduction of about 60%. The temperature of the cladding in the affected region ranged from 1230 to 1510 K. The cladding ruptured about 1 min after the ballooning occurred, at a temperature of 1567 K. No changes

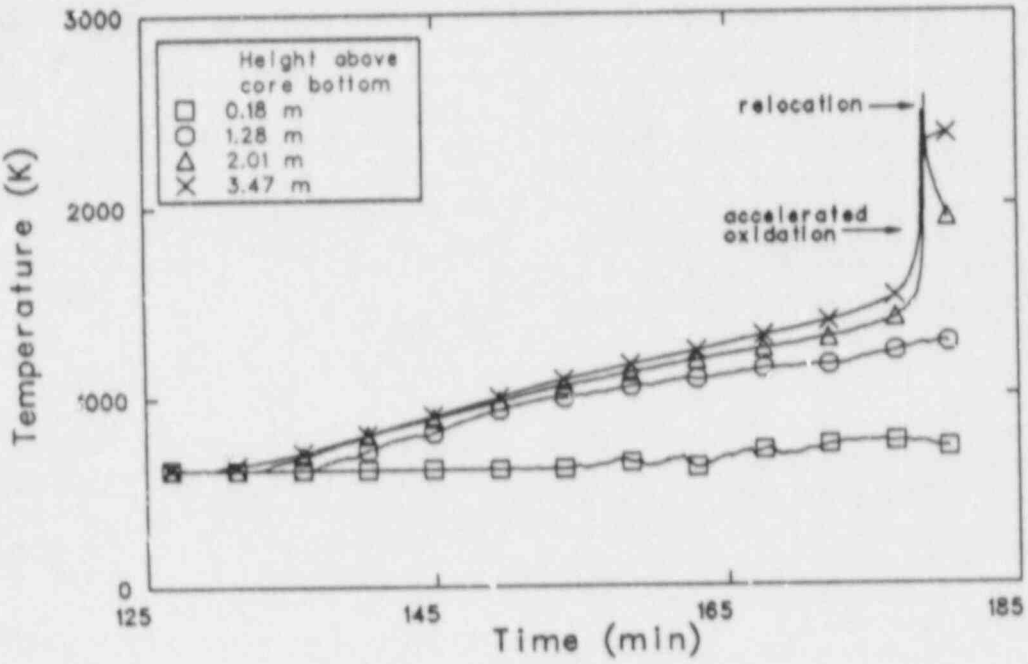

Figure 18. Center channel fuel rod cladding surface temperatures at 0.18, 1.28, 2.01, and 3.47 m above the bottom of the core for scoping Case 3.

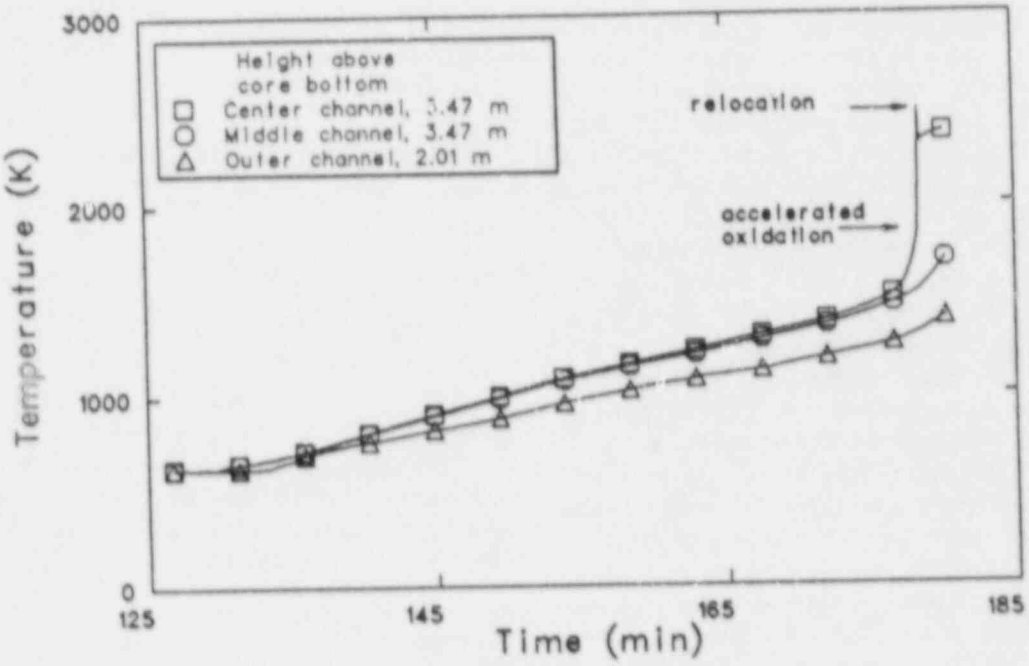

Figure 19. Fuel rod cladding surface temperatures from the three core channels for scoping Case 3.

in the flow patterns in the core were caused by the ballooning, but some of the vapor flowing through the center channel was diverted around the ballooned region.

The cladding rupture also initiated the release of fission products from the fuel rods to the coolant. Because the calculation ended shortly after fuel rod relocation began in the center channel, most of the core was at lower temperatures. The low temperatures resulted in the release of less than 0.3% of the noble gases, cesium, iodine, and tellurium by the end of the calculation.

Approximately 21% of the energy that was removed from the core during the heatup was deposited in the coolant loops along the path of the hot leg natural circulation flow. Of this, 18% was retained in the hot leg piping, 6% was deposited in the steam generator plena, 19% was transferred to the steam generator tube sheets, and 24% was stored in the steam generator tubes. The remaining 33% was transferred through the steam generator tubes to the steam and structures on the secondary side of the steam generators. The pressurizer surge line absorbed 1% of the heat removed from the core.

The effect of this energy transfer on the structure temperatures in the loop is seen in Figure 20, which presents the highest hot leg, surge line, and steam generator tube volume-average temperatures in the pressurized loop. The hot leg temperature decreased from the reactor vessel to the steam generator. The steam generator tube temperature also steadily decreased from the inlet plenum to the outlet plenum along the hot flow tubes, and then from the outlet plenum to the inlet plenum along the cold flow tubes. The surge line temperature increased more rapidly when the PORVs were open because there was more flow, and hence more heat transfer, through the surge line. The oscillations in the steam generator tube temperature were caused by the PORV cycling. When the PORV was open, the flow through the steam generator end of the hot leg reversed. With no source of hotter vapor, the vapor in the steam generator inlet plenum cooled because heat was transferred to the structures in the plenum and because cooler vapor was entering the plenum from the tubes. Thus, the vapor entering the hot flow tubes was cooler, and the tube temperature decreased. As in scoping Case 2, the average temperature of the surge line was higher than that of the other structures in the loop, and was high enough at the end of the calculation that creep rupture failure of the surge line could occur before reactor vessel failure. The presence of the hot leg flow carried hot vapor to the steam generator tubes, causing them to heat up as well. However, the temperature of the tubes was still low enough that they would not be expected to fail. The largest temperature difference between the inside and outside surfaces of the pipe at 180 min was 97 K in the hot leg, 25 K in the surge line, and 0.2 K in the steam generator tubes.

3.4 Loop Flow

Natural circulation flow through the coolant loops was not calculated in the Surry analyses. However, previous analyses of severe accidents in the Bellefonte plant[12] showed that natural circulation through the loops reduced the heatup rate of the core by an order of magnitude, to about 0.06 K/s, because all of the piping in the RCS was available as a heat sink. The pipe temperatures lagged behind the maximum fuel rod cladding temperature by about 100 K. Such high temperatures in the loop structures would cause the RCS pressure boundary to fail long before the fuel rods began to relocate, probably in the steam generator tubes since they are the thinnest structures. Although Bellefonte is a Babcock and Wilcox plant with once-through steam generators, similar results would be expected in a U-tube steam generator plant, such as Surry, should the loop seals clear of liquid.

3.5 Result Comparisons

Results of the Surry natural circulation calculations presented in the previous sections will be compared with one another. This will provide an indication of the effects and importance of modeling the various natural convection flows that may exist during a severe accident. The results of these analyses will then be compared with the Surry station blackout analyses performed for draft NUREG-1150. This comparison will provide some insight into differences in the timing and extent of core damage that result from the models used to analyze the plant behavior.

3.5.1 Effects of Natural Circulation Flows. The inclusion of the various natural circulation flows into the model used to calculate the TMLB' transient did not affect the events that occurred up to the early part of core relocation. Rather, these

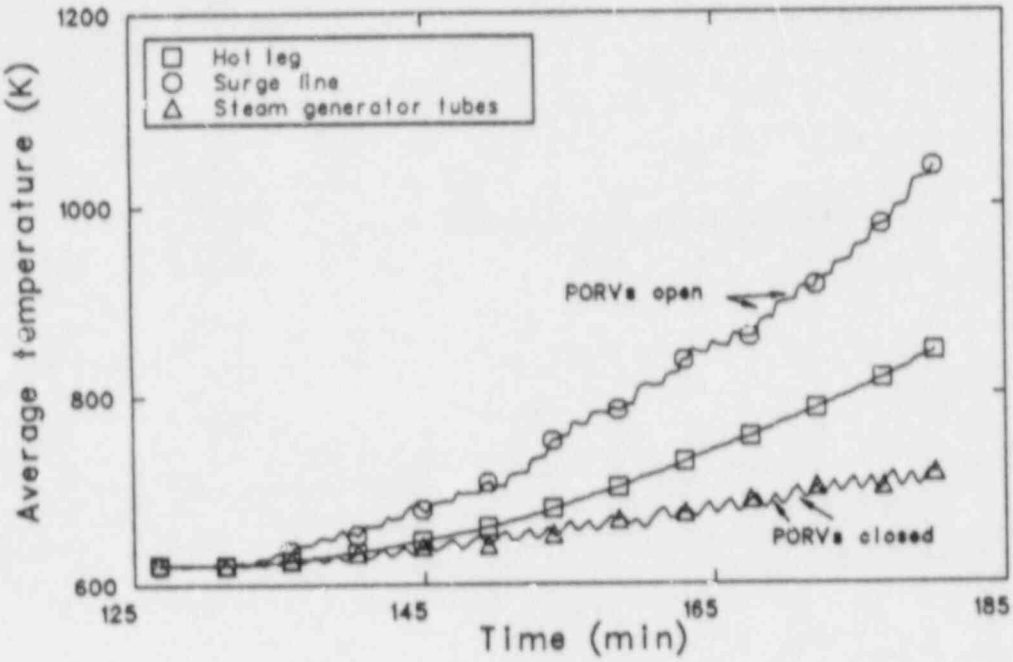

Figure 20. Volume-average temperatures of the hottest part of the hot leg pipe, surge line, and steam generator tubes for scoping Case 3.

flows served to extend the transient by removing energy from the core and transferring it to other parts of the reactor coolant system. The ultimate effect of these flows on the plant behavior cannot be completely evaluated until the transient proceeds to failure of the reactor vessel bottom head. At that time, differences in RCS pressure, melt composition, and fission product distribution will affect the containment response and ultimately the source term resulting from the transient.

The most significant effect of the natural circulation flows was the heating of ex-vessel structures, which was not seen in the once-through calculation. The heating was sufficient so that failure of the RCS boundary would occur before the vessel is breached, probably in the surge line. Such a failure may allow the RCS to depressurize before the vessel fails, perhaps sufficiently to significantly change the containment load at the time of melt ejection. The higher piping temperatures will also affect the fission product behavior in the RCS.

Table 3 lists the sequence of major events for the three scoping calculations. Since the addition of natural circulation flows extended the core heatup, a comparison of the three analyses at a specific time is not very meaningful. However, it is meaningful to examine the state of the plant at the time a specific event occurs. The latest common event in the three analyses was the beginning of fuel rod relocation.

Table 4 presents several major parameters that describe the state of the Surry plant at the time fuel rod relocation began in the three scoping calculations. Fuel rod relocation began in the scoping calculations when the cladding in one of the ten axial nodes reached a temperature of 2500 K.

Although they had been exposed to superheated vapor for a longer time, the hot leg and surge line temperatures were only slightly higher when fuel rod relocation began in the hot leg natural circulation case than with only in-vessel circulation modeled. Although more energy was transferred out of the core, the participation of both the steam generators and all three coolant loops (rather than just the pressurizer loop) as heat sinks resulted in a more even distribution of the energy throughout the RCS.

The temperature difference between the center and middle channels caused by the different average power was accentuated by the natural convection flows. The cooling provided by the coolant loops in Case 3 reduced the temperatures of both

Table 3. Sequence of events for the scoping calculations

Event	Time (min)		
	Case 1	Case 2	Case 3
Transient initiation	0	0	0
Calculation begins	0	126.7	126.7
PORV cycling begins	71.8	—	—
Steam generators dry	75.4-77.2	—	—
Hot legs reach saturation	100.6	—	—
Loop natural circulation flow ends	109.7	—	—
Core heatup begins	129.6	129.8	129.6
Cladding oxidation begins	144.1	146.3	148.0
Control rod relocation begins	157.2	166.2	178.2
Fuel rod cladding balloons	—	166.7-170.0+	176.4
Fuel rod cladding fails	—	167.0,170.0+	177.3
Accelerated oxidation begins	157.9	167.2	178.0
Fuel rod relocation begins	160.5	167.3	178.3
Calculation ends	200.0	200.0	180.0

Table 4. Conditions when fuel rod relocation began in the three scoping calculations

Parameter	Case 1	Case 2	Case 3
Time (min)	160.5	167.3	178.3
Hydrogen generated (kg)	96.9	47.2	33.7
Maximum middle channel fuel cladding temperature (K)	—	1747	1546
Maximum upper plenum structure temperature (K)	1100	1748	1153
Hot leg nozzle temperature (K)	633	789	829
Maximum surge line temperature (K)	637	973	1001
Maximum steam generator tube temperature (K)	624	629	731
Reactor vessel liquid level (m)	3.26	2.59	2.11
Pressurizer liquid level (m)	4.03	3.07	1.99
Core outlet flow (kg/s)	1.2	10	11
Core return flow (kg/s)	—	8	8
Upper plenum recirculating flow (kg/s)	—	38	49

the core and upper plenum structures compared to Case 2. When fuel rod relocation began in the center channel, the maximum cladding temperature in the middle channel was 1747 K in Case 2, and 1546 K in Case 3. Similarly, the hottest upper plenum structure was 100 K cooler with the hot leg countercurrent flow considered. The lower cladding temperatures also resulted in less hydrogen having been generated when relocation began.

The amount of hydrogen generated when fuel rod relocation began was about 97 kg in Case 1, 47 kg in Case 2, and 34 kg in Case 3. This comparison must be viewed with the understanding that different amounts of material are at high temperature when relocation begins. In Case 1, the once-through calculation, all of the fuel rods in the core are affected. In the other two cases, fuel rod relocation begins in the 25 fuel assemblies in the center core channel, with an accordingly smaller amount of material being relocated, and most of the core still undergoing oxidation.

The core damage was affected by the behavior of the fuel rod cladding. In Case 1, no ballooning occurred, and the molten Zircaloy was able to dissolve some of the fuel pellets. Ballooning did not occur because the axial average temperature of the fuel rods was low enough that the gap pressure never exceeded the coolant pressure (the bottom of the core was still submerged in liquid when the top of the core was relocating). With in-vessel natural circulation modeled (Cases 2 and 3), sausage-type ballooning occurred in the higher powered regions of the core. With an oxide shell on the inner surface of the cladding, no contact was made between the fuel pellets and the molten Zircaloy in the cladding. Thus, no dissolution of the fuel occurred and only Zircaloy relocated in the inner core channels.

Reactor vessel collapsed liquid levels from the three cases are presented in Figure 21. The liquid level decreased more rapidly with in-vessel natural circulation modeled because vapor was being recirculated to the lower parts of the core and lower plenum, accelerating the boiling of the liquid that was there. The liquid level in the once-through calculation eventually decreased to the level of the other two calculations as molten core material

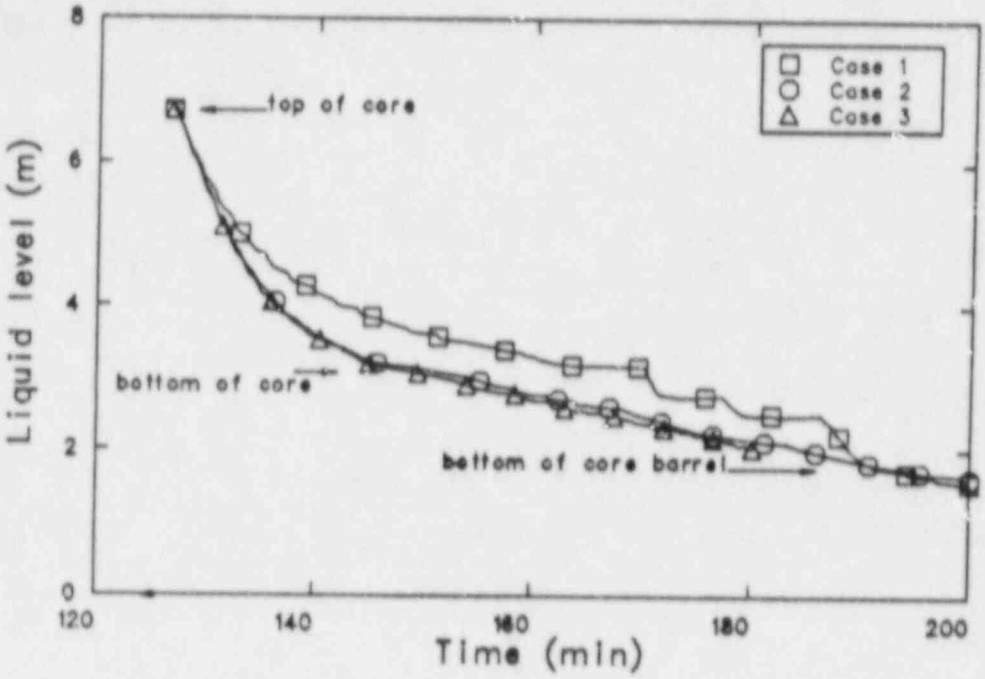

Figure 21. Reactor vessel collapsed liquid level for the three scoping cases.

relocated to the lower plenum, where it boiled the remaining liquid.

The pressurizer collapsed liquid level from the three calculations is shown in Figure 22. More liquid was retained in the pressurizer in Case 1 because the vapor flowing out the surge line was near the saturation temperature throughout the transient. In contrast, the amount of liquid decreased more rapidly with the natural circulation flows modeled because superheated vapor was flowing into the pressurizer, where it could transfer heat to the remaining liquid. Also, the heating of the surge line pipe by the superheated vapor allowed it to transfer heat to the liquid that drained from the pressurizer when the PORVs were closed, again increasing the amount of liquid that was boiled.

3.5.2 Comparisons with Draft NUREG-1150. Surry was one of the reference plants investigated in the "Reactor Risk Reference Document," NUREG-1150 (Draft). Natural circulation in the RCS was not explicitly considered in the thermal-hydraulic analyses performed for NUREG-1150. Therefore, it is of interest to examine differences in event timing and core damage caused by the natural circulation flows.

Table 5 presents the sequence of events for the draft NUREG-1150 analysis (obtained from Reference 13), the three scoping calculations presented earlier, and a MELPROG calculation.[14] The table shows that the transient was extended both by the inclusion of the natural circulation flows and by the more detailed modeling provided by the SCDAP/RELAP5 and MELPROG codes. Scoping Case 1 was similar to the MARCH calculation used in draft NUREG-1150 in the hydraulic treatment of the core. Yet the SCDAP/RELAP5 calculation reached the temperature at which fuel rod relocation began over 5 min after the bottom head failed in the MARCH calculation. While part of this difference can be attributed to a difference in decay power, which led to an earlier steam generator dryout, some is also attributable to the manner in which the codes treat the system behavior. The SCDAP/RELAP5 and MELPROG event timings were similar.

This lengthening of the transient could lead to very different conditions at the time of vessel failure. By heating the pipes in the coolant loops, failure of the RCS is likely to occur before the core melts through the reactor vessel. The resulting depressurization may be sufficient to reduce the impact of direct containment heating on the

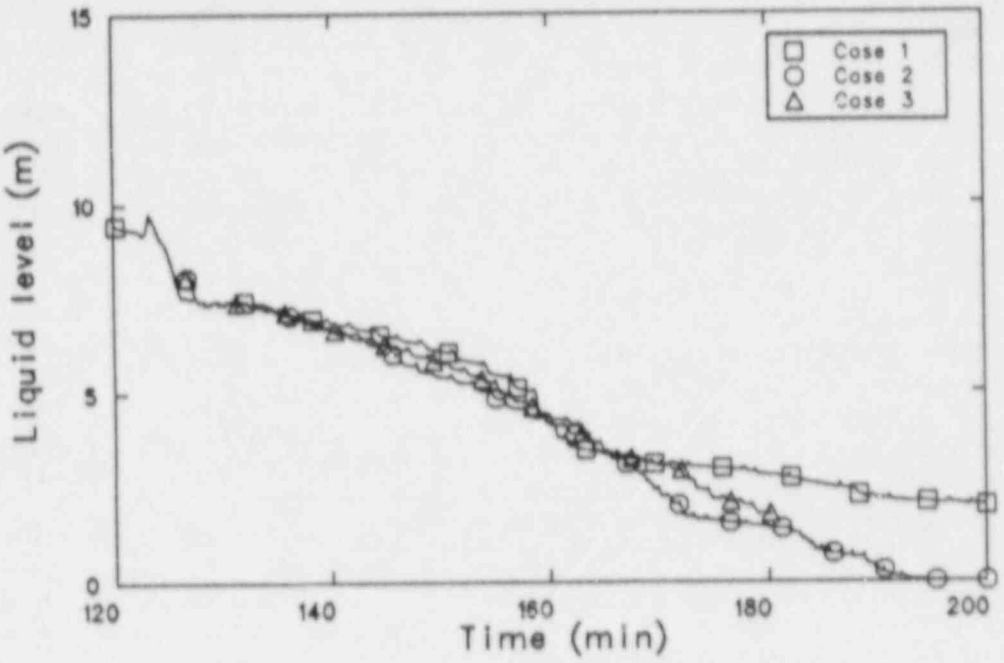

Figure 22. Pressurizer collapsed liquid level for the three scoping cases.

Table 5. Sequence of events for the Surry TMLB' transient from five different calculations

	Time (min)				
	MARCH	SCDAP/RELAP5			MELPROG
Event	Draft NUREG-1150	Once-Through	In-Vessel	Hot Leg and In-Vessel	NUREG/CR-4742
Steam generators dry	69.0	77.2	77.2	77.2	69.5
Core heatup began	97.2	129.6	129.8	129.6	117.8
Fuel rod relocation began[a]	118.5	160.5	167.3	178.3	169.7
Core slumped[b]	143.5	>200.0	>200.0	>180.0	248.0
Bottom head failed	155.3	>200.0	>200.0[c]	>180.0[c]	265.5

a. Fuel rod relocation corresponded to the fuel rod melting temperature of 2550 K in the draft NUREG-1150 calculation, to the cladding oxide shell breach temperature of 2500 K in the SCDAP/RELAP5 calculations, and to 2200 K in the MELPROG calculation.

b. Core slumping occurred when the bottom node in a region relocated or when the debris crust failed.

c. Failure outside the vessel is likely to occur before the bottom head failure.

containment response. The longer time before vessel failure may also allow more oxidation of the material in the reactor vessel. Additional oxidation in the vessel could affect the containment behavior through the core/concrete interaction. If less unoxidized material is involved in the interaction, less hydrogen may be generated in containment after vessel failure and fewer fission products may be released.

Another difference in the calculations is the amount of hydrogen produced. At the time of fuel rod relocation, the MARCH calculation predicted that 5% of the cladding would have been oxidized. When fuel rod relocation began in the center channel in the SCDAP/RELAP5 calculations, 14% of the cladding was oxidized in the once-through case, 7% was oxidized with in-vessel natural circulation modeled, and 5% was oxidized with both hot leg and in-vessel natural circulation modeled.

3.6 Uncertainties and Limitations

This section describes some of the uncertainties associated with the analyses presented in previous sections, and some of the limitations of the models and codes used in the analyses. Areas for future analysis are also discussed. Some of the uncertainties are addressed by the sensitivity studies described in the next chapter.

Because the flow in the coolant loops is modeled in a one-dimensional manner, the countercurrent hot leg flow is not strictly mechanistically treated. This introduces an uncertainty into the results, because the model was developed to reflect the behavior during a similar transient calculated by the COMMIX computer code. Differences in the flows and heat transfer rates predicted by the two codes dictate that the results will not be identical; one can only match the results of the COMMIX calculations as best as possible. The resulting heatup is believed to be close to that which would actually occur, but the distribution of the energy in the coolant loops may be somewhat different. The results under these conditions are also dependent on the applicability of the modeling used to simulate low pressure, low temperature experiment data to the high pressure, high temperature conditions of the transient being investigated. The sensitivity analyses investigate effects of hot leg flow rates on the plant transient response.

With the hot leg flows physically separated in the model, the piping temperature difference between the top and bottom halves is too large. Circumferential conduction would transfer heat from the top of the pipe to the bottom. By increasing the temperature of the pipe wall along the bottom of the pipe, the vapor flowing past may also increase in temperature, thus reducing the temperature difference between the hot and cold flow streams and reducing the natural circulation flow rate. This temperature variation around the pipe may also introduce stresses in the pipe that would accelerate its failure. The physical separation of the opposing flows also precludes accounting for any interactions that may occur between the flows, such as heat and mass transfer.

The pipe temperatures are also affected by the boundary conditions imposed on the outer surface. In these calculations, the surfaces exposed to the containment atmosphere were assumed to be adiabatic. In reality, there would be some heat loss through the pipes to the containment atmosphere. The heat loss would increase as the pipe temperature increased because the insulation may begin to break down, allowing a higher heat transfer rate, and because the temperature difference between the pipe surface and the containment is increasing. While the temperatures of the surge line and hot leg would be lower than those calculated, it is expected that the relative temperatures would remain the same. That is, the surge line would be hotter than the hot leg, which would be hotter than the steam generator tubes. The lower pipe temperatures would also allow more heat to be removed in the coolant loops by the hot leg countercurrent flow, extending the time to various stages of core damage even further. Heat loss from the hot legs and surge line is addressed in the sensitivity analyses.

The amount of hydrogen generated is also an area of uncertainty. The SCDAP/RELAP5 code does not calculate the oxidation of Zircaloy that is relocating. Nor does the code calculate the oxidation of structures outside the core, such as the steel structures in the upper plenum that are certainly hot enough to oxidize in the presence of steam.

The ballooning that occurred in Case 2 may not occur in the plant because of interactions between the Zircaloy cladding and the Inconel grid spacers. These materials form eutectics such that the cladding may be breached at temperatures below

1500 K. Since the ballooning in the calculation did not occur until some of the cladding had reached nearly 1800 K, it is likely that the cladding would have breached before then. That would allow the coolant and gap pressures to equalize, and thereby preclude ballooning. This may also be true for Case 3, in which the cladding temperatures were above 1500 K when failure occurred.

Another area of the code in which improved modeling is needed is in the cladding breach model. Currently, the user inputs a temperature at which the zirconium dioxide shell on the cladding breaches, initiating the flow of molten material from inside the fuel rod. A more realistic model would account for failure of the oxide shell by dissolution of the oxide phase by the molten Zircaloy on the inside of the cladding. This would allow a more accurate prediction of the timing and physical content of the relocation.

The formation of a cohesive debris in the once-through calculation had a significant impact on the transient progression. With very little steam flowing through the core, the heatup of the top of the core stopped, and oxidation throughout the core nearly ceased. Flow through the core bypass cooled the upper part of the core. While a cohesive debris that blocked the entire core would not be expected in an actual transient, it does demonstrate the drawbacks of using a single channel to model the entire core.

The transport of fission products was not included in these analyses. Consequently, the heating of the structures in the RCS by deposited fission products was not accounted for. However, the amount of fission products released during the calculations was generally small enough that there would be little effect on the structure temperatures. The physical separation of the opposing flows in the hot legs may affect the fission product transport. If a significant portion of the deposition in the hot leg is the result of gravitational settling, then the fission products would drop into the flow stream returning toward the reactor vessel, where they may be retained on the cooler piping in contact with the cooler flow stream.

The "bottom line" of the natural circulation analyses is how these flows affect the condition of the core and RCS at the time of reactor vessel lower head failure. To that end, the location, size, and timing of any RCS failure before the vessel failure needs to be determined. The surge line or hot leg appears to be the likely location, but the actual time at which failure occurs and the size of the hole are still unknown. The size is important in that a large enough break may permanently disrupt the natural circulation flows. The size of the failure may also be dynamic, in that continued heating of other parts of the RCS may result in additional failures or the hot vapor flowing through the original failure location may ablate the pipe and increase the size of the hole. By diverting flow from other parts of the RCS, those locations may cool, increasing the retention of fission products. Finally, the depressurization resulting from the failure needs to be calculated to determine the pressure of the RCS when the vessel fails, in order to determine the importance of direct containment heating on the containment response.

4. SENSITIVITY ANALYSES

A series of sensitivity calculations was performed to further investigate the effects of multidimensional natural circulation flows on the response of the plant. In each of these calculations, both in-vessel and hot leg natural circulation flows were modeled. These sensitivity calculations addressed uncertainties in the modeling of the Surry reactor coolant system and within the SCDAP/RELAP5 code itself, including some uncertainties identified in the scoping analyses.

Several changes in the code and input model were made from the version used for the scoping analyses. The decay power was reduced by about 9%. The axial power profile used was flatter. Interactions between the Inconel grid spacers and Zircaloy cladding were simulated, so that the cladding failure was based on either strain or temperature. The surge line model was also changed, so that it connected to both the top and bottom halves of the hot leg piping. These changes are discussed in more detail in Appendices A and B. The impact of these changes is that the results of the sensitivity analyses cannot be compared directly with the results of the scoping calculations.

The nine sensitivity calculations presented in the following sections are shown in Table 6. The case numbers will be used in most of the discussions for simplicity and clarity. Following these sensitivity calculations, a final case will be presented in which Case 1 was continued with failure of the surge line piping modeled.

As was the case with the scoping calculations, each of the sensitivity calculations began as the core began to uncover and heat up (at 160 min), and continued until shortly after the RCS pressure boundary failed. The conditions at this time were taken from a calculation of the plant response from transient initiation into the core heatup using a model without in-vessel or hot leg natural circulation flows. Table 7 presents the sequence of events for this early part of the transient. For comparison, the event timings from the scoping calculation are also presented. The difference in timing was caused by the use of a lower decay power in the sensitivity calculations. The two calculations were consistent in that the core uncovering began in both cases when the same amount of energy had been generated in the core. The RCS pressure throughout the transients cycled between the PORV open and close setpoints of 16.2 and 15.7 MPa, respectively. The secondary sides of the steam generators contained superheated steam, with the pressures varying between the relief valve setpoints of 7.24 and 6.89 MPa.

4.1 Base Case

The first calculation used best-estimate values for the steam generator inlet plenum mixing, and the core and upper plenum crossflow resistances. These values were the same as those used in the scoping calculation with both in-vessel and hot leg natural circulation flows modeled (Case 3). An end-of-life power profile was modeled, and the heat structures in contact with the containment atmosphere were adiabatic. This calculation is referred to as the base case.

Table 8 contains the sequence of events for the base case. The calculation began at 160 min, when the core heatup was just beginning. As the heatup continued, the cladding reached 1000 K, the temperature at which SCDAP/RELAP5 begins to calculate oxidation of the Zircaloy cladding. This occurred about 5 min before the core completely dried out. Eutectic formation between the Zircaloy cladding and Inconel grid spacers caused failure of the fuel rod cladding in all three channels when the temperature exceeded 1470 K; no ballooning was calculated to occur. Creep rupture of the pressurizer surge line occurred at 246.3 min, shortly before the onset of fuel rod relocation. The calculation was terminated at 250 min, since the RCS failure time and location had been established for comparison with the sensitivity calculations to follow.

The collapsed liquid level in the reactor vessel is presented in Figure 23. The level decreased below the bottom of the core at about 186 min, and below the bottom of the core barrel at about 228 min. At the end of the calculation, the level was within the lower head. The only other liquid in the RCS was in the three loop seals, which did not clear during the transient.

Figure 24 presents the peak cladding temperature in the core. The initial heatup rate of about 0.27 K/s decreased to 0.20 K/s at about 187 min. At that time, the core bypass cleared of liquid, allowing steam to flow from the upper plenum to the lower plenum. This increased the core inlet flow, reducing the core heatup rate. The peak temperature increased steadily until the oxidation kinetics changed at about 245 min, when the peak

Table 6. Matrix of sensitivity calculations

Parameter	Sensitivity Calculation Case Number								
	1	2	3	4	5	6	7	8	9
Axial power profile									
End-of-life	X		X	X	X	X	X	X	X
Beginning-of-life		X							
Inlet plenum mixing									
Best-estimate	X	X			X	X	X	X	X
Reduced			X						
None				X					
Piping heat loss									
None	X	X	X	X			X	X	X
Convection					X	X			
Radiation						X			
Upper plenum crossflow resistance									
Best-estimate	X	X	X	X	X	X		X	
Decreased							X		
Increased									X
Core crossflow resistance									
Best-estimate	X	X	X	X	X	X	X		
Decreased								X	
Increased									X

Table 7. Sequence of events up to core heatup for the sensitivity and scoping calculations

Event	Time (min)	
	Sensitivity	Scoping
Transient initiation	0	0
PORV cycling begins	82.9	71.8
Steam generators dry	85.4-90.2	75.4-77.2
Hot legs reach saturation	120.9	100.6
Loop natural circulation flow ends	129.9	109.7
Core heatup begins	159.8	129.6

Table 8. Sequence of events for the base case

Event	Time (min)
Calculation begins	160.0
Center channel oxidation begins	185.3
Middle channel oxidation begins	186.1
Two-phase liquid level below core	190.2
Outer channel oxidation begins	192.6
Center channel fuel rod cladding fails	223.4
Pressurizer empties of liquid	224.8
Middle channel fuel rod cladding fails	225.3
Outer channel fuel rod cladding fails	241.3
Pressurizer surge line fails	246.3
Center channel fuel rod relocation begins	248.0
Middle channel fuel rod relocation begins	248.8
Outer channel fuel rod relocation begins	—
Calculation ends	250.0

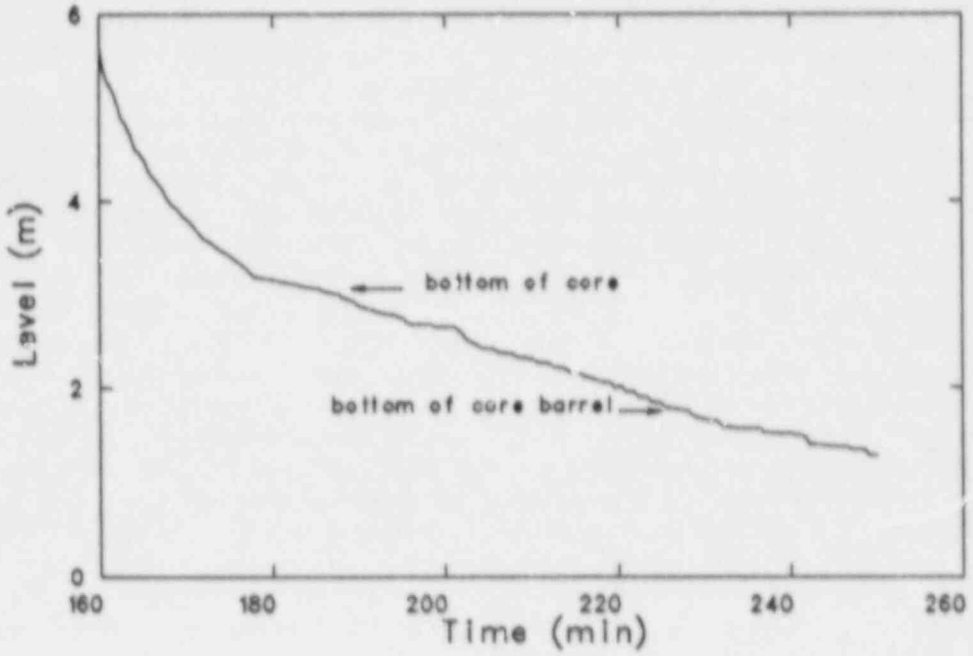

Figure 23. Reactor vessel collapsed liquid level for sensitivity Case 1.

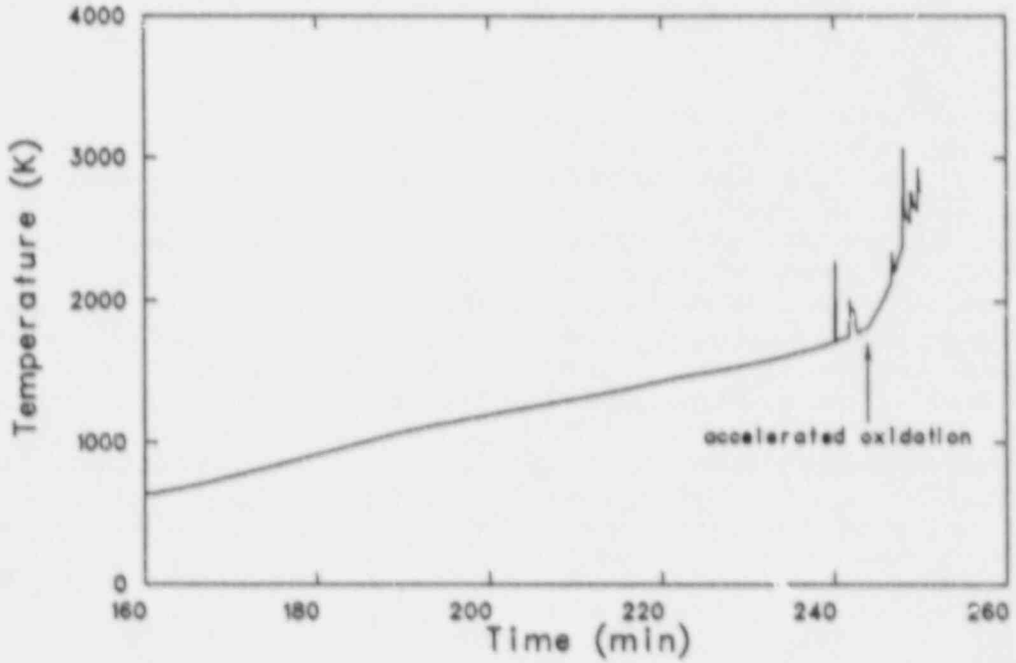

Figure 24. Peak cladding temperature for sensitivity Case 1.

cladding temperature increased rapidly. The short temperature excursions just prior to this time reflected the calculated behavior of the control rod guide tubes. The later temperature excursions showed the behavior of individual nodes in the core. The temperature increased as the cladding rapidly oxidized. The temperature then decreased when the cladding in a node was completely oxidized, because the decay heat alone was unable to sustain the higher temperature.

Fuel rod cladding surface temperatures from the top node in each of the three core channels are presented in Figure 25. The center and middle channel temperatures were very close together throughout the transient. The outer channel temperature was lower because it had a lower power and because steam reentering the outer channel from the upper plenum helped to cool the fuel rods. However, after accelerated oxidation began in the inner two channels, the hot vapor from the upper plenum helped to accelerate the temperature increase in the outer channel. That is why there was a rapid heatup in the outer channel prior to the change in oxidation kinetics, beginning at a temperature of about 1500 K. The heatup rate increased further as the temperature increased and accelerated oxidation occurred.

Figure 26 shows the center channel fuel rod cladding surface temperatures at several elevations. Changes in the core inlet conditions generally had a greater impact on the lower half of the fuel rod. As discussed previously, the core bypass cleared of liquid at about 187 min, and the increased flow into the core cooled the cladding in the lower part of the core while slowing the heatup rate in the top part. An increase in the center channel inlet flow shortly after 200 min resulted in more cooling of the bottom part of the core. At about 218 min, the downcomer liquid level dropped below the core barrel, allowing cooler vapor to flow into the core, again cooling the lower regions of the core. With the core barrel cleared, a flow path was established from the upper head to the downcomer into the core. Relocation of control rod absorber material to the lower plenum began at about 240 min. This material boiled liquid in the lower plenum, which resulted in some cooling in the lower elevations of the core. After the accelerated oxidation, the temperature of the cladding in the top node peaked and then decreased. The decrease occurred because the cladding was completely oxidized, so that the only heat generation in that node was the decay heat in the fuel. Without the exothermic Zircaloy oxidation reaction, there was not enough heat being generated to keep the temperature near the melting point of zirconium dioxide (2973 K) or uranium dioxide (3013 K).

Because the calculation was terminated shortly after temperatures exceeded 2000 K, the core damage was primarily in the form of Zircaloy oxidation, with some material relocation. Figure 27 shows the total hydrogen generation rate during the transient. The oxidation increased steadily until parts of the cladding became completely oxidized and the rate decreased. At its peak, the energy released by the oxidation reaction was about 6 times the decay power. At the end of the calculation (250 min), 222 kg of hydrogen had been generated, corresponding to oxidation of about 32% of the Zircaloy in the core. Material relocation was essentially confined to the control rods, as only about 0.03 kg of fuel melted in the core and there was no relocation of Zircaloy from the fuel rods. The upper 60% of the control rods in the center and middle channels relocated, with all of the Zircaloy and stainless steel and 25% of the relocated Ag-In-Cd control material refreezing in the core. The remaining 75% of the relocated absorber dropped into the lower plenum. In the outer channel, the top 50% of the control rods relocated, with 70% of the relocated absorber being the only material to drop below the core. The calculation was terminated before the outer channel fuel rod temperatures were high enough to initiate relocation. Fission product release during the transient was also relatively minor, with 4% of the noble gases, 3% of the cesium and tellurium, and 2% of the iodine originally in the core being released by the end of the calculation.

Figure 28 shows the flow entering the upper plenum from each of the three core channels and from the core bypass, and the upper plenum recirculating flow. The recirculating flow moves down the outer channel of the upper plenum and turns inward just above the core exit rather than entering the core. The flow in the upper plenum was about four times greater than the flow returning to the core through most of the transient. The increase in the flow from the upper plenum to the core bypass at about 187 min occurred when the liquid level cleared the core bypass, allowing vapor to flow freely from the upper plenum to the lower plenum. A slight decrease in the flow reentering the outer channel from the upper plenum can also be observed at that time. The relation between the upper plenum recirculating flow and the upper plenum vapor temperature just above the center core channel is shown in Figure 29. The flow decreased with increasing temperature because the density difference driving the flow was decreasing.

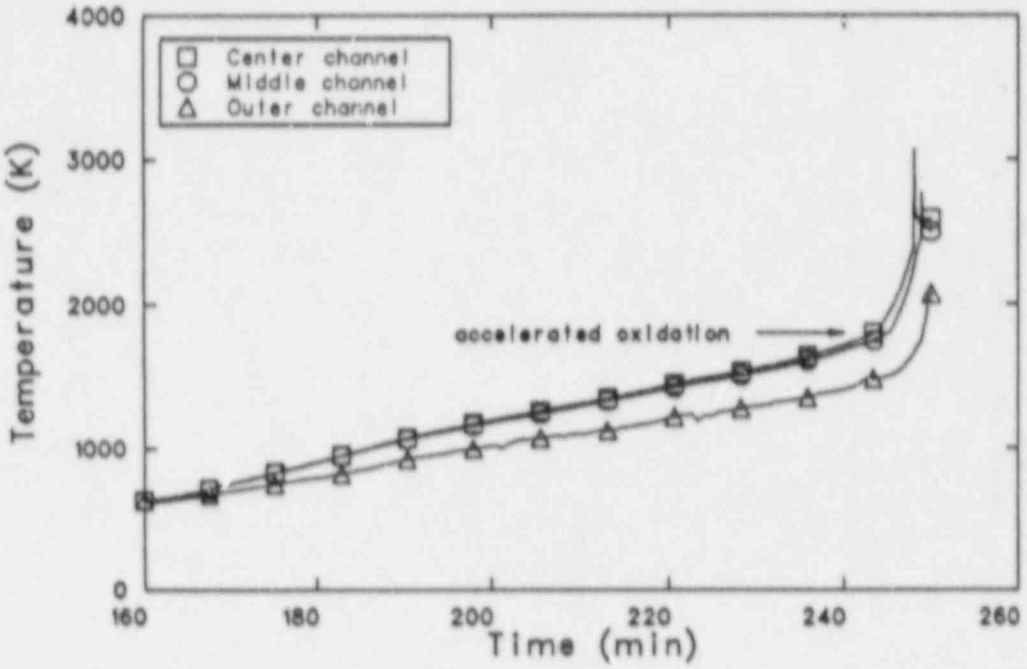

Figure 25. Fuel rod cladding surface temperatures at the top of the three core channels for sensitivity Case 1.

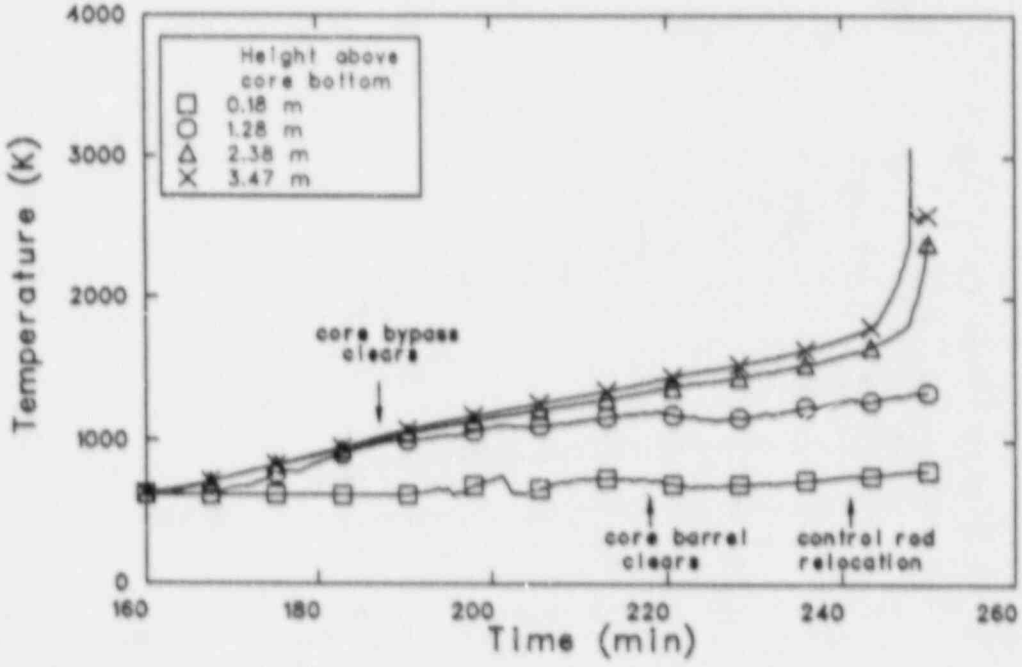

Figure 26. Center channel fuel rod cladding surface temperatures at 0.18, 1.28, 2.38, and 3.47 m above the core bottom for sensitivity Case 1.

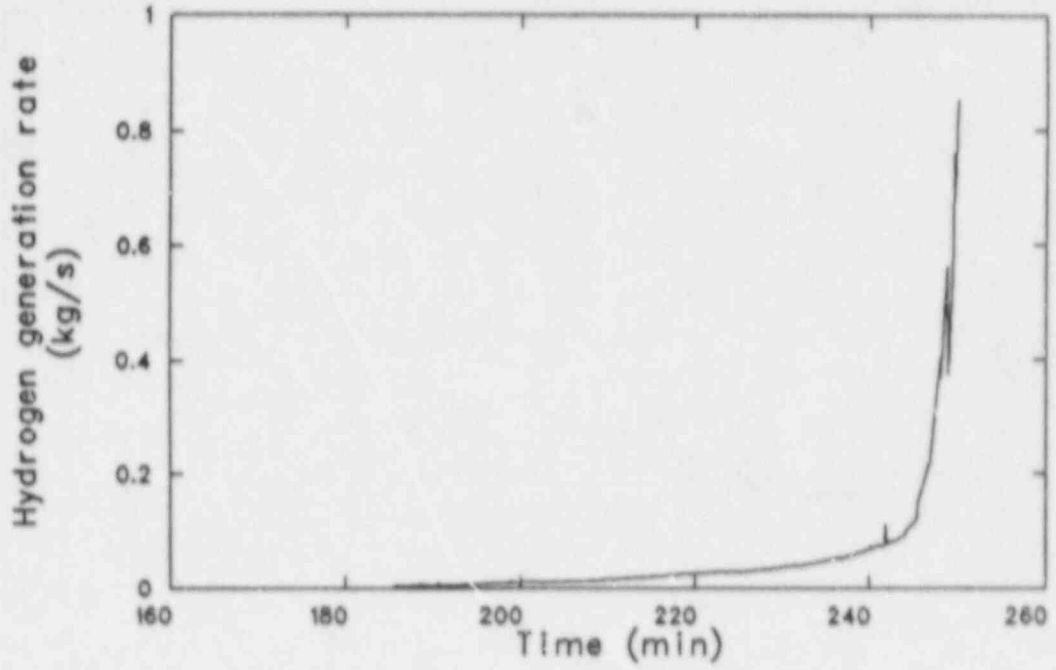

Figure 27. Total hydrogen generation rate for sensitivity Case 1.

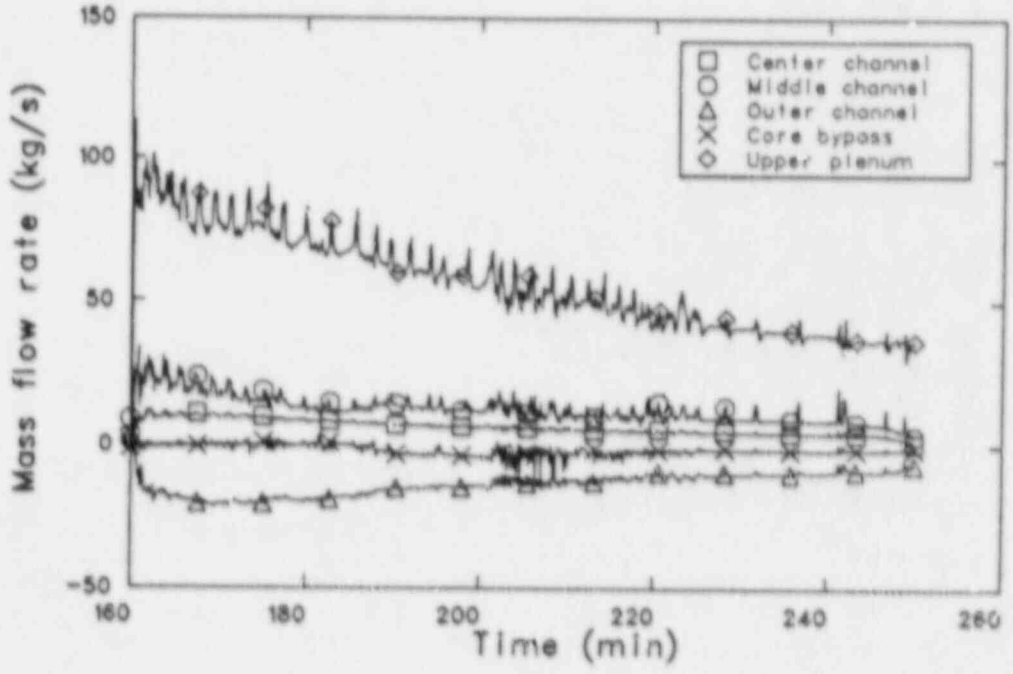

Figure 28. Mass flow rates exiting the three core channels, the core bypass, and recirculating in the upper plenum for sensitivity Case 1.

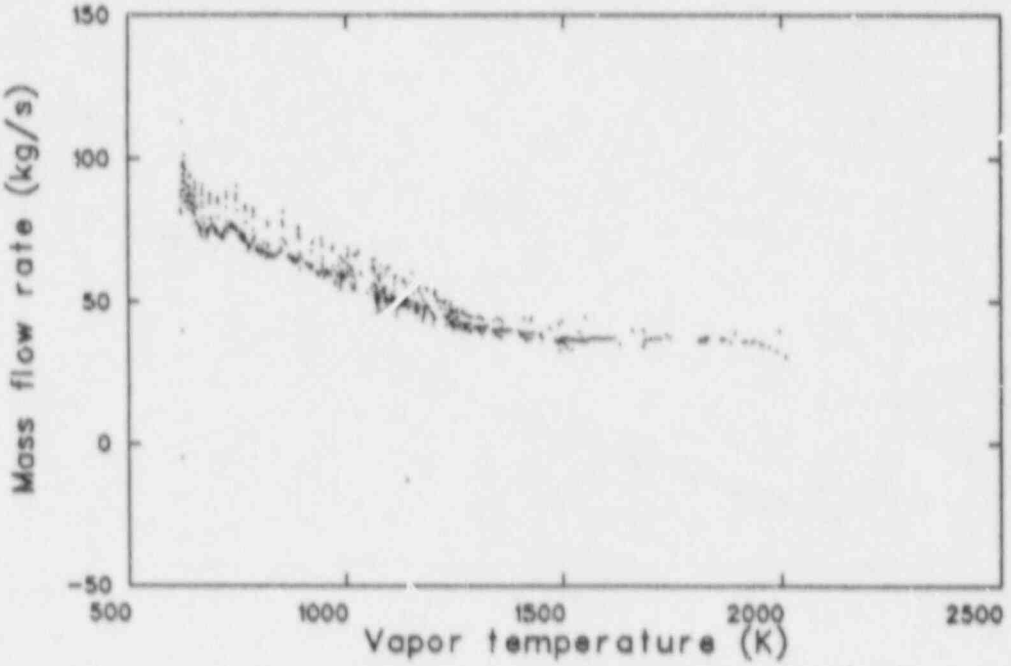

Figure 29. Upper plenum recirculating mass flow rate as a function of maximum upper plenum vapor temperature for sensitivity Case 1.

Upper plenum structure temperatures in each channel just above the core outlet are shown in Figure 30. The center channel temperature was highest because it was above the hottest part of the core. The outer channel temperature was the lowest because the vapor in that channel had been cooled as it flowed down; the upper plenum outer channel temperatures increased with increasing elevation. The middle channel temperature was between the center and outer channel temperatures, and might have been closer to the center channel structure temperature except that the recirculating flow within the upper plenum caused cooler vapor from the outer channel to mix with that above the middle channel, cooling the structures there. The hottest structures within the upper plenum were the control rod housings. These very thin structures had a temperature of 1803 K at the end of the calculation. This temperature is high enough to melt these stainless steel housings, although that behavior was not modeled. Other volume-average structure temperatures of note at the end of the calculation were a maximum of 1196 K for the core barrel, 1477 K for the core baffle plates, and 733 K for the upper head, which was the highest reactor vessel wall temperature. The local temperature in the region of the reactor vessel head bolts was 621 K at the end of the calculation. The high structure temperatures in the upper plenum and baffle plates indicate that more hydrogen would have been produced had the oxidation of these steel structures been accounted for in the calculations. There may also have been melting and relocation of some of these structures.

Figure 31 presents the fraction of the core heat that had been removed by the coolant at any time. The integral core heat removal remained near 75% for most of the calculation. Of the energy removed from the core at the time of the surge line failure (246.3 min), 9.0% had been transferred to structures in each of the non-pressurizer loops and 11.8% to Loop C structures. The hot leg piping in all three loops had absorbed 4.8% of the energy removed from the core, the surge line piping 0.8%, and the steam generator tubes and tube sheets 23.1%. Some of the energy transferred to the steam generator tubes was in turn transferred to the steam on the secondary side of the steam generators, so that the net energy storage in these structures was less than 23.1%.

More energy was deposited in the pressurizer loop (Loop C) than in the other loops because the PORVs drew flow into that loop when they were

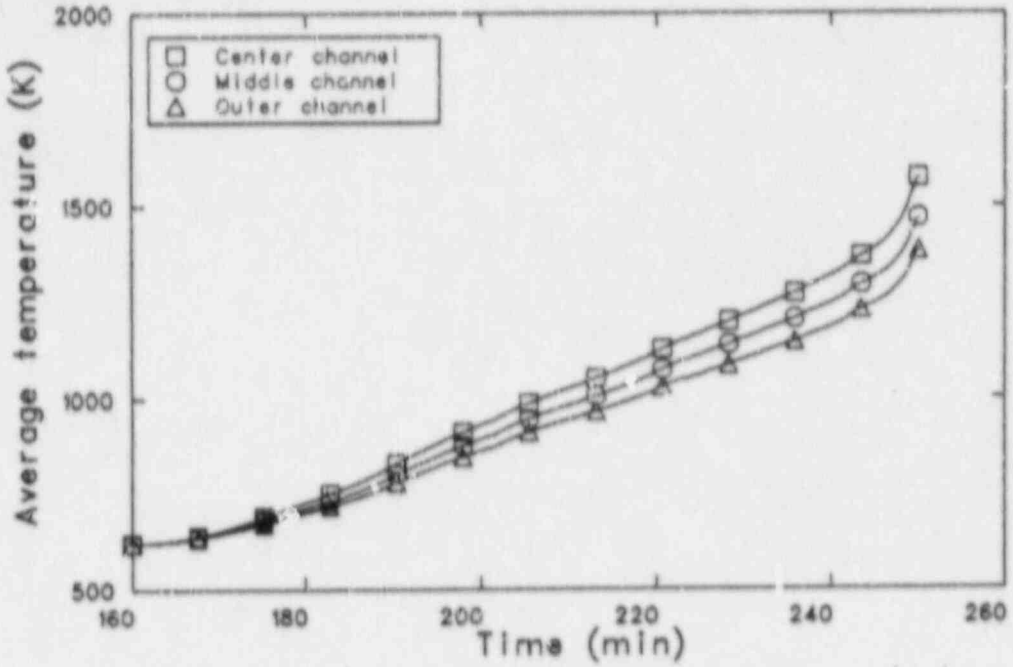

Figure 30. Volume-average temperatures of the upper plenum structures at the outlet of the three core channels for sensitivity Case 1.

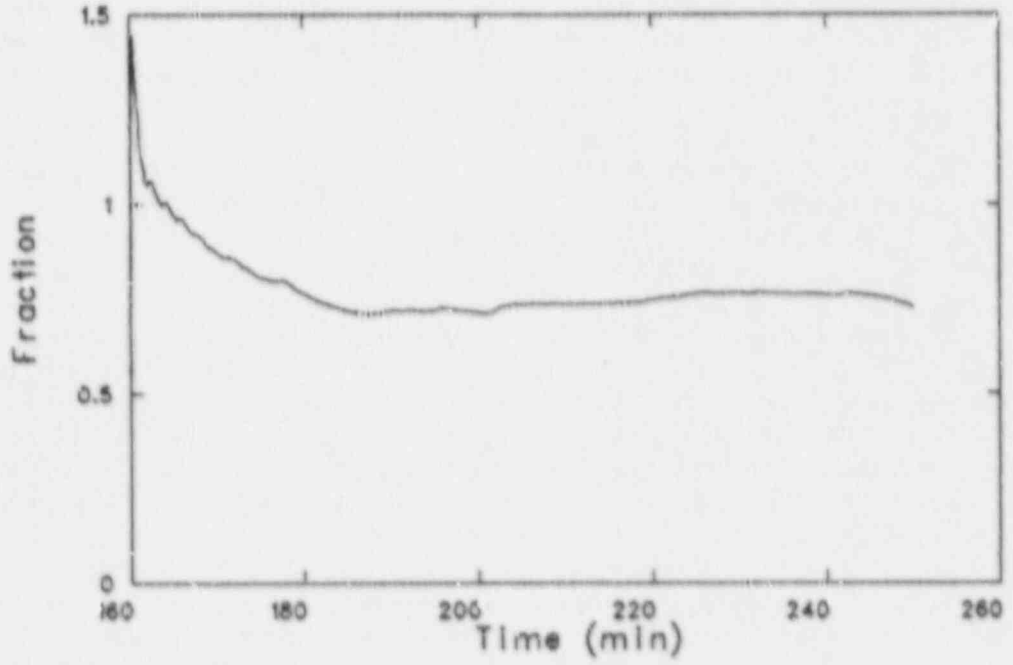

Figure 31. Fraction of the core heat removed by the coolant for sensitivity Case 1.

open. The increased flow in the hot leg, combined with the decreased flow into the other two hot legs, resulted in about 5% more energy being absorbed by the structures in Loop C than in Loop A or B. A result of this difference is illustrated in Figure 32, which presents the volume-average temperatures of the three hot legs near the reactor vessel. The Loop A and B hot leg temperatures are identical, and slightly cooler than the Loop C hot leg. Similar temperature differences were observed in the rest of the hot legs and in the steam generators.

Figure 33 shows the highest temperatures in the Loop C hot leg, surge line, and steam generator tubes. Also included in the figure are the corresponding structure temperatures on the bottom of the hot leg and surge line. All of the structures began to heat up above the saturation temperature immediately. The surge line heated up the fastest because it had nearly the same vapor temperatures as the hot leg, but it is only one-third as thick. The steam generator tubes are the thinnest structures, but they had the coolest vapor (of the structures shown). Also, the steam generator tubes are somewhat protected by the tube sheet, which has a large thermal capacity and helps to cool the vapor before it encounters the tubes. Creep rupture of the surge line was predicted to occur at 246.3 min, at a temperature of 1219 K. At that time, the hot leg was near 1000 K, and the steam generator tubes were near 800 K. The surge line temperature was affected most by the cycling of the PORVs. When the PORVs were open, hot vapor was drawn from the reactor vessel to the pressurizer, heating the surge line. When the PORVs were closed, very little flow passed through the surge line. Until the pressurizer emptied at 224.8 min, liquid draining into the surge line when the PORVs were closed cooled the pipe. After the pressurizer emptied, the temperature increased slowly when the valves were closed. By contrast, the hot leg temperature did not follow the PORV cycling. The greater thickness, and hence longer time constant, of the hot leg piping, together with the fact that there was always flow from the reactor vessel into the hot leg, resulted in a steady heatup of the hot leg. Several short decreases in the upper hot leg temperature between 170 and 200 min were the result of liquid draining from the pressurizer; the saturated liquid cooled the pipe. The large temperature differences between the top and bottom halves of the surge line (up to 450 K) and hot leg (up to 250 K) would induce circumferential stresses in the pipes. There would also be conduction heat transfer from the top of the pipe to the bottom. However, this cannot be modeled with the one-dimensional heat structures in SCDAP/RELAP5.

The temperature of the vapor entering and exiting the reactor vessel from the Loop A and C hot legs is presented in Figure 34. The vapor temperatures in the top halves of the hot legs were nearly identical throughout the transient. The temperatures in the bottom part of the hot legs were fairly close together, except when the PORVs were open. When the PORVs were open, flow reversed in the bottom of the Loop C hot leg, drawing vapor from the reactor vessel toward the surge line. This caused the large increases in temperature. When the PORVs closed, the flow was quickly reestablished toward the reactor vessel, and the temperature decreased. The open PORVs caused slight decreases in the temperature in Loop A because the flow rate through the bottom of the hot leg increased, resulting in higher heat transfer rates to the piping and correspondingly lower fluid temperatures. The hot leg bottom temperatures did diverge slightly as the transient progressed. This was the result of higher pipe temperatures in Loop C, which were developed during the PORV cycles when hot vapor from the upper plenum was drawn into Loop C.

The mass flow into the top of two of the hot legs is presented in Figure 35. The flow rate increased as the transient began, reaching a maximum at about 170 min. Displacement of the saturated vapor in the loops and heat transfer to the structures combined to keep the return flow at the saturation temperature during this time. The flow then gradually decreased as the return flow temperature increased above saturation, because the density difference between the opposing hot leg flows was decreasing even though the temperature difference was increasing. When the PORVs were closed, the flow in Loop C was higher than that in Loop A. The Loop B flow was the same as that in Loop A. About 5% less of the hot leg flow mixed in Loop C than in Loops A and B. This resulted in a higher flow rate in Loop C, as will be discussed in the steam generator inlet plenum mixing sensitivity section. When the PORVs were open, the flow in the pressurizer loop increased because flow was being drawn to the surge line, while the Loop A flow decreased for the same reason. When the PORVs closed, the two flows quickly returned to their quasi-steady values. Unlike the Westinghouse experiments[5] and COMMIX calculations[11], the

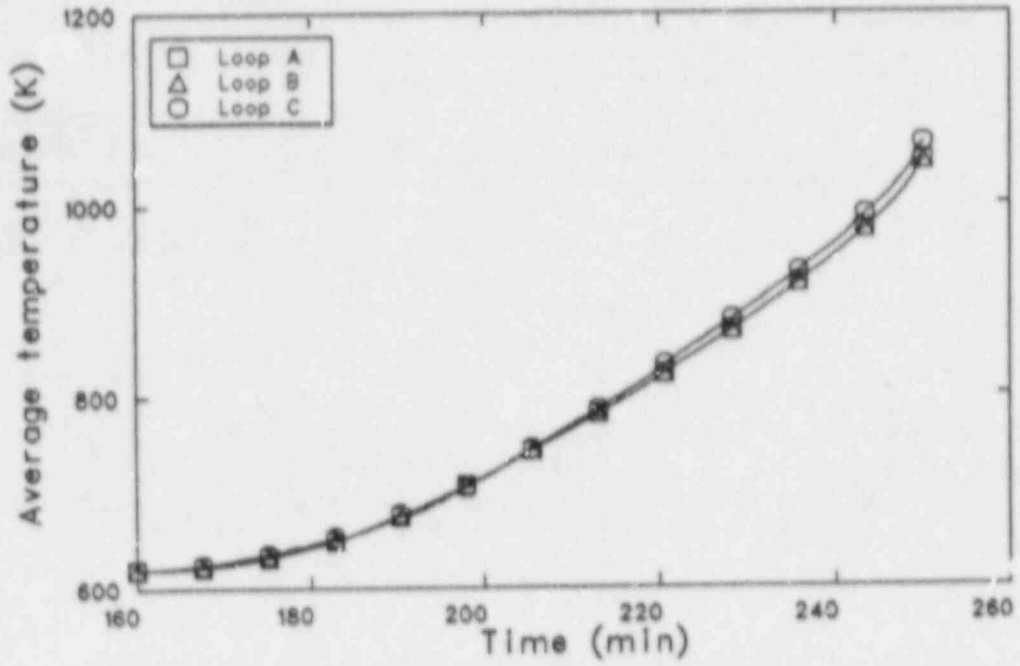

Figure 32. Volume-average temperatures of the three hot leg pipes near the reactor vessel for sensitivity Case 1.

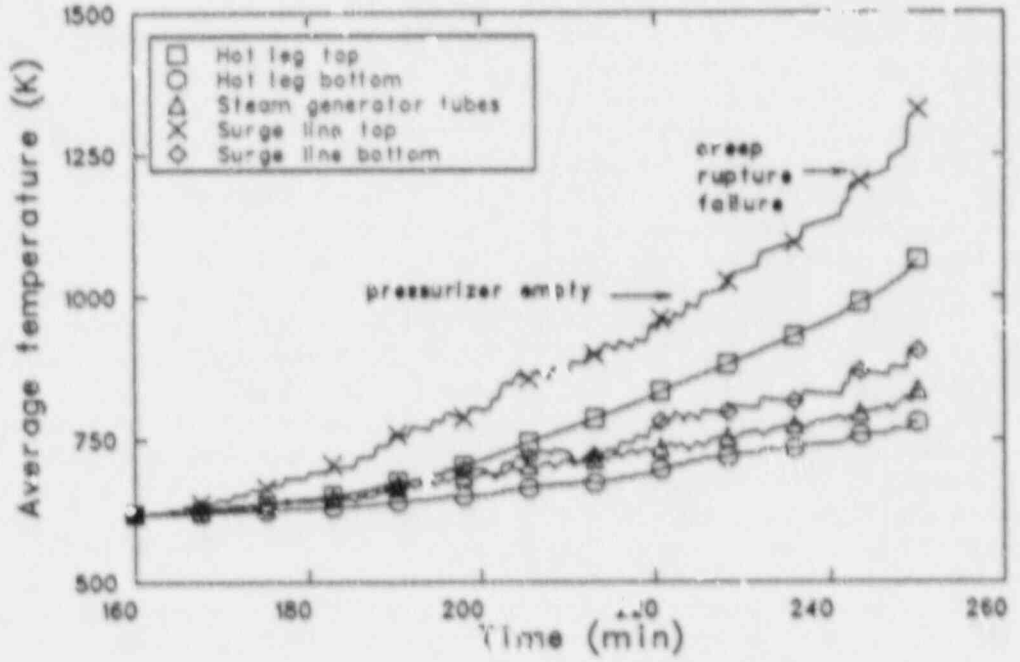

Figure 33. Volume-average temperatures of the hottest Loop C hot leg, surge line, and steam generator tubes for sensitivity Case 1.

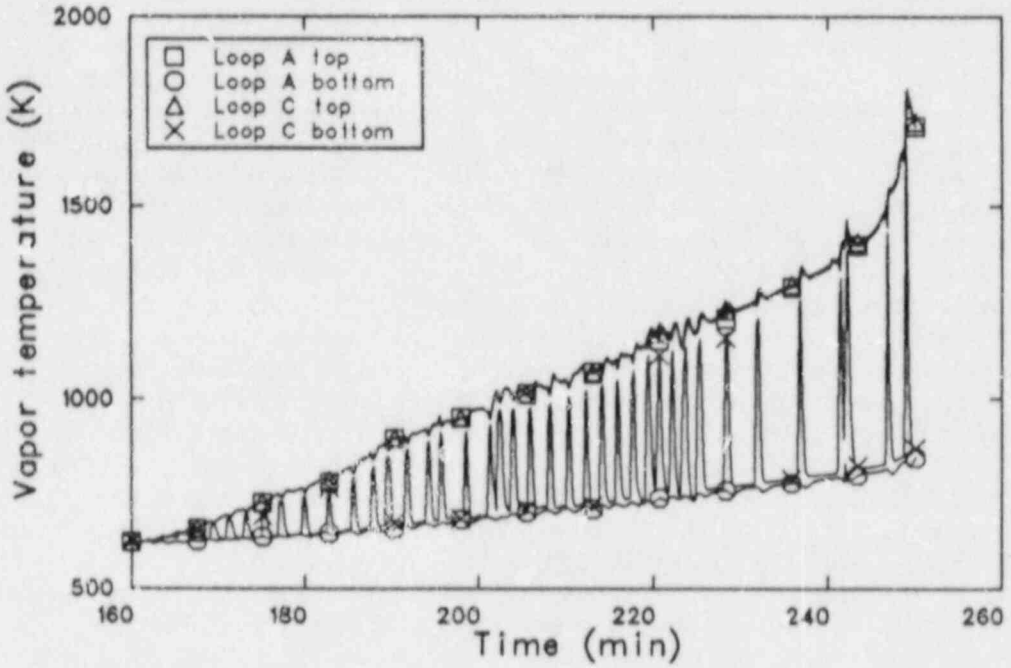

Figure 34. Hot leg nozzle hot and cold vapor temperatures in Loops A and C for sensitivity Case 1.

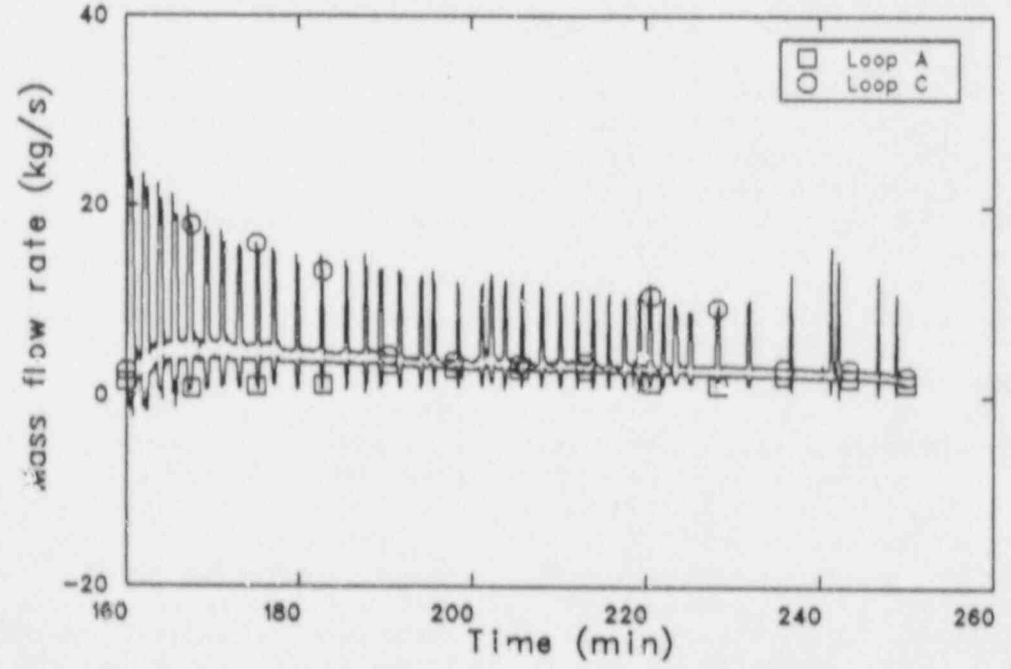

Figure 35. Upper hot leg mass flow in Loops A and C for sensitivity Case 1.

flow in the non-pressurizer loop did not reverse completely when the PORVs were open; a small positive flow toward the steam generator persisted. While this behavior does not reproduce the desired behavior, it was also present in the calculations that were performed to test the hot leg countercurrent flow nodalization. Hence the mixing in the steam generator inlet plenum was adjusted to provide the correct total heat transfer with this flow present. The flow into the Loop A hot leg is correlated with the vapor temperature in the upper plenum at the hot leg nozzle in Figure 36. The lower flow values at each temperature, which occurred less frequently than the higher flows, reflect times when the PORVs were open.

The flow through the steam generator tubes was about 70% larger than the flow in the hot legs in Loops A and B, and about 120% higher in Loop C. About 88% of the hot vapor flow in the hot leg mixed in the steam generator inlet plenum, with the other 12% proceeding directly into the steam generator tubes in Loops A and B; about 84% of the hot leg flow mixed in Loop C. The same fraction of the flow returning from the cold flow steam generator tubes mixed in the inlet plenum, with the rest proceeding directly into the bottom of the hot leg. In the Westinghouse natural circulation experiments, it was estimated that about 30% of the hot leg flow participated in the inlet plenum mixing.[5]

Figure 37 shows the pressurizer liquid volume. The liquid volume decreased when the PORVs were open for two reasons. First, the pressure was decreasing, causing some of the liquid to flash to steam. Second, the vapor entering from the surge line was superheated, and transferred heat to the liquid, causing it to boil. Virtually no liquid was entrained with the flow through the PORVs. The amount of liquid in the pressurizer increased slightly when the PORVs were closed, because the increasing pressure resulted in the condensation of some of the steam, which compensated for the loss of a small amount of liquid that drained back through the surge line to the hot leg. A brief calculation was also performed in which the Wallis flooding correlation[15] was applied at the junction between the surge line and the pressurizer. Over the 40 min that the calculation covered, there was little change in the pressurizer liquid volume.

4.2 Axial Power Profile Sensitivity

The effect of a different axial power profile was investigated with sensitivity Case 2. In this calculation, a chopped cosine axial power profile with a peak-to-average power ratio of 1.200 was used in all three core channels. In the base case (Case 1), a flatter profile with a peak-to-average power ratio of 1.155 was used. All other parameters were the same as in the base case.

Table 9 presents the sequence of events for the base case and the axial power profile sensitivity case. There was very little difference between the two calculations. The onset of various stages of core damage occurred slightly earlier in Case 2, as did the surge line failure. However, a difference in failure time of just over 1 min for a nearly 250 min transient is insignificant.

Figure 38 shows peak cladding temperatures from Cases 1 and 2. As with most comparisons between the two cases, there was little difference in the temperatures. The temperature in Case 2 increased slightly faster. The short increases before the temperature reached 1850 K were again the result of oxidation excursions in the control rod guide tubes.

There were small differences in the flows in the reactor vessel between Cases 2 and 1. In Case 1, the return flow from the upper plenum to the outer core channel was slightly higher than in Case 2. The flow also penetrated further down the outer channel in the base case. Both of these changes in flow resulted from the faster heatup of the downward flow in Case 2. This downward flow was heated faster because of the steeper power gradient, which transferred more energy to the fluid in the top half of the core, reducing the density gradient between the outer and inner channels. Similar decreases in the outer channel flow and flow penetration were observed in the base case when the cladding in the top part of the outer channel began to oxidize heavily. This oxidation had the effect of changing the axial power profile to be more like that of Case 2.

The energy removal from the core and redistribution throughout the system were nearly identical in the two cases. The hot leg mass flow rate at a given hot leg inlet temperature was identical to the base case. Figure 39 presents the highest hot leg, surge line, and steam generator tube temperatures from the pressurizer loop, as well as the surge line temperature from the base case. The temperatures increased throughout the transient, with the surge line failing at 245.0 min at a temperature of 1238 K. There was little difference in the surge line temperature until close to the time of failure, when the vapor temperatures leaving the core were higher

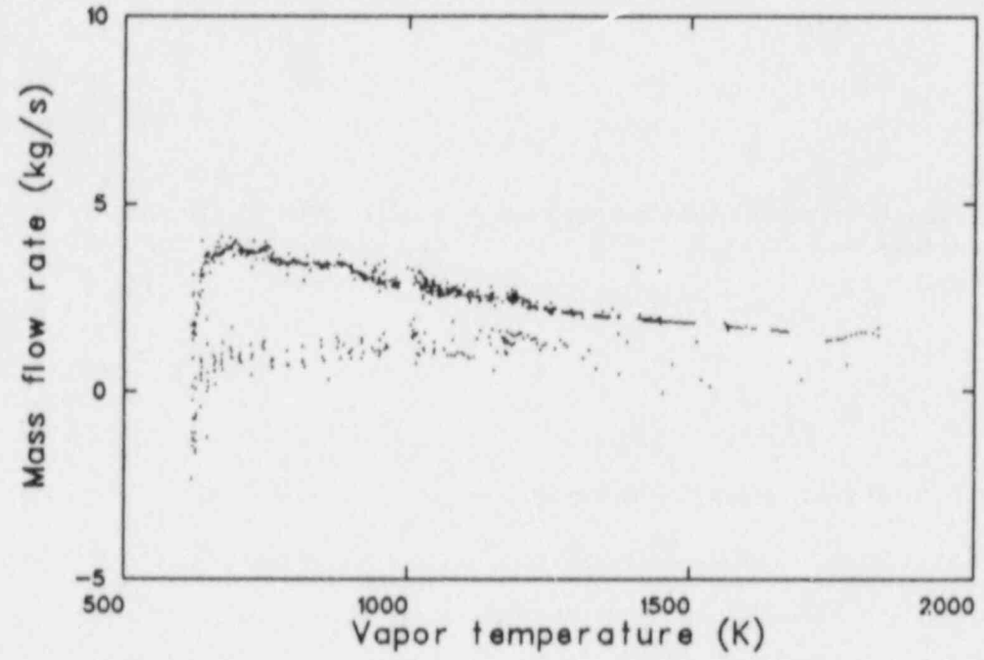

Figure 36. Hot leg flow as a function of the hot leg inlet vapor temperature in Loop A for sensitivity Case 1.

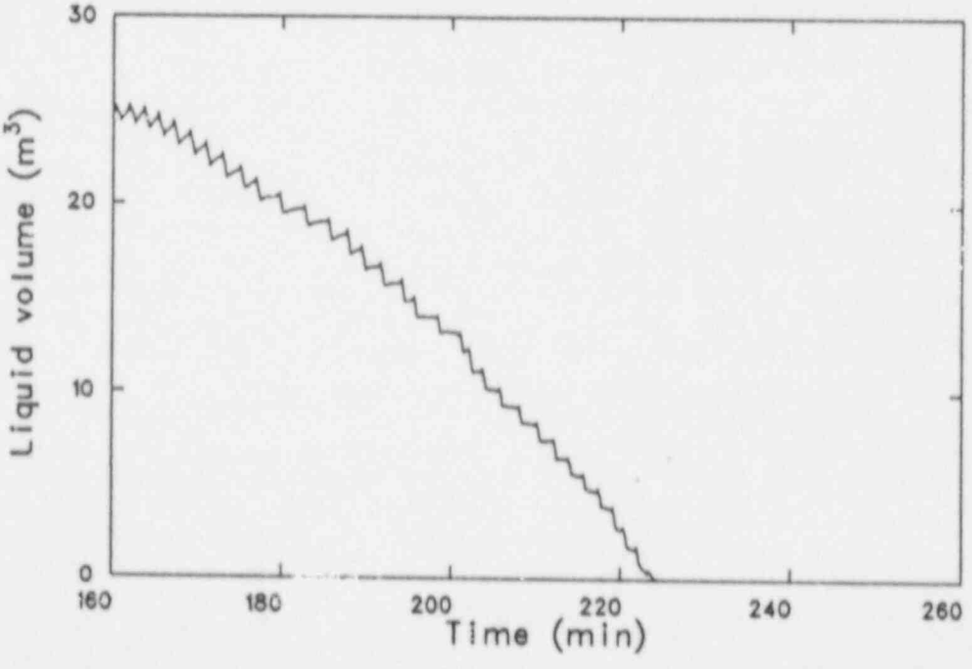

Figure 37. Pressurizer liquid volume for sensitivity Case 1.

Table 9. Sequence of events for the base case and axial power profile sensitivity calculations

Event	Time (min) Case 1	Case 2
Fuel rod cladding oxidation begins		
Center channel	185.3	185.3
Middle channel	186.1	185.7
Outer channel	192.6	191.7
Liquid level drops below core	190.2	190.2
Pressurizer empties of liquid	224.8	224.8
Fuel rod cladding fails		
Center channel	223.4	222.0
Middle channel	225.3	223.5
Outer channel	241.3	239.3
Fuel rod relocation begins		
Center channel	248.0	245.2
Middle channel	248.8	246.2
Outer channel	—	—
RCS pressure boundary fails	246.3	245.0
RCS failure location	Surge line	Surge line
Calculation terminated	250.0	248.2

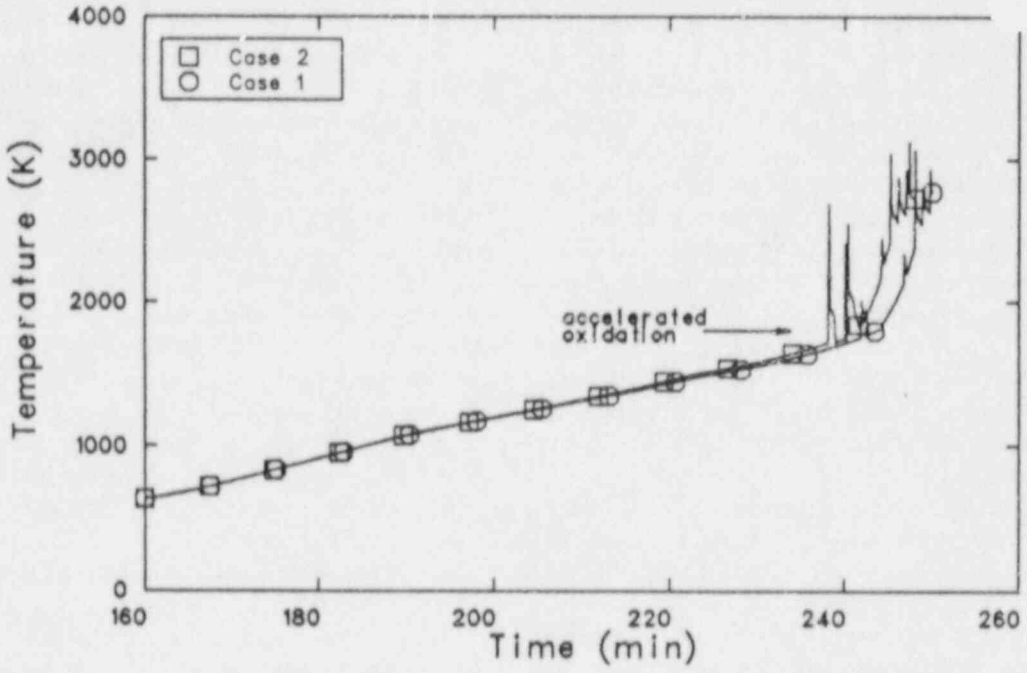

Figure 38. Peak cladding temperatures for sensitivity Cases 2 and 1.

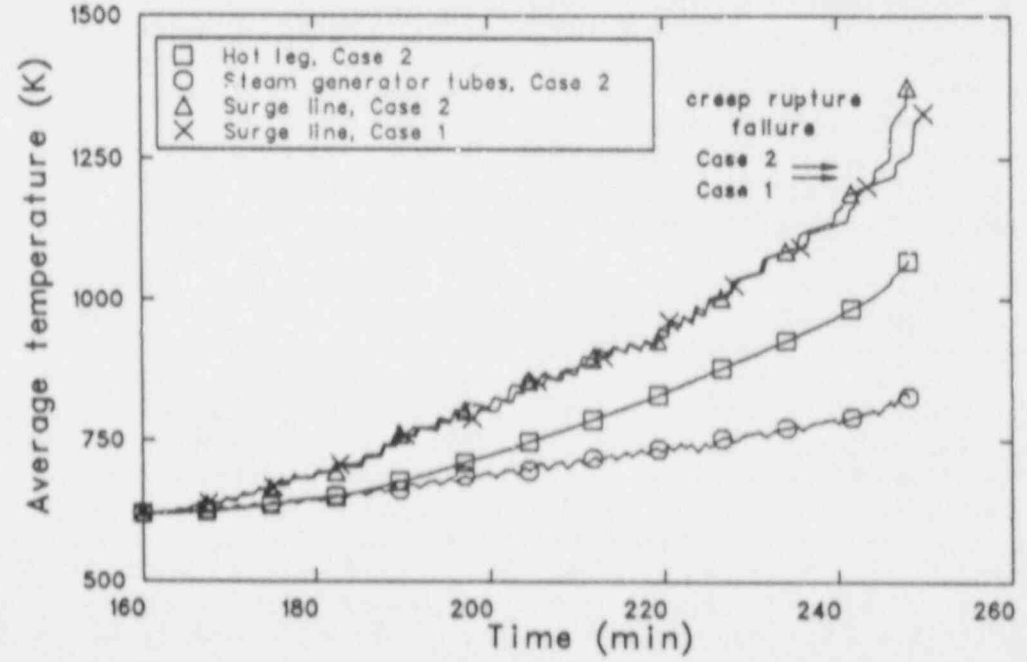

Figure 39. Highest volume-average pipe temperatures in the Loop C hot leg, surge line, and steam generator tubes for sensitivity Case 2, and the surge line for Case 1.

in Case 2 than in Case 1 because of the higher cladding temperatures.

Some of the plant conditions shortly before the surge line failure for Cases 1 and 2 are contained in Table 10. As in the sequence of events, there was very little difference between the two calculations at about 242 min. The peak cladding temperatures in each channel were slightly higher in Case 2, as was the hydrogen generation. The higher middle channel cladding temperatures in Case 2 resulted in more control rod relocation than in Case 1 at that time. The fission product release was slightly higher in Case 1 because the fuel rod temperatures in the bottom half of the core were higher in Case 1 than in Case 2.

Changing the axial power profile had little effect on the plant transient response. A slight decrease in the outer channel core flow resulted in slightly higher cladding temperatures, which led to surge line failure 1.3 min earlier than in the base case. The hot leg flow characteristics and energy removal were nearly identical to the base case.

4.3 Inlet Plenum Mixing Sensitivity

The natural circulation flow in the hot leg and steam generators is the most uncertain of the flows modeled because of the method used to develop the model. A model for full scale commercial plant severe accident conditions was developed from computer code calculations and low pressure, low temperature experiments in a scaled facility using a steam simulant. Accordingly, the hot leg model was changed significantly in these sensitivity calculations.

As discussed in Chapter 2, the amount of mixing in the steam generator inlet plenum determines the density difference between the opposing hot leg flows, and hence the hot leg flow rate. The amount of energy deposited in the loops is therefore directly influenced by the inlet plenum mixing. Two calculations were performed with decreased mixing, and hence higher hot leg flows. In sensitivity Case 3, the mixing was decreased arbitrarily. In sensitivity Case 4, there was no mixing at all. Case 4 provided an upper bound for the steam generator tube temperatures and for the heat transfer to the loops with hot leg countercurrent flow because the steam generator tubes were exposed to vapor at the same temperature as that entering the steam generators from the hot leg. In the limiting case of complete mixing in the inlet plenum, there would be no flow in the steam generator tubes, and therefore, no heatup of the tubes. The hot leg countercurrent flow would be driven only by heat transfer to the hot leg piping itself, and the behavior would be similar to that with no hot leg natural circulation modeled.

4.3.1 Reduced Inlet Plenum Mixing. As in the base case, the calculation with reduced inlet plenum mixing proceeded until shortly after the RCS pressure boundary failed. Table 11 presents the sequence of events for the base case (Case 1) and the two inlet plenum mixing sensitivity cases. By increasing the flow in the coolant loops, the transient was extended. Ballooning in the center and middle core channels, which resulted from the slower heatup, was the major difference between this and the base case.

With reduced mixing in the steam generator inlet plena, the hot leg flow rates increased. Figure 40 shows the flow entering the top of the Loop A hot leg from the reactor vessel for Cases 1 and 3. The trends in the flows were the same, but the magnitudes were higher in Case 3. The hot leg flow as a function of inlet temperature is shown in Figure 41 for Case 3. Compared to the base case, the flow at any given temperature was about 25% higher. With cooler vapor returning to the upper plenum, the recirculating flow in the upper plenum was also higher than in the base case, by about 10%.

The higher loop flow rates also changed the energy distribution compared to the base case. First, more energy was removed from the core as the hot leg flow increased. Figure 42 shows the fraction of the core heat removed during Cases 1 and 3. Second, more of the energy removed from the core was transferred to the loops in general, and the steam generator tubes in particular. Near the time of the RCS failure in the base case, heat transfer to the hot legs accounted for 4.8% of the energy removed from the core, and heat transfer to the steam generator tubes and tube sheets accounted for 23.1% of the energy removed from the core. These values were 3.6% for the hot legs and 30.1% for the tubes and tube sheets in Case 3 near the time of the RCS failure.

The effect of the higher energy deposition on the loop structure temperatures is shown in Figures 43 and 44. Figure 43 presents the hot leg temperatures nearest the reactor vessel for each of the three loops. The Loop C hot leg temperature was slightly higher than that of the other two loops because of the PORV cycling, which periodically drew more flow into that hot leg. The temperatures increased steadily until shortly after accelerated oxidation

Table 10. Conditions near the time of the surge line failure for the base case and axial power profile sensitivity calculations

Parameter	Value	
	Case 1	Case 2
Time (min)	241.7	241.7
Center channel peak clad temperature (K)	1752	1815
Middle channel peak clad temperature (K)	1714	1756
Outer channel peak clad temperature (K)	1513	1543
Maximum upper plenum structure temp. (K)	1355	1381
Maximum hot leg temperature (K)	973	985
Maximum steam generator tube temp. (K)	783	791
Maximum surge line temperature (K)	1164	1191
Core outlet flow (kg/s)	12.9	12.2
Core return flow (kg/s)	8.6	8.9
Upper plenum recirculating flow (kg/s)	35.7	36.8
Reactor vessel collapsed liquid level (m)	1.48	1.43
Core heat removal (%)[a]	76.1	76.2
Core energy removed and deposited in:[a]		
Loop A structures (%)	8.9	8.9
Loop B structures (%)	8.9	8.9
Loop C structures (%)	11.6	11.6
Hot leg piping (%)	4.6	4.7
Steam generator tubes, tube sheets (%)	22.8	22.8
Surge line piping (%)	0.8	0.9
Center channel oxidation (%)	14	15
Middle channel oxidation (%)	12	14
Outer channel oxidation (%)	7	8
Hydrogen generated (kg)	80	89
Fuel relocation (%)	0.0	0.0
Fuel rod cladding relocation (%)	0.0	0.0
Control rod relocation (%)	3	45
Xenon/krypton release (%)	0.8	0.7
Cesium release (%)	0.5	0.4
Iodine release (%)	0.0	0.0
Tellurium release (%)	1.1	1.0
Surge line failure time (min)	246.3	245.0

a. Integral quantities from the start of the calculation.

Table 11. Sequence of events for the base case and steam generator inlet plenum mixing sensitivity calculations

Event	Time (min)		
	Case 1	Case 3	Case 4
Fuel rod cladding oxidation begins			
Center channel	185.3	187.8	193.5
Middle channel	186.1	188.3	194.7
Outer channel	192.6	197.4	206.4
Liquid level drops below core	190.2	191.3	191.1
Pressurizer empties of liquid	224.8	231.6	224.0
Fuel rod cladding balloons			
Center channel	—	233.3+	250.0+
Middle channel	—	233.3+	—
Outer channel	—	—	—
Fuel rod cladding fails			
Center channel	223.4	242.3	252.2
Middle channel	225.3	244.2	257.3
Outer channel	241.3	255.3	268.3
Fuel rod relocation begins			
Center channel	248.0	—	—
Middle channel	248.8	—	275.3
Outer channel	—	254.3	279.8
RCS pressure boundary fails	246.3	254.8	290.5
RCS failure location	Surge line	Surge line	Hot leg
Calculation terminated	250.0	266.7	300.0

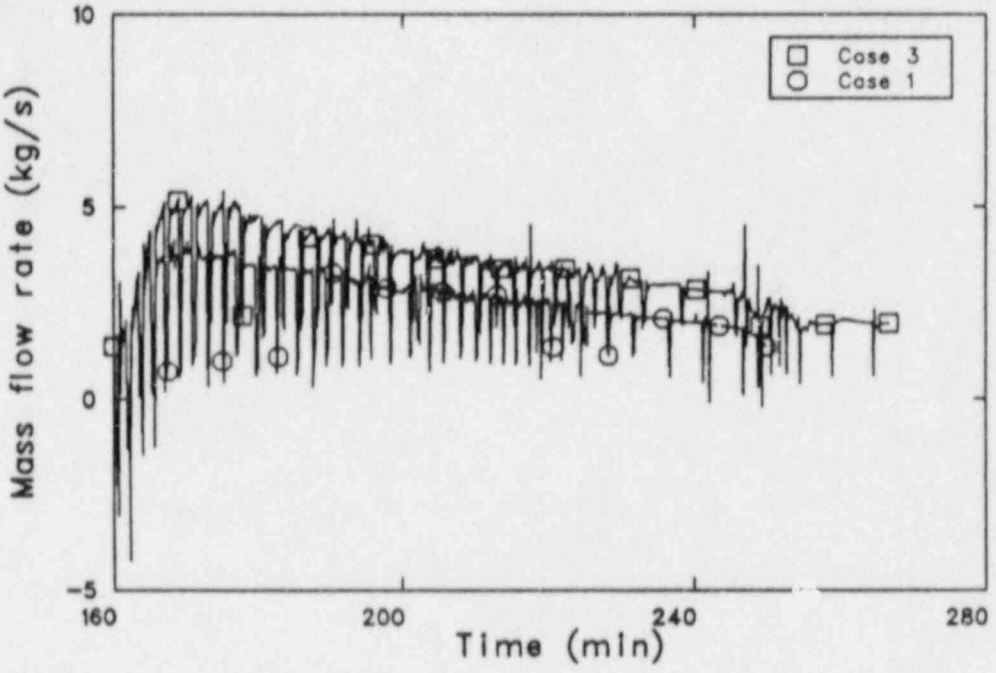

Figure 40. Upper hot leg mass flow in Loop A for sensitivity Cases 3 and 1.

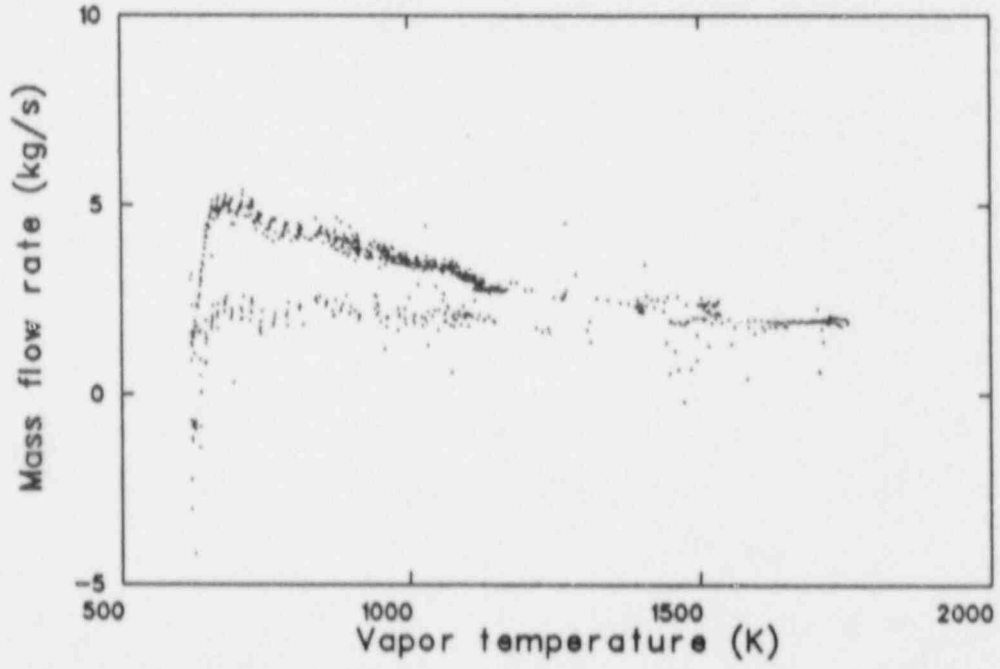

Figure 41. Hot leg flow as a function of hot leg inlet vapor temperature for sensitivity Case 3.

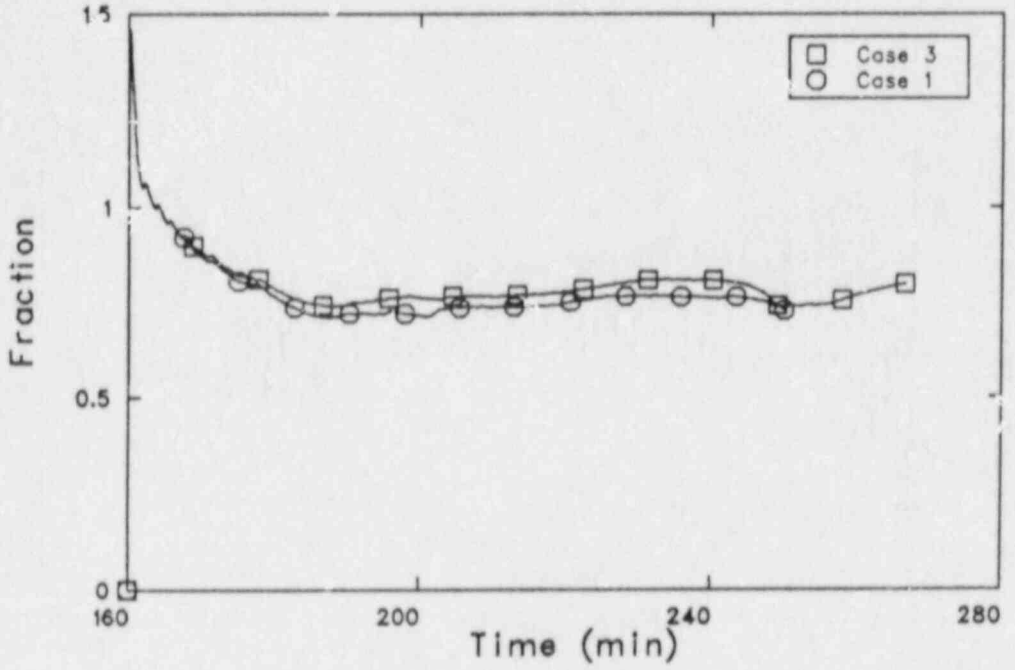

Figure 42. Fraction of the core heat removed by the coolant for sensitivity Cases 3 and 1.

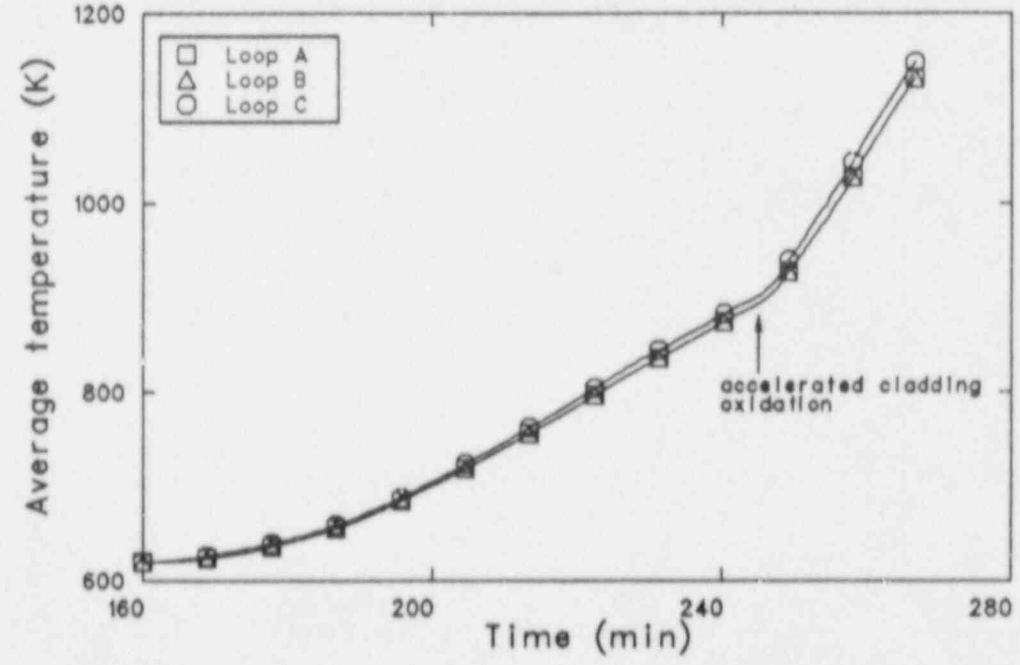

Figure 43. Volume-average hot leg pipe temperatures near the reactor vessel for sensitivity Case 3.

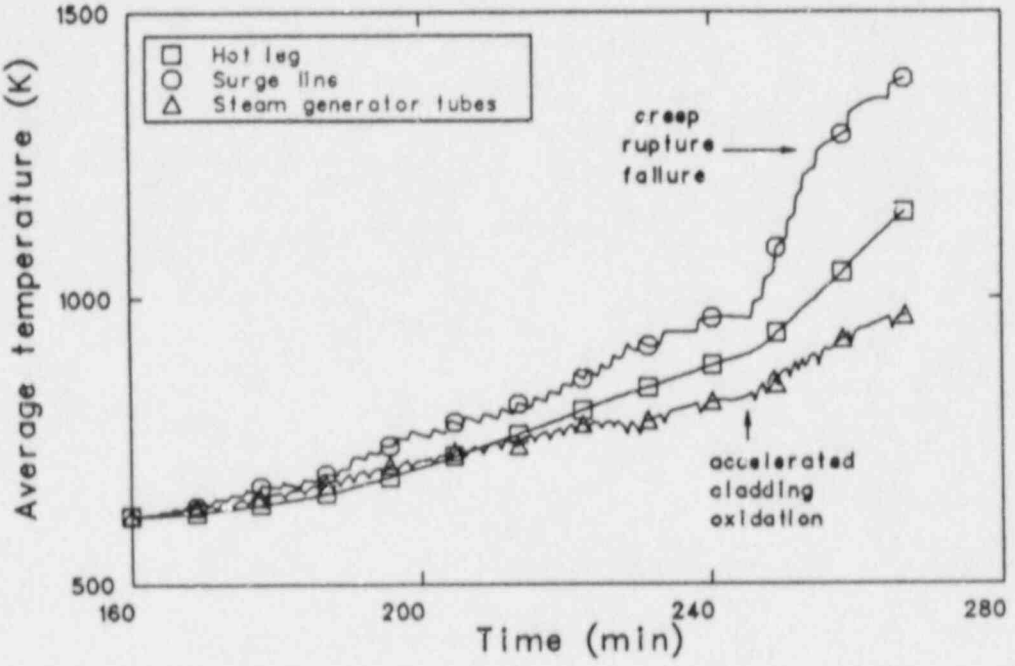

Figure 44. Highest volume-average pipe temperatures in the Loop C hot leg, surge line, and steam generator tubes for sensitivity Case 3.

began in the core, at about 250 min. The enhanced oxidation in the core increased the vapor temperature in the upper plenum and the heatup rate of the hot leg piping. There was little difference in the steam generator tube temperatures between the loops in Case 3. The highest volume-average temperatures in the hot leg, surge line, and steam generator tubes for Case 3 are presented in Figure 44. As with the hot leg, the surge line temperature increased much more rapidly after the core heatup accelerated. Creep rupture failure of the surge line was calculated to occur at 254.8 min, at a temperature of 1256 K.

Figure 45 shows the fuel rod cladding surface temperatures from the top node in each of the three core channels for Case 3. The delay in the onset of accelerated oxidation between the center and middle channel temperatures increased compared to the base case. This was because cooler vapor was being returned from the upper plenum to the core, where it provided cooler vapor first to the outer channel, then to the middle channel as it flowed inward. The heatup rate increased in the center and middle channels at about 240 min because the cladding ballooned. When the ballooned cladding ruptured, the inner surface of the cladding began to oxidize. The increased oxidation accelerated the heatup. The outer channel heatup rate did not increase until a few minutes later, when accelerated oxidation began in the center channel. The accelerated oxidation led to higher vapor temperatures in the upper plenum. This vapor then entered the outer channel, causing the cladding heatup rate to increase. However, the faster inner channel heatup associated with ballooning was not reflected in the outer channel, indicating that the additional oxidation energy was retained in the cladding rather than transferred to the coolant.

Peak cladding temperatures from Cases 1 and 3 are shown in Figure 46. The curves exhibited the same behavior, but with the time extended. The higher hot leg flow rates led to increased heat removal in the loops, which in turn led to increased heat removal from the core and a slower heatup. The slower core heatup allowed the cladding to balloon in both the center and middle channels at about 240 min. The ballooning in both channels extended over the top 60% of the cladding and reduced the axial flow area by just over 60%.

The ballooning caused an overall decrease in the core flows in Case 3. Figure 47 shows the mass flow rate entering the upper plenum from each of

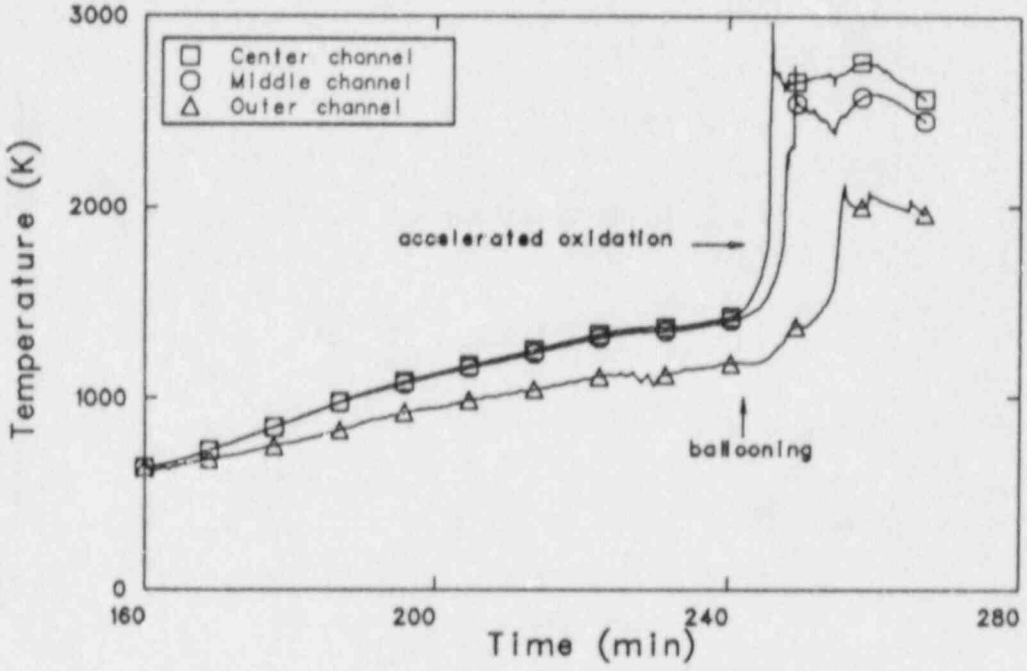

Figure 45. Fuel rod cladding surface temperatures at the top of the three core channels for sensitivity Case 3.

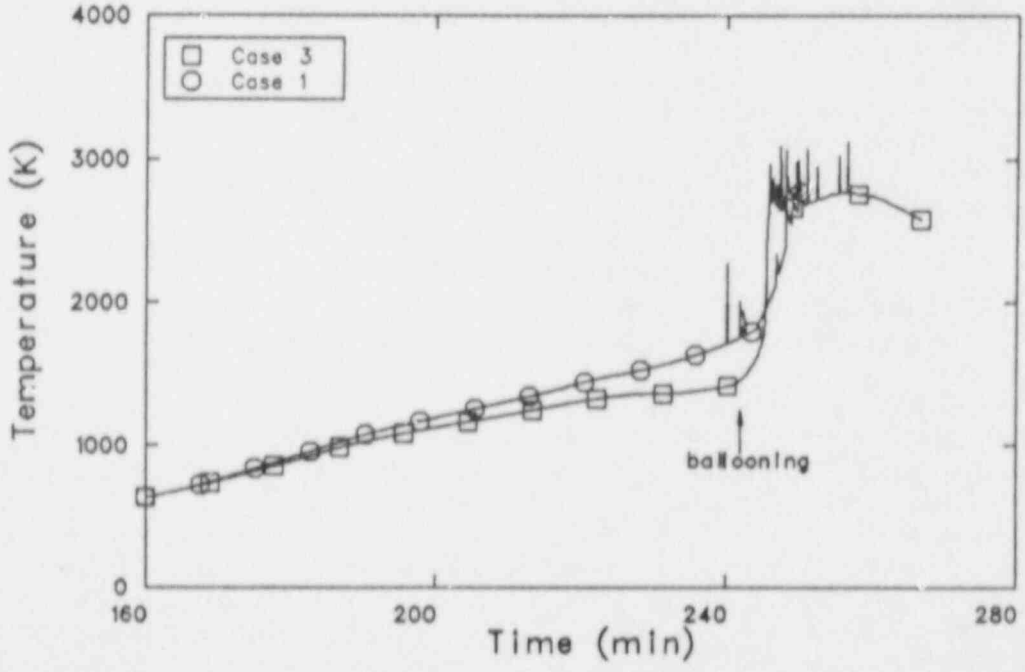

Figure 46. Peak cladding temperatures for sensitivity Cases 3 and 1.

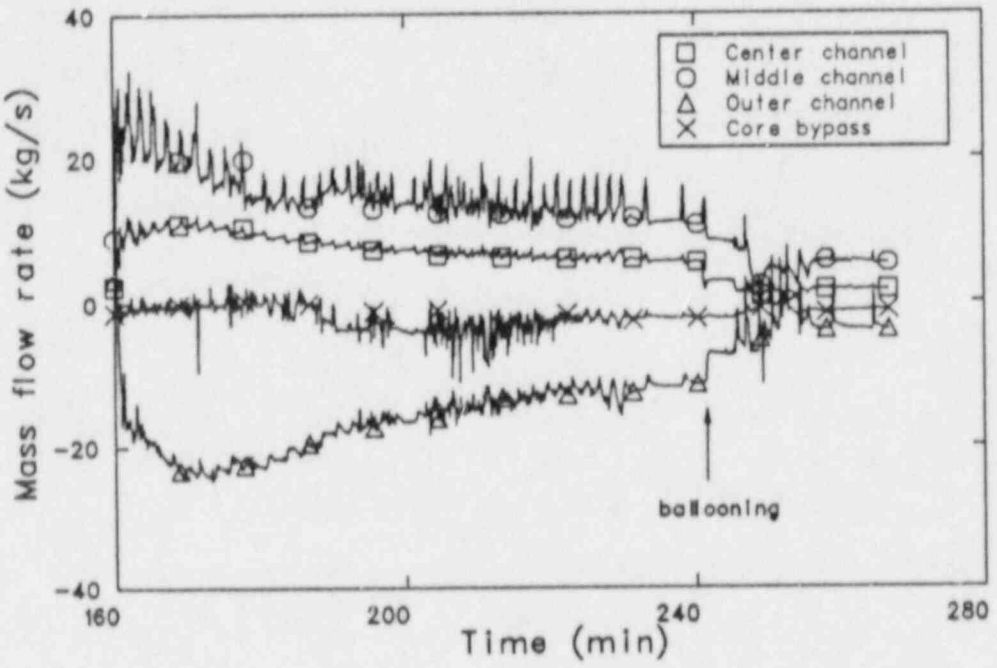

Figure 47. Mass flow rates exiting the three core channels and the core bypass for sensitivity Case 3.

the core channels and the core bypass. When ballooning occurred at about 240 min, the flows leaving the center and middle channels and entering the outer channel decreased. The flow penetration in the outer channel was also reduced, although the basic flow pattern in the core was maintained. The flow pattern did change briefly at about 250 min. When the cladding in the middle channel began to oxidize rapidly, causing a rapid heatup in that channel, the flow reversed in the center channel. Flow was drawn toward the middle channel from both the center and outer channels until the oxidation rate decreased when most of the cladding had been oxidized completely.

Temperatures of the upper plenum structures just above each of the core channels in Case 3 are presented in Figure 48. The temperatures increased steadily throughout the transient, with the heatup rate increasing at about 246 min as accelerated oxidation began in the core. By the end of the calculation, the structures above the center and middle channels were hot enough that they could begin to melt. The highest temperatures of other internal structures at the end of the calculations were 1734 K for the control rod guide housings, 1670 K for the core baffle plates, and 1315 K for the core barrel. The upper head had the highest reactor vessel temperature, 752 K, while the temperature in the region of the head bolts was 630 K.

The slower heatups led to more extensive oxidation of the cladding at the time of the RCS pressure boundary failure. In Case 3, 382 kg of hydrogen had been generated shortly after the surge line failure, compared to 109 kg at the time of surge line failure in the base case. Figure 49 shows the heat generated by the oxidation reaction together with the decay power. The peak oxidation power was about 7 times greater than the decay power.

The core damage was also affected by the ballooning. With the cladding ballooned, oxidation occurred on both the inner and outer cladding surfaces. By the time the temperature reached levels at which relocation might occur, the cladding was completely oxidized, so that no relocation of fuel rods occurred in the ballooned components. Relocation did occur in the control rods and the unballooned fuel rods. In Case 3, 31% of the Zircaloy in the outer channel fuel rods had melted and relocated by the end of the calculation. The molten Zircaloy dissolved 1.0% of the fuel in that channel, allowing it to relocate with the Zircaloy to lower portions of the fuel rods; none of the fuel rod material dropped into the lower plenum. The top 60% of the control rods in each of the channels

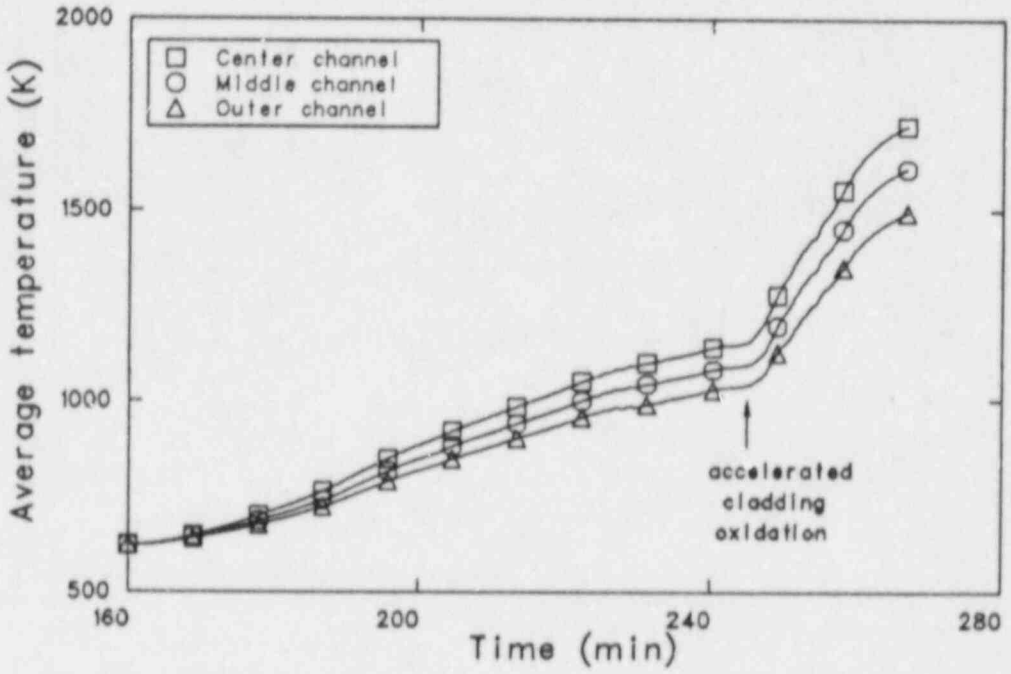

Figure 48. Volume-average temperatures of the upper plenum structures at the outlet of the three core channels for sensitivity Case 3.

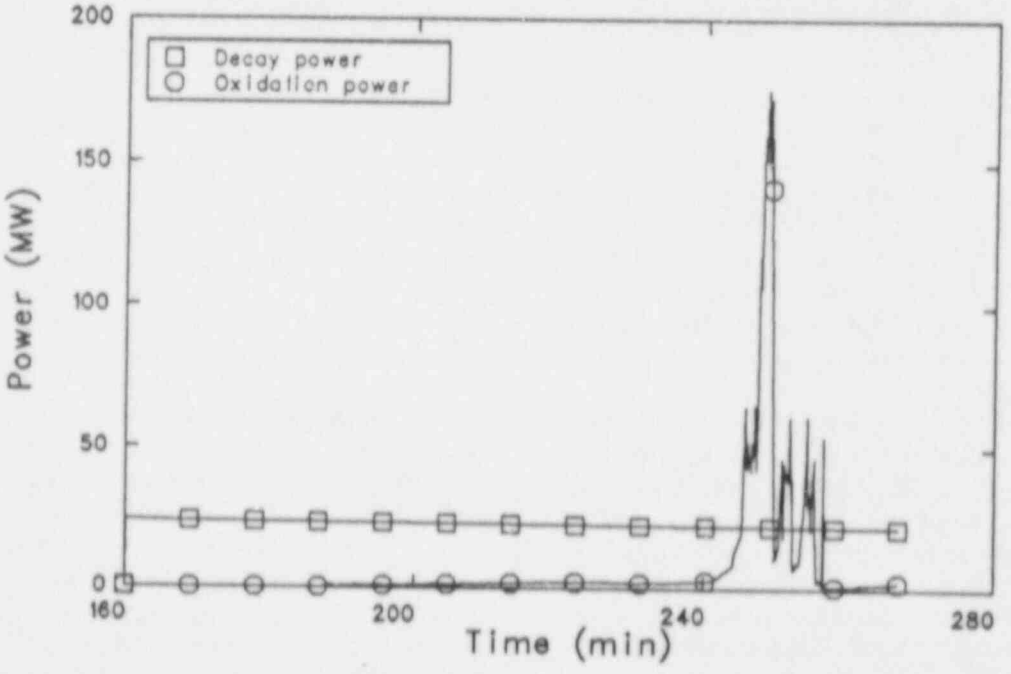

Figure 49. Decay and oxidation power for sensitivity Case 3.

relocated, with 75% of the relocated absorber material and none of the stainless steel and Zircaloy flowing into the lower plenum.

The longer transient also resulted in higher fission product releases than the base case. In Case 3, 6.1% of the xenon and krypton, 4.7% of the cesium, 3.0% of the iodine, and 6.6% of the tellurium in the fuel rods at the beginning of the transient was released by the time the surge line failed.

Table 12 presents the plant conditions for Cases 1, 3, and 4 near the time of the RCS failures. In general, the longer the transient lasted, the more severe the damage was at the time of the RCS failure. The integral core heat removal for Case 3 is somewhat misleading, in that Figure 42 shows that the fraction increased to a value above that of Case 1 after 260 min.

4.3.2 No Inlet Plenum Mixing. For Case 4, the flow from the top of the hot legs proceeded directly into the steam generator tubes, and the flow returning from the tubes went directly into the lower part of the hot legs. No interactions between the flows occurred in the steam generator inlet plena. Table 11 presents the sequence of events for this transient. Two major differences between this and the base case resulted from the slower heatup. Ballooning occurred in the center core channel and the RCS failure location was the pressurizer loop hot leg.

With no mixing in the steam generator inlet plenum, the hot leg flow rate increased more than in Case 3. Figure 50 shows the flow entering the top of the Loop A hot leg from the reactor vessel for Cases 1 and 4. The trend of the flow was the same in both cases, with higher flow rates in Case 4. The hot leg flow as a function of inlet temperature is shown in Figure 51. Compared to the base case, the flow at any given temperature was 50-60% higher in Case 4. Cooler vapor returning to the upper plenum increased the density gradient, so the recirculating flow in the upper plenum was also 10-20% higher in Case 4 than in the base case.

As in Case 3, more energy was removed from the core and deposited in the loops as a result of the hot leg flow increase. Figure 52 shows the fraction of the core heat removed during Cases 1 and 4. Near the time of the RCS failure, heat transfer to the hot legs accounted for 3.9% of the energy removed from the core, and heat transfer to the steam generator tubes and tube sheets accounted for 37.0% of the energy removed from the core, compared to values of 4.8% and 23.1%, respectively, in the base case.

The effect of the higher energy deposition on the loop structure temperatures is shown in Figures 53 through 55. Figure 53 presents the hot leg temperatures nearest the reactor vessel for each of the three loops. As in previous cases, the Loop C hot leg temperature was slightly higher than that of the other two loops because of the PORV cycling. The temperatures increased steadily until shortly after accelerated oxidation began in the core, at about 256 min in the center channel and at about 275 min in the middle channel. The enhanced oxidation in the core increased the vapor temperature in the upper plenum and the heatup rate of the hot leg piping. Figure 54 shows the highest steam generator tube temperatures in each of the loops. The pressurizer loop temperature was higher than the other loops, again because of the effect of the PORV cycling. The highest volume-average temperatures in the hot leg, surge line, and steam generator tubes for Case 4 are presented in Figure 55. The steam generator tubes were the hottest structure until 250 min because they were the thinnest structure and there was a smaller difference between the hot leg and steam generator tube vapor temperatures than in the other calculations. The hot leg near the reactor vessel was the hottest structure after 250 min. Its high temperature led to creep rupture failure at 290.5 min, at a temperature of 1233 K. The hot legs in the other two loops failed at 291.9 min, and the surge line at 296.9 min. None of the steam generator tubes had failed by the end of the calculation. The surge line temperature was strongly affected by the PORV cycling. When the valves were open, the surge line temperature increased rapidly. When the valves were closed, the temperature slowly decreased. The calculated surge line temperature was probably too low. The temperature remained near saturation until the pressurizer was nearly empty of liquid. Liquid draining from the pressurizer kept the upper part of the surge line cool, while the lower part heated up. In reality, this behavior should be reversed, with the liquid draining through the lower half of the surge line. The effect of the change may be that the surge line would fail before the hot legs, given the more rapid temperature increase of the surge line once it did begin to heat up.

Table 12. Conditions near the time of the reactor coolant system failure for the base case and steam generator inlet plenum mixing sensitivity calculations

Parameter	Value		
	Case 1	Case 3	Case 4
Time (min)	246.3	255.3	285.8
Center channel peak clad temperature (K)	2066	2763	2562
Middle channel peak clad temperature (K)	1926	2601	2600
Outer channel peak clad temperature (K)	1618	3017	2633
Maximum upper plenum structure temp. (K)	1430	1488	1718
Maximum hot leg temperature (K)	1012	1012	1175
Maximum steam generator tube temp. (K)	805	905	1110
Maximum surge line temperature (K)	1219	1262	1176
Core outlet flow (kg/s)	11.5	5.2	6.2
Core return flow (kg/s)	9.0	2.6	3.5
Upper plenum recirculating flow (kg/s)	37.1	36.5	32.2
Reactor vessel collapsed liquid level (m)	1.38	1.04	0.75
Core heat removal (%)[a]	75.4	74.1	79.4
Core energy removed and deposited in:[a]			
Loop A structures (%)	9.0	11.6	13.8
Loop B structures (%)	9.0	11.6	13.8
Loop C structures (%)	11.8	12.8	16.4
Hot leg piping (%)	4.8	3.6	3.9
Steam generator tubes, tube sheets (%)	23.1	30.1	37.0
Surge line piping (%)	0.8	0.7	0.5
Center channel oxidation (%)	20	61	63
Middle channel oxidation (%)	17	62	63
Outer channel oxidation (%)	10	28	62
Hydrogen generated (kg)	109	382	440
Fuel relocation (%)	0.0	0.3	0.0
Fuel rod cladding relocation (%)	0.0	4.1	0.0
Control rod relocation (%)	33	60	70
Xenon/krypton release (%)	1.0	6.1	19.4
Cesium release (%)	0.6	4.7	14.9
Iodine release (%)	0.0	3.0	12.4
Tellurium release (%)	1.3	6.6	13.3
Reactor coolant system failure time (min)	246.3	254.5	290.5

a. Integral quantities from the start of the calculation.

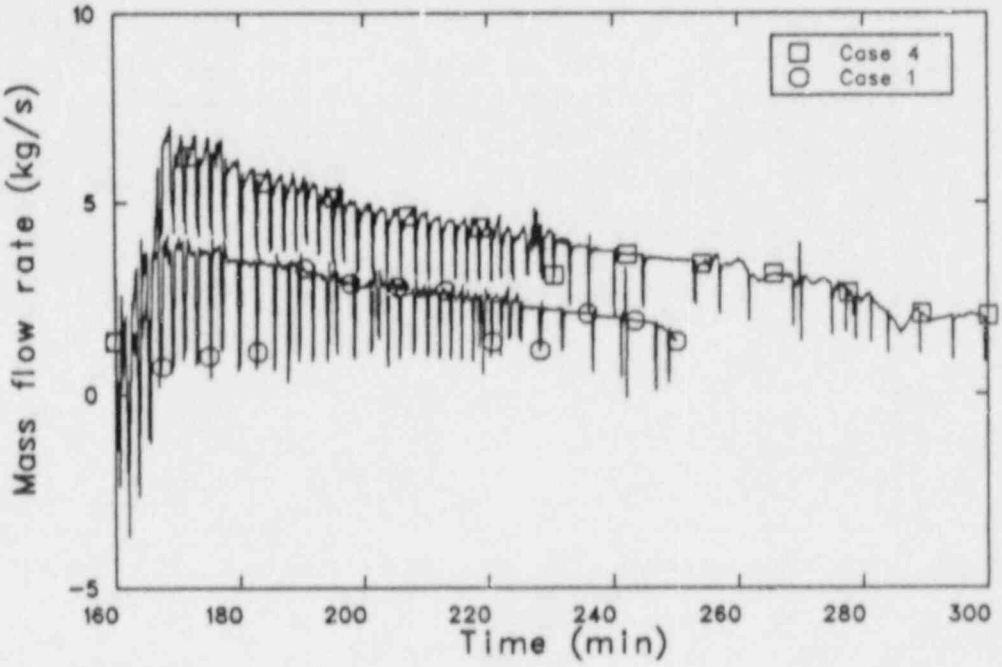

Figure 50. Upper hot leg mass flow in Loop A for sensitivity Cases 4 and 1.

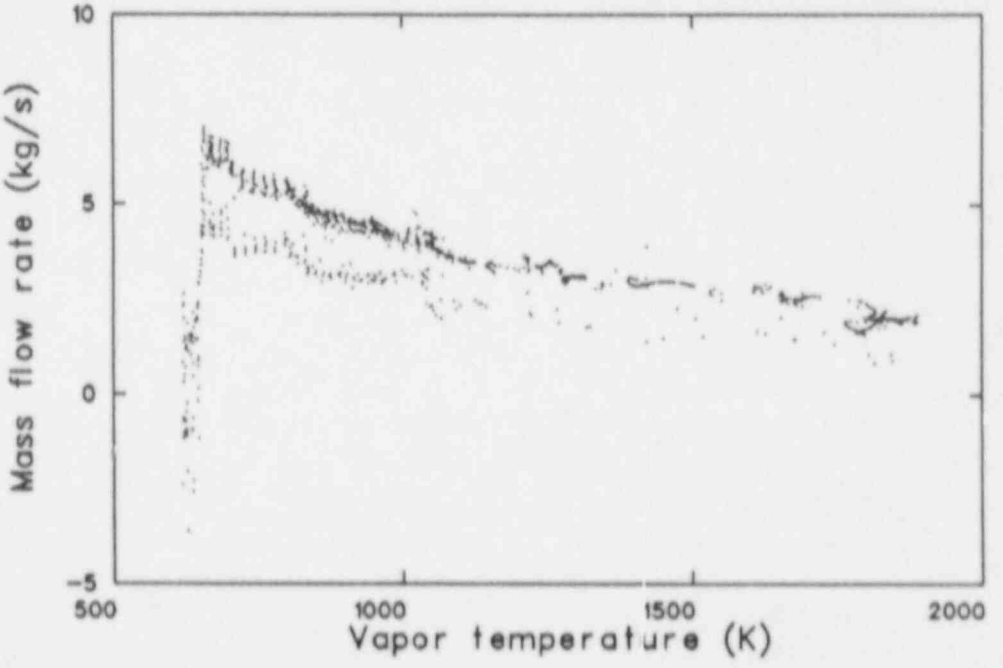

Figure 51. Hot leg flow as a function of hot leg inlet vapor temperature for sensitivity Case 4.

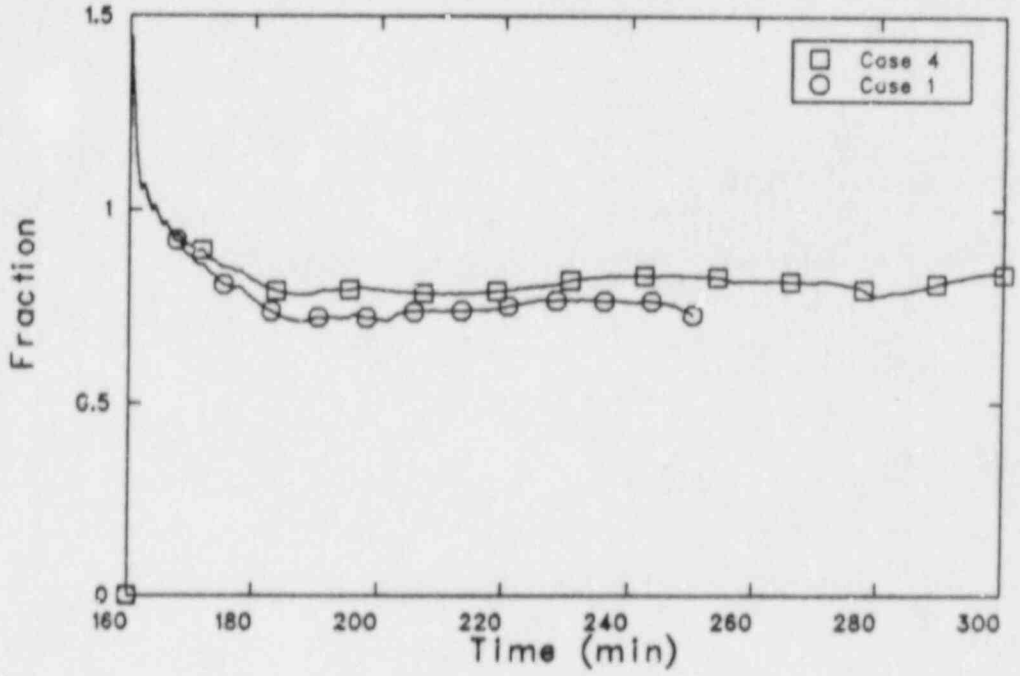

Figure 52. Fraction of the core heat removed by the coolant for sensitivity Cases 4 and 1.

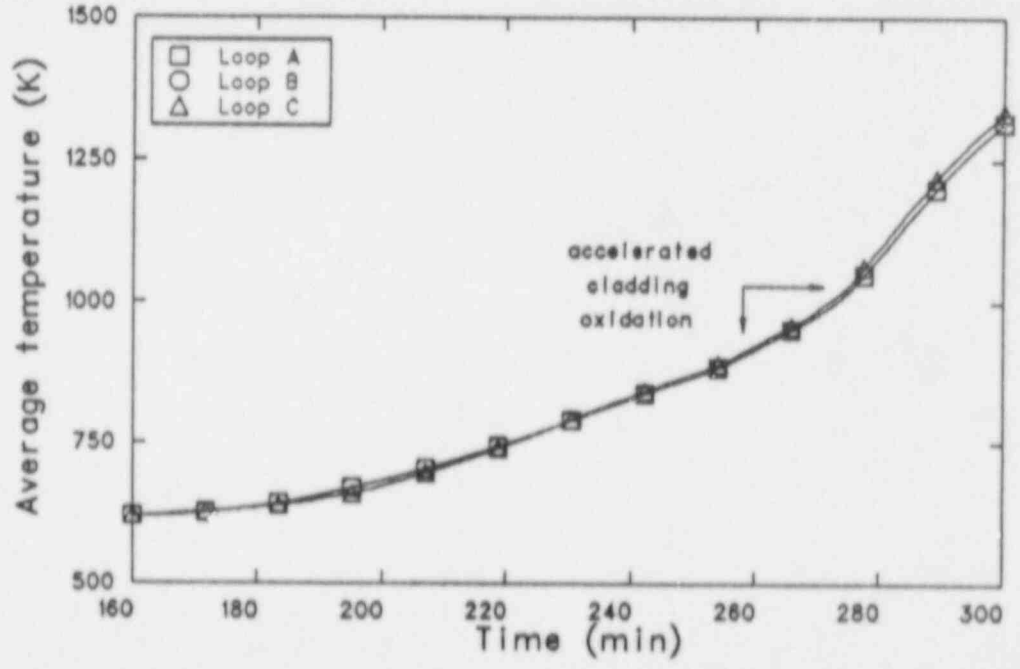

Figure 53. Volume-average hot leg pipe temperatures near the reactor vessel for sensitivity Case 4.

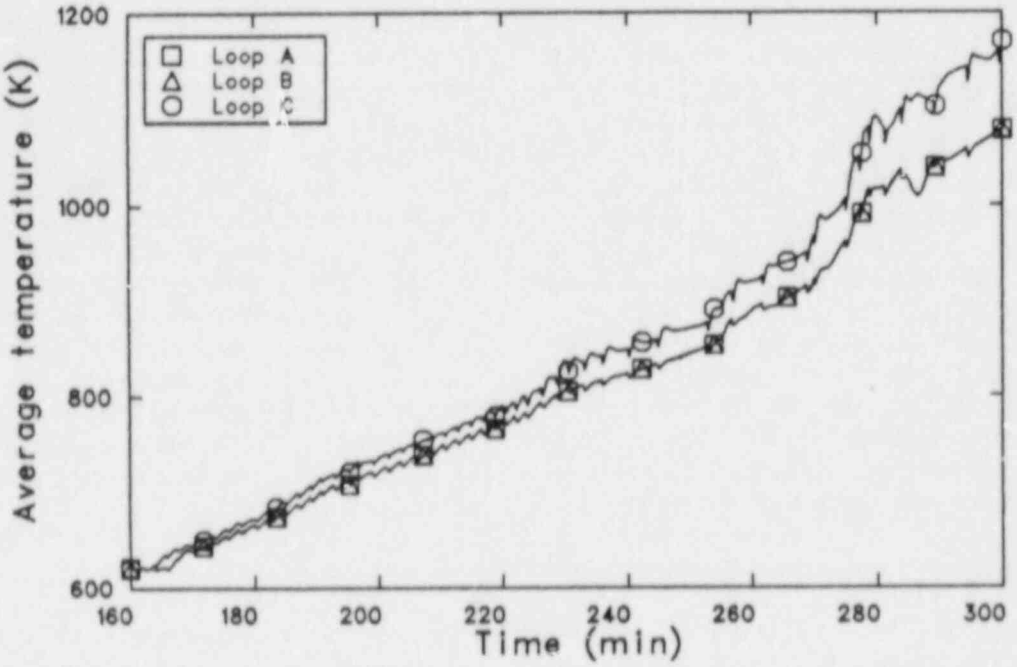

Figure 54. Highest volume-average steam generator tube temperatures in the three coolant loops for sensitivity Case 4.

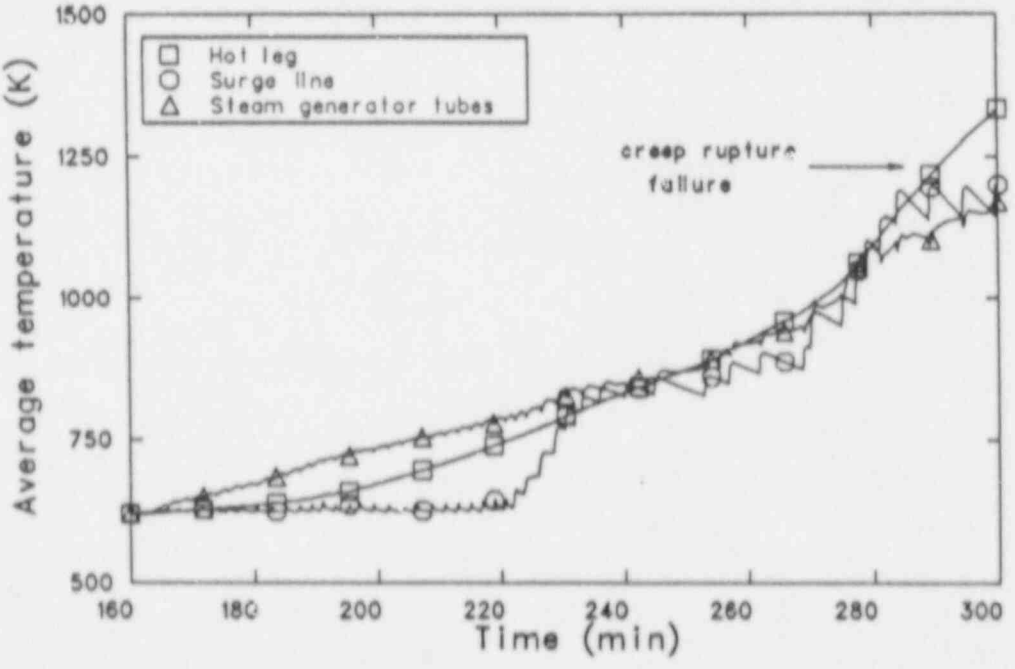

Figure 55. Highest volume-average pipe temperatures in the Loop C hot leg, surge line, and steam generator tubes for sensitivity Case 4.

Figure 56 shows the fuel rod cladding surface temperatures from the top node in each of the three core channels. The difference between the center and middle channel temperatures increased even more than in Case 3 because the heat transfer in the loops had increased more. The center channel heatup rate increased at about 250 min, when the cladding ballooned and ruptured. Oxidation of the inner cladding surface again caused the faster heatup.

Peak cladding temperatures from Cases 1 and 4 are shown in Figure 57. The curves exhibited the same behavior, but with the time extended in Case 4. The higher heat removal in the loops led to increased heat removal from the core and a slower heatup. The slower core heatup allowed the cladding to balloon in the center channel in Case 4, reducing the axial flow area by 62% over the upper 60% of the fuel rod at about 250 min.

The effects of the ballooning on the core flows were more localized in Case 4 than in Case 3. Mass flow rates entering the upper plenum from the three core channels and the core bypass are presented in Figure 58. The center channel core exit flow decreased when the ballooning occurred at about 250 min. Flow was diverted around the blocked region, increasing the middle channel flow. The flow into the outer channel, as well as the distance it penetrated down the channel, were essentially unchanged.

Figure 59 presents the core exit upper plenum structure temperatures for Case 4. Shortly after 250 min, rapid heatup of the center core channel caused a more rapid heatup of the upper plenum structures. The heatup rate slowed as much of the cladding in the center channel had been oxidized, then increased again at about 268 min when the rapid heatup of the middle core channel began. The temperatures were high enough at the end of the calculation that significant oxidation and melting of the stainless steel structures in the upper plenum might occur. At the end of the calculation, the highest temperatures in other structures in the reactor vessel were 1507 K for the core barrel, 1840 K for the control rod guide housings, 832 K for the reactor vessel at the nozzle elevation, and 654 K for the head bolt region. The top 60% of the core baffle was above 1760 K, so that these plates would be expected to melt.

The slower heatup led to more extensive oxidation of the cladding at the time of the RCS pressure boundary failure. In Case 4, 440 kg of hydrogen had been generated before the hot leg failure, compared to 382 kg near the time of surge line failure in Case 3 and 109 kg in Case 1. Figure 60 shows the heat generated by the oxidation reaction from Case 4 together with the decay power. The peak oxidation power was about eight times greater than the decay power.

The core damage was again affected by the ballooning, in that double-sided oxidation of the cladding led to no relocation of fuel rods in the center channel. The slow heatup also allowed the cladding in the other channels to oxidize completely before Zircaloy relocation could occur. Relocation did occur in the control rods and the unballooned fuel rods. In Case 4, 0.3 kg of fuel melted and relocated in the middle and outer channels. The upper 70% of the control rods in each of the channels relocated, with none of the structural material and 79% of the absorber relocating to the lower plenum.

More fission products were released than in the base case because of the longer heatup and time at high temperature prior to the RCS pressure boundary failure. In Case 4, 19% of the noble gases, 15% of the cesium, 12% of the iodine, and 13% of the tellurium had been released before the hot leg failed.

Table 12 presents the plant conditions for Cases 1, 3, and 4 near the time of the RCS failures. In general, the damage was at the time of the RCS failure was more severe in Case 4 because the transient lasted longer and was at higher temperatures for a longer period of time than the other two cases. The loop heat structure temperatures in Case 4 showed that the temperatures were relatively close together throughout the loops.

4.3.3 Summary. Decreasing the amount of mixing in the steam generator inlet plena resulted in slower core heatups and more energy deposition in the loop structures. Despite the increased energy deposition in the loops, the steam generator tubes were not predicted to fail in either sensitivity calculation. The surge line failed 8.5 min later than in the base case with a 25% increase in the hot leg countercurrent flow (Case 2). With a 50% increase in the hot leg flow (Case 4), the RCS failure location was the hot leg, 44.2 min later than the failure in the base case. The slower heatup also resulted in ballooning of the fuel rod cladding. Extensive sausage-type ballooning in both Cases 3 and 4 resulted in flow redistributions, but not in a change of the basic flow pattern in the core. Temperatures in the core and upper plenum were high enough that melting of some internal structures could occur near the time the RCS piping fails.

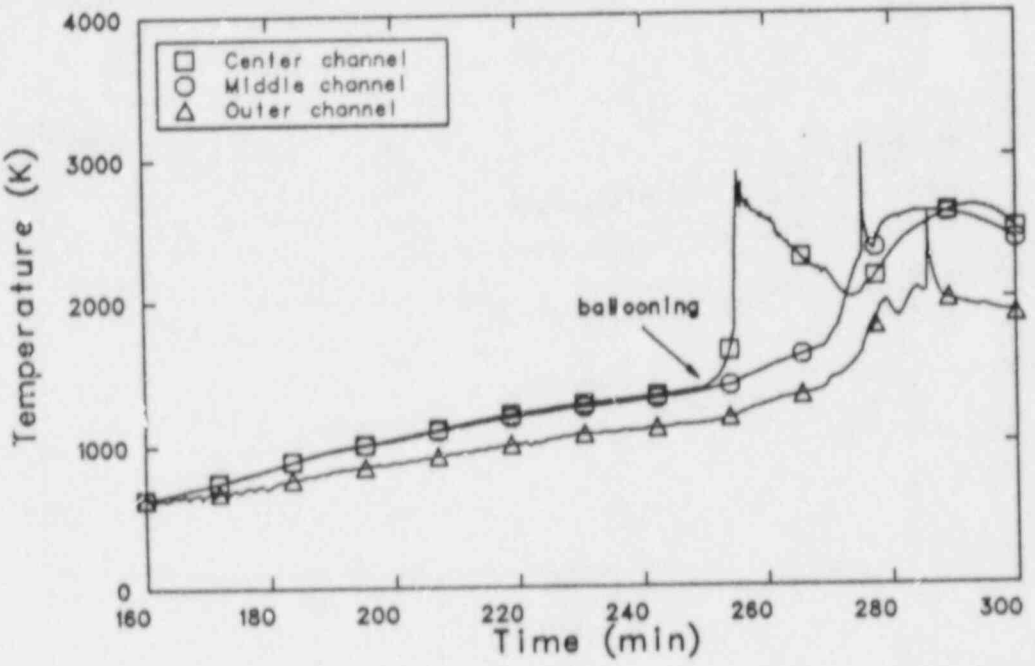

Figure 56. Fuel rod cladding surface temperatures at the top of the three core channels for sensitivity Case 4.

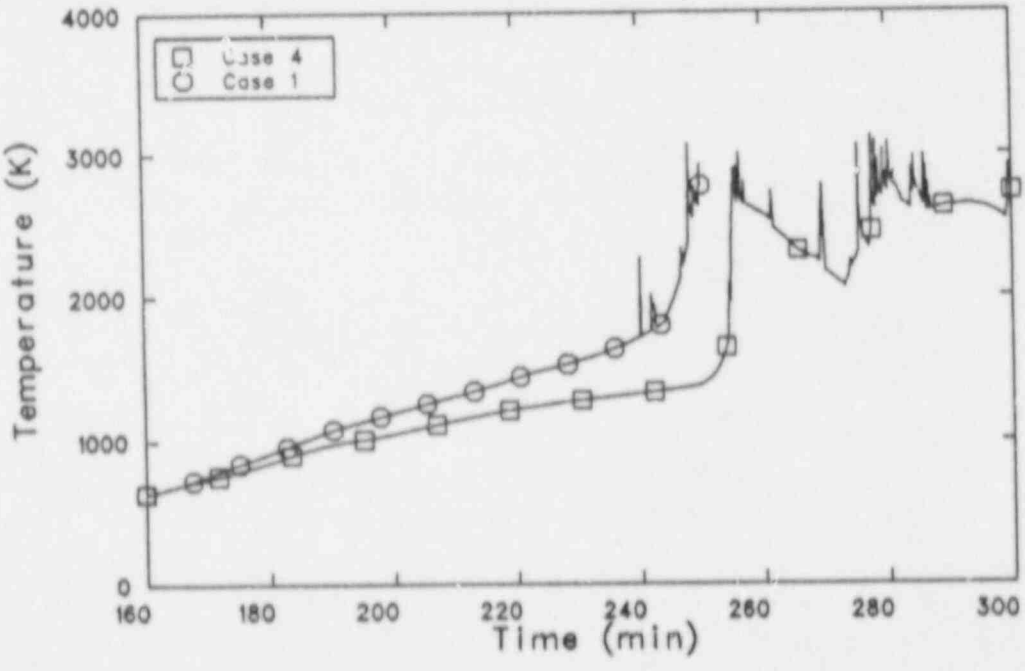

Figure 57. Peak cladding temperatures for sensitivity Cases 4 and 1.

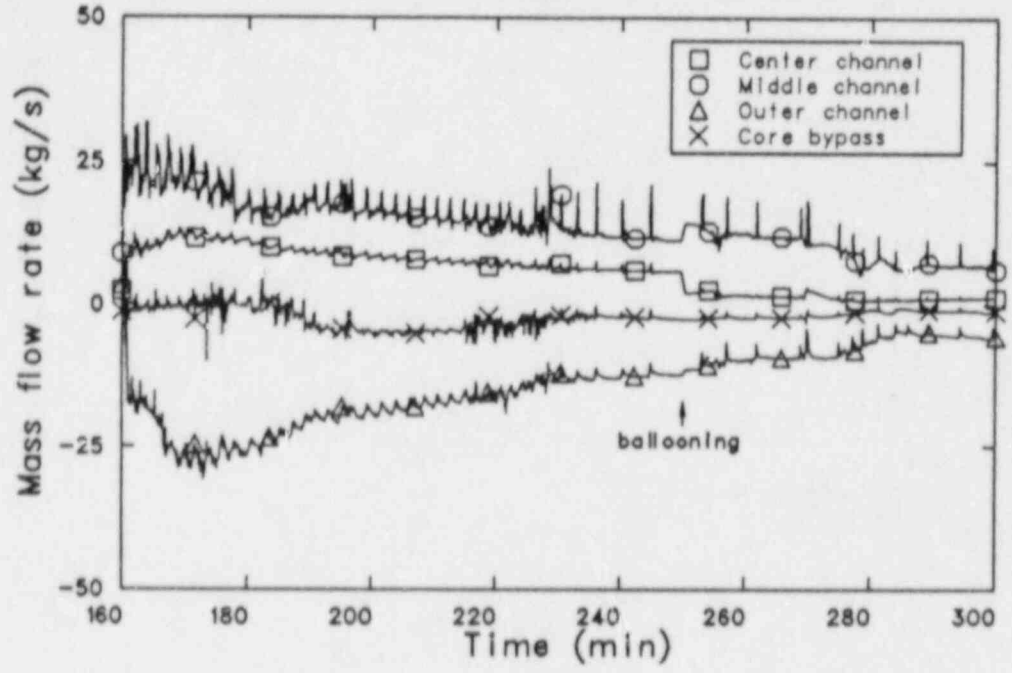

Figure 58. Mass flow rates exiting the three core channels and the core bypass for sensitivity Case 4.

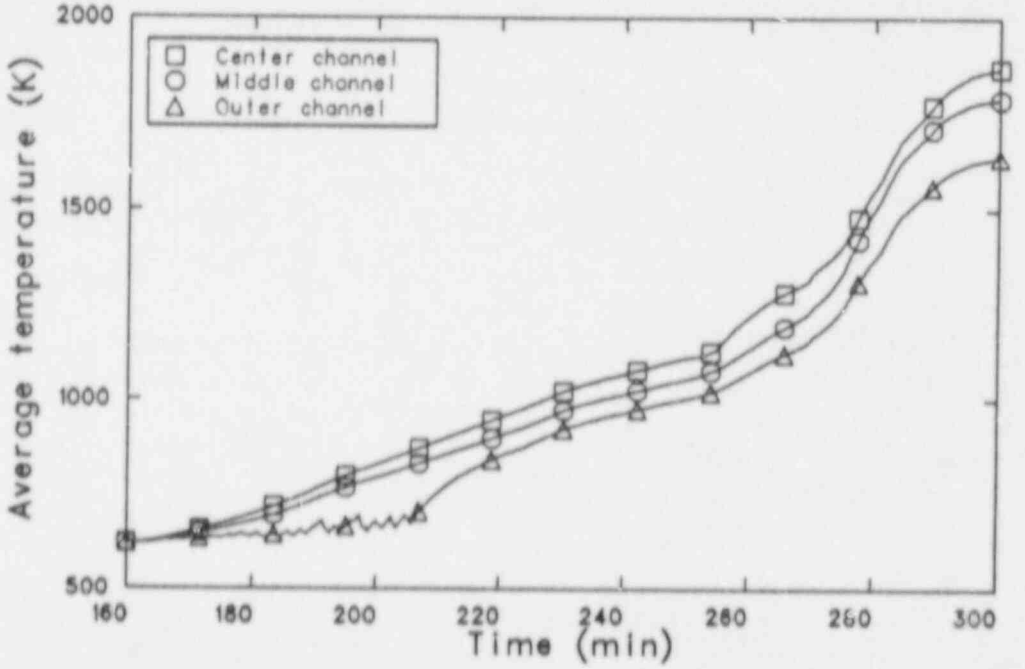

Figure 59. Volume-average temperatures of the upper plenum structures at the outlet of the three core channels for sensitivity Case 4.

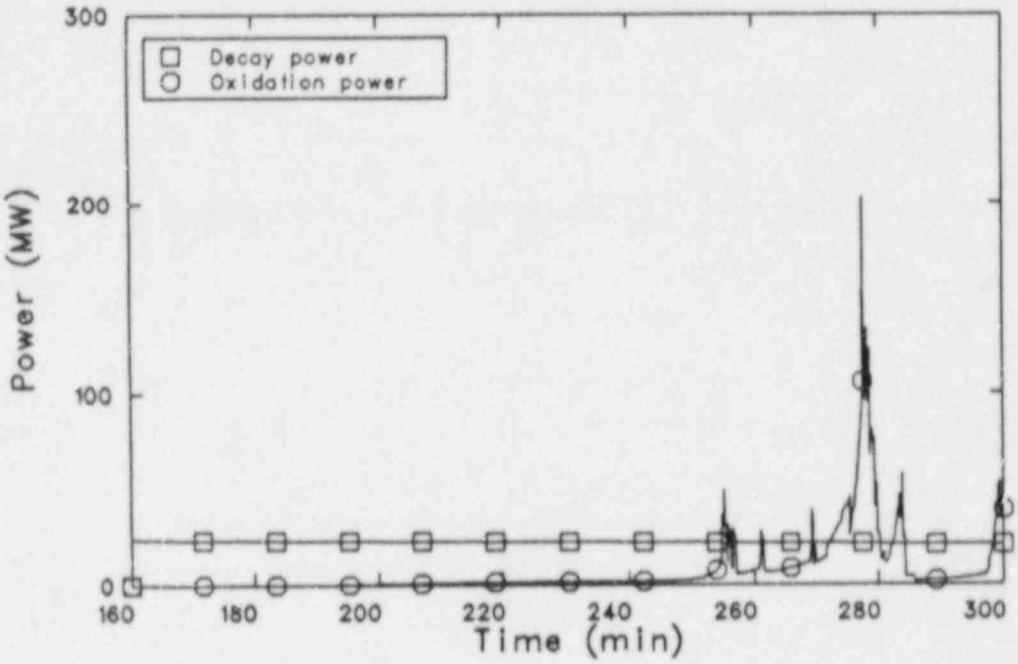

Figure 60. Decay and oxidation power for sensitivity Case 4.

4.4 Piping Heat Loss Sensitivity

How the insulation on the plant will perform under severe accident conditions is not well known. Two sensitivity calculations were performed to investigate the effects of heat loss from the hot leg and surge line piping. The first applied a convective heat transfer coefficient to the outer surface of the pipes. The second applied convective and radiative heat transfer coefficients to the outer surface of the pipe.

4.4.1 Convective Boundary Condition. For Case 5, a constant convective heat transfer coefficient of 28.4 W/m^2K was applied to the outside surface of the hot leg and surge line piping. This is a high heat transfer coefficient for natural convection vapor flow,[16] and, since it is applied directly to the pipe outer wall, no credit is taken for any insulation. The heat sink (containment) temperature was assumed to be a constant 311 K.

The sequence of events for the base case and both heat loss sensitivity cases are contained in Table 13. Convective heat loss through the piping in Case 5 delayed the onset of various stages of core damage, but only by 1-2 min. The surge line failure was delayed by 6.6 min. The larger difference in the surge line failure time occurred because the effects of the heat loss were localized in the piping. The overall energy removal from the core was nearly the same as in the base case, as illustrated in Figure 61, which shows the integral energy removal from the core for Cases 5 and 1. Heat transfer to the coolant loops was slightly higher than in the base case. Heat loss from the piping kept the hot legs and surge line cooler than in the base case.

Figure 62 shows the fraction of the energy removed from the core that was lost through the piping to the containment. The fraction remained fairly constant near 0.04 through most of the transient, indicating that 4% of the energy was being lost at any point in time as well. Since about 75% of the core power was being removed by the coolant, about 3% of the core power (roughly 0.65 MW) was being transferred through the uninsulated pipes. The decrease in the fraction near the end of the calculation occurred when the core was heating up rapidly, with more of the energy removed from the core being stored in structures within the reactor vessel. This was a temporary redistribution of the energy, in that the heat loss would be expected to return to about 4% if the calculation were continued.

The fraction of the energy removed from the core that was deposited in the steam generator tubes and

Table 13. Sequence of events for the base case and piping heat loss sensitivity calculations

Event	Time (min) Case 1	Case 5	Case 6
Fuel rod cladding oxidation begins			
Center channel	185.3	185.5	185.7
Middle channel	186.1	186.0	186.0
Outer channel	192.6	193.1	193.7
Liquid level drops below core	190.2	192.2	192.4
Pressurizer empties of liquid	224.8	225.8	225.0
Fuel rod cladding fails			
Center channel	223.4	224.1	227.5
Middle channel	225.3	226.2	228.9
Outer channel	241.3	241.8	243.0
Fuel rod relocation begins			
Center channel	248.0	249.8	251.8
Middle channel	248.8	250.7	252.5
Outer channel	—	253.2	255.0
RCS pressure boundary fails	246.3	252.9	259.2
RCS failure location	Surge line	Surge line	Surge line
Calculation terminated	250.0	262.9	266.7

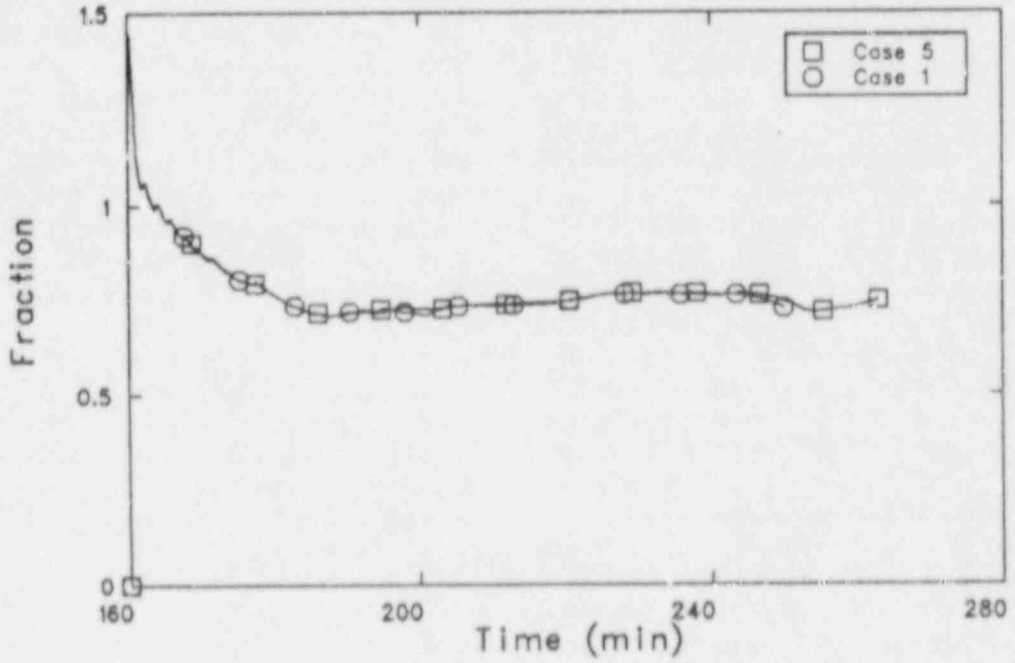

Figure 61. Fraction of the core heat removed by the coolant for sensitivity Cases 5 and 1.

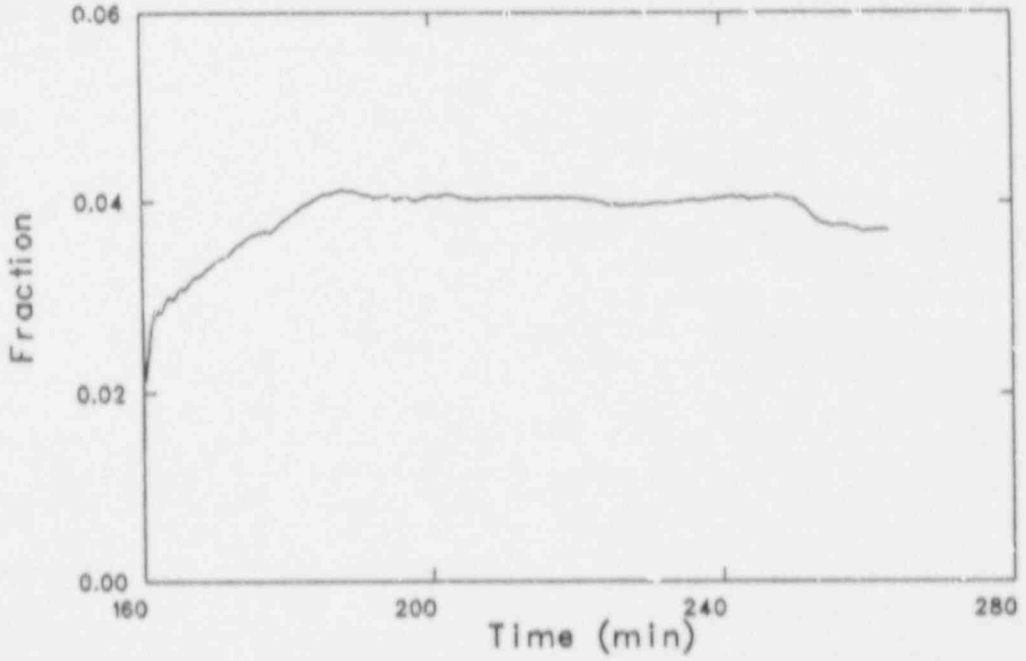

Figure 62. Fraction of the heat removed from the core that was lost through the piping to the containment for sensitivity Case 5.

tube sheets is presented in Figure 63 for Cases 5 and 1. Slightly less energy was deposited in Case 5 because slightly cooler vapor was entering the steam generators. There was more heat transfer from the vapor to the hot leg in Case 5 because of the heat loss to the containment.

The volume-average temperatures of the hottest parts of the hot leg, steam generator tubes, and surge line are presented in Figure 64. As in previous cases, the pressurizer loop structure temperatures were slightly higher than similar structures in the other two loops. The hot leg and surge line temperatures were lower than in the base case because of the heat loss through those pipes, while the steam generator tubes were also cooler than in the base case because of the heat loss through the hot leg piping, which reduced the temperature of the vapor entering the steam generator tubes. The surge line was the hottest structure throughout the transient and the steam generator tubes the coldest for most of the time. The temperatures increased at a faster rate at about 249 min, after the rapid heatup in the core began. Failure of the surge line occurred at 252.9 min, at a temperature of 1256 K. The heat loss through the piping increased the temperature difference across the hot legs from 97 K in the base case to 193 K, and across the surge line from 8 to 45 K near the time of the surge line failure.

Figure 65 plots the hot leg inlet vapor flow against the inlet vapor temperature. The flow at any given temperature was the same as that in the base case (Figure 36). This means that heat loss through the hot leg piping was compensated for by less heat transfer in the steam generators.

Peak cladding temperatures from Cases 5 and 1 are presented in Figure 66. A slight delay in the onset of the rapid heatup near a temperature of 1850 K was the only real difference between the two calculations. The delay resulted from the slightly higher energy removal in the loops in Case 5. Other temperatures throughout the reactor vessel were also very similar in these two cases, as were the flows.

The conditions of the plant near the time of surge line failure are presented in Table 14 for Cases 1, 5, and 6. The differences between Case 5 and Case 1 were the result of the later time in Case 5, which allowed the core to heat up further, oxidize more, and release more fission products.

4.4.2 Convective and Radiative Boundary Condition. In addition to the convective boundary condition applied in Case 5, a radiative heat transfer coefficient was also modeled on the outer pipe wall in Case 6. The pipe was assumed to be a diffuse gray emitter, and the containment was assumed to be a black body absorber at a constant temperature of 311 K. The emissivity varied linearly from 0.24 to 0.31 as the pipe outer surface temperature increased from 480 to 1310 K.[17] The resulting radiation heat transfer coefficient was about 20% of the convection heat transfer coefficient at a wall surface temperature of 600 K, and about 130% at 1150 K.

The sequence of events for Case 6 is presented in Table 13. The effects of the additional heat loss became more evident as the transient progressed and the piping temperatures increased. Fuel rod relocation was delayed by nearly 4 min, and the surge line failure was delayed nearly 13 min, compared to the base case.

The heat loss through the piping represented about 5% of the energy removed from the core, or about 3.8% of the core heat generation. However, as in Case 5, this heat loss from the piping did not affect the hot leg flow rate. Figure 67 shows the hot leg inlet flow as a function of the inlet vapor temperature. The flows at any temperature were the same as those in Case 5 and the base case. The additional heat loss in the hot leg did lead to a further reduction in the heat transfer in the steam generators, and hence in the steam generator tube temperatures.

As in Case 5, the effects of the heat loss were primarily noticeable in the loop piping temperatures. Figure 68 shows the highest hot leg, steam generator tube, and surge line temperatures in the pressurizer loop. The temperatures in the other two loops were lower than those shown in the figure. Again, the loop structure heatup rates increased shortly after the core heatup rate increased at about 250 min. The surge line failed at 259.2 min, when its temperature was 1250 K. The heat loss through the pipes increased the temperature difference between the inner and outer walls. Near the time of the surge line failure, the hot leg temperature difference had increased from 97 K in the base case to 254 K in Case 6, and the surge line temperature difference had increased from 8 to 125 K.

Figure 69 shows the peak cladding temperatures from Case 6 and the base case. The heat loss through the pipes increased the heat removal in the loops, resulting in about a 4 min delay in the onset of the rapid core heatup. Like the cladding temperature, structure temperatures throughout the reactor vessel were very close to the values in the base case.

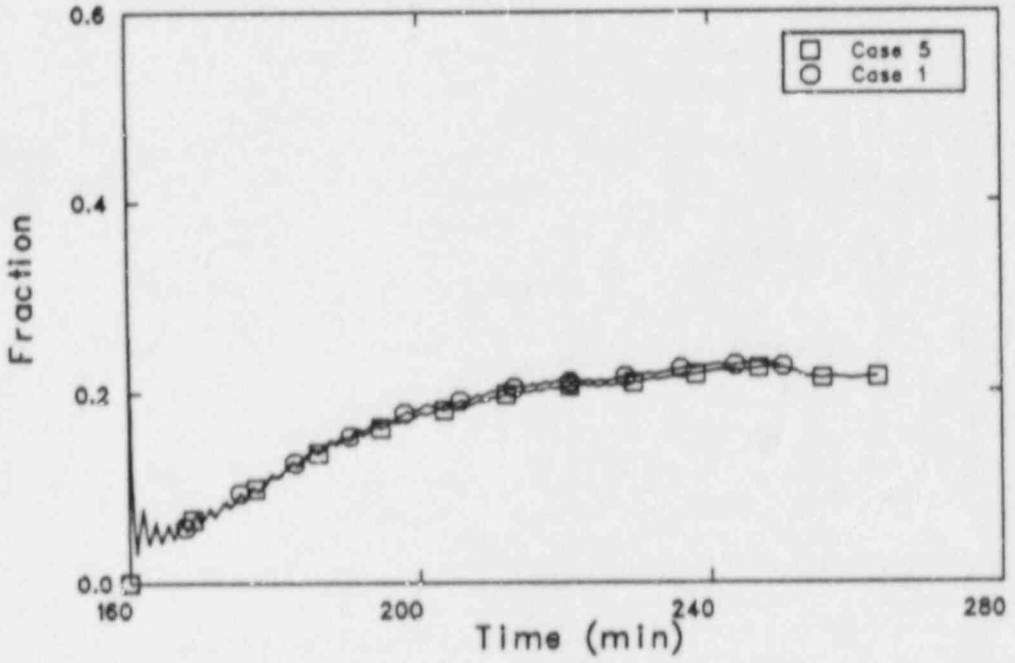

Figure 63. Fraction of the heat removed from the core that was transferred to the steam generator tubes and tube sheets for sensitivity Cases 5 and 1.

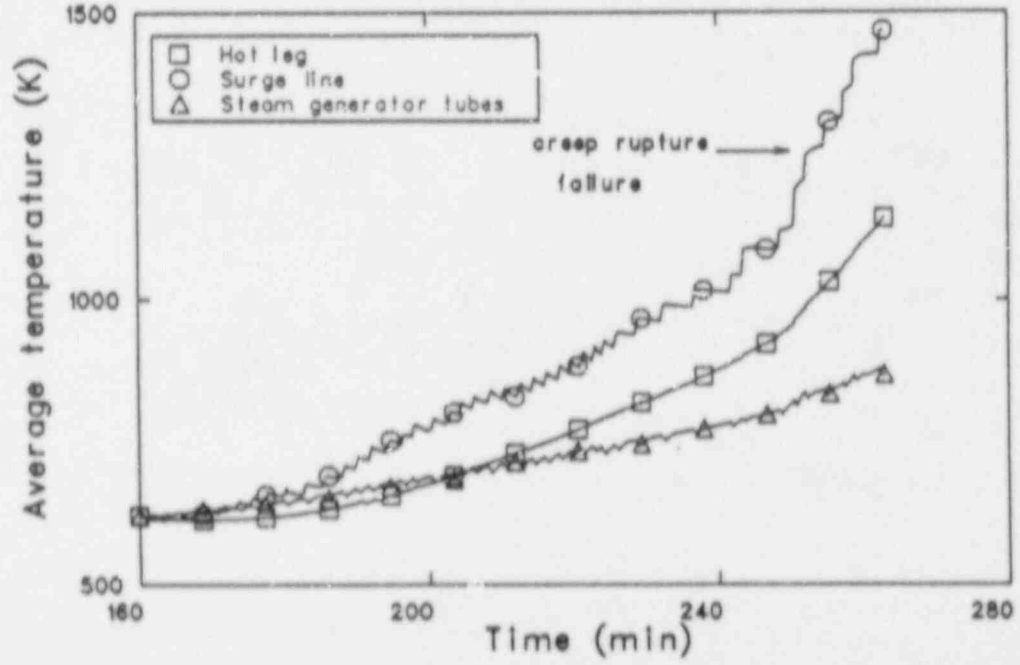

Figure 64. Highest volume-average pipe temperatures in the Loop C hot leg, surge line, and steam generator tubes for sensitivity Case 5.

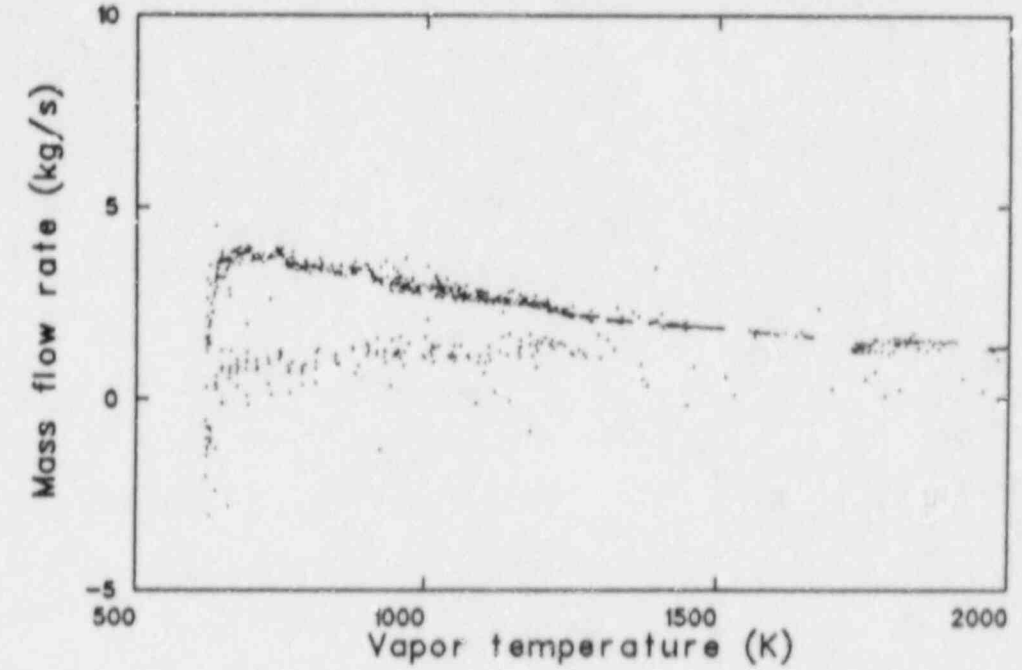

Figure 65. Hot leg flow as a function of hot leg inlet vapor temperature for sensitivity Case 5.

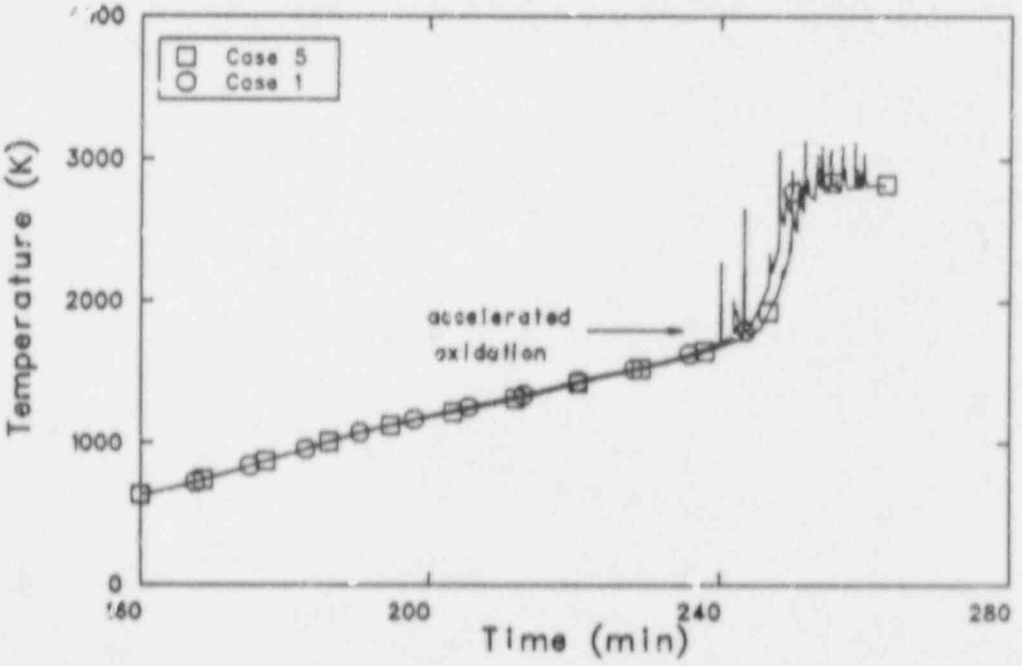

Figure 66. Peak cladding temperatures for sensitivity Cases 5 and 1.

Table 14. Conditions near the time of the surge line failure for the base case and piping heat loss sensitivity calculations

Parameter	Value		
	Case 1	Case 5	Case 6
Time (min)	246.3	250.0	258.3
Center channel peak clad temperature (K)	2066	2577	2809
Middle channel peak clad temperature (K)	1926	2300	2783
Outer channel peak clad temperature (K)	1618	1679	3120
Maximum upper plenum structure temp. (K)	1430	1500	1767
Maximum hot leg temperature (K)	1012	953	1014
Maximum steam generator tube temp. (K)	805	816	848
Maximum surge line temperature (K)	1219	1125	1202
Core outlet flow (kg/s)	11.5	9.4	6.9
Core return flow (kg/s)	9.0	8.0	5.2
Upper plenum recirculating flow	37.1	36.4	30.3
Reactor vessel collapsed liquid	1.38	1.33	1.11
Core heat removal (%)[a]	75.4	74.6	72.3
Core energy removed and deposited in:[a]			
Loop A structures (%)	9.0	8.3	8.1
Loop B structures (%)	9.0	8.3	8.1
Loop C structures (%)	11.8	11.1	10.7
Hot leg piping (%)	4.8	3.3	3.2
Steam generator tubes, tube sheets (%)	23.1	22.5	21.5
Surge line piping (%)	0.8	0.7	0.6
Core energy removed through piping (%)[a]	—	4.0	4.7
Center channel oxidation (%)	20	30	55
Middle channel oxidation (%)	17	23	55
Outer channel oxidation (%)	10	11	54
Hydrogen generated (kg)	109	152	384
Fuel relocation (%)	0.0	0.0	0.1
Fuel rod cladding relocation (%)	0.0	0.0	0.0
Control rod relocation (%)	33	50	60
Xenon/krypton release (%)	1.0	1.6	18.8
Cesium release (%)	0.6	1.0	14.8
Iodine release (%)	0.0	0.3	12.8
Tellurium release (%)	1.3	1.9	12.5
Surge line failure time (min)	246.3	252.9	259.2

a. Integral quantities from the start of the calculation.

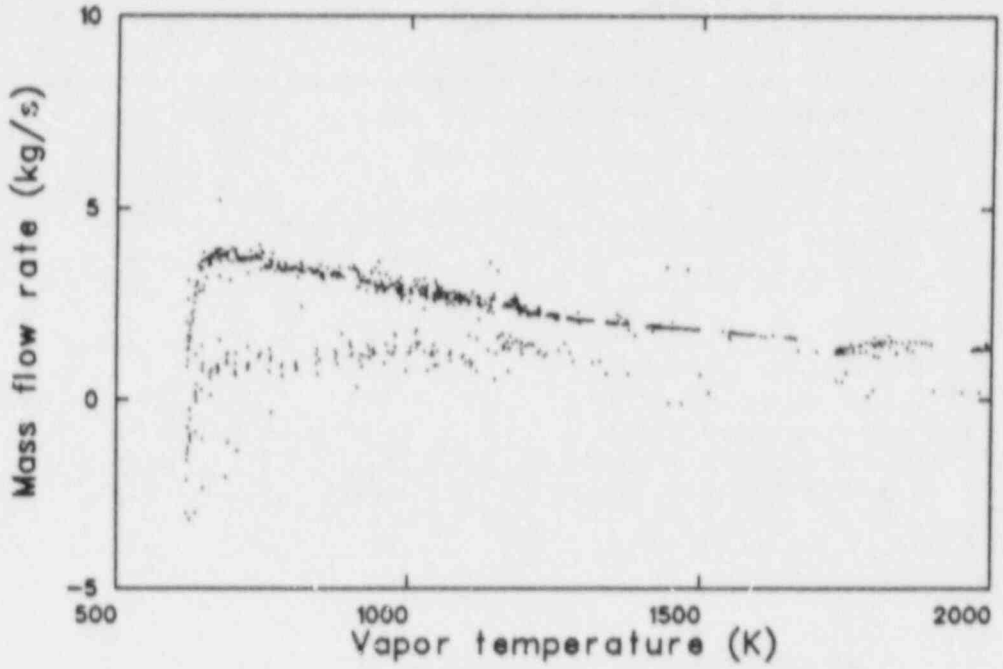

Figure 67. Hot leg flow as a function of hot leg inlet vapor temperature for sensitivity Case 6.

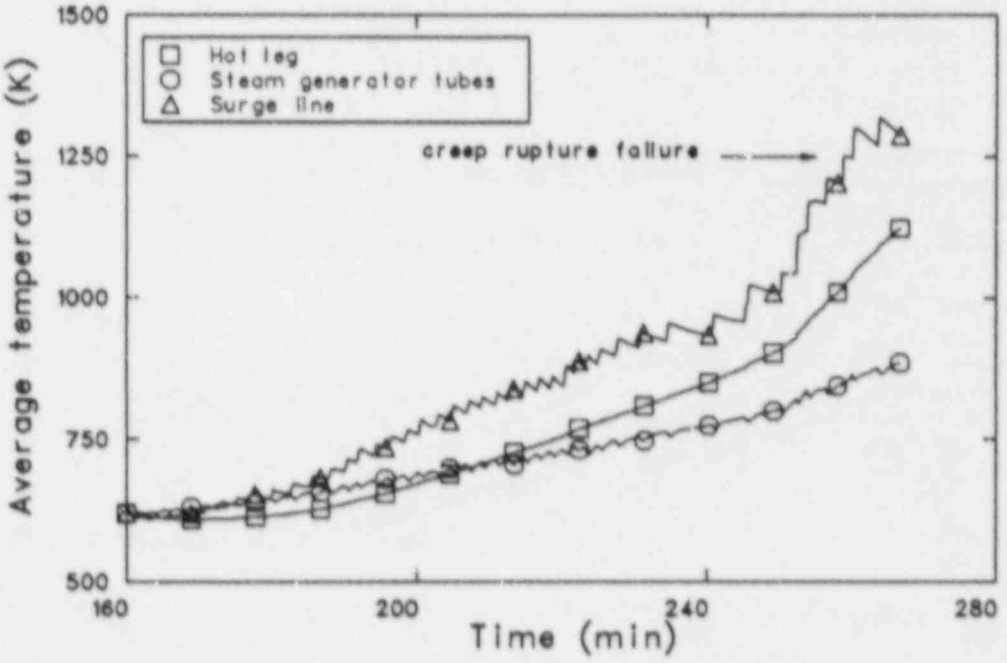

Figure 68. Highest volume-average pipe temperatures in the Loop C hot leg, surge line, and steam generator tubes for sensitivity Case 6.

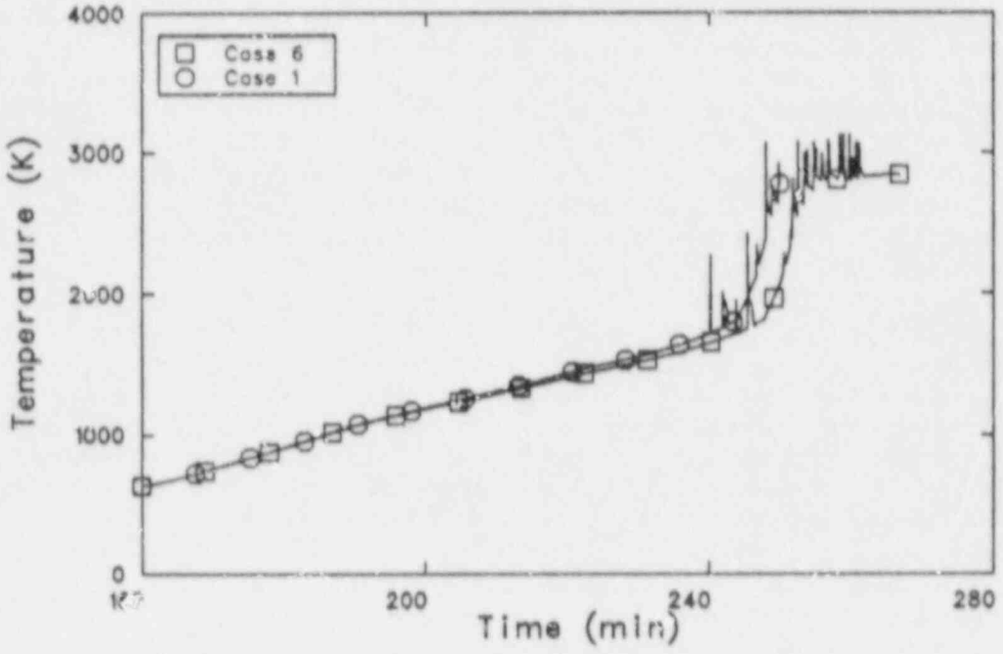

Figure 69. Peak cladding temperatures for sensitivity Cases 6 and 1.

Some of the plant conditions near the time of the surge line failure are presented in Table 14. Differences in the temperatures and the extent of core damage were attributable to the later time at which the conditions were evaluated in Case 6, since the core heatups were similar. The effects of the later time, and longer time at high temperatures, are seen particularly in the outer channel cladding temperature and the extent of the core damage. The cladding in the outer channel in Case 6 had already gone through the heatup associated with accelerated oxidation, so its peak temperature was much higher than in the other two cases. The longer time at high temperatures throughout the core also resulted in more oxidation and much greater fission product release in Case 6 than in Cases 1 and 5. Because of the increased heat transfer from the hot leg and surge line piping, those structures retained less of the energy removed from the core in Case 6 than in Case 1. As discussed above, the steam generator tubes and tube sheets also removed a smaller fraction of the core energy because of the heat loss along the hot legs.

4.4.3 Summary. Modeling of heat loss from the surge line and hot legs delayed the surge line failure compared to the base case. The delay was 6.6 min with a convective boundary condition, and 12.9 min with a convective and radiative boundary condition. The heat loss resulted in smaller delays in the onset of rapid core heatup and relocation because most of the effects of the heat loss were localized in the hot legs and surge line. Increased heat transfer from the vapor flowing in the hot legs led to lower temperatures in the steam generators, and hence lower steam generator tube temperatures than in the base case. The piping heat loss did not affect the hot leg flow rate, in that the flow rate at any given inlet vapor temperature was unchanged from the base case in both Case 5 and Case 6.

4.5 Crossflow Resistance Sensitivity

The natural circulation flow within the reactor vessel has both axial and radial components. Many structures are present in the upper plenum and core to provide resistance to flow in the radial direction, such as fuel rods, control rod drive shafts, control rod guide housings, and support columns. The sensitivity of the calculated in-vessel flows was investigated by changing the crossflow loss coefficients. These loss coefficients were increased and decreased by factors of 10.

4.5.1 Decreased Upper Plenum Crossflow Resistance. The Case 7 crossflow loss coefficients in the upper plenum were a factor of 10 lower than the base case model values. The upper plenum recirculating flow for Cases 7 and 1 are shown in Figure 70. The decreased crossflow resistance in Case 7 resulted in a higher recirculating flow in the upper plenum than in the base case. Figure 71 shows the upper plenum recirculating flow as a function of the vapor temperature at the outlet of the center core channel. The flow at any given temperature was 30-40% higher than in the base case.

The increased flow in the upper plenum changed the energy distribution in the upper plenum slightly, increasing the temperatures of the vapor and structures in the outer channel. The higher vapor temperatures resulted in slightly less flow returning to the core, which in turn caused the core to heat up slightly faster. Figure 72 shows the vapor temperature in the upper plenum just above the outer core channel for Cases 7 and 1. Slightly higher temperatures were also present in the structures above the outer core channel and in the core barrel temperatures in the upper plenum.

Figure 73 shows the peak cladding temperatures from Cases 7 and 1. The temperatures began to deviate after 215 min, the result of the lower return flow from the upper plenum. The more rapid heatup of the core associated with the change in the Zircaloy oxidation kinetics began at about 240 min.

The amount of core energy removed by the coolant is shown in Figure 74 for Cases 7 and 1. The energy removal was nearly identical in both cases until late in the calculations, when the difference in the timing of the rapid core heatup was reflected in an earlier drop in the removal fraction in Case 7.

Figure 75 presents the flow entering the top of the Loop A hot leg for Cases 7 and 1. The flow rates when the PORVs were closed were nearly identical, as was the flow at any given temperature.

The temperatures of some of the loop structures are shown in Figure 76. The temperature differences between the loops were small, with the pressurizer loop temperatures being higher. The temperature increase during the transient was steady, with the surge line heatup accelerating when the pressurizer emptied of liquid at about 225 min (because liquid was no longer draining through the surge line, helping to cool it), and both the surge line and hot leg heatup rates increasing when the core heatup accelerated at about 240 min (because hotter vapor was leaving the reactor vessel). Creep rupture of the surge line occurred at 244.9 min, at a temperature of 1258 K.

Table 15 presents the sequence of events for this case, as well as for the other crossflow resistance sensitivity cases and the base case. The damage progression was slightly accelerated compared to the base case, with fuel rod relocation beginning 3.3 min earlier and the surge line failing 1.4 min earlier.

Table 16 lists some of the plant conditions near the time of the surge line failure for the base case and the crossflow resistance sensitivity cases. In comparing Cases 7 and 1, it is seen that the temperatures in Case 7 were higher throughout the system, because of the earlier rapid core heatup. The core damage was slightly more extensive for the same reason. The energy removal in the loops was nearly identical in the two cases, indicating that the hot leg flow was unaffected by the changes in the upper plenum model, as would be expected.

4.5.2. Decreased Core Crossflow Resistance. In sensitivity Case 8, the crossflow loss coefficients between the three core channels were decreased by a factor of 10, making it easier for flow to move radially between the channels.

The sequence of events for Case 8 is presented in Table 15. The core heatup and the onset of various damage stages occurred slightly earlier than in the base case. An increased recirculating flow within the core was responsible for the faster core heatup. At the top of the core, the upper end boxes present a reasonably large axial flow resistance that tends to drive the flow radially. In the base case, the radial (crossflow) resistances were also large, so that the radial flow component between the uppermost core nodes was small. With the decreased crossflow resistance, this flow increased, providing more vapor from the top of the middle channel to the top of the outer channel. This vapor then mixed with the vapor entering the core from the upper plenum, increasing its temperature. The increased vapor temperature, and hence lower vapor density, in the outer channel resulted in a lower buoyant driving head, reducing both the recirculating flow between the core and upper plenum, and the distance the outer channel flow was able to penetrate down the core. With less flow, less cooling of the core occurred, and the core heated up faster.

The increased outer channel temperature is illustrated in Figure 77, which presents the fuel rod cladding surface temperatures at the top of the core for each of the three core channels. The temperatures were closer together than in the base case

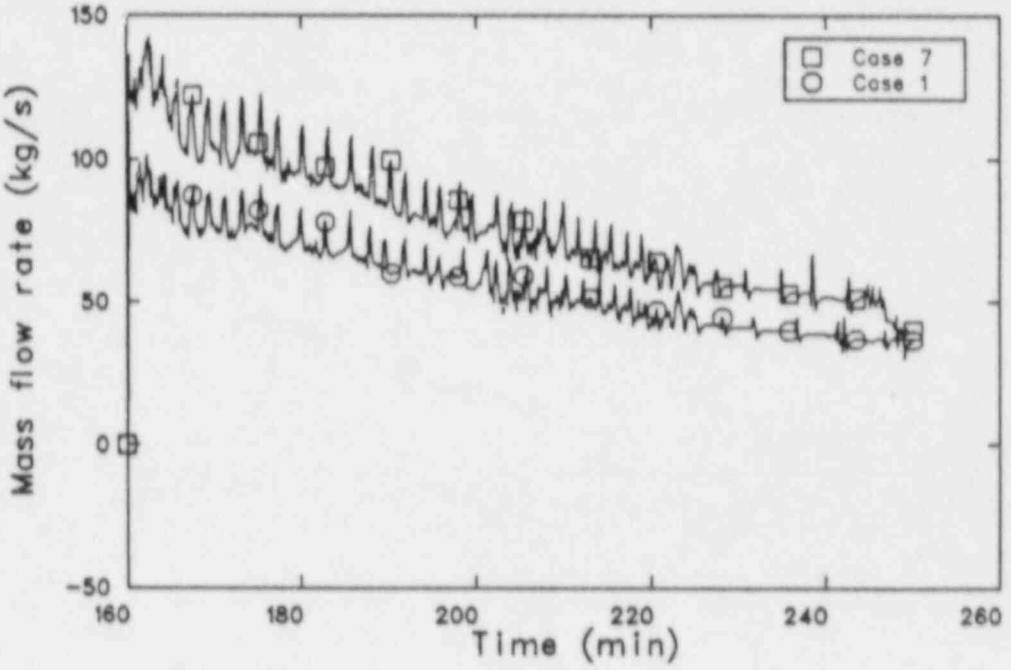

Figure 70. Upper plenum recirculating mass flow for sensitivity Cases 7 and 1.

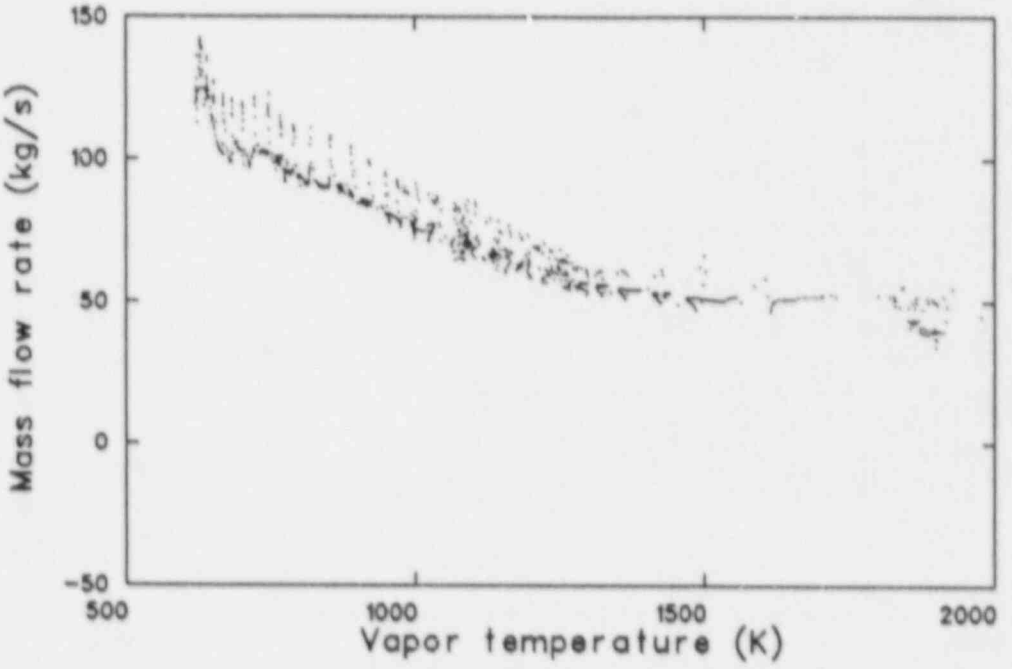

Figure 71. Upper plenum recirculating mass flow rate as a function of maximum upper plenum vapor temperature for sensitivity Case 7.

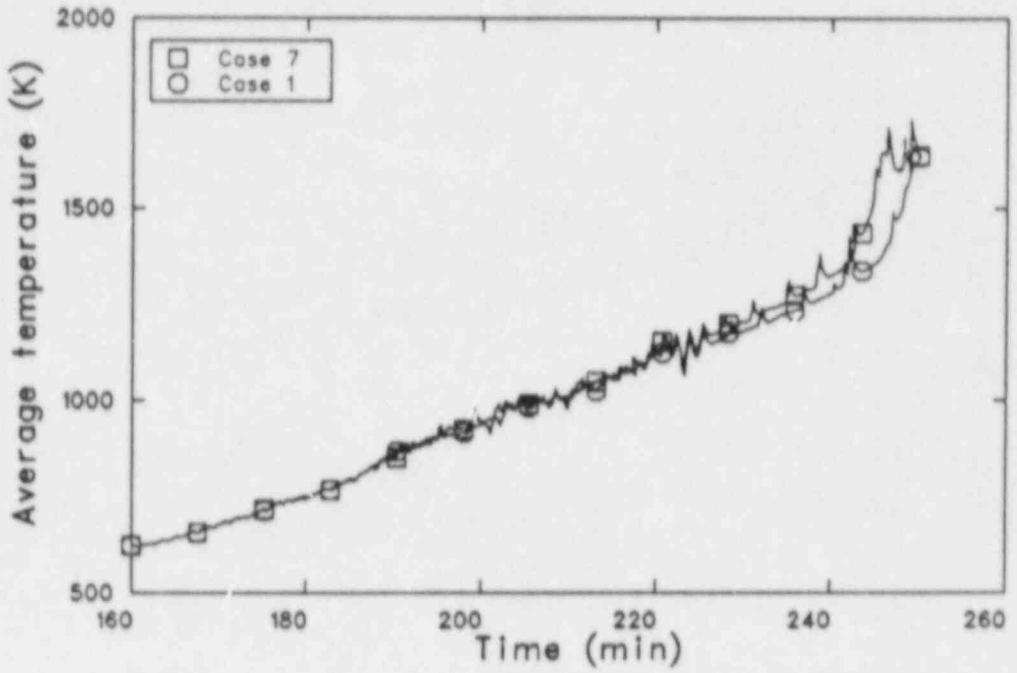

Figure 72. Volume-average temperature of the upper plenum structure at the outlet of the outer core channel for sensitivity Cases 7 and 1.

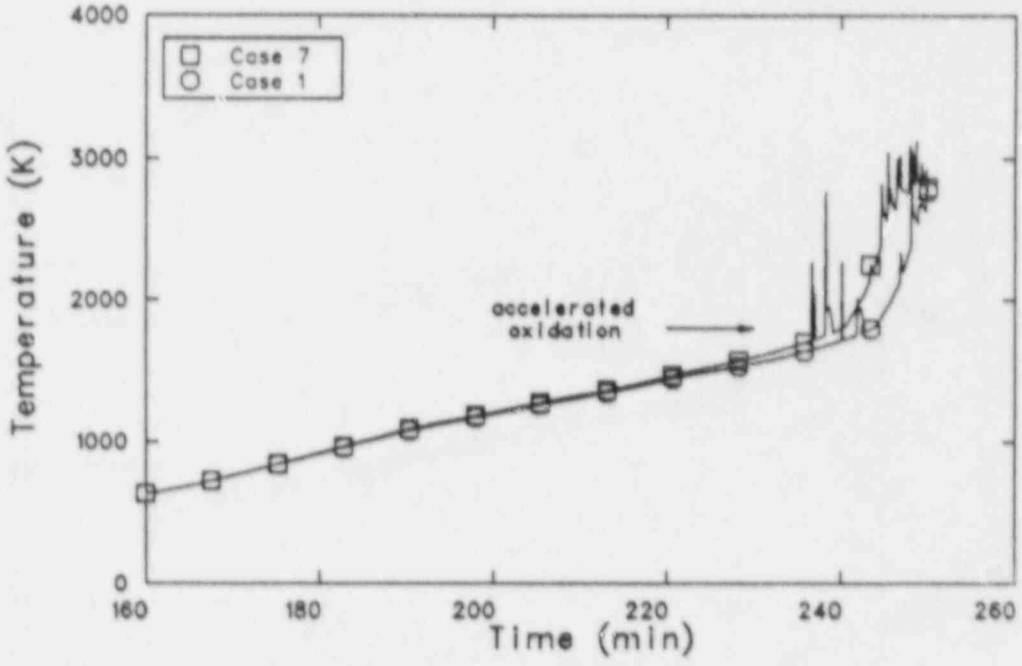

Figure 73. Peak cladding temperatures for sensitivity Cases 7 and 1.

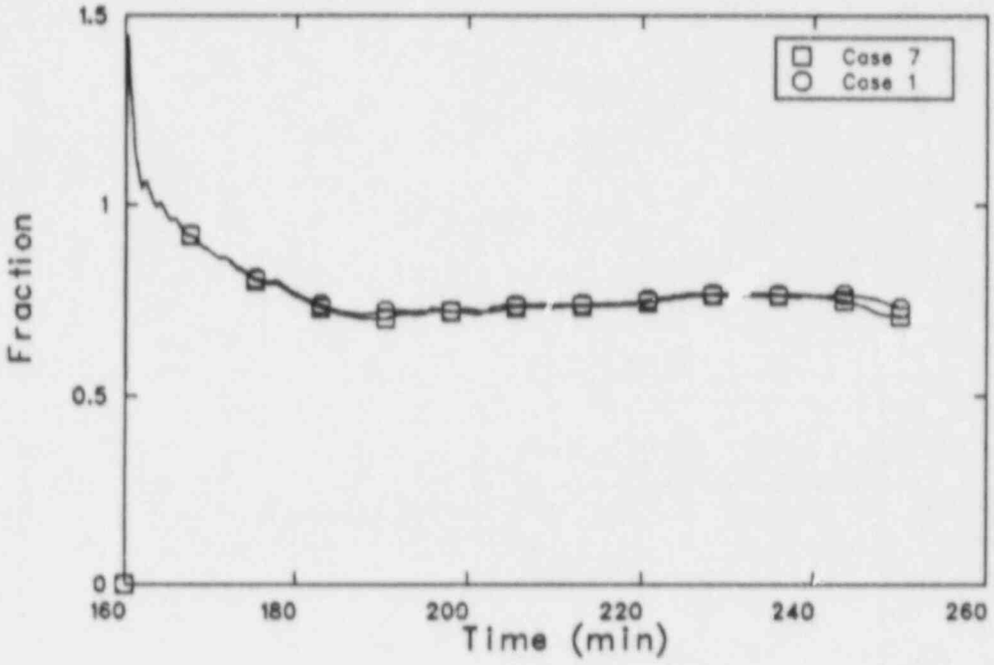

Figure 74. Fraction of the core heat removed by the coolant for sensitivity Cases 7 and 1.

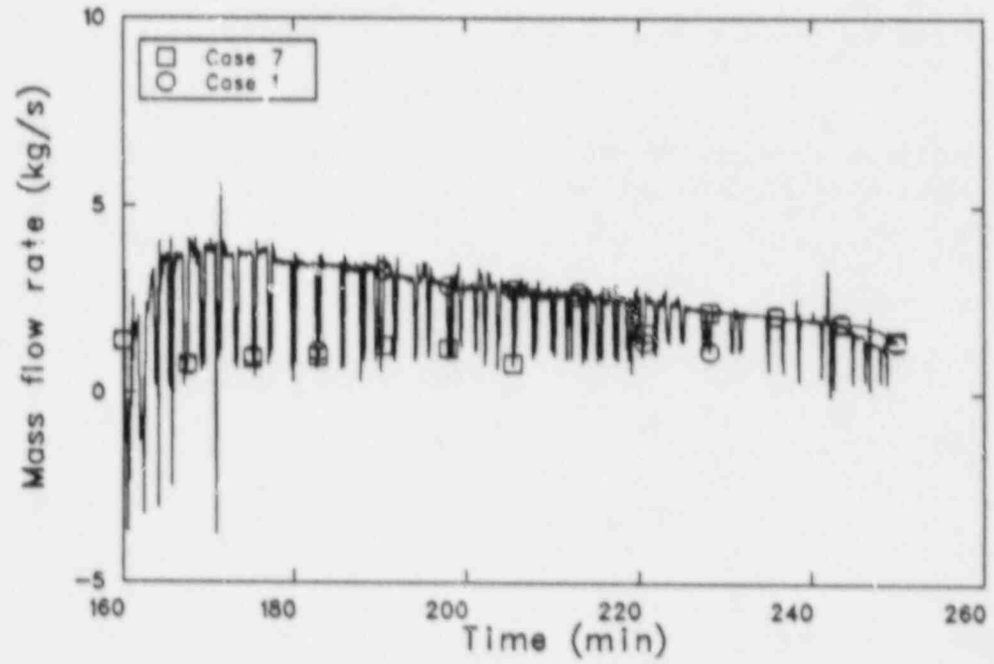

Figure 75. Upper hot leg mass flow in Loop A for sensitivity Cases 7 and 1.

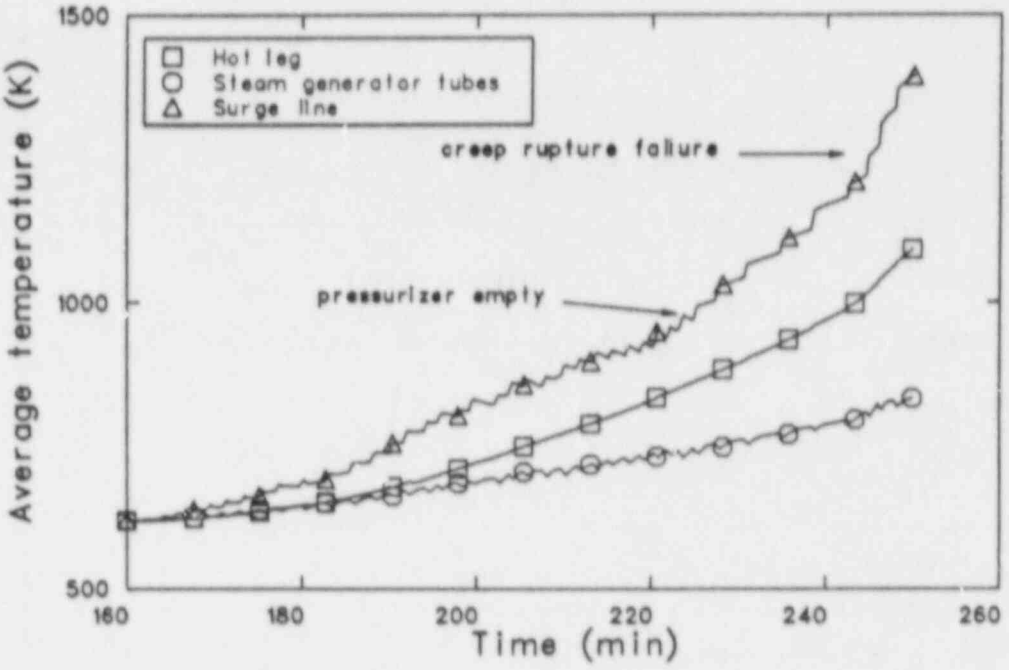

Figure 76. Highest volume-average pipe temperatures in the Loop C hot leg, surge line, and steam generator tubes for sensitivity Case 7.

Table 15. Sequence of events for the base case and crossflow resistance sensitivity calculations

Event	Time (min) Case 1	Case 7	Case 8	Case 9
Fuel rod cladding oxidation beings				
Center channel	185.3	184.8	185.0	185.6
Middle channel	186.1	185.3	185.3	186.9
Outer channel	192.6	191.5	191.5	194.3
Liquid level drops below core	190.2	189.5	189.4	192.2
Pressurizer empties of liquid	224.8	224.7	226.0	224.5
Fuel rod cladding balloons				
Center channel	—	—	—	216.7 +
Middle channel	—	—	—	227
Outer channel	—	—	—	—
Fuel rod cladding fails				
Center channel	223.4	220.9	221.3	223.7
Middle channel	225.3	222.9	222.9	226.8
Outer channel	241.3	237.5 +	236.3	236.4
Fuel rod relocation begins				
Center channel	248.0	244.7	243.5	236.5
Middle channel	248.8	245.3	244.0	233.2
Outer channel	—	247.8	246.0	242.2
RCS pressure boundary fails	246.3	244.9	244.6	233.9
RCS failure location	Surge line	Surge line	Surge line	Surge line
Calculation terminated	250.0	250.0	250.0	246.3

able 16. Conditions near the time of the surge line failure for the base case and crossflow resistance sensitivity calculations

Parameter	Value			
	Case 1	Case 7	Case 8	Case 9
Time (min)	241.7	241.7	241.7	233.3
Center channel peak clad temperature (K)	1752	1935	2058	1698
Middle channel peak clad temperature (K)	1714	1807	1972	2398
Outer channel peak clad temperature (K)	1513	1579	1636	1400
Maximum upper plenum structure temperature (K)	1355	1383	1396	1339
Maximum hot leg temperature (K)	973	982	980	949
Maximum steam generator tube temperature (K)	783	793	794	778
Maximum surge line temperature (K)	1164	1179	1159	1245
Core outlet flow (kg/s)	12.9	11.8	10.8	12.1
Core return flow (kg/s)	8.6	8.7	8.0	5.7
Upper plenum recirculating flow (kg/s)	35.7	50.7	39.2	16.8
Reactor vessel collapsed liquid level (m)	1.48	1.43	1.40	1.81
Core heat removal (%)[a]	76.1	75.4	74.4	72.6
Core energy removed and deposited in:[a]				
Loop A structures (%)	8.9	8.9	8.8	8.6
Loop B structures (%)	8.9	8.9	8.8	8.6
Loop C structures (%)	11.6	11.6	11.5	11.0
Hot leg piping (%)	4.6	4.7	4.7	4.5
Steam generator tubes, tube sheets (%)	22.8	22.7	22.6	21.9
Surge line piping (%)	0.8	0.8	0.8	1.0
Center channel oxidation (%)	14	17	19	11
Middle channel oxidation (%)	12	15	16	31
Outer channel oxidation (%)	7	9	10	4
Hydrogen generated (kg)	80	96	108	150
Fuel relocation (%)	0.0	0.0	0.0	0.5
Fuel rod cladding relocation (%)	0.0	0.0	0.0	7.2
Control rod relocation (%)	3	27	35	33
Xenon/krypton release (%)	0.8	0.9	0.9	1.8
Cesium release (%)	0.5	0.5	0.5	1.3
Iodine release (%)	0.0	0.0	0.0	0.6
Tellurium release (%)	1.1	1.2	1.3	2.1
Surge line failure time (min)	246.3	244.9	244.6	233.9

a. Integral quantities from the start of the calculation.

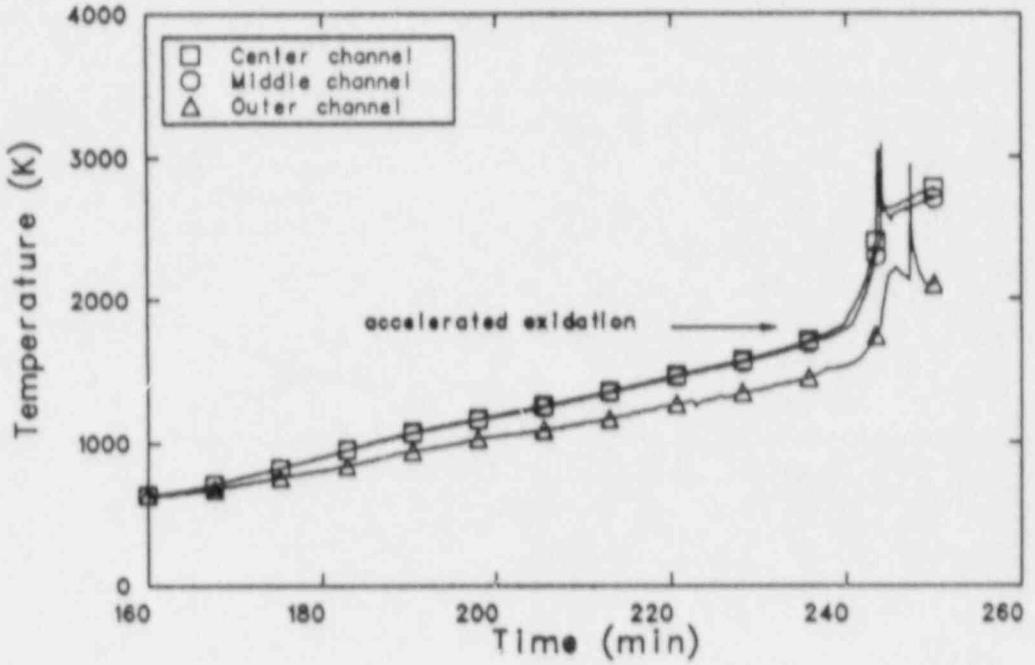

Figure 77. Fuel rod cladding surface temperatures at the top of the three core channels for sensitivity Case 8.

(Figure 25), particularly in the center and middle channels, which were nearly identical.

Peak cladding temperatures from Cases 8 and 1 are presented in Figure 78. The temperatures began to deviate at about 217 min, with the higher temperatures in Case 8 leading to the rapid core heatup about 4 min sooner than in the base case.

The increased recirculation within the core coupled with the decreased flow between the core and upper plenum combined to reduce the amount of energy removed from the core. Figure 79 shows the fraction of the core energy removed by the coolant during the transient for Cases 8 and 1. As did the temperatures, the energy removal began to deviate at about 217 min. The lower heat removal in Case 8 led to the faster core heatup. The faster core heatup led to a faster heatup of structures in the upper plenum and the coolant loops.

Figure 80 shows the upper plenum metal temperatures at the outlet of the center and outer core channels for Cases 8 and 1. The temperatures in Case 8 were lower until about 216 min because more energy was being retained in the core rather than transferred to the upper plenum. The Case 8 temperatures were higher later in the transient because the rapid core heatup provided hotter vapor to the upper plenum earlier than in the base case. Other structures in the reactor vessel exhibited similar behavior compared to the base case.

Flows leaving the top of the core and core bypass are shown in Figure 81, together with the flow leaving the outer channel in the base case. The flow behavior was the same as in the base case, but the magnitudes of the flows were lower, similar to what is shown for the outer channel. The upper plenum recirculating flow was the same as in the base case at any given center core channel outlet temperature. However, as discussed earlier, the initial upper plenum heatup was slower than in the base case, so the flow was lower.

Volume-average metal temperatures in the pressurizer loop hot leg, surge line, and steam generator tubes are shown in Figure 82. As in the other calculations, the non-pressurizer loop structure temperatures were lower than those in the pressurizer loop. The surge line heatup rate increased at about 226 min, when the pressurizer dried out, because liquid draining from the pressurizer was no longer available to help cool the pipe. The hot leg and surge line heatup rates both increased when the core heatup rate increased at about 235 min. Creep rupture of the surge line occurred at 244.6 min, when its temperature was 1252 K.

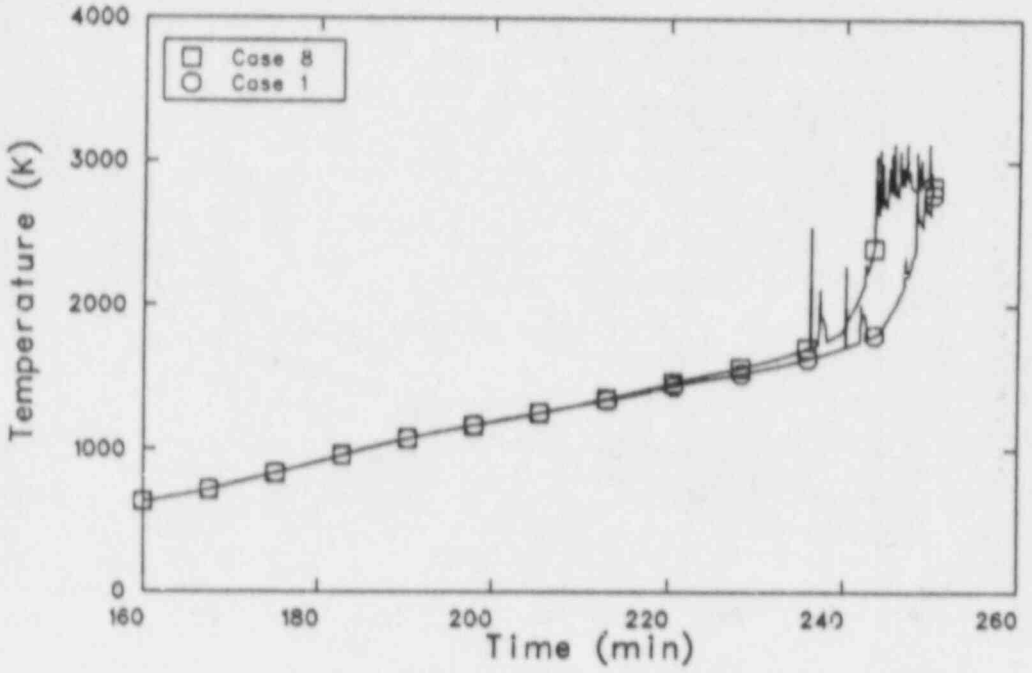

Figure 78. Peak cladding temperatures for sensitivity Cases 8 and 1.

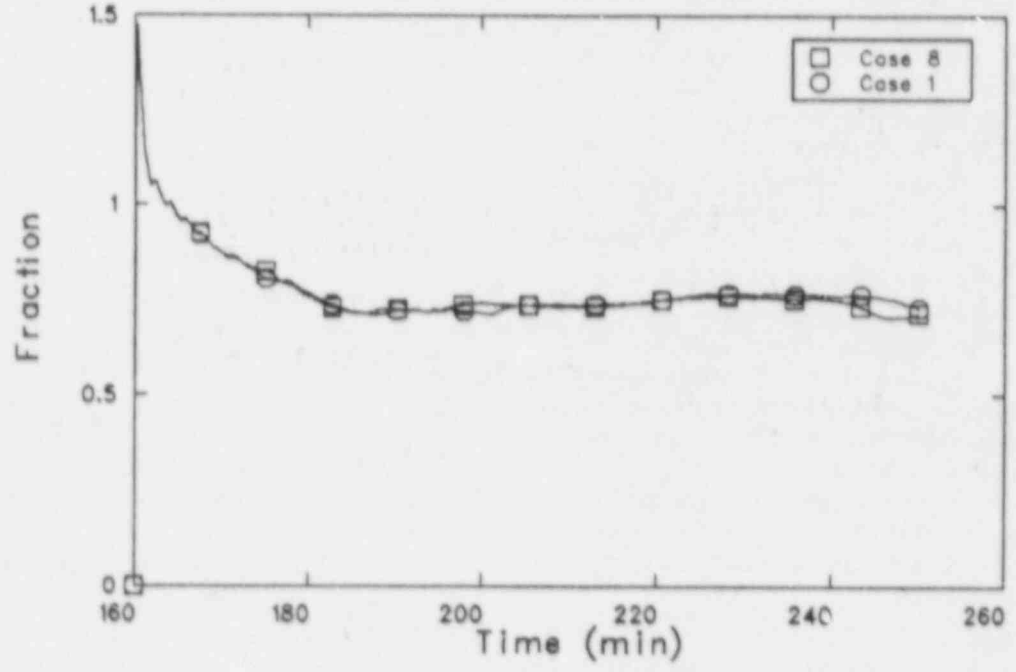

Figure 79. Fraction of the core heat removed by the coolant for sensitivity Cases 8 and 1.

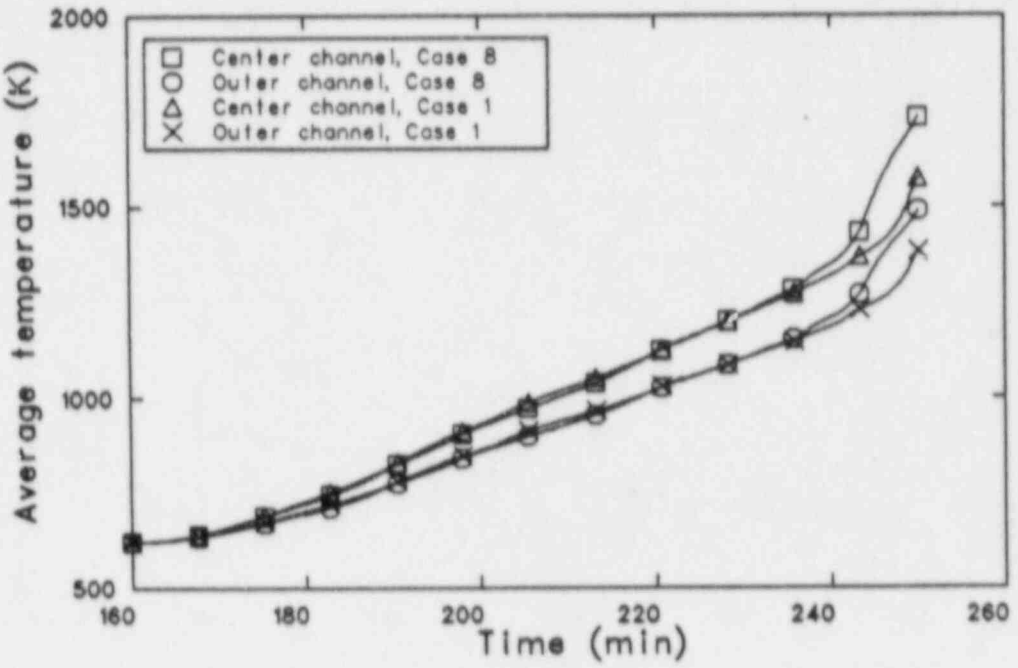

Figure 80. Volume-average temperatures of the upper plenum structures at the outlet of the center and outer core channels for sensitivity Cases 8 and 1.

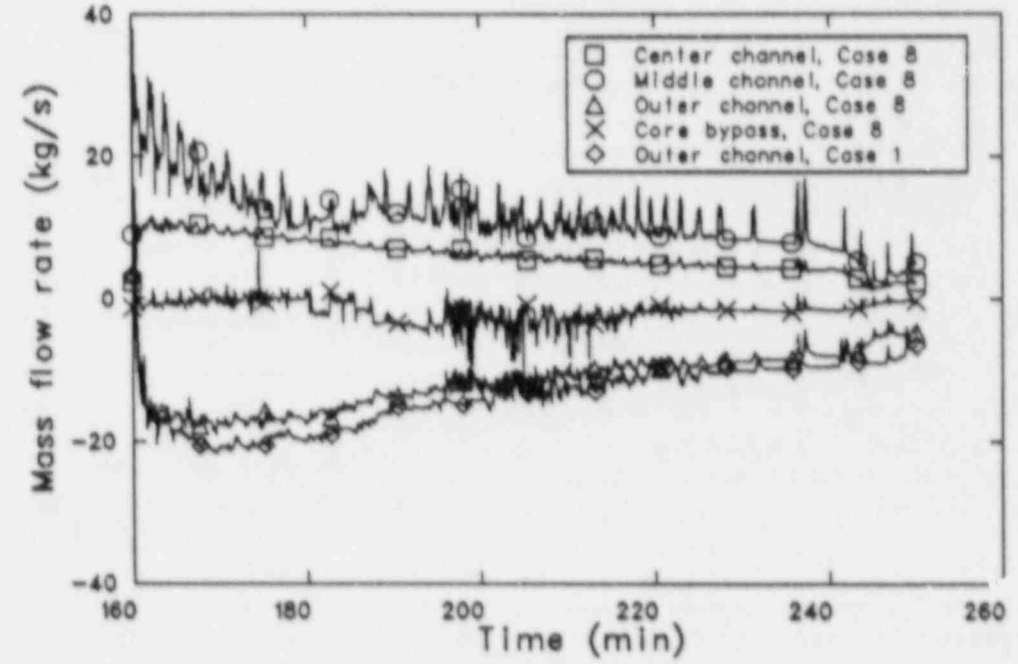

Figure 81. Mass flow rates exiting the three core channels, the core bypass, and recirculating in the upper plenum for sensitivity Case 8.

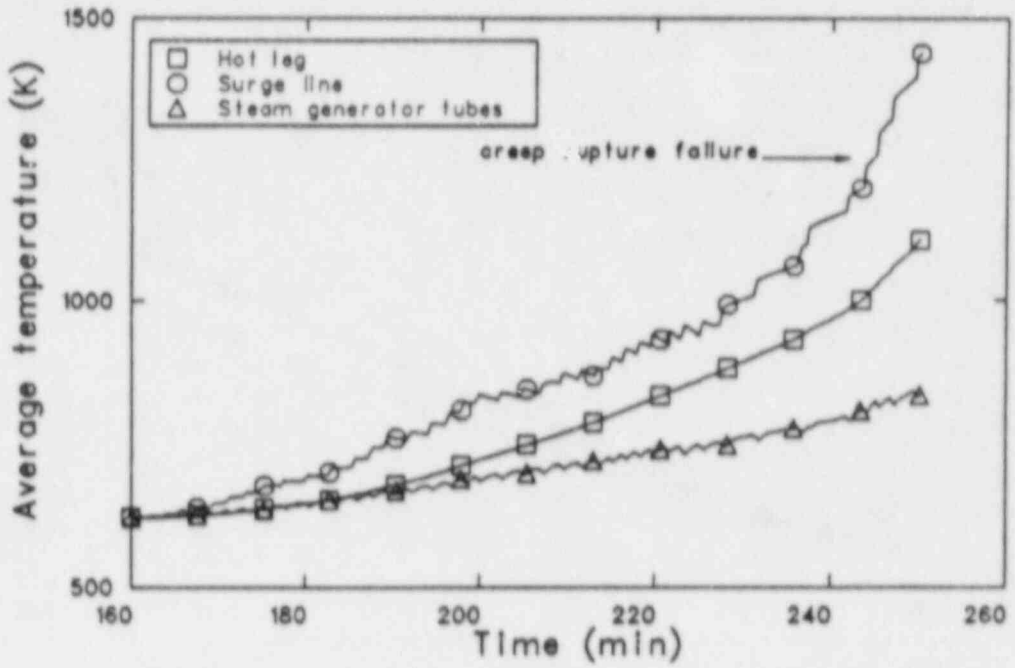

Figure 82. Highest volume-average pipe temperatures in the Loop C hot leg, surge line, and steam generator tubes for sensitivity Case 8.

Table 16 lists some of the conditions in the RCS near the time of the surge line failure. The reactor vessel temperatures were higher in Case 8 than in the base case because the rapid core heatup had already begun. The loop structure temperatures were only slightly higher, or in the case of the surge line lower, than those in the base case, indicating that the temperature increase in the reactor vessel had not yet propagated fully into the loops. The lower surge line temperature may also indicate that the PORVs had not cycled since the core heatup rate increased, since PORV cycling is needed to draw hotter vapor into the surge line. The heat transfer to the loops was nearly the same as in the base case. The higher hydrogen generation and fission product release in Case 8 resulted from the higher core temperatures.

4.5.3 Increased Core and Upper Plenum Crossflow Resistance. The crossflow loss coefficients in both the core and the upper plenum in Case 9 were increased by a factor of 10 over the values used in the base case. This change tended to make the flow more one-dimensional in the axial direction.

The sequence of events for Case 9 is contained in Table 15. Several important differences from the base case are indicated. Ballooning occurred in both the center and middle core channels. Core relocation began sooner, and started in the middle channel, not in the center channel as had all the other sensitivity calculations. Finally, the surge line failure occurred more than 12 min earlier than in the base case.

The core flow pattern was affected by the ballooning in the center and middle channels. Prior to the ballooning, the flow through the core was from the inlet to the outlet in the center and middle channels, and from the outlet to the inlet in the outer channel. When a localized balloon formed after 217 min in the fifth node of the center channel, reducing the flow area by 57%, the flow pattern changed. Flow in the center channel below the balloon was downward to the lower plenum, while vapor flowed upward from the lower plenum into the middle and outer channels. The flows in the upper part of the core were as before, with the outer channel downflow penetrating to the third node from the bottom of the core. A sausage-type balloon occurred in the middle channel at about 227 min, resulting in a 60% flow area reduction

from nodes 4 through 8. The return flow in the outer channel penetrated as far as before, but the flow magnitude was reduced. The outer channel flow penetrated only to the seventh node from the bottom after the rapid heatup of the middle channel began. That rapid heatup also caused the center channel flow to reverse, flowing from the upper plenum into the core for a few minutes.

Mass flow rates leaving the three core channels and the core bypass, and recirculating within the upper plenum are shown in Figure 83. The center channel outlet flow is seen to reverse during the rapid heatup of the middle channel around 233 min. The axial flows generally exhibited similar behavior to the other sensitivity calculations, but with higher magnitudes. The upper plenum recirculating flow, however, was much lower than in any of the other calculations. Figure 84 shows the upper plenum recirculating flow as a function of the vapor temperature above the center core channel. The flow at any given temperature was nearly 60% lower than in the base case.

The flow in the outer channel was heated as it flowed downward. Because of the increased radial flow resistance, which reduced the amount of flow turning in to the middle channel, the temperatures in the lower part of the core increased with increasing radius; that is, the outer channel had the highest temperatures, and the center channel the lowest. Figure 85 illustrates this by showing the fuel rod cladding surface temperatures from node 3 in each of the core channels. The temperature distribution was such that the lower part of the core was hotter than in the base case, while the upper part was cooler. The effect of the increased crossflow resistance was to make the temperatures more uniform axially.

Fuel cladding surface temperatures at several different elevations in the middle core channel are shown in Figure 86. The temperatures in the top half of the channel were close together throughout the transient. When the core bypass dried out at about 185 min, the core inlet flow increased, cooling the fuel rods near the bottom of the core. The entire core then heated up until ballooning occurred in the center channel at about 217 min. The change in the flow pattern in the bottom part of the core resulted in cooler vapor entering the middle channel from the lower plenum, with no recirculation of hotter vapor from the outer channel; the result was a slowly decreasing temperature in the bottom two nodes of the middle channel, with a slower increase in nodes 3 and 4. When ballooning occurred in the middle channel, the increased surface area coupled with the oxidation of the cladding inner surface caused an increase in the oxidation rate in the ballooned region, accelerating the heatup in nodes 4 through 8 so that they were hotter than the top two nodes. The temperatures in the upper two nodes soon followed, as the temperature of the vapor available to cool the fuel rods increased. The heatup rate increased further when the temperature reached 1850 K and the oxidation kinetics changed. At about 232 min, the liquid level in the downcomer dropped below the core barrel, allowing cooler vapor from the downcomer to enter the lower plenum and core. This cooler vapor caused a short decrease in the temperatures in the bottom half of the channel, but did not affect the temperatures of the top four nodes because those elevations were above 1850 K and oxidizing rapidly.

The peak cladding temperature in the core during the transient is shown in Figure 87, together with the temperature from the base case. The more uniform axial temperatures in Case 9 resulted in a lower peak cladding temperature than in the base case until ballooning occurred in the middle channel. After that time, the Case 9 temperature increased much more rapidly.

Figure 88 presents the fuel rod cladding surface temperatures at the top of the core for the three core channels. As in the other sensitivity calculations, the center channel was the hottest for the first part of the transient. However, the middle channel ballooning and associated heatup allowed the middle channel temperature to exceed that of the center channel, leading to fuel rod relocation 3 min earlier than in the center channel. The outer channel temperature was lower than in the base case because there was less mixing in the upper plenum. Cool flow returning from the bottom of the hot legs to the upper plenum was not mixed with much hotter vapor, so that the vapor entering the outer channel was cooler than in the base case. The lower temperature caused the outer channel relocation to be delayed, compared to the inner channel relocation and the other crossflow sensitivity calculations.

The total core hydrogen generation rate is shown in Figure 89. When ballooning occurred in the middle channel at about 227 min, a step increase to a more rapidly increasing hydrogen generation rate occurred. The rate then increased and decreased as different regions of the core went through accelerated cladding oxidation at temperatures above 1500 K.

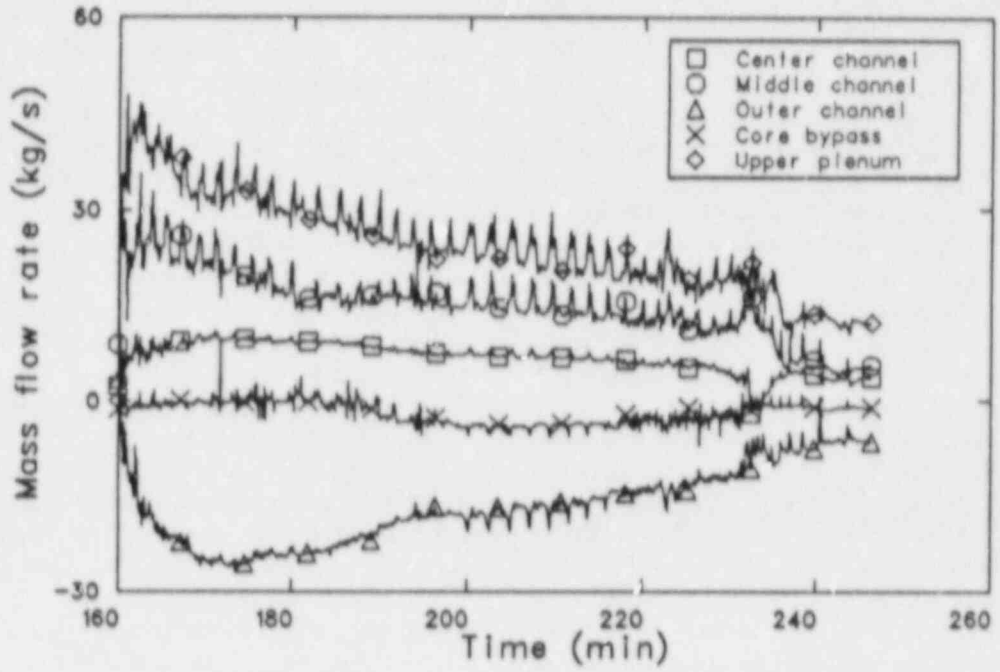

Figure 83. Mass flow rates exiting the three core channels, the core bypass, and recirculating in the upper plenum for sensitivity Case 9.

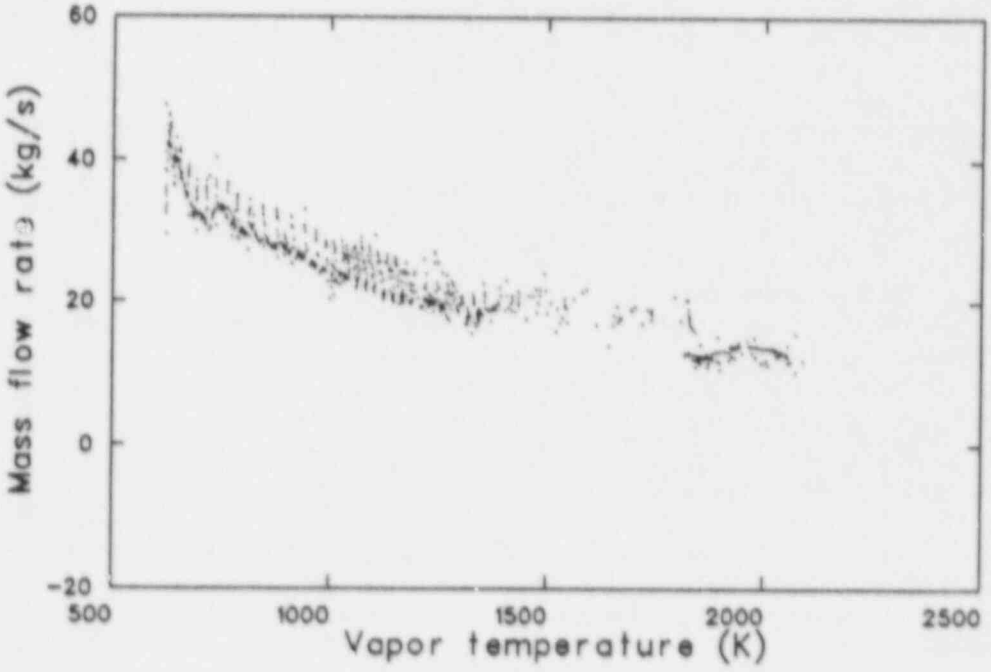

Figure 84. Upper plenum recirculating mass flow rate as a function of maximum upper plenum vapor temperature for sensitivity Case 9.

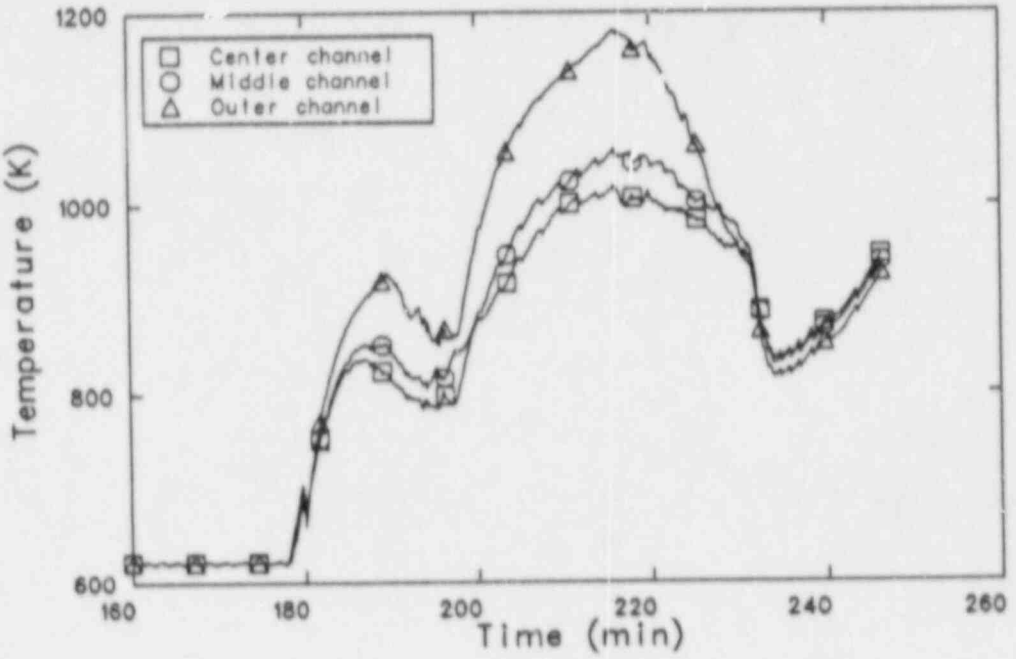

Figure 85. Fuel rod cladding surface temperatures at 0.55 m above the core bottom in the three core channels for sensitivity Case 9.

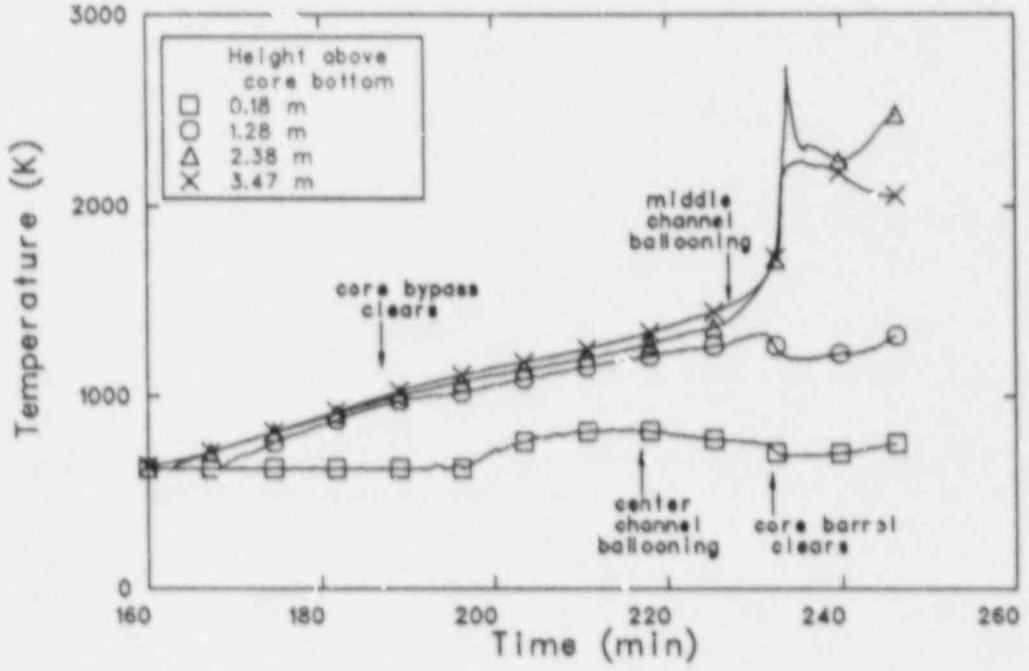

Figure 86. Center channel fuel rod cladding surface temperatures at 0.18, 1.28, 2.38, and 3.47 m above the core bottom for sensitivity Case 9.

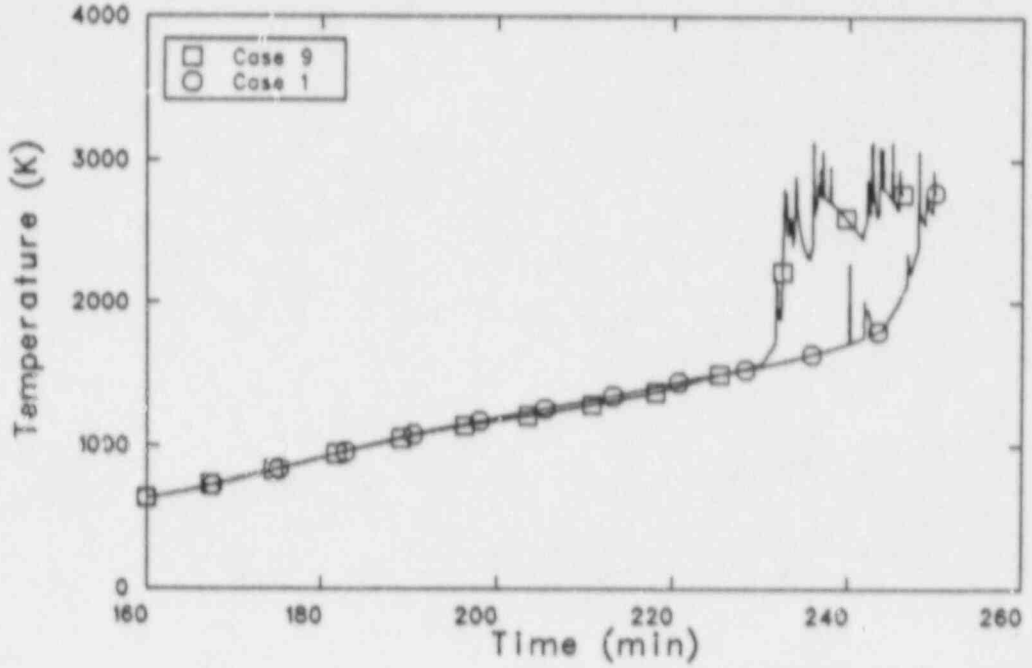

Figure 87. Peak cladding temperatures for sensitivity Cases 9 and 1.

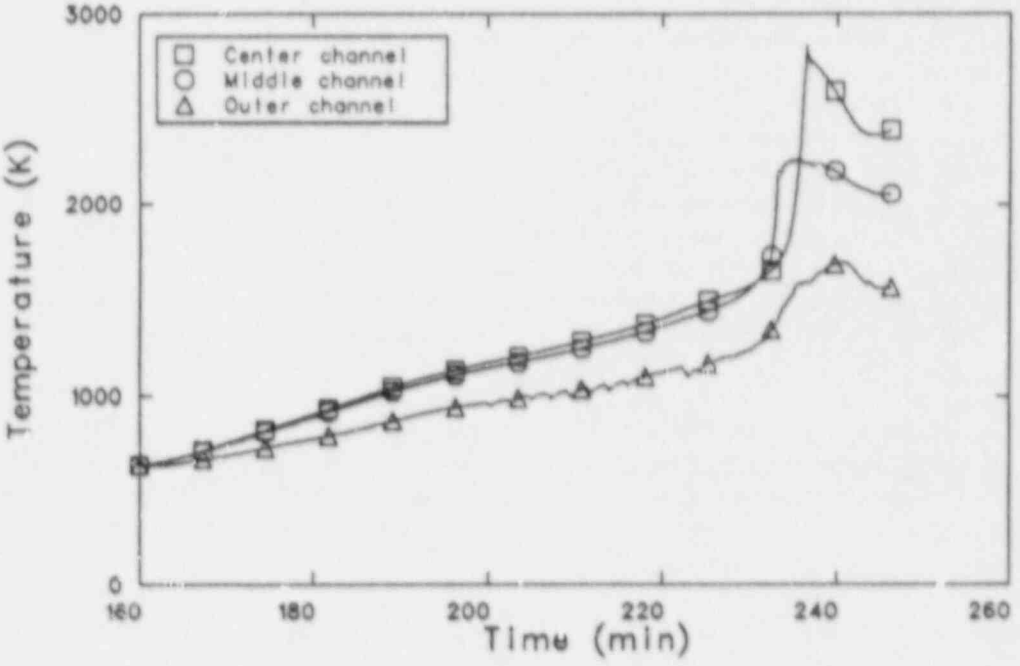

Figure 88. Fuel rod cladding surface temperatures at the top of the three core channels for sensitivity Case 9.

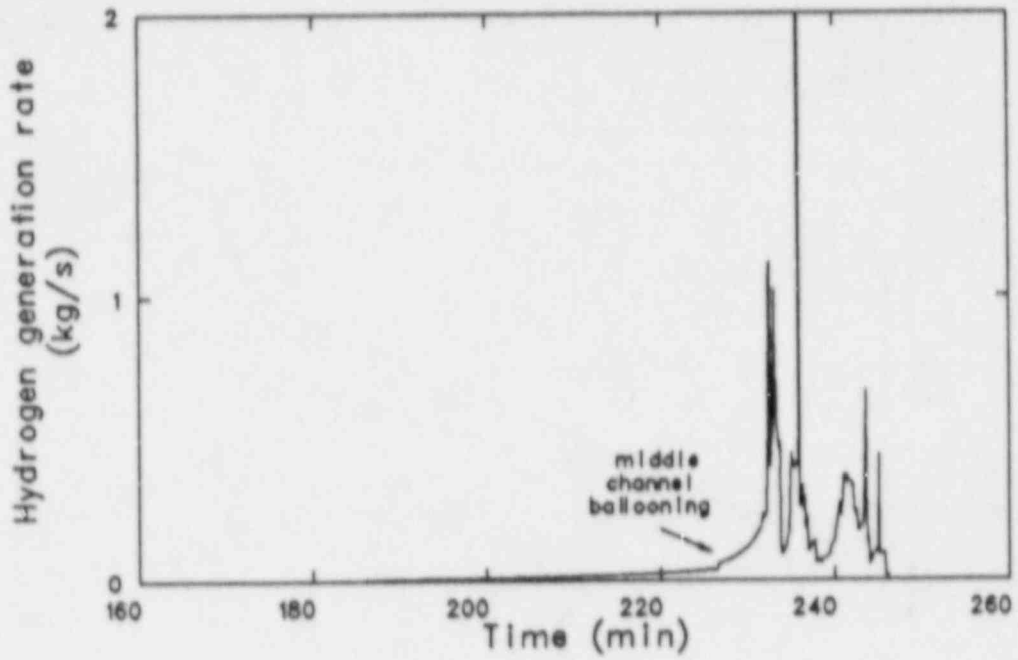

Figure 89. Total hydrogen generation rate for sensitivity Case 9.

The structure temperatures throughout the upper plenum were higher in Case 9 than in the base case, with the exception of the outer channel just above the core outlet. The higher core exit flows seen in Figure 83 transferred more of the core energy to the upper plenum early in the transient. Lower temperatures were seen in the fluid volume into which the cooler hot leg flow returns. With a lower recirculating flow in the upper plenum, there was not as much mixing with higher temperature vapor in this volume, keeping the structure temperature cooler. Figure 90 shows the upper plenum structure temperatures just above each of the three core channels.

Collapsed liquid levels in the reactor vessel for Cases 9 and 1 are shown in Figure 91. The level in Case 9 decreased more slowly after the core dried out because of the lower temperature above the outer core channel. The fluid in this volume also flowed down the core bypass to the lower plenum, where it transferred heat to the liquid. The heat transfer to the liquid caused it to boil, reducing the reactor vessel liquid level. Since the flow entering the top of the core bypass was cooler than that in the base case, the flow exiting the bottom was also cooler. Less energy was transferred to the liquid because of the smaller temperature difference between the vapor and the liquid. When the rapid core heatup occurred at about 230 min, hotter vapor flowed through the core bypass, and the level approached that of the base case.

Vapor temperatures at the top and bottom of the hot leg for two of the coolant loops are shown in Figure 92. The rapid heatup in the core led to about a 400 K temperature increase over 2 min in the top of the hot legs. The vapor temperatures in the pressurizer loop were slightly higher after the rapid increase, because the PORV cycling had increased the heat transfer to the hot leg piping, and not as much heat could be transferred from the vapor to the piping. The cooler (hot leg bottom) vapor temperatures were the same in the two loops through most of the transient except when the PORVs were open. When they were open, hotter vapor was drawn from the reactor vessel to the surge line through the bottom of the pipe. The temperatures also diverged briefly during the rapid heatup in the top of the pipe. The PORVs cycled often during this period, so that the hotter vapor in the piping did not have time to completely clear the loops between cycles, and the pressurizer loop temperature was higher. The temperatures were closer together after the cycling frequency decreased again.

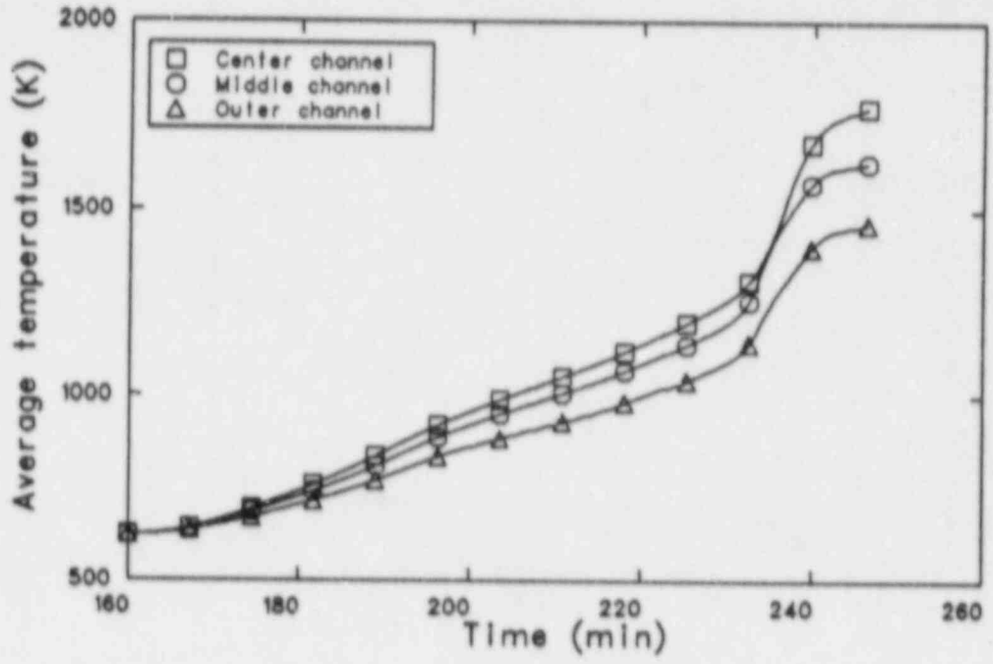

Figure 90. Volume-average temperatures of the upper plenum structures at the outlet of the three core channels for sensitivity Case 9.

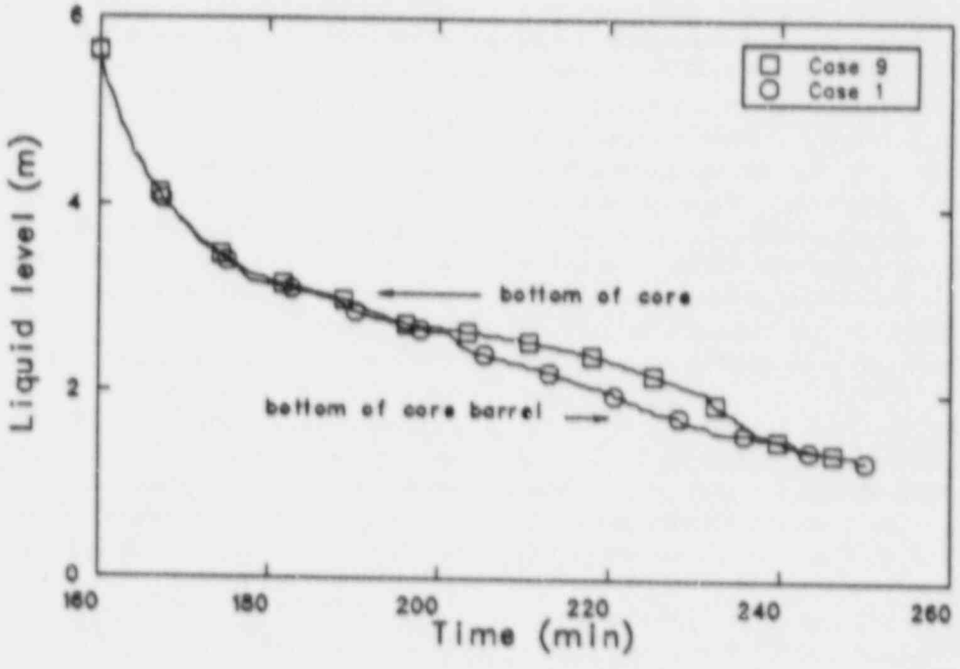

Figure 91. Reactor vessel collapsed liquid level for sensitivity Cases 9 and 1.

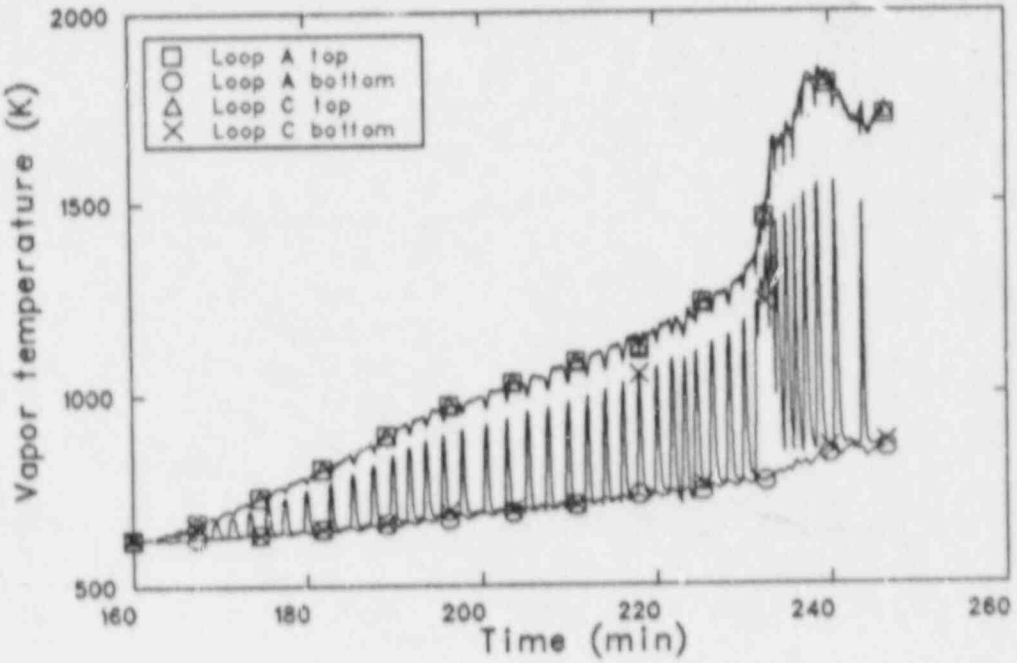

Figure 92. Hot leg nozzle hot and cold vapor temperatures in Loops A and C for sensitivity Case 9.

Figure 93 shows the pressurizer loop hot leg, surge line, and steam generator tube maximum temperatures, as well as the surge line temperature from Case 1. The surge line heated up faster in Case 9 than in the base case, as did the hot leg. The temperature increase associated with the rapid core heatup was more pronounced in Case 9 because the middle core channel heated up first rather than the center core channel. The middle core channel represents 96 fuel assemblies while the center channel represents 25. Since the middle channel was heating up in Case 9, there was a larger amount of hot vapor entering the upper plenum, which resulted in higher average vapor temperatures in the upper plenum and hot legs. The surge line failed at a temperature of 1252 K at 233.9 min. The heatup of the surge line occurred rapidly because the PORVs cycled five times in 2.5 min during the time of the rapid core heatup, drawing hot vapor into the relatively thin surge line often.

Figure 94 shows the fraction of the heat removed from the core that was transferred to the steam generator tubes and tube sheets in Cases 9 and 1. The higher upper plenum temperatures in Case 9 at the hot leg inlet led to increased flow in the hot legs and more energy transfer to the steam generators. The decrease in Case 9 near the end of the calculation was caused by the rapid core heatup, which heated the structures closest to the core first. The calculation was terminated before that energy could be redistributed to the loops, and one would expect the ratio to increase had the calculation continued further.

Conditions of the RCS near the time of the surge line failure are presented in Table 16. The temperatures in the system were generally lower than in the base case, except for the middle channel cladding and surge line. The more extensive total oxidation and fission product release were primarily caused by the heatup of the middle channel occurring before that of the center channel, since the middle channel represents nearly 4 times as many fuel assemblies as does the center channel. The lower energy deposition in the loops is misleading, in that a rapid core heatup was occurring at 233.3 min, and the energy removed from the core had not yet been redistributed to the loop structures. Similarly, the core heat removal fraction is probably a bit low. The higher reactor vessel liquid level is the only other major difference between Case 9 and the other calculations.

Reviewing the figures, it can be seen that the core and surge line heatups in Cases 9 and 1 were quite similar before the fuel rod cladding ballooned. The

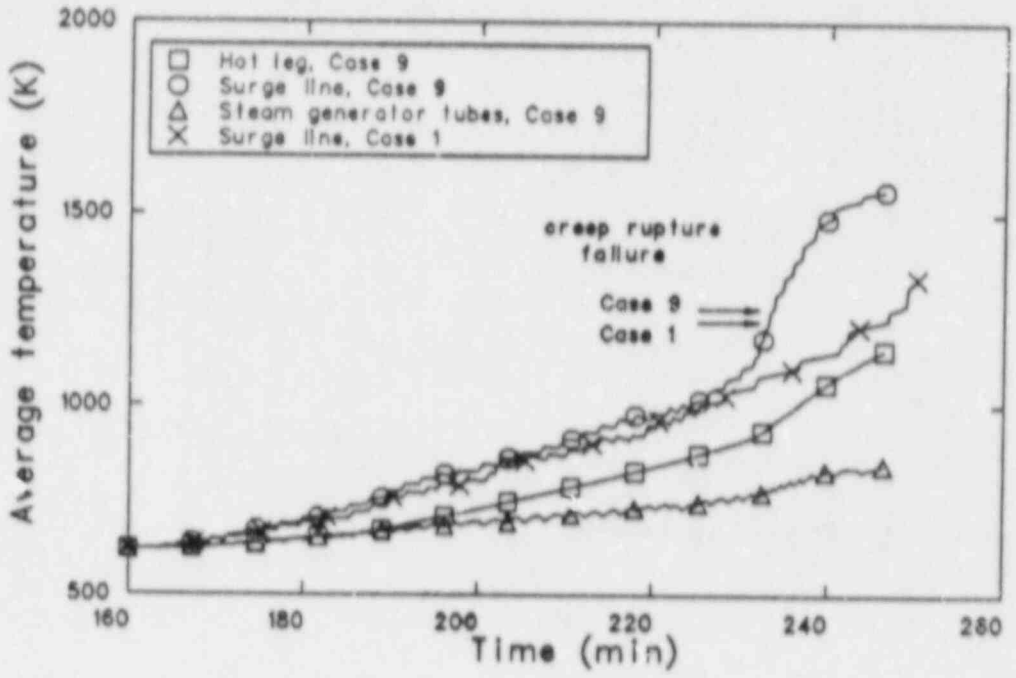

Figure 93. Highest volume-average pipe temperatures in the Loop C hot leg, surge line, and steam generator tubes for sensitivity Case 9, and the surge line for Case 1.

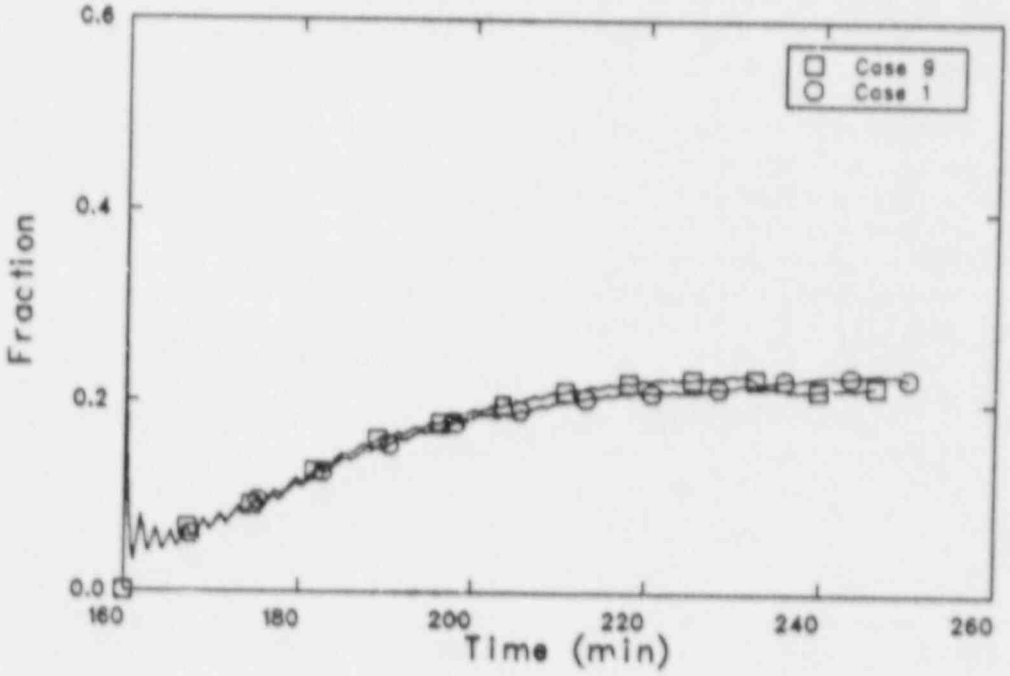

Figure 94. Fraction of the core heat removed by the coolant for sensitivity Cases 9 and 1.

ballooning then changed the flow and heatup, accelerating the core damage and surge line failure. Had ballooning not occurred, the difference in timing of the surge line failure would probably have been much less than 12.4 min.

4.5.4 Summary. Decreasing the crossflow resistances in either the core or the upper plenum led to surge line failure less than 2 min earlier than in the base case. Increasing the resistances in both locations resulted in lower crossflows, which reduced the mixing in both the core and upper plenum. The more one-dimensional flow led to ballooning in the center and middle core channels, which accelerated the core heatup. Surge line failure occurred 12.4 min earlier than in the base case.

With a reduced crossflow resistance, the upper plenum recirculating flow increased by more than 30%. The increased mixing resulted in higher temperatures above the outer core channel, which reduced the flow returning to the core. This led to slightly higher core temperatures and earlier core damage.

With reduced crossflow resistances in the core, more flow recirculated within the core, turning radially outward at the top of the core because of the relatively large axial flow resistance at the upper end boxes. This flow heated the vapor at the top of the outer channel, reduced its density, and thus, reduced the buoyant driving force. The higher outer channel temperatures and reduced core flow rates accelerated the core heatup and the onset of core damage, but only by a few minutes.

Increased crossflow resistances in both the core and upper plenum led to a more one-dimensional flow. A more uniform axial temperature distribution in the core resulted, as did a higher core flow rate. The higher flow rate removed more of the core energy early in the transient, and allowed the fuel rod cladding to balloon in both the center and middle channels. The localized balloon in the center channel altered the flow pattern in the bottom of the core, changing the axial temperature distribution. The sausage-type balloon in the middle channel caused an increased heatup rate by increasing the cladding surface area, and allowing oxidation of the inner surface, both of which increased the Zircaloy oxidation rate. A rapid heatup of the core ensued, followed closely by a rapid heating of the surge line to failure. The rapid core heatup started when the cladding temperature was around 1400 K, well below the temperature at which the Zircaloy oxidation kinetics change (1850 K). Without ballooning, the surge line failure time probably would have been much closer to the base case than it was.

The changes in the reactor vessel modeling did not alter the hot leg countercurrent flow characteristics. The hot leg flow rate was affected by the changes in the upper plenum only in that the hot leg inlet temperature was changed; the flow at any given inlet temperature did not change from the base case.

4.6 Surge Line Failure Calculation

A final analysis was performed in which failure of the surge line was modeled. The base case calculation was changed at 246.3 min to include a 0.15-m diameter break in the side of the surge line near the hot leg. The calculation was then continued to examine the effects of the blowdown on the system behavior. Since the transient up to the time of surge line failure is the base case, which has already been presented, the discussion that follows will concentrate on the behavior during the blowdown. Similarly, the time scale on most of the figures will focus on the later part of the transient.

The sequence of events for the transient is presented in Table 17. After the surge line failed, the RCS pressure decreased rapidly, initiating accumulator liquid injection. The accumulator water, together with water from the loop seals, entered the reactor vessel and core, eventually quenching the entire core. The pressure continued to decrease, and the accumulators emptied completely. At the end of the calculation, the two-phase liquid level in the reactor vessel was just above the top of the core, indicating that core uncovering and heatup were about to begin again.

The pressurizer pressure after 245 min is shown in Figure 95. The pressure cycled between the PORV opening and closing setpoints of 16.2 and 15.7 MPa, respectively, until the surge line failed. A rapid pressure decrease ensued, with the pressure decreasing from 16.2 to 1.7 MPa in 1.25 min. This rapid depressurization caused the loop seals to clear of liquid, with the water flowing to the reactor vessel. The pressure then increased as water from the accumulators and loop seals boiled in the core. A pressure decrease allowed more water to be injected from the accumulators, resulting in more boiling and another pressure increase. Subsequent accumulator injection cycles caused only slight pressure increases, with the pressure slowly

Table 17. Sequence of events for the surge line failure calculation

Event	Time (min)
Calculation begins	160.0
Center channel oxidation begins	185.3
Middle channel oxidation begins	186.1
Two-phase liquid level below core	190.2
Outer channel oxidation begins	192.6
Center channel fuel rod cladding fails	223.4
Pressurizer empties of liquid	224.8
Middle channel fuel rod cladding fails	225.3
Outer channel fuel rod cladding fails	241.3
Pressurizer surge line fails	246.3
Accumulator injection begins	247.2
Core quench begins	247.4
Core quench complete	250.3
Accumulators empty of liquid	255.5
Calculation ends	266.7

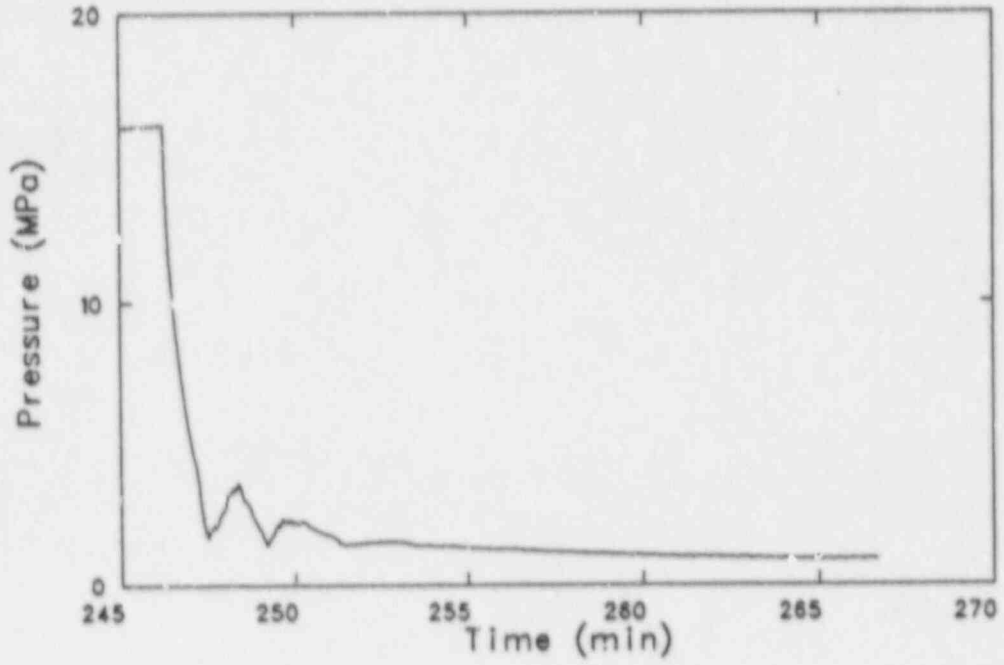

Figure 95. Pressurizer pressure for the surge line failure calculation.

decreasing until the end of the calculation. At that time, the pressurizer pressure was 0.91 MPa.

Figure 96 presents the liquid volume in one of the three accumulators, which was nearly identical to that of the other two. Each accumulator contained 29.4 m^3 of 322 K water at the beginning of the transient. Accumulator injection began at 247.2 min, and the accumulators were dry by 255.5 min. The injection occurred in five stages. Liquid flow from the accumulators was interrupted four times by repressurization of the RCS. This is shown by the rapid level decreases, followed by periods where the level was not changing. The final injection stage was a slow injection as the RCS pressure gradually decreased.

The peak cladding temperature is shown in Figure 97. The temperature had reached about 2100 K when the surge line failed. Depressurization of the RCS allowed some of the liquid remaining in the lower head to flash to steam, and increased steam flow through the core cooled the core structures. When the accumulator and loop seal water reached the core, a more rapid cooldown began, followed by a quench of the core. The entire core was at the saturation temperature at the end of the calculation.

Figure 98, which presents the fuel rod cladding surface temperatures at several elevations in the center channel, better illustrates the cooling of the core. Temperatures over the entire length of the fuel rod decreased as soon as the surge line failed at 246.3 min. The cooldown then slowed, and the top of the core began to heat up again. The temperatures decreased again at 247.4 min, when water from the accumulators began entering the bottom of the core. The bottom core node quenched (reached the saturation temperature) at 247.6 min. At 250.3 min, the top of the core was also quenched. Quenching of the oxidized, embrittled cladding was predicted to shatter it, initiating formation of a debris bed within the core. However, a rod-like geometry was assumed for the remainder of the calculation.

The center core channel collapsed liquid level is presented in Figure 99. The level increased rapidly when the accumulators injected. The brief decreases in level occurred when the RCS pressure was temporarily above the accumulator pressure, so that no liquid was being added to the system. The collapsed level nearly reached the top of the core before decreasing at the end of the transient. The two-phase level at the end of the calculation was in the top core node.

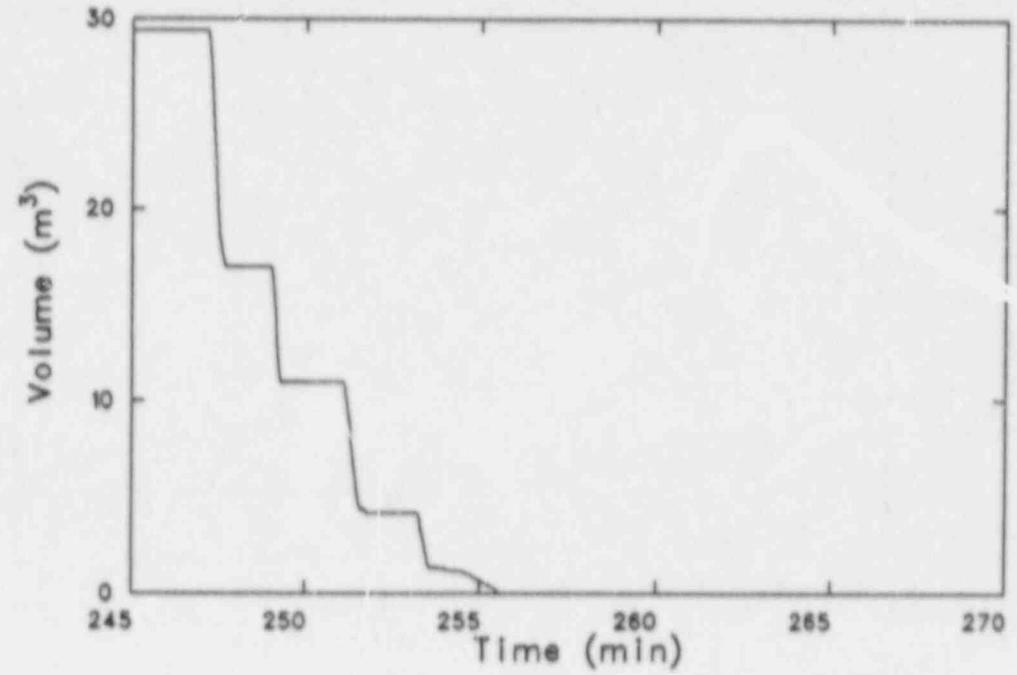

Figure 96. Liquid volume in one accumulator for the surge line failure calculation.

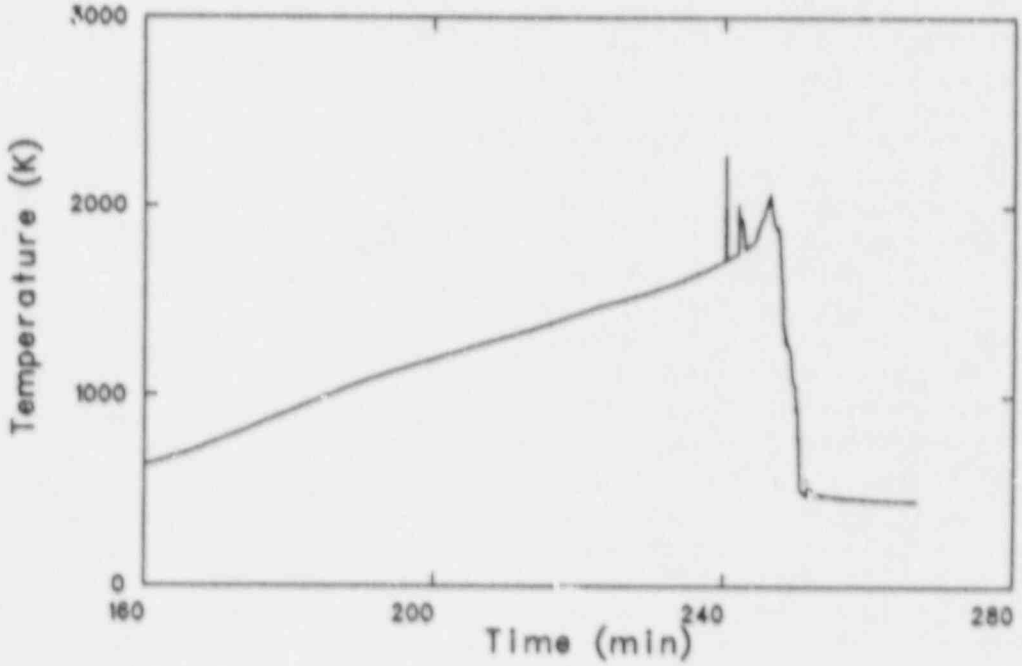

Figure 97. Peak cladding temperature for the surge line failure calculation.

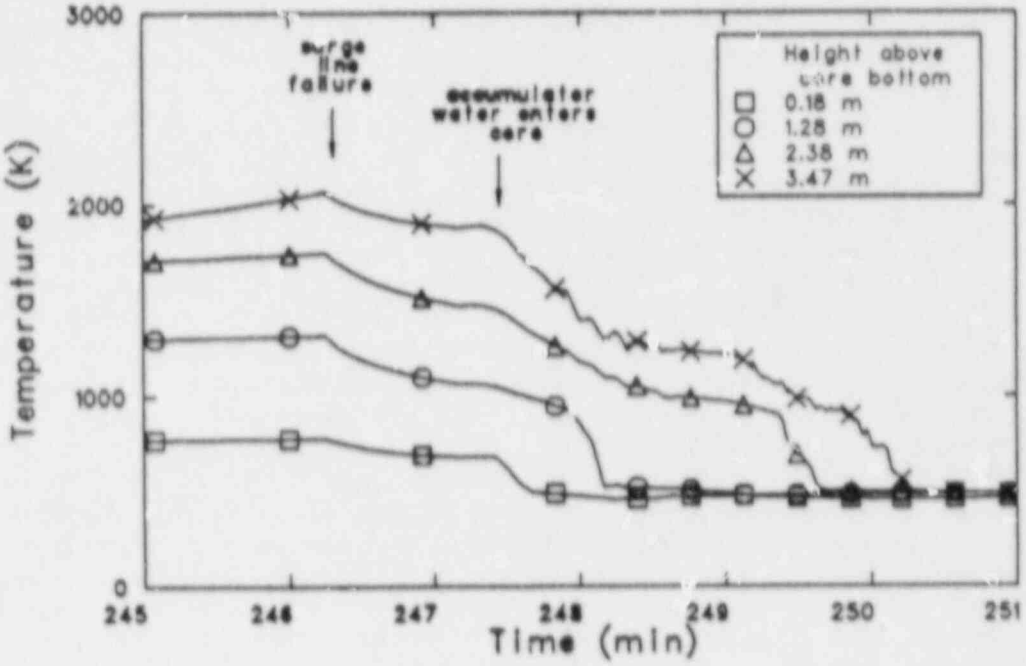

Figure 98. Center channel fuel rod cladding surface temperatures at 0.18, 1.28, 2.38, and 3.47 m above the core bottom for the surge line failure calculation.

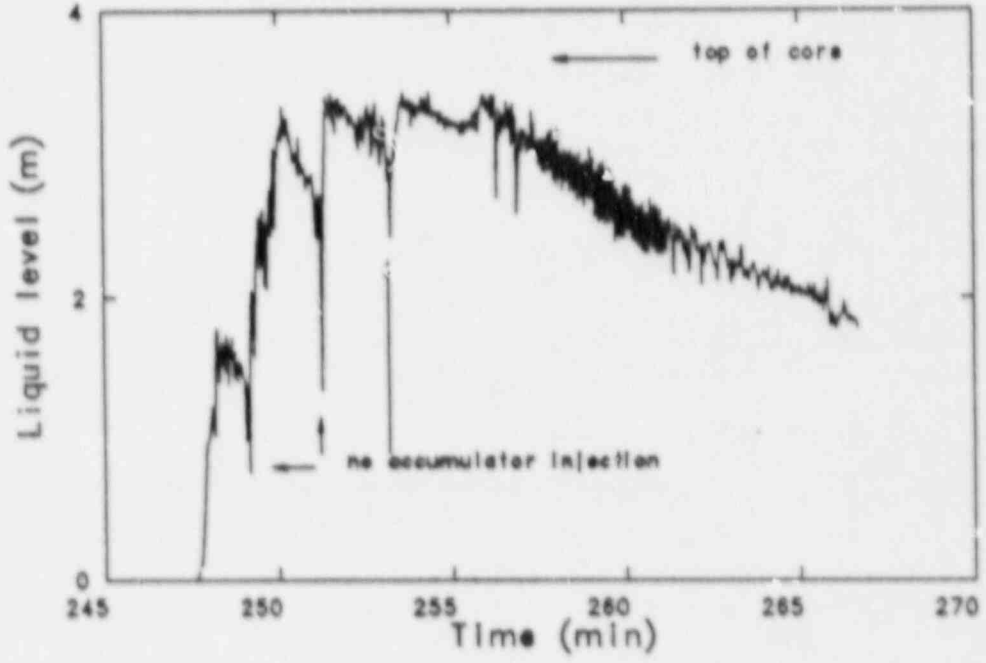

Figure 99. Collapsed liquid level in the center core channel for the surge line failure calculation.

Figure 100 shows the reactor vessel collapsed liquid level during the transient. A sharp drop in the level occurred when the surge line failed, as some of the water that remained in the vessel lower head flashed as the RCS depressurized. Water from the loop seals and accumulators then partially refilled the vessel. As in the core, the level decreased briefly when the accumulators were not injecting, and continuously after they emptied.

Upper plenum structure temperatures in the three volumes above the center core channel are shown in Figure 101. The temperatures were close together through the heatup and initial stage of the blowdown. However, the reactor vessel liquid level increased sufficiently so that the structures in the upper plenum just above the core quenched, while those higher in the plenum did not. Another feature of interest is that the structure at the core outlet was cooler than the structure in the next higher volume, even though the vapor temperature was higher. The acceleration of the flow in the upper plenum yielded a higher flow velocity in the second volume and hence, a higher heat transfer coefficient, leading to the higher structure temperature.

Figure 102 presents the void fraction at the bottom of the Loop A loop seal. The pipe was full of water throughout the transient until the surge line failed. The rapid depressurization of the RCS caused all of the loop seals to clear. The water from Loops A and B flowed into the reactor vessel. Flow from Loop C entered both the reactor vessel and the steam generator tubes; the latter occurred because flow was drawn toward the surge line. There was about 12.7 m^3 of liquid in the loop seals when the surge line failed, not enough to refill the vessel from its level at that time to the bottom of the core. By 252 min, when the pressure had stabilized, water from the accumulators refilled the loop seals.

The hottest steam generator tube temperatures from each loop are shown in Figure 103. The temperatures in each decreased when the surge line failed and the loops seals cleared as steam flowed toward the surge line on the Loop C hot leg. Some liquid entered the Loop C steam generator because of its proximity to the break, resulting in a more rapid cooling of the tubes, although they did not reach the saturation temperature. The temperatures began to increase again when the loop seals refilled with liquid, preventing flow from entering the steam generators from the cold legs. The temperatures at the end of the transient were slowly decreasing (Loops A and B) or increasing (Loop C), depending on whether the superheated steam on the secondary side of the steam generators was cooler or hotter than the RCS vapor temperature.

The hot leg pipe temperatures near the reactor vessel are presented in Figure 104. When the surge line failed, the temperature in Loop C increased because hot vapor was being drawn from the reactor vessel toward the surge line, and the increased velocity increased the heat transfer rate. In the other two loops, the temperature decreased because the flow reversed in the top of the hot legs, and cooler vapor was drawn from the steam generators toward the reactor vessel. The increased flow, combined with lower vapor temperatures emanating from the vessel as the core cooled and quenched, then led to a more rapid cooling of the Loop C hot leg. Cooling of all the piping, together with the RCS depressurization, indicates that creep rupture failure of another RCS structure subsequent to the surge line failure is unlikely for this failure size.

Figure 105 presents the mass flow through the break in the surge line. The flow rate decreased as the pressure dropped, then increased as the RCS repressurized. The flow rate then generally followed the system pressure behavior, although there were increases in the flow caused by local increases in vapor density as cooler vapor entered the surge line.

In the base case, fuel rod relocation did not begin until after the surge line was predicted to fail. Because the cooling and quench of the core began as soon as the surge line failed, there was no fuel rod relocation in the blowdown calculation. The calculated core damage was limited to oxidation of the cladding, which resulted in the generation of 114 kg of hydrogen, and to relocation of 27% of the control rods in the core from the center and middle channels. The code predicted that the quench of the core would result in the fragmentation of the fuel rods and the formation of a debris bed at about 248 min, but a rod-like geometry was assumed to be maintained until the end of the calculation.

4.7 Summary of Sensitivity and Surge Line Failure Analyses

This section provides an overview of the results of the various sensitivity calculations and the surge line failure calculation. General patterns of behavior are described, and the results of different analyses are compared to better understand how the natural circulation flows affect the plant severe accident response.

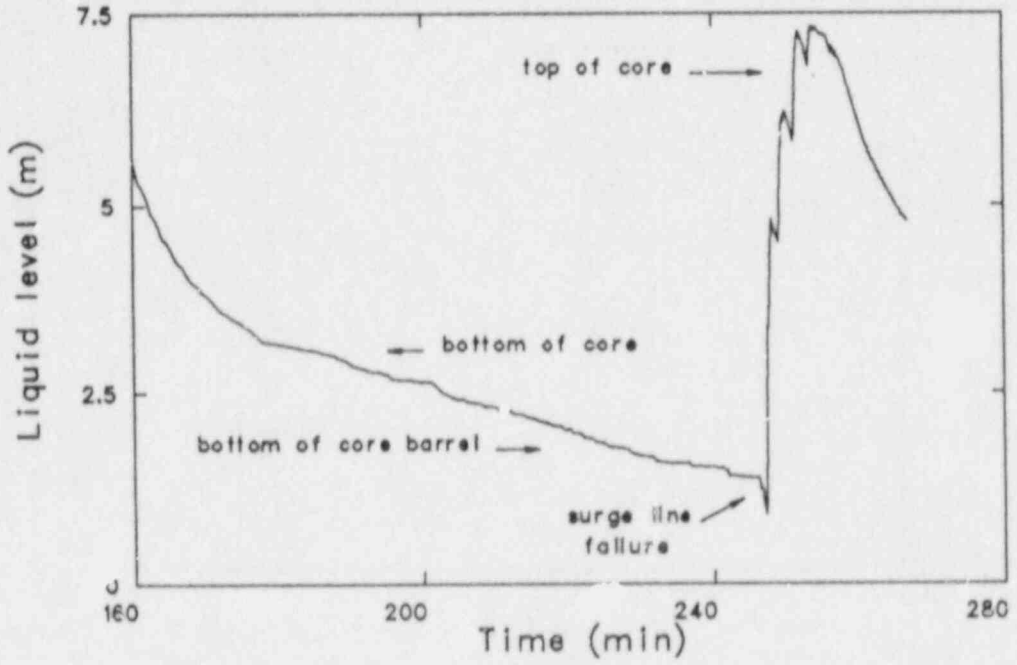

Figure 100. Reactor vessel collapsed liquid level for the surge line failure calculation.

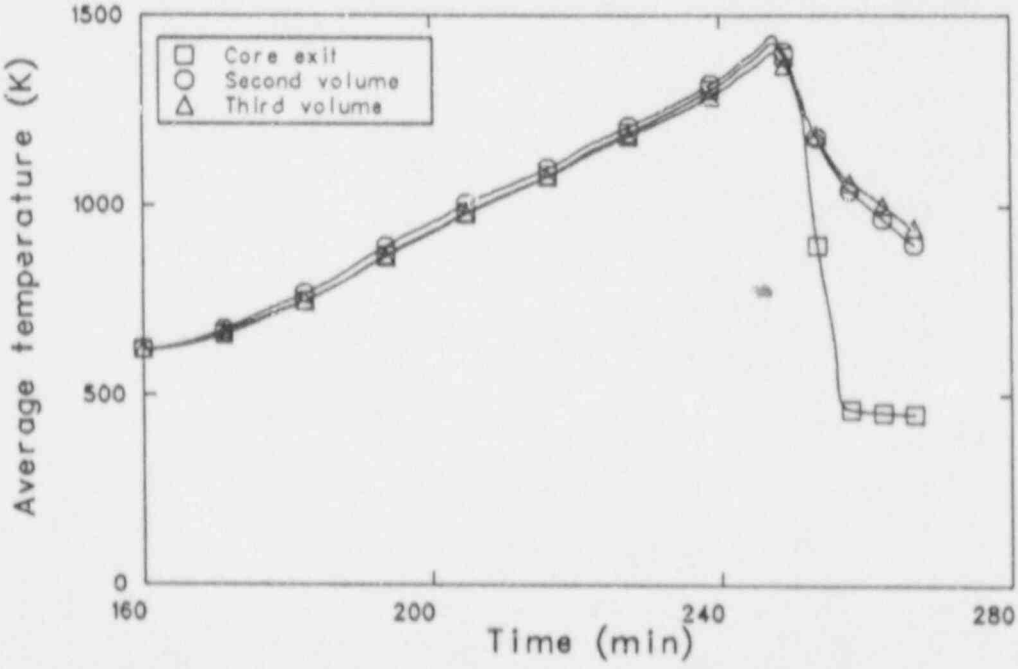

Figure 101. Volume-average structure temperatures in the three volumes above above the center core channel for the surge line failure calculation.

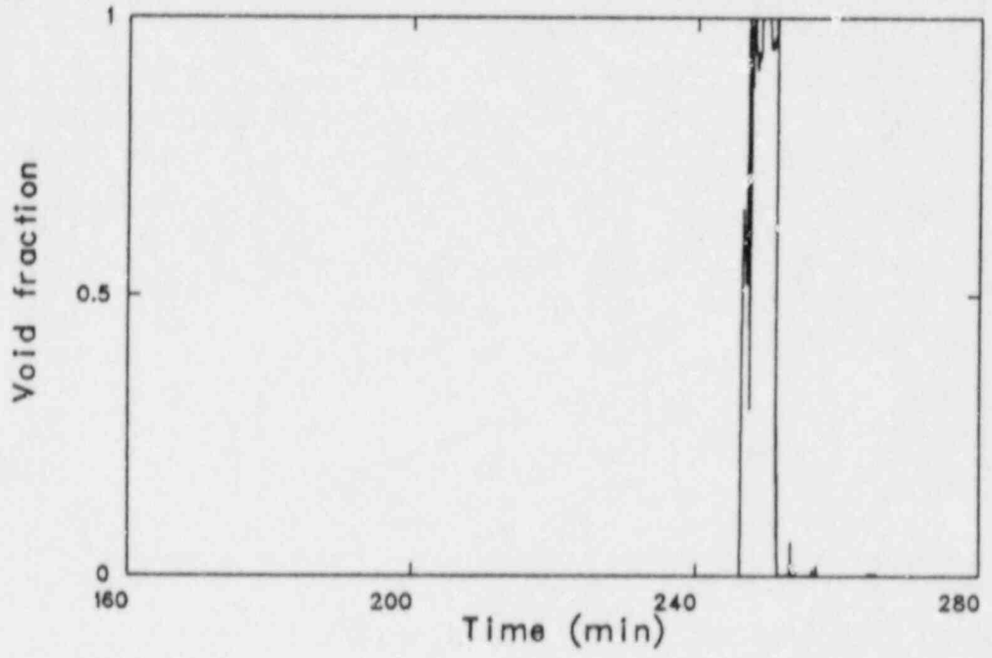

Figure 102. Void fraction in the bottom of the Loop A loop seal for the surge line failure calculation.

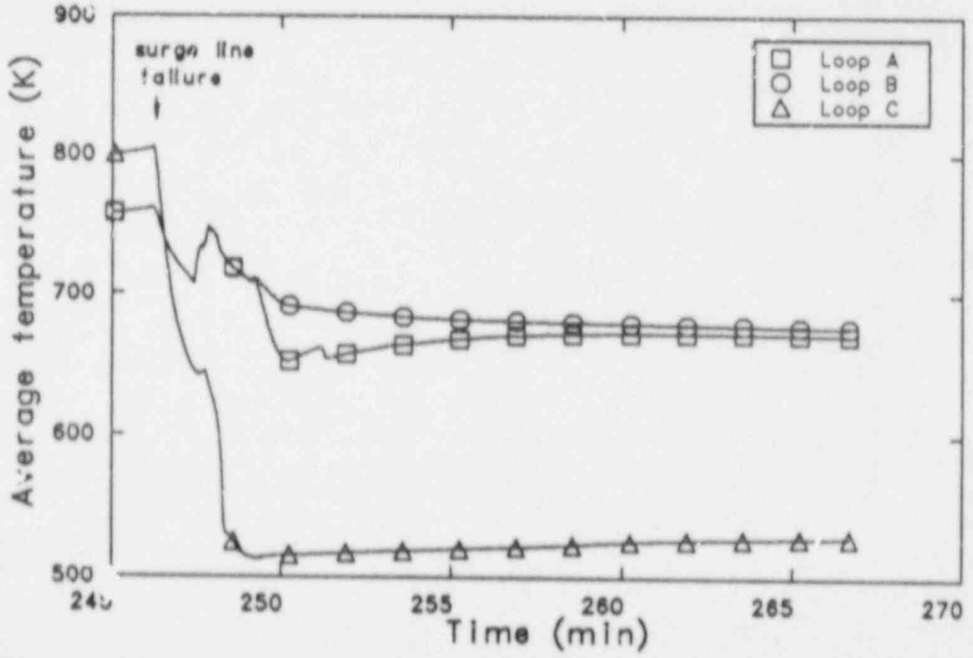

Figure 103. Highest volume-average steam generator tube temperatures in the three coolant loops for the surge line failure calculation.

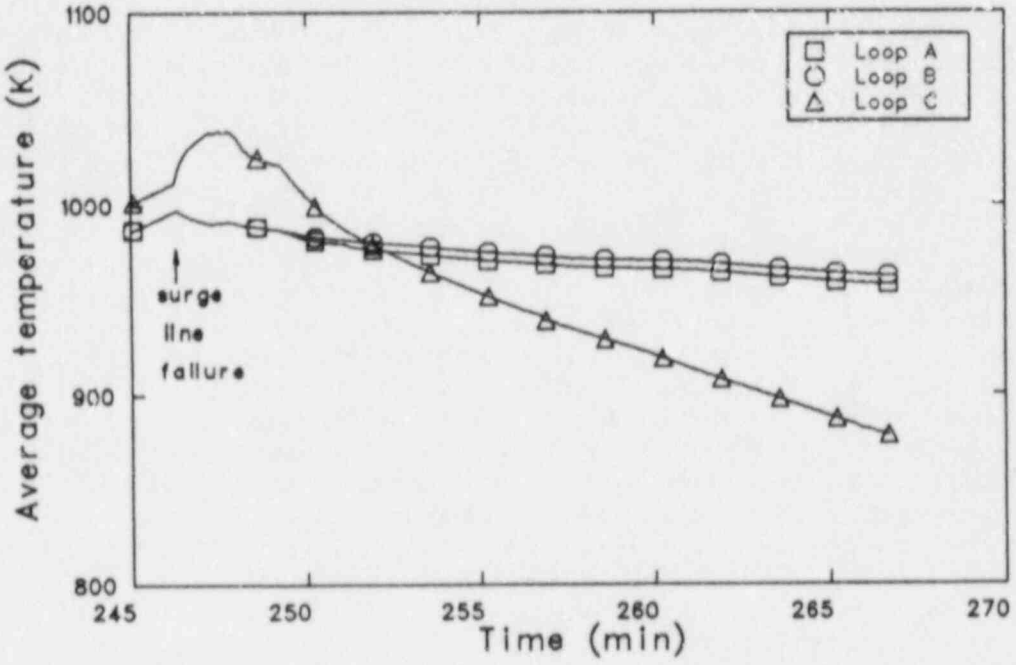

Figure 104. Volume-average hot leg pipe temperatures near the reactor vessel for the surge line failure calculation.

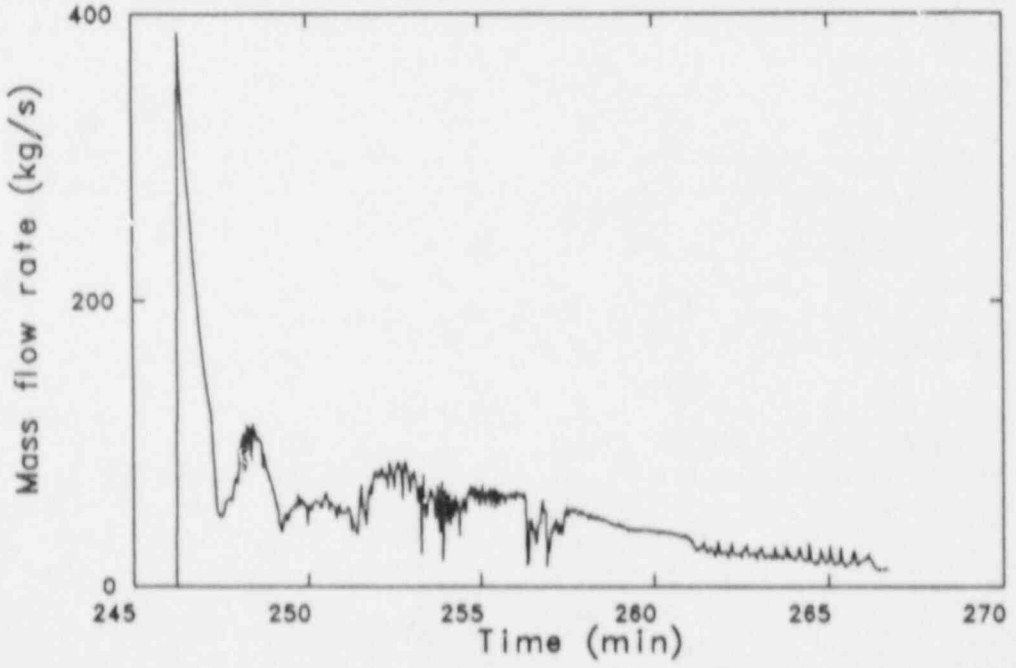

Figure 105. Mass flow out the break for the surge line failure calculation.

The hot leg flow was affected only by the inlet vapor temperature and the steam generator inlet plenum mixing. With decreased inlet plenum mixing, the flow increased, increasing the heat transfer in the loops and moving more of the energy to the steam generator tubes. In all of the sensitivity calculations except Cases 3 and 4, the hot leg flow as a function of temperature did not change. Any changes in the upper plenum conditions affected the hot leg flow only by altering the hot leg inlet vapor temperature.

Heat loss through the hot leg pipe also affected only the loop energy distribution, and not the hot leg flow. The heat loss through the pipe reduced the temperature of the vapor entering the steam generators. With lower temperatures, the steam generators removed less energy, and the tube temperatures were reduced.

The upper plenum flow was affected by the local modeling and by the hot leg behavior. Increasing the upper plenum crossflow resistance reduced the flow recirculating within the upper plenum, while decreasing the resistance increased the flow. Increasing the heat transfer in the coolant loops also increased the upper plenum flow by returning cooler vapor from the hot legs to the upper plenum, with the same hot leg inlet temperature. The cooler vapor had a higher density, increasing the buoyant driving force in the upper plenum and consequently the flow.

With a simple model in SCDAP/RELAP5 simulating the effects of cladding/grid spacer material interactions, ballooning did not occur as frequently as in past calculations. In most of the sensitivity calculations, the fuel rod cladding failed when the calculated temperature reached 1470 K, a value input to simulate the effects of eutectic formation between the Zircaloy and iron or nickel, rather than failing because of excessive strain following ballooning. By contrast, ballooning occurred in both of the scoping calculations in which in-vessel natural circulation was modeled.

The ballooning that did occur affected the core damage more than it affected the core flows and early heatup behavior. Only in Case 9 did the ballooning have a significant effect on the core flow pattern and heatup rate, causing the flow in the bottom of the center channel to reverse while changing the temperature distribution in the core. Ballooning of the middle channel led to increased oxidation of the ballooned cladding, and the middle channel heated up faster than the center channel. In the other cases in which ballooning occurred, the flow magnitude changed while the overall flow pattern did not. There was some reduction in the flow penetration in the outer channel, but the recirculating flow between the core and upper plenum was maintained in all the calculations. Double-sided oxidation of the ballooned cladding accelerated the heatup and allowed the cladding to be completely oxidized at relatively low temperatures. With no unoxidized Zircaloy, dissolution of the fuel by molten cladding could not occur, and fuel liquefaction and relocation could only occur when the temperatures reached the melting point of uranium dioxide. This reduced the amount of fuel relocation that occurred by the time of the RCS pressure boundary failure.

The pressure boundary failure in all the cases occurred very close to the time that fuel rod relocation began. The largest differences in the timing of these two events were 7.4 min in Case 6 and 15.2 min in Case 4; the initial fuel rod relocation and surge line failure occurred within 3.1 min of each other in all the other calculations. The significance of that is its relation to the timing of the reactor vessel lower head melt-through. The results of a MELPROG calculation presented in Table 5 in the scoping analyses chapter showed that the melt-through occurred nearly 100 min after the initial fuel rod relocation. While relocation occurred at lower temperatures than in the SCDAP/RELAP5 calculations, the core damage occurred at a higher decay power, so that the delay indicated by the MELPROG calculation is probably not too long. Since the RCS failure occurred no more than 15.2 min later than the initial fuel rod relocation in the sensitivity calculations, it should occur at least an hour before the vessel failure. This allows a long time for the RCS to depressurize.

With a 0.15-m diameter failure, this would be more than enough time to depressurize the RCS to nearly the containment pressure. In the surge line failure calculation, the pressure decreased from 16.2 to less than 1.0 MPa within 16 min.

Liquid remained in the loop seals for all of the sensitivity calculations, so the effects of loop natural circulation flow on the structure temperatures were not calculated. However, sensitivity Case 4, in which there was no mixing in the steam generator inlet plena, gave an indication of what those effects would be. With no mixing, the flow traveled from the reactor vessel, through the top of the hot leg and the hot flow steam generator tubes to the outlet plenum, where the flow turned back into the cold flow steam generator tubes, proceeding to the reactor vessel through the bottom of the hot leg. With loop natural circulation flow, the flow in all of the

tubes would be from the inlet plenum to the outlet plenum. The flow rate would also be much higher than in the sensitivity calculation because the elevation over which the density difference was driving the flow would be much larger (from the top of the steam generators to the bottom of the core, rather than half the height of the hot leg). Even with the lower flow, the steam generator tube temperatures were very close to the hot leg and surge line piping temperatures. The higher flow rate in loop natural circulation would probably increase the tube temperatures even further, so that they may fail before the other RCS structures.

The RCS failure time and location were fairly insensitive to the parameters varied in the sensitivity calculations. The surge line was predicted to fail in all of the calculations except Case 4, where the hot leg failed shortly before the surge line. However, even in that case, the calculated surge line behavior may have resulted in lower surge line temperatures than one might expect. Failure of the surge line occurred within 13 min of the base case time of 246.3 min in all of the cases, again with the exception of Case 4, where the hot leg failed 44.2 min later. It must be remembered that Case 4 was a bounding calculation that maximized the hot leg countercurrent flow, so a longer delay was expected.

The largest effect on the failure time was the decay power. Although it was not specifically part of the sensitivity calculations, the main difference between scoping Case 3 and sensitivity Case 1 was a decrease in the decay power. The result was that surge line failure occurred about 50 min later in the sensitivity calculation than in the scoping calculation.

4.8 Uncertainties and Limitations

This section identifies some of the uncertainties in the plant modeling and calculations. Also addressed are some of the limitations of the analyses. Some of these uncertainties were the subject of the sensitivity calculations.

Uncertainties exist in the decay power during the transient. The difference between the scoping and sensitivity calculations showed the importance of the power in determining the timing of the RCS failure.

The hot leg countercurrent flow rate is very uncertain, but was addressed in sensitivity Cases 3 and 4. The uncertainty stems from the way the model was developed. Scaled experiments at low pressure and temperature were modeled with COMMIX, which was then used to calculate a transient in a full-scale plant. The SCDAP/RELAP5 model was adjusted to provide the same heat transfer for the large plant calculation, then was applied to the Surry station blackout transient. The analyses that have been performed have bounded the flow rate, in that Case 4 provided an upper flow limit and that the lower flow limit is no countercurrent flow, which was addressed in scoping Case 2.

The behavior of the liquid in the loop seals is also uncertain. Although the loop seals did not clear in any of these calculations, the effect on the transient would be significant if they did clear. Other studies[18] have indicated that the loop seal clearing is a random process, so its potential should be considered when analyzing the plant response.

Effects of insulation degradation on the piping temperatures were examined in sensitivity Cases 5 and 6. Heat loss from the piping, which is an uncertainty in the plant modeling, was shown to delay the surge line failure by 6-13 min.

The size of the RCS failure is not known. The rate and extent of the depressurization depend on the failure size. A large enough failure, such as that in the blowdown calculation, may lead to core quenching and low reactor vessel pressures at the time the core melts through the lower head. Smaller failures may lead to different core damage scenarios, with slow intermittent injection of accumulator liquid that cools only part of the core while the rest continues to heat up.

How much flow blockage actually occurs during ballooning is another area of uncertainty. With all of the fuel rods in a region of the core behaving identically, blockages caused by localized ballooning may be too high. In the plant, while all of the fuel rods in a region may indeed balloon, the blockage would probably not be coplanar, as is the case with a code calculation.

The transient timing could be greatly affected by changes in the initial conditions. A lower steam generator liquid level would accelerate the time of steam generator dryout, leading to an earlier core heatup. With the core heating up earlier in the transient, the decay power would be higher, causing a faster core heatup and possibly changing the nature of the core damage (less oxidation and more relocation, for example). A lower initial reactor power would reduce the fission product decay heat, lengthening the transient. A lower burnup would reduce the actinide decay power, which would affect the core damage portion of the transient more than the initial heatup because the actinide

power is a larger fraction of the total power later in the transient.

Failure of components other than those that define the accident sequence were not considered. For example, the loss of cooling water to the reactor coolant pumps may lead to failure of the shaft seals, initiating a small break loss of coolant accident, or there may be insufficient battery power or air pressure to keep the relief valves operating throughout the transient.

The model of the Surry plant included only the major components. Small pipes and instrument penetrations of the system were not modeled, so that their behavior was not calculated. Features such as these on the hot leg may be subject to conditions such that they would fail before the surge line.

Oxidation and melting of structures outside of the core were not considered. The temperatures in the upper plenum were high enough during many of the calculations that the stainless steel would oxidize, adding to the amount of hydrogen generated. Melting temperatures were also attained in some cases, but the relocation of those structures was not calculated. Core debris formation caused by fragmenting fuel rods also was not accounted for. The core quench in the surge line failure calculation caused the embrittled fuel rods to shatter, but an intact geometry was maintained for the duration of the calculation. Changing this model would not affect the surge line failure, since it occurred earlier, but it would affect the subsequent reheating of the core.

The calculations were not continued to vessel failure. Accordingly, while the pressure at that time can be estimated, it has not yet been determined, so that the extent of any direct containment heating is unknown. In particular, the effect on the pressure of molten core relocation into a water pool in the lower head is unknown, as are the effects of smaller creep rupture failures with different accumulator injection rates.

6. CONCLUSIONS AND RECOMMENDATIONS

A comprehensive analysis of the response of the Surry plant to a station blackout transient has been performed. The analysis has provided insight into the phenomena that control the plant response and natural circulation flows, and to the level of detail needed to model the plant. Conclusions drawn from the natural circulation analyses performed for the Surry plant are presented below. Based on the results of the analyses, recommendations are also made for further investigation to help resolve the phenomenological uncertainties related to RCS natural circulation during severe accidents.

1. The modeling of each additional natural circulation flow slowed the core heatup, extending the transient.

   The in-vessel and hot leg natural circulation flows slowed the core heatup by transferring energy from the core to the upper plenum and coolant loops, respectively. The slower heatup allows more time to recover systems to mitigate core damage. Fuel rod relocation began at about 161 min in the once-through calculation, 7 min later with in-vessel circulation modeled, and 18 min later with both in-vessel and hot leg natural circulation modeled.

2. The decay power had the greatest effect on the event timings.

   The predominant difference between scoping Case 3 and sensitivity Case 1 was about a 9% decrease in decay power. This delayed steam generator dryout by 10 min, core heatup by 30 min, and RCS failure by about 50 min. By comparison, the longest delay of the RCS failure in the sensitivity calculations was about 45 min for the bounding analysis in which no steam generator inlet plenum mixing occurred.

3. Natural circulation flows resulted in high ex-vessel structure temperatures.

   Modeling of the multidimensional flows in the vessel and hot leg resulted in hot vapor flowing through the upper plenum and hot leg. The temperatures of the upper plenum, hot leg, steam generator, and surge line structures were high enough that oxidation, melting, or creep rupture failure may occur. With no natural circulation flows modeled, the ex-vessel structures remained at or near the saturation temperature. The hot leg countercurrent flow transferred about 30% of the energy removed from the core to the coolant loops.

4. Hot leg countercurrent flow led to the likely creep rupture failure of the pressurizer surge line about 4 hr into the transient.

   Creep rupture failure of the surge line was predicted in all of the sensitivity calculations within 13 min of the base case time of 246 min, except when there was no mixing in the steam generator inlet plena (Case 4). In that calculation, the lot legs failed at about 290 min, shortly before the surge line, although the calculated surge line temperature may have been too low. Two important points should be remembered in regard to this conclusion. Should the loop seals clear, there will be no hot leg countercurrent flow, and the steam generator tubes may fail first. Second, no penetrations of the hot legs were modeled besides the surge line (instrument taps, small pipes, etc.).

5. Steam generator tube failure will probably not occur.

   The temperature of the steam generator tubes remained near the saturation temperature without hot leg natural circulation modeled. With the hot leg flow, the tube temperatures were generally several hundred K lower than the surge line temperature. In the limiting hot leg flow case of no inlet plenum mixing, the tube temperatures were close to the hot leg and surge line temperatures, yet those structures failed by the end of the calculations, while the tubes did not. Should the loop seals clear of liquid, the tubes may be heated fast enough to fail first. Without failure of the tubes, containment bypass

through the secondary system relief valves would not occur.

6. The RCS will have time to depressurize before the reactor vessel melt-through.

   In seven of the nine sensitivity calculations, the RCS failure occurred within 3.1 min of the onset of fuel rod relocation; relocation began 7.4 and 15.2 min before the RCS failure in the other two. Since the MELPROG calculation showed that vessel melt-through occurred nearly 100 min after fuel rod relocation began, the RCS failure should occur at least 85-100 min before the core leaves the reactor vessel.

7. The RCS depressurization may quench the core.

   With a 0.15-m diameter surge line failure, the rapid injection of accumulator water quenched the entire core. Smaller failures may result in slow accumulator injections that may quench only part, or none, of the core. The quench may also result in debris bed formation as the oxidized cladding fragments.

8. The hot leg countercurrent flow was determined by the inlet vapor temperature and the steam generator inlet plenum mixing.

   The hot leg flow as a function of the inlet vapor temperature only changed when the amount of mixing in the inlet plenum changed. Changes in the upper plenum behavior affected the hot leg flow only in that they altered the hot leg inlet vapor temperature. Heat loss from the piping did not affect the hot leg flow rate because cooler vapor then entered the steam generator tubes, reducing the heat transfer in the steam generators commensurately.

9. The upper plenum flow was affected by the hot leg behavior.

   As expected, changing the upper plenum crossflow resistances changed the flow circulating in the upper plenum. The hot leg flow also affected the upper plenum flow by changing the temperature of the vapor returning from the steam generators. As the loop heat transfer increased, for the same hot leg inlet temperature, cooler vapor was returned to the upper plenum, increasing the buoyant driving force and the recirculating flow in the plenum.

10. Fuel rod cladding ballooning generally had little effect on the core flows.

    The ballooning that occurred in most cases changed the core flow rates without changing the flow pattern. However, in sensitivity Case 9, ballooning changed the flow pattern and heatup rate by accelerating the oxidation of the ballooned cladding in the middle channel.

11. Ballooning did affect the core damage.

    Cladding that ballooned and failed oxidized on both the inner and outer surfaces, so that the cladding was completely oxidized by the time Zircaloy would begin to melt. With no molten Zircaloy, fuel dissolution and relocation at temperatures below the fuel melting point could not occur. Oxidation of the cladding inner surface increased the hydrogen generation rate and accelerated the core heatup.

12. Increasing the hot leg flow extended the time to RCS failure.

    A 25% increase in the hot leg flow (sensitivity Case 3) delayed the surge line failure by 3.5 min compared to the base case. With a bounding 50-60% flow increase, the RCS failure occurred in the pressurizer loop hot leg 44.2 min later than the surge line failure in the base case.

13. Heat loss from the hot leg and surge line piping did not significantly alter the transient.

    With a convective boundary condition on the pipe outer wall (Case 5), heat loss to the containment accounted for 4% of the heat removed from the core, delaying the surge line failure by 6.6 min compared to the base case. Adding a radiative heat transfer coefficient as well (Case 6) increased the heat loss by 25% and delayed

the surge line failure an additional 6.3 min.

14. Changing the crossflow resistances had a small effect on the transient.

    Reducing the upper plenum (Case 7) or core (Case 8) crossflow loss coefficients by a factor of 10 resulted in surge line failure less than 2 min earlier than in the base case. Increasing the loss coefficients in both locations by a factor of 10 (Case 9) had a similarly small effect on the temperatures until ballooning occurred, accelerating the heatup and leading to surge line failure 12.4 min earlier than the base case.

15. Changing the axial power profile had little effect on the transient.

    In the base case, a bottom-peaked, relatively flat axial power profile was used. In sensitivity Case 2, a center-peaked chopped cosine profile was used, resulting in slightly different core flows that accelerated the surge line failure by 1.3 min.

16. The slow draining of liquid from the pressurizer will have little effect on the fission product behavior.

    If fission products must pass through the liquid in the pressurizer before entering the containment through the PORV discharge piping, many of them may be scrubbed by the liquid so that few are released to the containment. Although liquid remains in the pressurizer for a long time, the scrubbing benefits will be minimal because of the small release (less than 3%) of fission products before all of the liquid is boiled.

17. Mechanistic analyses are needed to accurately describe the plant severe accident response.

    A comparison of the once-through calculation (scoping Case 1) with the draft NUREG-1150 results, which should have similar detail in the core modeling, showed that vessel failure occurred in the draft NUREG-1150 analysis before fuel rod relocation began in the SCDAP/RELAP5 analysis. Addition of the natural circulation flows enlarged the difference in timing, and added the structural failure concerns that were not addressed in the draft NUREG-1150 calculations. These differences demonstrate the importance of performing deterministic analyses of severe accidents.

18. Detailed calculations of the effects of the natural circulation flows should be performed to the time of vessel failure.

    The effects of the natural circulation flows and slower heatup on the core debris formation and composition need to be investigated. The composition of the melt will affect the core/concrete interaction in containment, and subsequently the containment loading, fission product behavior, and ultimately the source term for the accident.

19. The RCS failure size should be determined, and the resultant depressurization calculated.

    The relation between natural circulation and direct containment heating dictates that the transient be continued until vessel failure to determine the RCS pressure that will drive the melt ejection. A 0.15-m diameter surge line break caused the RCS to depressurize fast enough to quench the entire core before fuel rod relocation could begin, indicating that the vessel melt-through would probably occur at low pressure, reducing the impact of direct containment heating. A larger failure size would affect the plant similarly, while the effects of a smaller break need to be determined.

20. The effects of natural circulation flows on fission product transport and deposition should be investigated.

    With the natural circulation flows providing a path for moving released fission products through most of the RCS, significant retention of fission products may occur. Fission products deposited on the pipes may also heat the structures, leading to their reevolution or to structural failure.

The disposition of these deposited fission products after the vessel fails, or after an ex-vessel failure, needs to be determined since it will directly affect the fission product inventory in the containment, and thus the source term.

21. Experiment data from more prototypic conditions would aid in the modeling of the hot leg countercurrent flow.

    The experiments that have been performed to date have been at relatively low pressures and temperatures with cooling water provided in the steam generator secondary. Computer simulations of these experiments have been used to build models for full-scale plant applications at high pressure and high temperature. Data at higher temperatures, in which heat transfer to the hot leg piping may be significant, and with no cooling water flow in the steam generators would be very useful in evaluating the applicability of the current modeling approach.

22. The effects of noncondensibles on the natural circulation flows should be investigated.

    The computer codes being used to model the natural circulation flows can only separate and concentrate noncondensibles by condensing the steam. Additional investigation would be useful in determining whether significant separation of the steam and noncondensibles may occur in these low velocity flows, and whether any such separation would affect the flows or the heat transfer.

23. The fuel rod model in SCDAP/RELAP5 should be modified to account for cladding interactions with the grid spacers.

    In the scoping calculations, ballooning was being calculated under conditions in which failure of the cladding may have already occurred. In the sensitivity calculations, cladding/grid spacer interactions were simulated by imposing a temperature failure criterion on the cladding in addition to the strain failure criterion associated with ballooning. The cladding failed before ballooning in nearly all of the sensitivity calculations.

REFERENCES

1. M. Silberberg, J. A. Mitchell, R. O. Meyer, and C. P. Ryder, *Reassessment of the Technical Bases for Estimating Source Terms*, NUREG-0956, July 1986.

2. U.S. Nuclear Regulatory Commission, *Reactor Risk Reference Document (Draft for Comment)*, NUREG-1150, February 1987.

3. U.S. Nuclear Regulatory Commission, *Uncertainty Papers on Severe Accident Source Terms*, NUREG-1265, May 1987.

4. T. C. Cheng et al., "RELAP5/SCDAP - An Integrated Code for Severe Accident Analysis," *Proceedings of the Thirteenth Water Reactor Safety Research Information Meeting, Gaithersburg, MD, October 22-25, 1985*, NUREG/CP-0072, pp. 347-355.

5. W. A. Stewart, A. T. Pieczynski, and V. Srinivas, "Experiments on Natural Circulation Flows in Steam Generators During Severe Accidents," *Proceedings of the International ANS/ENS Topical Meeting on Thermal Reactor Safety, San Diego, CA, February 2-6, 1986.*

6. H. M. Domanus, R. C. Schmitt, W. T. Sha, and V. L. Shah, *Analysis of Natural Convection Phenomenon During Postulated Station Blackout Transient Accident*, ATHRP-30, January 1987.

7. M. Hansen and K. Anderko, *Constitution of Binary Alloys, Second Edition*, Schenectady, NY: Genium Publishing Corporation, August 1986, pp. 742,1060.

8. S. Hagen and P. Hoffmann, *Physical and Chemical Behavior of LWR Fuel Elements up to Very High Temperatures*, KfK4104, June 1987.

9. S. Hagen, L. Sepold, P. Hoffmann, and G. Schanz, "Out-of-Pile Experiments on Severe Fuel Damage Behavior of LWR Fuel Elements (CORA Program)," *IAEA International Symposium on Severe Accidents in Nuclear Power Plants, Sorrento, Italy, March 21-25, 1988.*

10. B. L. Harris, V. N. Shah, and G. E. Korth, *Creep Rupture of Three Components of the Reactor Primary Coolant System During the TMLB' Accident*, EGG-EA-7431, November 1986.

11. H. M. Domanus and W. T. Sha, *Analysis of Natural-Convection Phenomena in a 3-Loop PWR during a TMLB' Transient Using the COMMIX Code*, NUREG/CR-5070, ANL-87-54, January 1988.

12. P. D. Bayless, C. A. Dobbe, and R. Chambers, *Feedwater Transient and Small Break Loss of Coolant Accident Analyses for the Bellefonte Nuclear Plant*, NUREG/CR-4741, EGG-2471, March 1987.

13. R. S. Denning et al., *Radionuclide Release Calculations for Selected Severe Accident Scenarios (PWR, Subatmospheric Containment Design)*, NUREG/CR-4624, BMI-2139, Vol. 3, July 1986.

14. J. E. Kelly, R. J. Henninger, and J. F. Dearing, *MELPROG-PWR/MOD1 Analysis of a TMLB' Accident Sequence*, NUREG/CR-4742, SAND86-2175, January 1987.

15. G. B. Wallis, *One-Dimensional Two-Phase Flow*, New York: McGraw-Hill, 1969.

16. W. M. Rohsenow and H. Choi, *Heat, Mass, and Momentum Transfer*, Englewood Cliffs, NJ: Prentice-Hall, Inc., 1961, pg. 102.

17. R. Siegel and J. R. Howell, *Thermal Radiation Heat Transfer, Second Edition*, Washington: Hemisphere Publishing Corporation, 1981, pg. 834.

18. N. Lee, "Discussion on Loop Seal Behavior During Cold Leg Small Break LOCAs of a PWR," *Nuclear Engineering and Design 99*, pp. 453-458, 1987.

APPENDIX A

PLANT AND MODEL DESCRIPTIONS

APPENDIX A

PLANT AND MODEL DESCRIPTIONS

The SCDAP/RELAP5 model of the plant included all of the major components necessary to perform the station blackout analyses. The reactor vessel, three coolant loops, three steam generators, and the pressurizer were modeled. Information was obtained from References A-1 and A-2.

Each of the three coolant loops was modeled, as were the associated steam generators. The loop model included both the fluid volume and the metal structures. Figure A-1 shows the nodalization of one of the coolant loops. The piping was assumed to be adiabatic on the outer surface. The pressurizer and surge line were attached to one of the coolant loops (Loop C). The surge line piping and pressurizer shell were modeled as heat structures, again with adiabatic outer surfaces. The pressurizer heaters were not modeled, as power was not available to them during the transient. The two pressurizer power-operated relief valves (PORVs) were modeled as a single valve connected to the top of the pressurizer. The valve was sized to provide a saturated steam flow rate of 45.1 kg/s at 16.2 MPa, which is twice the rated capacity of one PORV. Similarly, the three safety relief valves (SRVs) on the pressurizer were modeled as a single valve. It was assumed that there was sufficient battery power and plant air to operate the PORVs as long as the transient continued. Piping downstream of the PORVs and SRVs was not modeled. The accumulators were the only available part of the emergency core cooling system for these transients. Each of the three accumulators injected into a different cold leg and contained 29100 kg of 322 K borated water with a nitrogen cover gas pressure of 4.24 MPa.

The steam generator model included the tubes, downcomer, riser, separator, steam line, main and auxiliary feedwater systems, main steam isolation valve, PORVs, and SRVs. The metal masses associated with the steam generator walls and internals were modeled, with the outer surface of the steam generators assumed to be adiabatic.

Two reactor vessel models were developed for the analyses. The single-channel model, whose nodalization is shown in Figure A-2, was used for the once-through calculation. The fluid volumes modeled include the downcomer, lower head, lower plenum, core, core bypass, upper plenum, and upper head. The core bypass represented the fluid volume between the core barrel and the core baffle, and connected the lower plenum and the upper plenum. Flow paths were modeled between the inlet annulus and the upper head and between the inlet annulus and the upper plenum (leakage around the hot leg nozzles). Flow between the upper plenum and upper head occurred only through the guide tube assemblies. Heat structures modeled include the reactor vessel walls, the core barrel and baffle, the thermal shield, the upper and lower core support plates, and structures in the lower and upper plena. The three-channel model nodalization is shown in Figure A-3. The core and upper plenum volumes were divided into three radial regions. The core regions were selected so that similarly powered fuel assemblies were grouped together. The upper plenum regions were extensions of the core region boundaries. The three channels were connected at each elevation (except the top of the upper plenum) by crossflow junctions, so that a nearly two-dimensional model of the core and upper plenum was available for the in-vessel natural circulation calculations. The deep beam weldments were assumed to provide barriers to radial flow in the top of the upper plenum, so that the uppermost volumes in the upper plenum were not connected to each other. Figure A-4 shows a cross-section of the three channel core model. The number of fuel assemblies in each region, along with their relative powers, is also provided.

The 3.66 m active fuel length was divided into ten equal axial nodes, numbered 1 to 10 from bottom to top, corresponding to the nodalization of the fluid volumes in the core. SCDAP structures were used to model the fuel rods, control rods, and instrument tubes and empty control rod guide tubes in each channel in the core. Thus, three SCDAP components were used in the once-through core model, and nine SCDAP components were used in the three-channel model. Figure A-5 shows a typical fuel assembly. Grid spacers were assumed to be located at the bottom of nodes 1, 3, 5, 6, 7, and 9. There are 48 full length and 5 partial length control assemblies in the Surry core: 8 full and 1 partial length in the center channel, 32 full and 4 partial length in the middle channel, and 8 full and 0 partial length in the outer channel. The

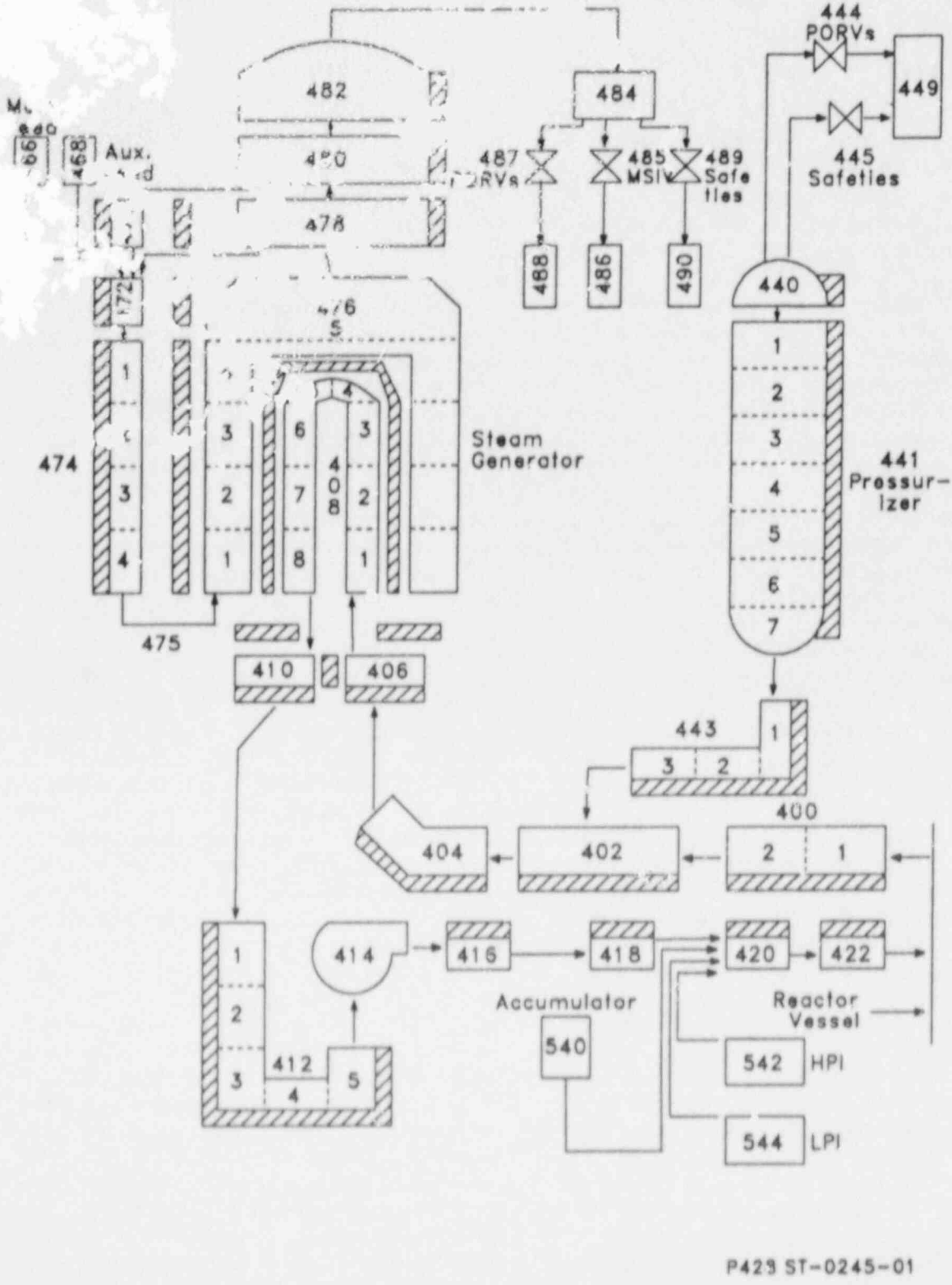

Figure A-1. Nodalization of the pressurizer coolant loop for the Surry SCDAP/RELAP5 calculations.

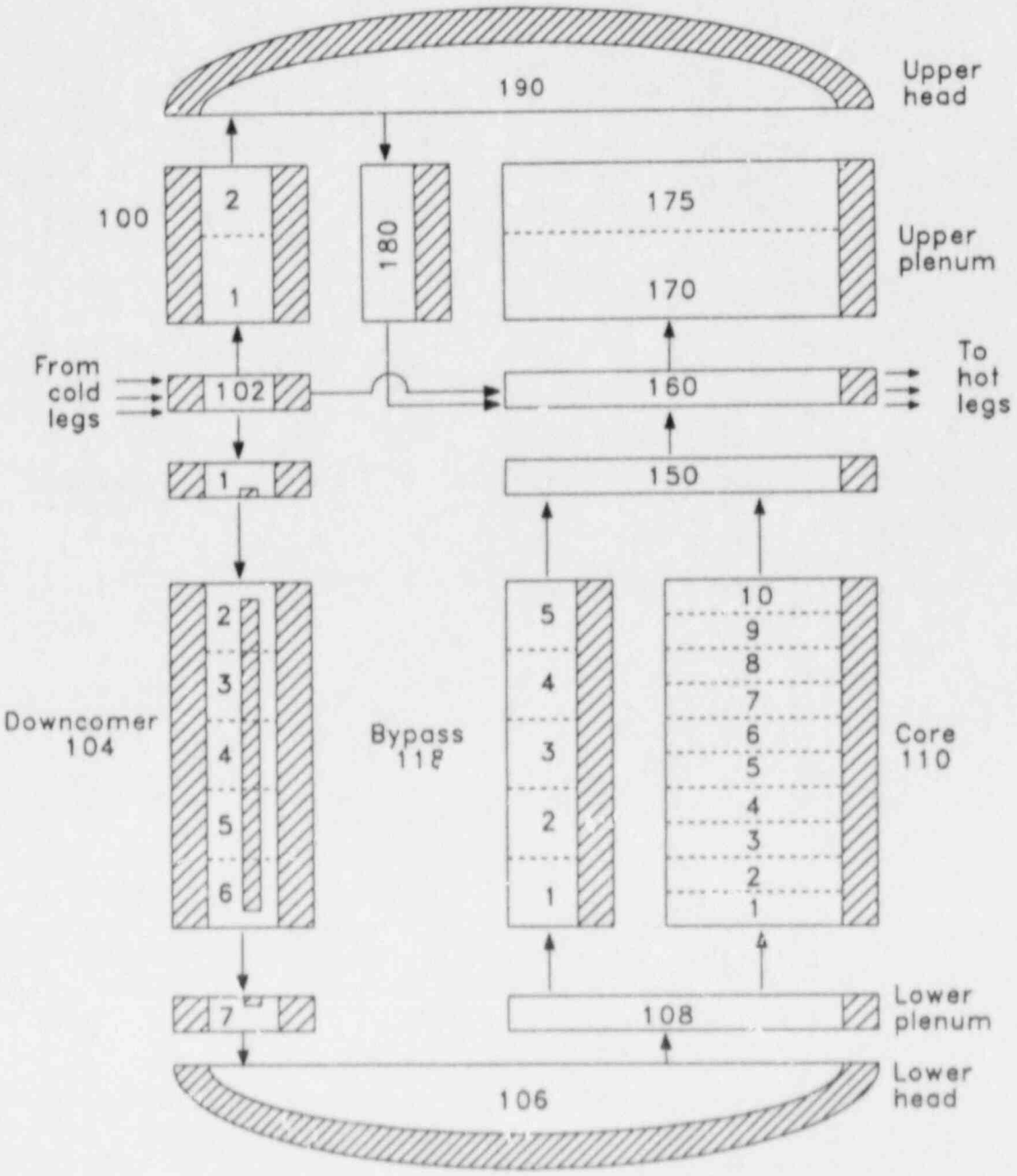

P428 ST-0245-03

Figure A-2. Nodalization of the single-channel reactor vessel for the once-through Surry SCDAP/RELAP5 calculation.

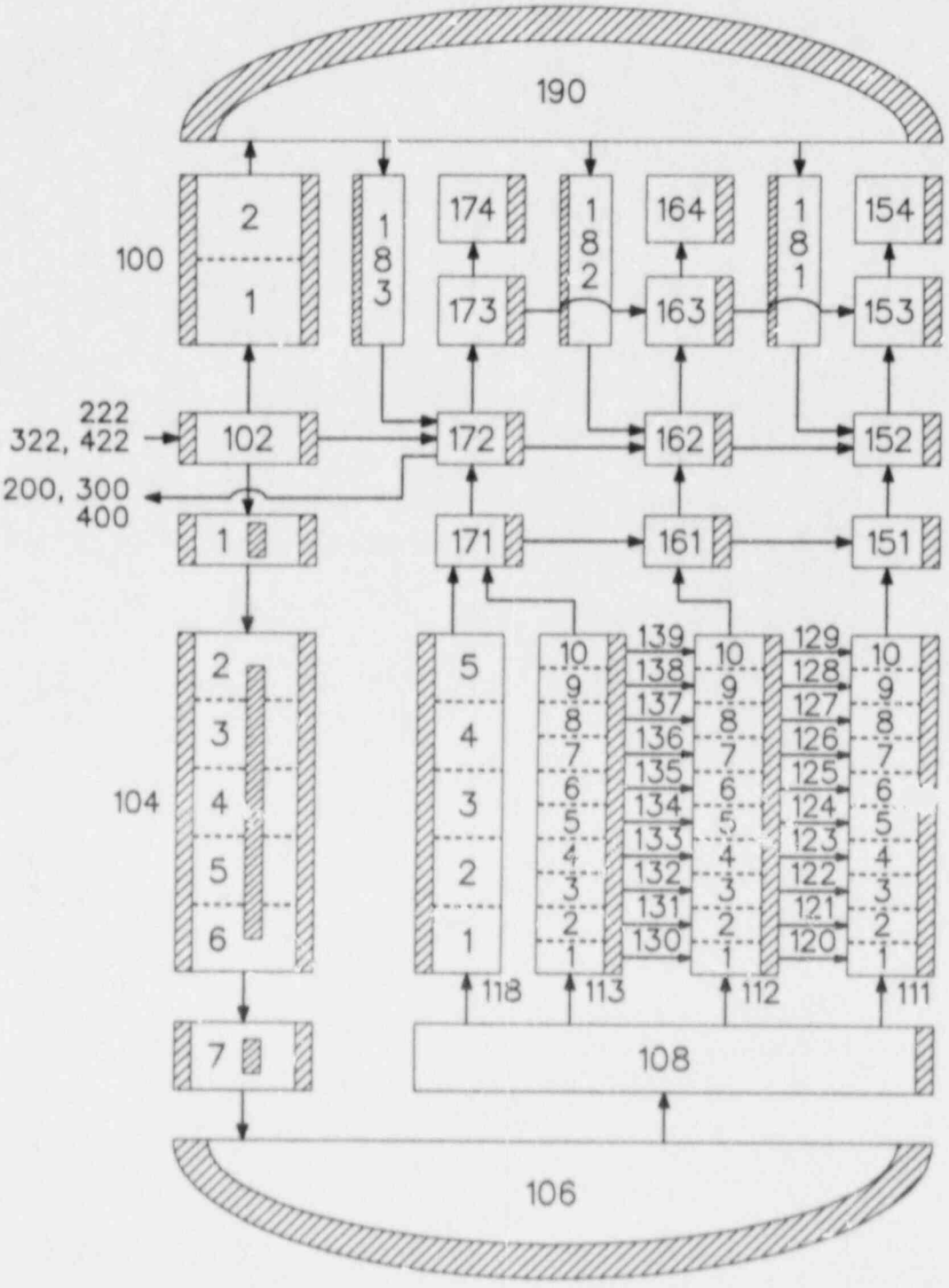

P394-LN87017-1

Figure A-3. Nodalization of the reactor vessel for the Surry SCDAP/RELAP5 calculations with in-vessel natural circulation.

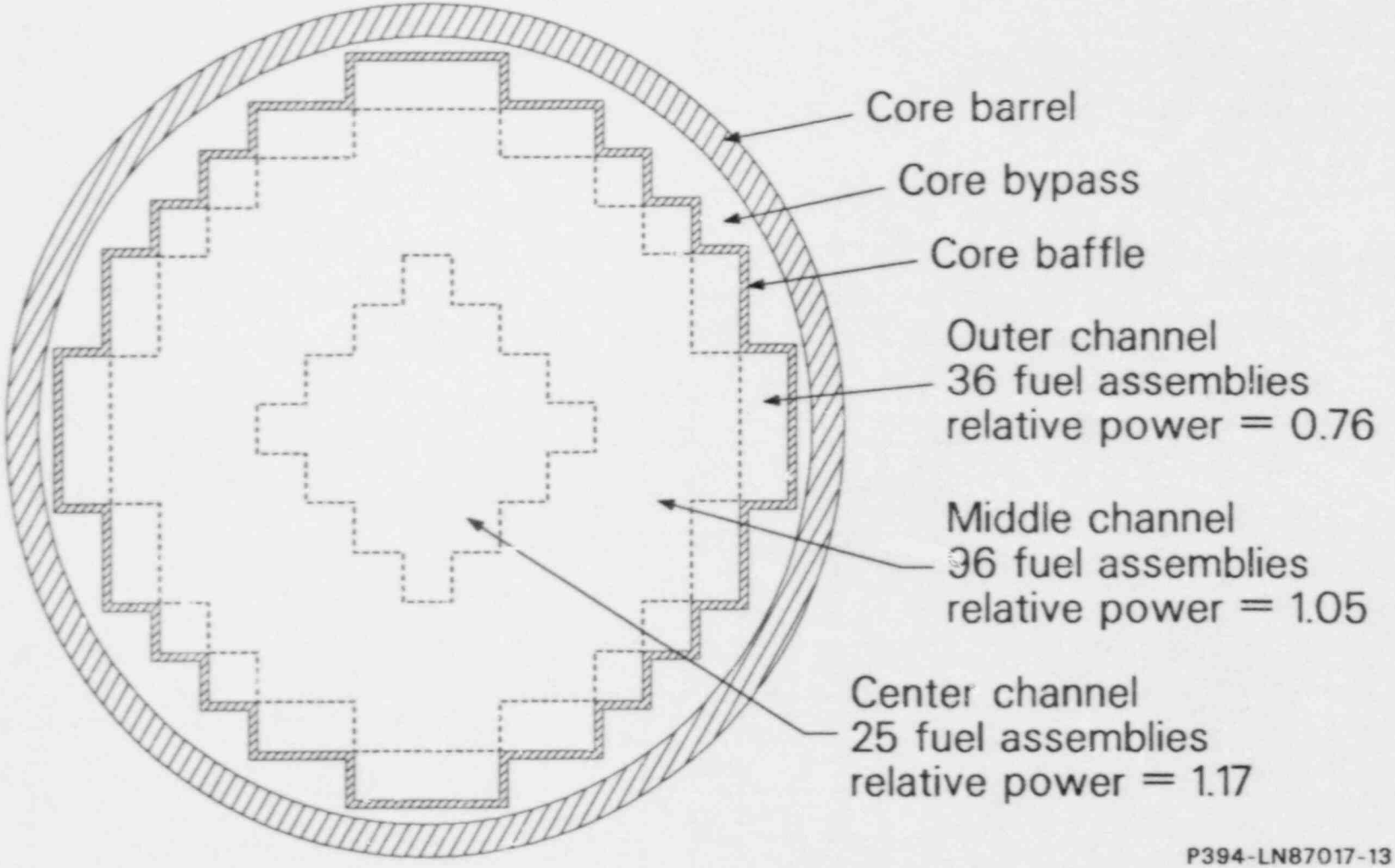

Figure A-4. Cross section of the three-channel core region.

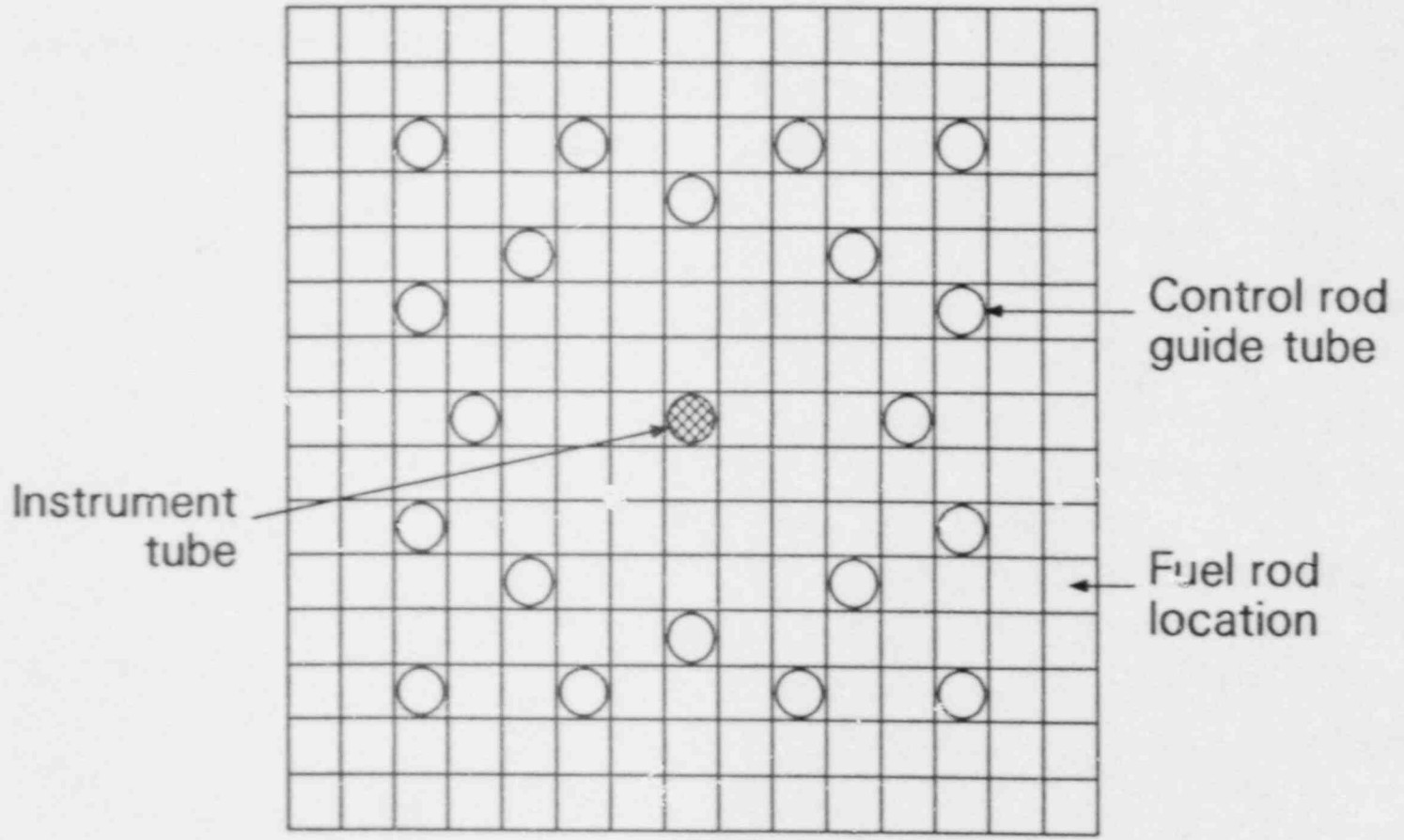

P431-LN87031-1

Figure A-5. Typical arrangement of a Surry fuel assembly.

control material is Ag-In-Cd. The fuel rods were assumed to be prepressurized to 2.4 MPa. The same axial power profile was used in each of the core channels. The scoping calculations and sensitivity Case 2 used an axisymmetric chopped cosine axial power profile with a peak-to-average power ratio of 1.200 located in nodes 5 and 6. The rest of the calculations used a flatter axial power profile having a peak-to-average power ratio of 1.155 located in node 3. The core was assumed to be at the end of an equilibrium cycle, which corresponded to an average burnup of 21,000 MWd/t.[A-1] Both radial and axial conduction were accounted for in the cladding heat transfer calculations. A control system was used to approximate the behavior of molten material that relocated below the core. A heat structure was located in the lower plenum that received the energy of the relocated material. The structure then dissipated this energy, allowing water in the lower plenum to be boiled.

In order to simulate the hot leg countercurrent flow, several modeling changes were made. Figure A-6 shows the nodalization of one loop for the hot leg countercurrent flow calculations. All three loops were modeled this way, except that the surge line was connected only to Loop C. The hot leg was divided into top and bottom halves. The return flow from the bottom half of the hot leg entered the reactor vessel at the top of the volume below the hot leg nozzle connection. This approximated the elevation difference between the top and bottom halves of the hot leg, so that the driving head for the natural circulation flow should be close to that of the actual situation. It also prevented the hot and cold steam flows from mixing immediately in the upper plenum. The steam generator inlet plenum was divided into three volumes. A mixing volume in the middle connected to the flows entering and leaving both the hot leg and the steam generator tubes. The volumes on either side of the mixing volume passed the hot and cold vapor that did not mix with the other fluid in the inlet plenum between the hot leg and steam generator tubes. The amount of flow entering and leaving the mixing volume was adjusted by changing the loss coefficients and flow areas. Guidance in adjusting the flows was obtained from calculations of a similar transient performed at Argonne National Laboratory using the three-dimensional COMMIX computer code.[A-3] The unmixed fluid flow areas were reduced to 5% of the flow area leaving the hot leg and steam generator tubes. Large loss coefficients were added to the junctions in the hot legs and steam generator plena to provide the desired amount of heat transfer to the steam generator tubes and hot leg piping for a given hot leg inlet temperature, based on the COMMIX calculation. Two sets of tubes connected the inlet and outlet plena. The hot flow tubes represented 35% of the flow and heat transfer area; the cold return flow tubes represented 65% of the total flow and heat transfer area. This division of the steam generator tubes was based on results of the Westinghouse natural circulation experiments.[A-4] The reactor coolant pump suction piping was still connected to the steam generator outlet plenum, so that clearing of the liquid from the loop seals could occur if appropriate conditions existed. Since the pressurizer surge line connected to the side of the hot leg, the horizontal portion of the surge line (the two volumes at the hot leg end) was also split into top and bottom halves, connected to the top and bottom halves of the hot leg, respectively, in the sensitivity calculations. For the scoping calculations, the pressurizer surge line was not split. Because of difficulties with reverse flow through the pressurizer loop (encountered during testing of the model), a valve was inserted at the connection of the bottom of the hot leg to the reactor vessel for the scoping calculations. This valve was closed when the PORVs were open, preventing vapor in the vessel from entering the bottom of the hot leg until the PORVs closed. This valve was not needed with the split surge line model. Creep damage calculations were performed for each hot leg near the reactor vessel, for the hottest part of the steam generator tubes in each loop, and for the hot leg end of the surge line.

This hot leg model evolved from low pressure, low temperature experiments performed by Westinghouse using SF_6 as the working fluid.[A-4] These experiments were then simulated using the COMMIX computer code. COMMIX was then used to simulate a high pressure, high temperature transient in a commercial plant. The plant model included the core, upper plenum, hot legs, steam generators, surge line, and PORV. Pipes and steam generator tubes were modeled with adiabatic outer boundary conditions. The transient was a 2000 s heatup from saturated vapor conditions throughout the model. This transient was then calculated using SCDAP/RELAP5. The mixing volume, junction areas in the inlet plena, and loss coefficients were adjusted to reproduce the COMMIX-calculated integral heat transfer in the loops as a function of the hot leg inlet vapor temperature. The model developed, which did not have a split surge line, was within 7% of the COMMIX values. The

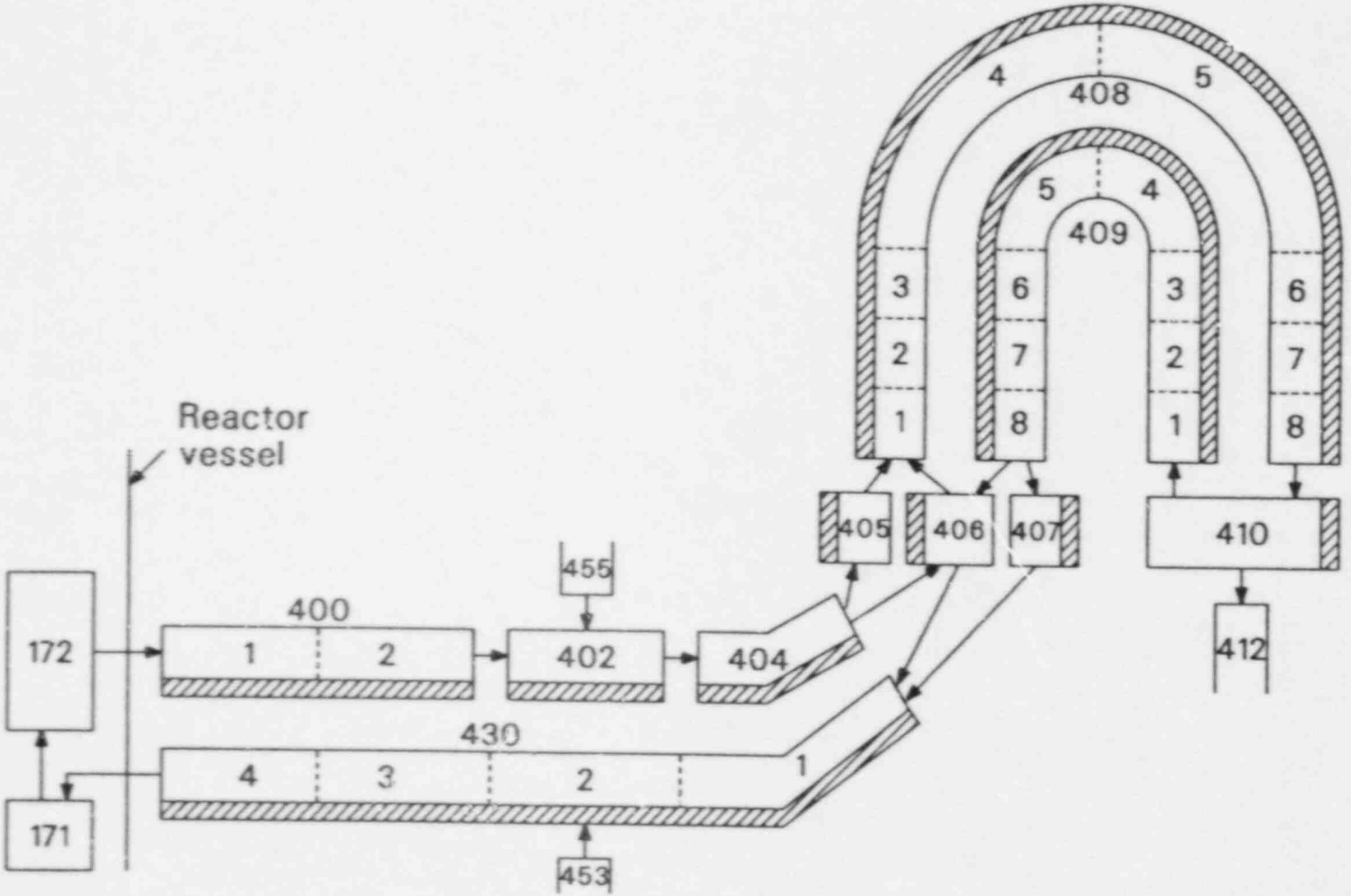

P431-LN87031-2

Figure A-6. Nodalization of the hot leg and steam generator for the Surry SCDAP/RELAP5 calculations with hot leg natural circulation.

hot leg flow rates were lower than those calculated by COMMIX, but that was not a large concern because the heat transfer to the loops was the most important parameter, and the one that was being matched. The flow characteristics were also somewhat different than in the COMMIX calculation and the Westinghouse experiments, in that the flows in the tops of the non-pressurizer loop hot legs did not reverse when the PORVs were open, although their magnitudes were reduced. This hot leg model was then used for the scoping calculations, and the split surge line was added for the sensitivity calculations.

For the calculation in which inlet plenum mixing was not considered, the mixing volume was removed. The two through-flow volumes were increased in size, so that each modeled one-half of the inlet plenum. The steam generator tubes were not changed from the model discussed above.

Full power steady state calculations were performed for both the scoping and sensitivity analyses, since different versions of the code were used. Results of the steady state calculations are presented in Table A-1, together with the desired values for several key parameters. There was good agreement between the calculated and desired steady state conditions.

Table A-2 presents the initial inventory of five significant fission product elements for the various calculations. It can be seen that there is a significant difference in initial inventory for four of the elements for the sensitivity analyses, for which calculations were performed using both SCDAP/RELAP5 and ORIGEN2[A-5], with the ORIGEN2 values being 8-40% lower. SCDAP/RELAP5 uses PARAGRASS[A-6] to calculate the fission product initial inventory and subsequent release. The values calculated by ORIGEN2 are believed to be more accurate because of the more extensive physics and cross section data used, and because PARAGRASS was primarily developed for trace-irradiated fuel rather than the high-burnup fuel associated with the end of an equilibrium fuel cycle. ORIGEN2 calculations were not performed for the scoping studies.

The power used in SCDAP/RELAP5 is divided into three components: prompt (fission) power, fission product decay power, and actinide decay power. Different decay power values were used in the scoping and sensitivity calculations.

For the scoping calculations, the decay heat was calculated internally by the code. This calculation uses the ANS 5.1[A-7] standard and assumes only one fissile isotope (U^{235}). A core-average burnup for the end of an equilibrium cycle (21000 MWd/MT) was assumed. To achieve this burnup, the fuel assemblies in each channel were assumed to have been in that region of the core during a 22.5 month period of full power reactor operation. The prompt power was assumed to decrease linearly from full power to zero in the first 2 s. Table A-3 lists the decay power for these calculations.

For the sensitivity calculations, ORIGEN2 calculations were performed to generate input power tables for SCDAP/RELAP5. It was assumed that fuel is loaded such that fresh fuel is added to the core periphery, from where it moves radially inward on subsequent refuelings until it is eventually removed from the center of the core. It was assumed that 52 assemblies were added at the beginning of the current cycle, 52 assemblies were in their second cycle, and 53 assemblies were in their third and final cycle. Accordingly, the center channel contained 25 assemblies with three cycle burnup, the middle channel contained 28 assemblies with three-cycle burnup, 52 assemblies with two-cycle burnup, and 16 assemblies with one-cycle burnup, and the outer channel contained 36 assemblies with one-cycle burnup. ORIGEN2 calculations were performed to determine the fission product and actinide decay after the reactor scram. Calculations were performed for the irradiation of assemblies in each of the three core channels. The last irradiation cycle was assumed to be at the relative radial power described earlier (see Figure A-4). The two- and three-cycle burnup assemblies were assumed to have been irradiated at average core power prior to the current cycle. The resulting fission product decay power values were multiplied by a factor to account for neutron absorption by the fission products [G(t) in ANS 5.1], which had a very small effect on the power until after 10000 s. The prompt power decay was developed from a RELAP5 kinetics calculation. It was assumed that the prompt power began to decay when the control rods started to enter the core, at 0.7 s after the loss of power. The decay of the fission products and actinides was assumed to begin at 1.0 s after the start of the transient. Table A-4 lists the decay power input for the sensitivity calculations.

Table A-5 provides some details on the sizes of the various models used and the computer time needed to perform the natural circulation calculations. The scoping calculations were performed on a CRAY-1S computer, while the sensitivity calculations were performed on a CRAY X-MP/24.

Table A-1. Comparison of computed and desired steady state parameters

Parameter	Scoping Study	Sensitivity Study	Desired
Core thermal power, MW	2442	2443	2441
Pressurizer pressure, MPa	15.5	15.5	15.5
Pressurizer liquid level, m	6.05	6.62	6.62
Hot leg temperature, K	592.0	591.7	591.9
Cold leg temperature, K	557.3	557.0	557.0
Coolant flow per loop, kg/s	4230	4230	4230
Steam generator pressure, MPa	5.49	5.71	5.41
Steam generator liquid mass, kg (each)	44000	44000	44000
Steam generator feedwater flow, kg/s	443.9	444.6	441.8

Table A-2. Initial inventory for five fission product elements

	Fission Product Mass (kg)			
	Scoping Calculations		Sensitivity Calculations	
Element	One-channel	Three-channel	SCDAP/RELAP5	ORIGEN2
Xenon	257.4	253.9	258.3	238.4
Krypton	28.99	29.16	28.10	17.44
Cesium	186.1	187.2	186.7	125.5
Iodine	10.39	10.45	10.42	10.79
Tellurium	23.91	24.05	23.98	21.12

Table A-3 Decay power for the scoping calculations

Time (s)	Center Channel (MW)			Middle Channel (MW)		
	Prompt	Fission Product	Actinide	Prompt	Fission Product	Actinide
0.0	419.8	31.00	1.465	1446.8	106.8	5.050
2.0	0.0	27.03	1.465	0.0	93.12	5.045
10.0	0.0	21.90	1.461	0.0	75.43	5.035
100.0	0.0	14.18	1.428	0.0	48.86	4.919
1000.0	0.0	8.574	1.163	0.0	29.53	4.007
5000.0	0.0	5.238	0.747	0.0	18.04	2.574
7600.0	0.0	4.572	0.693	0.0	15.74	2.389
8000.0	0.0	4.496	0.689	0.0	15.48	2.374
8500.0	0.0	4.408	0.684	0.0	15.18	2.359
9000.0	0.0	4.328	0.681	0.0	14.90	2.346
9500.0	0.0	4.252	0.678	0.0	14.64	2.335
10000.0	0.0	4.182	0.675	0.0	14.40	2.325
10500.0	0.0	4.338	0.672	0.0	14.95	2.317
11000.0	0.0	4.275	0.670	0.0	14.73	2.310
11500.0	0.0	4.216	0.668	0.0	14.53	2.303
12000.0	0.0	4.160	0.667	0.0	14.34	2.297
12500.0	0.0	4.109	0.665	0.0	14.16	2.292
13000.0	0.0	4.060	0.664	0.0	13.99	2.287
14000.0	0.0	3.968	0.661	0.0	13.68	2.277
20000.0	0.0	3.559	0.647	0.0	12.26	2.229

Table A-3. (continued)

Time (s)	Outer Channel (MW)			Single Channel (MW)		
	Prompt	Fission Product	Actinide	Prompt	Fission Product	Actinide
0.0	392.7	28.99	1.371	2267.8	166.4	7.866
2.0	0.0	25.26	1.370	0.0	145.0	7.862
10.0	0.0	20.44	1.367	0.0	117.5	7.845
100.0	0.0	13.25	1.336	0.0	76.12	7.666
1000.0	0.0	8.008	1.088	0.0	46.00	6.244
5000.0	0.0	4.887	0.699	0.0	28.09	4.010
7600.0	0.0	4.264	0.648	0.0	24.51	3.721
8000.0	0.0	4.193	0.644	0.0	24.11	3.699
8500.0	0.0	4.110	0.640	0.0	23.63	3.674
9000.0	0.0	4.034	0.637	0.0	23.20	3.654
9500.0	0.0	3.963	0.634	0.0	22.80	3.637
10000.0	0.0	3.898	0.631	0.0	22.42	3.623
10500.0	0.0	4.057	0.629	0.0	23.29	3.610
11000.0	0.0	3.998	0.627	0.0	22.75	3.598
11500.0	0.0	3.943	0.625	0.0	22.63	3.589
12000.0	0.0	3.892	0.624	0.0	22.34	3.579
12500.0	0.0	3.844	0.622	0.0	22.05	3.570
13000.0	0.0	3.796	0.621	0.0	21.79	3.563
14000.0	0.0	3.711	0.618	0.0	21.30	3.548
20000.0	0.0	3.329	0.605	0.0	19.11	3.472

Table A-4. Decay power for the sensitivity calculations

Time (s)	Center Channel (MW)			Middle Channel (MW)		
	Prompt	Fission Product	Actinide	Prompt	Fission Product	Actinide
0.0	427.5	25.85	1.412	1472.8	90.13	4.324
0.7	427.5	25.85	1.412	1472.8	90.13	4.324
1.0	382.8	25.85	1.412	1318.7	90.13	4.324
1.5	324.3	24.68	1.412	1117.2	85.96	4.323
2.0	276.3	23.92	1.412	951.9	83.28	4.323
3.0	61.29	22.86	1.411	211.1	79.58	4.321
6.0	8.887	21.03	1.410	30.62	73.15	4.318
11.0	5.550	19.36	1.409	19.12	67.33	4.313
16.0	4.115	18.30	1.407	14.18	63.64	4.308
21.0	3.291	17.52	1.405	11.34	60.92	4.302
31.0	2.307	16.41	1.402	7.948	57.05	4.290
51.0	1.299	14.98	1.395	4.476	52.11	4.269
101.0	0.397	13.06	1.378	1.368	45.45	4.216
201.0	0.068	11.29	1.345	0.234	39.32	4.115
501.0	0.001	9.325	1.255	0.005	32.46	3.838
1001.0	0.0	7.918	1.132	0.0	27.58	3.458
2501.0	0.0	6.030	0.900	0.0	21.02	2.741
5001.0	0.0	4.755	0.744	0.0	16.55	2.263
10001.0	0.0	3.760	0.675	0.0	12.99	2.052
20001.0	0.0	3.215	0.646	0.0	11.11	1.965

Table A-4. (continued)

Time (s)	Outer Channel (MW)		
	Prompt	Fission Product	Actinide
0.0	399.1	25.24	1.013
0.7	399.1	25.24	1.013
1.0	357.4	25.24	1.013
1.5	302.8	24.03	1.013
2.0	258.0	23.26	1.013
3.0	57.22	22.20	1.013
6.0	8.297	20.37	1.012
11.0	5.182	18.71	1.011
16.0	3.842	17.67	1.009
21.0	3.072	16.91	1.008
31.0	2.154	15.83	1.005
51.0	1.213	14.45	1.000
101.0	0.371	12.61	0.988
201.0	0.063	10.91	0.964
501.0	0.001	9.000	0.898
1001.0	0.0	7.654	0.807
2501.0	0.0	5.839	0.637
5001.0	0.0	4.583	0.523
10001.0	0.0	3.567	0.474
20001.0	0.0	3.027	0.454

Table A-5. Computer calculation statistics

Calculation	Number of Volumes/ Junctions	Number of RELAP5 Heat Structures/ Mesh Points	Number of SCDAP Componeats	Transient Time (s)	CPU Time (s)
Scoping Analyses					
Case 1	168/177	195/909	3	12000	7269
Case 2	198/235	211/955	9	4400	11676
Case 3	240/289	259/1201	9	3200	8008
Sensitivity Analyses					
Case 1	247/297	262/1210	9	5400	7152
Case 2	247/297	262/1210	9	5289	7094
Case 3	247/297	262/1210	9	6400	10010
Case 4	244/285	259/1192	9	8400	13357
Case 5	248/297	262/1210	9	6174	8998
Case 6	248/297	262/1210	9	6400	9527
Case 7	247/297	262/1210	9	5400	7290
Case 8	247/297	262/1210	9	5400	7884
Case 9	247/297	262/1210	9	5176	7802
Surge line failure	247/297	262/1210	9	6400	19540

REFERENCES

A-1. Virginia Power Company, *Surry Power Station Updated Fin[illegible] Analysis Report*, Docket 05000280, 05000281, July 16, 1982.

A-2. J. D. Burtt, *Audit Calculations for a Main Steam Line Break in North Anna, Unit 2 Using the RELAP5 Computer Code*, EGG-NTAP-6082, November 1982.

A-3. H. M. Domanus and W. T. Sha, *Analysis of Natural-Convection Phenomena in a 3-Loop PWR during a TMLB' Transient Using the COMMIX Code*, NUREG/CR-5070, ANL-87-54, January 1988.

A-4. W. A. Stewart, A. T. Pieczynski, and V. Srinivas, "Experiments on Natural Circulation Flows in Steam Generators During Severe Accidents," *Proceedings of the International ANS/ENS Topical Meeting on Thermal Reactor Safety, San Diego, CA, February 2-6, 1986.*

A-5. A. G. Croff, *A Users Manual for the ORIGEN2 Computer Code*, ORNL-TM-7175, July 1985.

A-6. Argonne National Laboratory, *Light-Water-Reactor Safety Research Program: Quarterly Progress Report, July-September 1981*, NUREG/CR-2437 Vol. III, ANL-81-77 Vol. III, February 1982.

A-7. *American National Standard for Decay Heat Power in Light Water Reactors*, ANSI/ANS-5.1-1979.

APPENDIX B

COMPUTER CODE DESCRIPTION

APPENDIX B

COMPUTER CODE DESCRIPTION

The computer code used in the transient analyses was SCDAP/RELAP5.[B-1] A brief general description of the code, together with information on the specific versions used, is presented below.

The SCDAP/RELAP5 computer code is a light water reactor (LWR) system transient analysis code that is currently being developed. It can be used for simulation of a wide variety of system transients of interest in LWR safety but is designed especially to calculate the behavior of the reactor coolant system during severe accidents. The core, primary system, secondary system, feedwater train, and system controls can be simulated. The code models have been designed to permit simulation of postulated accidents ranging from small break loss of coolant accidents to severe accidents. Transient conditions can be modeled up to the point of vessel failure.

SCDAP/RELAP5 was produced by incorporating models from the SCDAP[B-2] and TRAP-MELT[B-3,4] codes into the RELAP5/MOD2[B-5] code. The SCDAP components model the structures in the reactor core. The TRAP-MELT models were used as a basis for the fission product transport and deposition models. RELAP5 models the fluid behavior throughout the system, as well as the thermal behavior of structures outside the core. The feedbacks between the various parts of the code were developed to provide an integral analysis capability. For example, the changes in coolant flow area associated with fuel cladding ballooning or relocation are taken into consideration in the hydrodynamics.

SCDAP/RELAP5 uses a one-dimensional, two fluid, nonequilibrium, six equation hydrodynamic model with a simplified capability to treat multidimensional flows. This model provides continuity, momentum, and energy equations for both the liquid and the vapor phases within a control volume. The energy equation contains source terms which couple the hydrodynamic model to the heat structure conduction model by a convective heat transfer formulation. The code contains special process models for critical flow, abrupt area changes, branching, crossflow junctions, pumps, accumulators, valves, core neutronics, and control systems. A flooding model can also be applied at vertical junctions. Appendix C contains more information on the crossflow junction, which is used to treat multidimensional flow.

SCDAP components simulate core disruption by modeling heatup, geometry changes, and material relocation. Detailed modeling of cylindrical and slab heat structure geometries is allowed. Thus, fuel rods, control rods and blades, instrument tubes, and flow shrouds can be represented. All structures of the same type, geometry, and power in a coolant channel are grouped together and one set of input parameters is used for each of these groupings or components. Code input identifies the number of rods or tubes in each component and their relative positions for the purpose of radiation heat transfer calculations. Models in SCDAP calculate fuel and cladding temperatures, Zircaloy and stainless steel oxidation, hydrogen generation, cladding ballooning and rupture, fuel and cladding liquefaction, flow and freezing of the liquefied materials, and release of fission products. Fragmentation of fuel rods during reflood is calculated. Oxidation of the inside surface of the fuel rod cladding is calculated for ballooned and ruptured cladding.

The fission product behavior includes aerosol agglomeration, aerosol deposition, evaporation and condensation, and chemisorption of vapors by stainless steel. Fission products are assumed to be released equally over the entire length of the fuel rods. The released fission products enter the coolant as aerosols, being put into the smallest size bin and allowed to agglomerate or evaporate as conditions dictate. The number of aerosol size bins used, as well as the fission product species tracked, is selected by the user. The chemical form of the fission products is fixed. All of the iodine is assumed to be in the form of CsI, with the remaining cesium being transported as CsOH. Fission products do not interact with the surfaces of SCDAP components (fuel rods, control rods, control blades, and shrouds).

The versions of the code used for the scoping calculations were SCDAP/RELAP5/MOD0 Cycles 48 and 51, with updates. The updates included error corrections that have been added to subsequent versions of the code, using steam properties in a control volume when the noncondensible quality was less than 0.001, and a generalized creep rupture model for RELAP5 heat structures. The sensitivity calculations used an updated version of SCDAP/RELAP5/MOD1 Cycle 5. Updates to the

code included several error corrections, and a change in the cladding failure subroutine that caused the cladding to fail when its temperature exceeded 1470 K, if it had not already failed following ballooning. This change simulated the interaction between the Zircaloy cladding and the Inconel grid spacers, which would be expected to form holes in the cladding by the time this temperature was attained.[B-6,7]

The core damage part of the SCDAP/RELAP5 code does not consider the metallurgical interaction of Zircaloy cladding and grid spacers. As mentioned above, a simple model of the effect of such interactions on the intact fuel rod cladding was used in the sensitivity calculations. Interactions between molten material and the fluid below the core were not explicitly modeled in these versions of the code, although enough information was available to use a control system to dissipate the energy in the molten material. Models of the debris formation and behavior in the reactor vessel lower head have been developed and incorporated in more recent versions of SCDAP/RELAP5. The oxidation of control rod stainless steel occurs only if the surrounding Zircaloy guide tube is completely oxidized. The control material in the control rods is assumed to be Ag-In-Cd. Breaching of the oxidized fuel rod cladding by the molten material within the fuel rod is controlled by the user. In the scoping studies, the oxide shell failure depended only on temperature; a temperature of 2500 K was selected. In the sensitivity calculations, the breach was dependent on both temperature and oxide layer thickness. The cladding would breach when the temperature reached 2500 K only if the cladding were less than 60% oxidized. The code does not allow oxidation of material (Zircaloy) while it is relocating.

REFERENCES

B-1. T. C Cheng et al., "RELAP5/SCDAP - An Integrated Code for Severe Accident Analysis," *Proceedings of the Thirteenth Water Reactor Safety Research Information Meeting, Gaithersburg, MD, October 22-25, 1985*, NUREG/CP-0072, pp. 347-355.

B-2. G. A. Berna, C. M. Allison, and L. J. Siefken, *SCDAP/MOD1/VO: A Computer Code for the Analysis of LWR Vessel Behavior During Severe Accident Transients*, IS-SAAM-83-002, Rev. 1, July 1984.

B-3. H. Jordan, J. A. Gieseke, and P. Baybutt, *TRAP-MELT User's Manual*, NUREG/CR-0632, BMI-2017, February 1979.

B-4. H. Jordan and M. R. Kuhlman, *TRAP-MELT2 User's Manual*, NUREG/CR-4205, BMI 2124, May 1985.

B-5. V. H. Ransom et al., *RELAP5/MOD2 Code Manual, Volumes 1 and 2*, NUREG/CR-4312, EGG-2396, August 1985.

B-6. S. Hagen and P. Hoffmann, *Physical and Chemical Behavior of LWR Fuel Elements up to Very High Temperatures*, KfK4104, June 1987.

B-7. S. Hagen, L. Sepold, P. Hoffmann, and G. Schanz, "Out-of-Pile Experiments on Severe Fuel Damage Behavior of LWR Fuel Elements (CORA Program)," *IAEA International Symposium on Severe Accidents in Nuclear Power Plants, Sorrento, Italy, March 21-25, 1988.*

APPENDIX C

USE OF RELAP5 THERMAL-HYDRAULIC MODELS IN THE SEVERE CORE DAMAGE ACCIDENT ANALYSIS PACKAGE

APPENDIX C

USE OF RELAP5 THERMAL-HYDRAULIC MODELS IN THE SEVERE CORE DAMAGE ACCIDENT ANALYSIS PACKAGE[a]

A Position Paper

V. H. Ransom
J. C. Lin
C. M. Allison
P. E. MacDonald

Introduction and Summary

The mission of the Severe Core Damage Analysis Package (SCDAP)[C-1] is to predict, in best-estimate fashion, the consequences of a severe accident in a light water reactor up to the point of accident termination or major core relocation. The accumulation within and the release from the primary coolant system of hydrogen and radiologically significant fission products along with the overall geometry and coolability of the damaged core must be described. The thermal-hydraulic behavior within the reactor vessel and the entire primary system will both influence and be influenced by the core damage progression and the fission product release. For example, natural circulation within the primary system may lead to early structural failures in either or both the vessel and primary system, changes in core heating rates, and changes in fission product retention during certain risk dominant transients. Natural circulation flows can move significant thermal energy from the core to peripheral structures, and the evaporation, condensation and re-evaporation of the volatile fission products can also relocate a significant fraction of the decay heat source. In addition, the runaway oxidation and core heatup is influenced by the steam supply which is, in turn, influenced by core geometry changes. Therefore, a best estimate calculation of core damage progression, fission product transport and coolant flow patterns can only be achieved when the couplings and interactions between these processes are modeled simultaneously.

Considerable thought and planning has been addressed to the issue of which thermal-hydraulic model should be incorporated into SCDAP. The TRAC-PWR[C-2], TRAC-BWR[C-3], and RELAP5[C-4] models were considered along with the idea of developing a new vessel multidimensional thermal-hydraulic model. A link with RELAP5 was chosen for the following reasons. First, the combined RELAP5/SCDAP/TRAP-MELT code will be able to treat all of the important processes including loss of geometry, release and transport of hydrogen and the important radionuclides, two-phase primary coolant system thermal-hydraulics, and multidimensional flow in the vessel driven by increased axial pressure drops across blockage regions or buoyancy forces. Second, RELAP5 is fast running, and is based on a modular and user friendly architecture that can easily accommodate linking with SCDAP and TRAP-MELT[C-5]. Finally, the cost to develop and maintain the linked code is significantly less than would be required to develop new capability since RELAP5 provides a proven capability to model pressurized and boiling water reactors, as well as the light water reactor (LWR) safety experimental facilities.

However, questions have been raised regarding the ability of RELAP5 to adequately model multidimensional flow phenomena within a damaged core. Specifically the modeling of recirculating flow downstream of a blockage has been mentioned.[C-6] The recirculation region formed downstream of a blockage is the result of flow separation and reattachment with a semi-stagnant flow within the separated region. The separated flow region results from laminar/turbulent boundary layer separation that accompanies an adverse pressure gradient in the mean flow. The

a. This position paper was written in 1984, before the SCDAP and RELAP5 codes were integrated. Although some of the discussion in that regard is dated, it is reproduced here because the discussion of the crossflow junctions and viscous flow effects is still applicable.

modeling of such viscous/turbulent effects requires a boundary layer model for the flow at the wall coupled with a turbulence model for the mean flow. None of the LWR system codes have such models. Only the COBRA[C-7] code contains a viscous mean flow model, but even this model is a simple isotropic eddy viscosity model that is limited to mean flow shear; specifically, shear effects near a boundary cannot be modeled and thus flow separation/reattachment cannot be modeled. TRAC and RELAP5 do not have viscous/turbulent shear models and separated flow regions with recirculation cannot be calculated, let alone accurately modeled. However, we believe that the uncertainty resulting from neglect of these effects is small in comparison to the uncertainties associated with modeling mechanical behavior of severely damaged fuel.

Recirculating flows that result from body forces, such as gravity, play an important role in the severe accident process and must be modeled. These effects can be modeled by all the system codes and do not require viscosity/turbulence models. The TRAC vessel component uses a full three-dimensional nonviscous flow model, COBRA contains user-specified options either/or a three-dimensional viscous flow model or a nonviscous crossflow model for parallel channel flow, and RELAP5 uses a simplified multi-region crossflow model in which some of the momentum flux cross-product terms are neglected. All buoyancy and wall shear forces are included in RELAP5 for both the axial as well as crossflow models. Thus, RELAP5 can predict recirculation resulting from natural convection.

The redistribution of flow in a damaged core resulting from local flow blockage can also have a significant effect on the coolability of the core and the circulation within the primary coolant system. This effect can also be accurately modeled without consideration of bulk viscous/turbulent shear models and all the system codes have this capability. The flow redistribution is dominated by anisotropic wall shear effects (that result from the embedded matrix of fuel rods) and the change in flow resistance due to local blockage. These effects are modeled in all the codes by empirical Darcy type friction factors.

The status of two-phase system modeling in relation to the phenomena of importance to severe accident modeling is discussed in greater detail in the following section of this paper. In particular, the RELAP5 severe accident core-wide fluid modeling capabilities are discussed.

Severe Accident Modeling Requirements

SCDAP is a significant step forward in the mechanistic modeling of the fuel and coolant behavior during severe accidents. However, uncertainties still exist in the modeling of processes such as clad metal-water reaction, fuel liquefaction and fragmentation, and core material relocation. The spatial variation of these processes is modelled in SCDAP by dividing the core into regions or nodes. The numbers of nodes which can be used is mostly a matter of computer economics in terms of core storage and execution time. The modeling work at the Idaho National Engineering Laboratory (INEL) on SCDAP and at Sandia National Laboratory on TRAC/MIMAS indicates that nodes smaller than about 30 cm characteristic dimensions are impractical. This node size is about the same as nodalizations which are used for core thermal-hydraulic modeling (even for accidents not involving fuel damage) and consistent with the length scale of two-phase mixtures.

Viscous/turbulent flow effects can be modeled by either a microscopic approach using nodes smaller than the smallest turbulent eddies of interest or by a bulk shear model in which the details of the flow near a boundary are approximated by a boundary layer model to provide boundary conditions. Only bulk viscous/turbulent effects could be modeled using a node size of 30 cm or larger in a reactor core and thus special boundary layer models would be required in order to model the details of flow separation and reattachment with formation of recirculation regions. However, the anisotropic effects of the fuel geometry could not be modeled by a bulk shear model and must be approximated by an empirical Darcy law formulation anyway. The primary reason for this is that the length scale of the viscous/turbulent effects is less than the pore size (i.e., approximately 1 cm or smaller) and cannot be represented mechanistically at the characteristic length of most numerical models (i.e., greater than 30 cm).

The primary motivations for core-wide and system thermal-hydraulic models for use in severe accident simulation are to properly represent the availability of coolant to the core, the transport of energy from the core to other parts of the system, and the transport of fission products throughout the primary system and into the containment. The inclusion of fluid viscous/turbulent shear models would mainly affect the coolant velocity field

downstream of abrupt changes in flow area or direction where flow separation and formation of regions with recirculation would exist.

However, the heat transfer correlations for natural convection steam cooling or boiling (the convective cooling mechanisms of most importance in a damaged core) are not strong functions of the fluid velocity and thus accurate descriptions of such flow regions are not necessary. The transport of energy and entrained fission products throughout the system by the bulk flow also is not significantly influenced by viscous/turbulent shear effects. In summary, a detailed viscosity/turbulence model is not feasible with present mathematical modeling and computational technology and is not required for best estimate modeling of the severe accident progression.

Thermal-Hydraulic Models for Severe Accidents

Best estimate models of the severe accident process require that the macroscopic thermal and mass transport processes throughout the entire nuclear steam supply system be included. The rate at which energy is transported away from the core to other components significantly affects the course and severity of core damage and associated fission product release. Thus it is clear that a system thermal-hydraulic modeling capability is required for coupling with the SCDAP code. Additional thermal-hydraulic requirements include the ability to model the fluid processes in the core and vessel such as flow redistribution resulting from local blockage and natural circulation within the core and plenum regions. Both of these effects are significant mechanisms for core cooling and fission product transport within the vessel and must, therefore, be included in the thermal-hydraulic model.

The candidate codes that have been considered for integration with SCDAP to provide the system and core wide thermal-hydraulic modeling include TRAC-PWR, TRAC-BWR, COBRA/TRAC, and RELAP5. The TRAC and COBRA/TRAC codes include three-dimensional vessel thermal-hydraulic models, while RELAP5 uses a multi-region crossflow model to approximate multidimensional effects. The RELAP5 approach is the simplest and results in a highly versatile fast running code. The COBRA/TRAC model includes a viscous/turbulent flow model for the mean flow shear effects. However, the model is based on an isotropic eddy viscosity formulation that is inappropriate for flow with embedded structures such as the vessel core and upper plenum. Thus none of the available codes can model viscous/turbulent flow effects in a reactor core nor is it necessary that such effects be included.

The RELAP5 multi-region model is a simplified formulation obtained by deleting the cross-product momentum flux terms from the axial momentum equation and by deletion of all momentum flux terms from the crossflow momentum equation. The validity of this approach for moderate or low flow velocities can be verified by an order of magnitude analysis using the equivalent two-fluid Navier-Stokes equations. The vector formulation for the ensemble and time averaged momentum equations has been derived by Ishii,[C-8] and appears as follows in nonconservative form for the k^{th} specie:

$$\rho_k (\partial \tilde{V}_k / \partial t) + \left(\tilde{\rho}_k \tilde{V}_k \cdot \nabla_k\right) \tilde{V}_k = - \nabla P + \bar{\rho}_k g + \nabla \cdot (\bar{\tau}_k - \overline{\rho V_k V_k}) - \tilde{V}_k \Gamma_k \qquad (1)$$

The terms of the equation can be interpreted as follows: the time rate of change of momentum, force gradient due to momentum convection, force gradient due to pressure, gravitational force gradient, and viscous/turbulent force gradient. Equation (1) in nondimensional form[C-9] becomes,

$$(1/N_{St})(\partial V_k^*/\partial t) + (V_k^* \cdot \nabla^*) V_k^* = - (1/N_{Ru}) \nabla^* P^* + (\Delta x / V_o^2) g + (1/N_{Re}) \nabla^* (\tau_k^* - \rho_k^* V_k^{*\prime} V_k^{*\prime}) - (\Delta x / \rho_k V_o) V_k^* \Gamma_k \qquad (2)$$

where

N_{St} = $(t_o V_o / L_o)$, Strouhal number

N_{Ru} = $(\rho V_o^2 / P_o)$, Ruark number

N_{Re} = $(L_o V_o \rho / \mu)$, Reynolds number.

The viscous stress tensor τ_k is assumed to have the same dependence on parameters of the flow as the viscous stress tensor of a Newtonian fluid.

In the low flow limit the momentum flux terms of Equation (2) are small in comparison to the other terms because the coefficients $1/N_{St}$, $1/N_{Ru}$, $1/N_{Re}$, and the coefficients of g and Γ_k, all become

large for small V_o. Thus the low flow limit of Equation (1) is

$$\bar{\rho}_k \, (\partial \tilde{V}_k / \partial t) = - \nabla P + \rho_k g$$

$$+ \nabla \cdot (\bar{\tau}_k - \overline{\rho_k V_k' V_k'}) - \tilde{V}_k \Gamma_k \qquad (3)$$

The flow is dominated by the forces due to pressure gradient, gravity, viscosity/turbulence, and mass transfer. The forces due to momentum flux may be neglected.[C-9]

A more severe test of the simplified RELAP5 momentum flux formulation is provided by examining the various terms of Equation (1) for calculated high velocity flows in a reactor core with blockage. The flow geometry and the RELAP5 nodalization for the case examined is illustrated in Figure C-1. The core is modeled by three concentric regions each divided into five axial nodes. Flow is totally blocked between the third and fourth nodes in the two innermost regions. An inflow boundary condition at the bottom of the core vessel is specified such that the flow through the unblocked core would be 1.0 m/s.

The magnitudes of each of the terms appearing in Equation (1) are tabulated in Table C-1 (using cylindrical coordinates) for the selected points indicated on Figure C-1 (points 1 through 5). The time rate of change of momentum is zero in all cases since the calculations were carried out to steady-state. For the axial nodes, only the radial momentum flux term is neglected in the RELAP5 calculation. This term is less than 10% of the total pressure gradient except at Node 3 where a strong radial gradient in the axial velocity exists in front of the blockage. Here the neglected term is 25% of the pressure gradient and is a result of the flat plate configuration of the idealized blockage. This value is still within the uncertainty of the flow resistance definition and the numerical approximation of the derivative terms.

The components of the radial momentum equation are tabulated in Table C-2 for selected points in the flow (points 6 through 10). In this case both momentum flux terms are omitted from the crossflow momentum equation. The neglected terms are again less than 10% of the total pressure gradient except at Node 10 where the velocities are very small. However, this is the region where recirculation would exist in real flow, but cannot be modeled by any of the system codes.

These calculations were made for flow velocities approximately equal to the flow velocity at full power operation (1.0 m/s through the core) and are much greater than velocities that could exist during the core damage phase of an accident. The reason that the momentum flux terms are not significant factors for flow in a light water reactor core is that the flow is dominated by the gravitational forces and the anisotropic wall friction (the ratio of hydraulic resistances in the radial to axial directions is approximately 50). The simplified momentum flux formulation used in RELAP5 is clearly adequate for predicting flow redistribution effects resulting from local blockage due to fuel damage.

Since the modeling of natural convection currents within a reactor vessel is necessary for best estimate modeling of a severe accident, a further numerical experiment was conducted. The RELAP5 multi-region approximation was used to simulate the natural circulation resulting from asymmetric heating. The configuration modeled is the same as the previous case, i.e., an axisymmetric core having three concentric vertical passages with each divided into five equal length nodes. Crossflow junctions link the axial nodes at each of the five levels. The core has no through-flow and heating occurs in the center channel. Once the calculation reached steady-state the flow pattern shown in Figure C-2 resulted. The maximum velocity in the heated channel is approximately 0.1 m/s and the downward flow velocities in the two outer channels are approximately 0.02 m/s. The momentum flux terms at these low velocities are negligible as previously shown by the order of magnitude analysis. These results confirm the ability of the RELAP5 multi-region modeling approach to approximate recirculation resulting from buoyancy forces.

Thermal-Hydraulic Model Expectations

Misconceptions exist with respect to what can be expected from the thermal-hydraulic models employed in the light water reactor safety codes. First, as discussed above, none of the system codes such as TRAC-PWR, TRAC-BWR, COBRA/TRAC, or RELAP5 can mechanistically model viscous-turbulence effects in an anisotropic porous medium, such as a reactor core. The reason for this is that the length scale of the turbulence is small compared to the length scale of the ensemble average two-phase fluid model and the spatial nodalization used is too coarse. The COBRA/TRAC code has a bulk viscosity/turbulence model suitable for free shear flows, but this model is inappropriate for LWR cores where the flow is dominated by anisotropic frictional effects due to embedded structures. Phenomena such as flow separation and

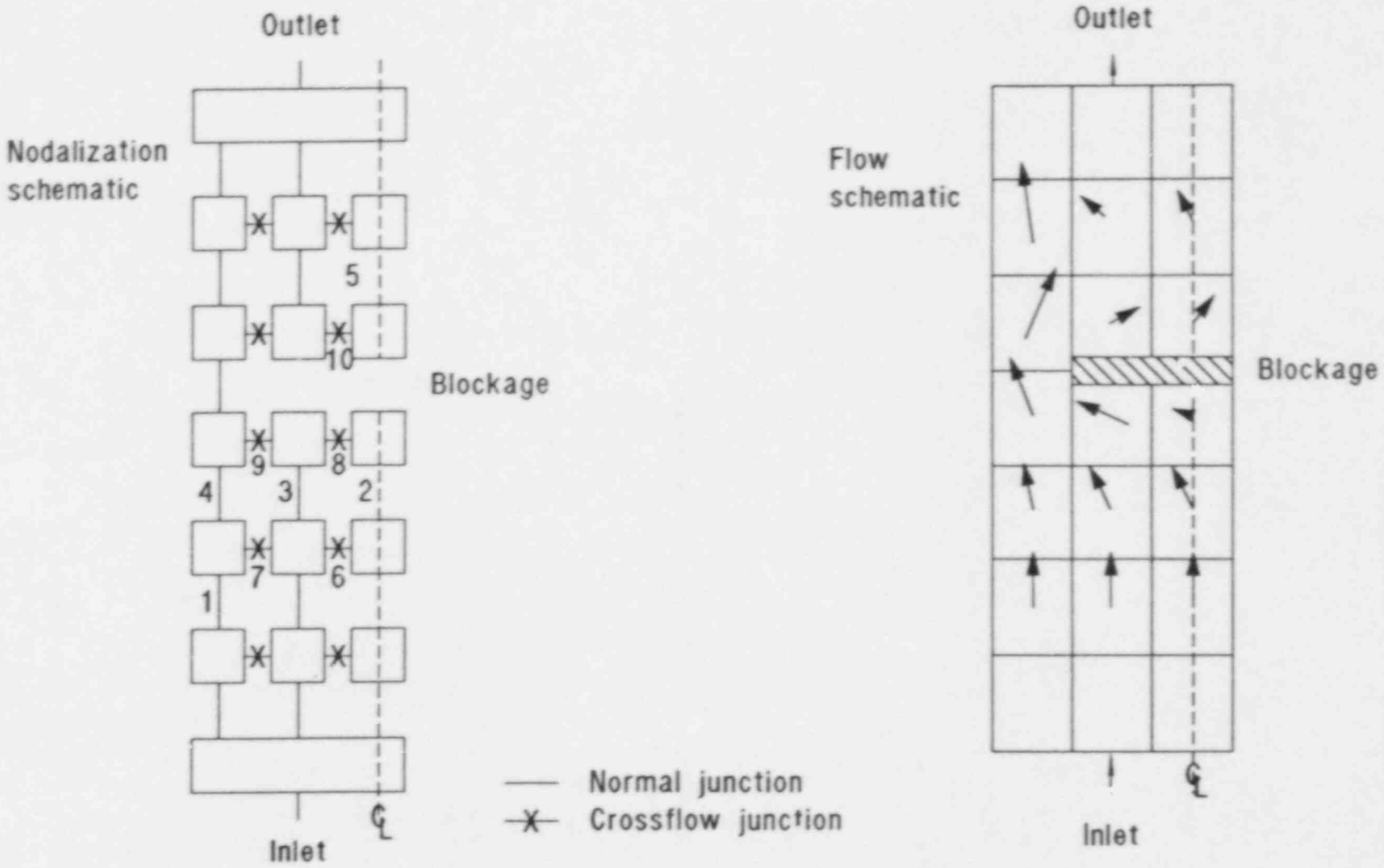

Figure C-1. RELAP5 multi-region core model with blockage, velocity vectors at volume centers.

Table C-1. Axial momentum equation components

Node	$\frac{\partial V_z}{\partial t}$	$V_r \frac{\partial V_z}{\partial r}$	$V_z \frac{\partial V_z}{\partial z}$	$\frac{1}{\rho} \frac{\partial P}{\partial z}$	Wall Friction and Form Loss	g
1	0.0	1.09[a]	3.32	-27.61	14.48	9.81
2	0.0	0.00[a]	1.05	-9.82	1.04	9.81
3	0.0	2.49[a]	-1.17	-10.38	1.74	9.81
4	0.0	2.25[a]	4.79	-32.25	17.65	9.81
5	0.0	0.00[a]	-0.00	- 9.82	- 0.01	9.81

a. Neglected terms in RELAP5 formulation.

Table C-2. Radial momentum equation components

Node	$\frac{\partial V_r}{\partial t}$	$V_r \frac{\partial V_r}{\partial r}$	$V_z \frac{\partial V_r}{\partial z}$	$\frac{1}{\rho} \frac{\partial P}{\partial r}$	Wall Friction and Form Loss	g
6	0.0	0.11[a]	0.06[a]	- 7.61	7.61	0.00
7	0.0	0.68[a]	1.78[a]	-18.63	18.63	0.00
8	0.0	0.12[a]	0.02[a]	- 8.03	8.03	0.00
9	0.0	0.85[a]	1.78[a]	-29.62	29.62	0.00
10	0.0	0.00[a]	0.08[a]	0.14	-0.14	0.00

a. Neglected terms in RELAP5 formulation.

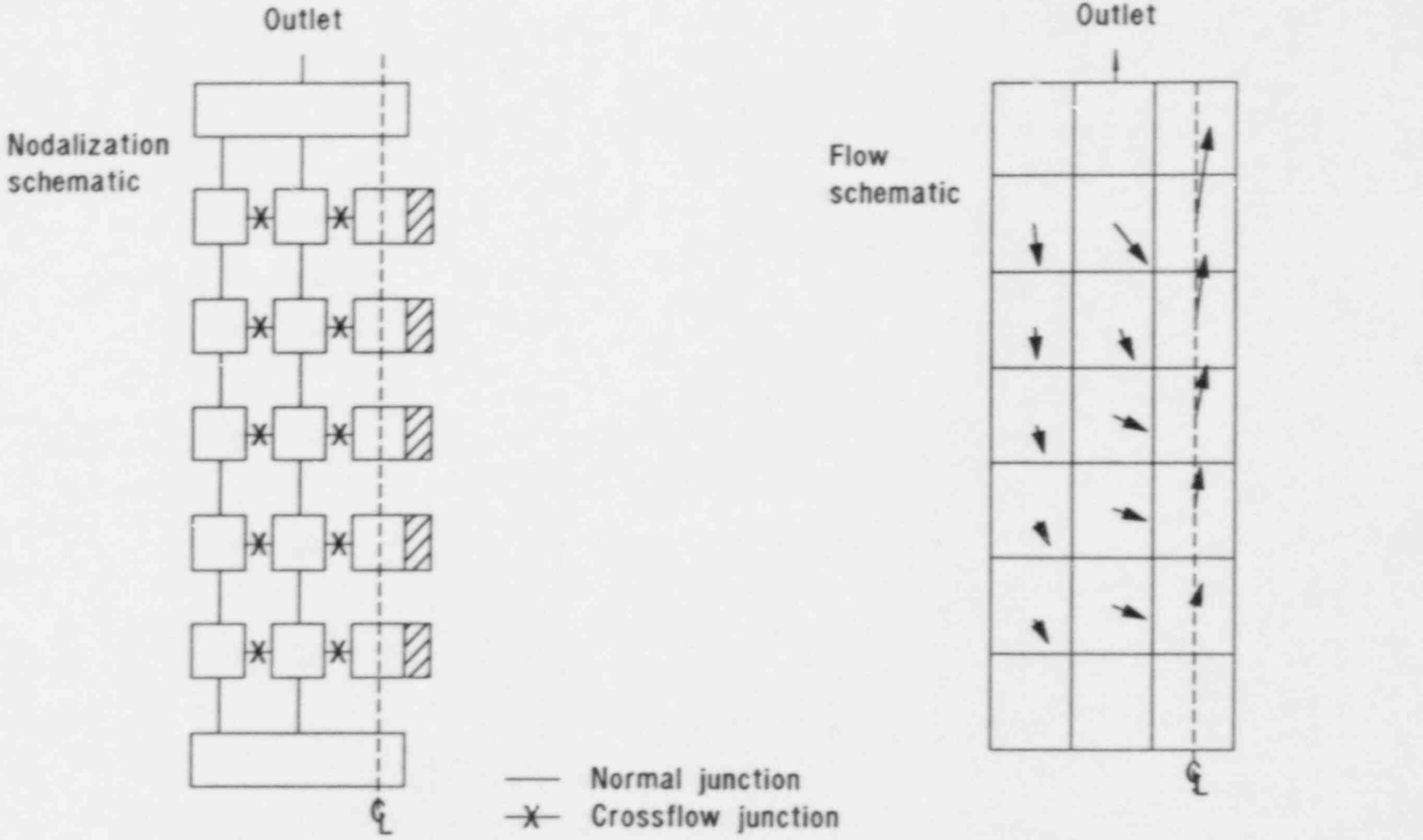

Figure C-2. RELAP5 multi-region core model with heated center channel, velocity vectors at volume centers.

reattachment with recirculation in the separated flow region are the result of viscous/turbulent effects near the wall or boundaries of the flow. Simulation of such effects would require a shear layer or boundary layer model coupled with a model for the bulk flow turbulence effect such as the k-ε model.[C-10] Thus, the recirculation that might occur behind a step or blockage in a core cannot be modeled by any of the LWR system codes.

Second, the modeling of separated flow regions with recirculation depends upon whether the viscous/turbulent effects are included in the model and not on whether all momentum flux terms are included. This fact is vividly illustrated by a calculated result obtained using the BEACON[C-11] code which is a containment version of the KACHINA[C-12] code. Both of these codes have a full multidimensional model including all the momentum cross-product terms, but do not consider viscous shear or turbulence. The results for simulation of a flow having several blockages are shown in Figure C-3. Note that no flow recirculation is predicted to exist downstream of any of the abrupt steps in the boundary. These results are similar to those obtained using the RELAP5 multi-region model for flow in a blocked core, see Figure C-1. Recirculation regions would form downstream of the rearward facing steps in a real flow. Boundary layer separations would result from the adverse pressure gradient in the mean flow. For comparison, a calculation by Roache[C-13] for a single-phase flow over a backstep using a viscous flow code is illustrated in Figure C-4. Note the boundary layer separation at the rearward facing step followed by reattachment downstream. A viscous shear-driven recirculation region is formed within the separated flow region. This calculation was made using a very detailed nodalization in order to resolve the flow process near the wall. A comparable calculation for a reactor core flow is not technically feasible using either a detailed or a bulk flow model. This is due to lack of a detailed two-phase model with viscous/turbulent effects and in addition the large number of nodes that would be required for solution due to the need to include detailed boundary layer considerations for use with a bulk shear model.

Conclusions

None of the LWR system codes can model boundary-governed viscous/turbulent effects on the bulk flow in an LWR core or plenum region. Thus, none of the LWR system codes can predict the recirculation that occurs downstream of an abrupt step or blockage. However, the uncertainties associated with modeling the mechanical, thermal, and chemical behavior of the core components during a severe accident are judged to be far greater than any uncertainties resulting from omission of viscous/turbulent effects. Thus, such effects are not significant factors in the best estimate prediction of LWR system behavior for severe core damage accidents.

The flow in an LWR vessel does not depend strongly on the momentum flux cross-product terms and is dominated by gravity and kinetic loss effects. Thus the RELAP5 multi-region model is completely adequate for modeling the multidimensional core-wide flow effects that are associated with severe core damage accidents and large flow blockages.

The linking of RELAP5 with SCDAP and TRAP-MELT to obtain a system and core-wide severe fuel damage accident analysis capability is strongly recommended. This approach is completely adequate for modeling of the thermal-hydraulic system response and takes advantage of the superior code architecture, efficient execution, and user friendly features of RELAP5. The results of this review reinforce the correctness of the conclusions of an earlier INEL study concerning the selection of a thermal-hydraulic model to link with SCDAP. RELAP5 was also recommended in that study.

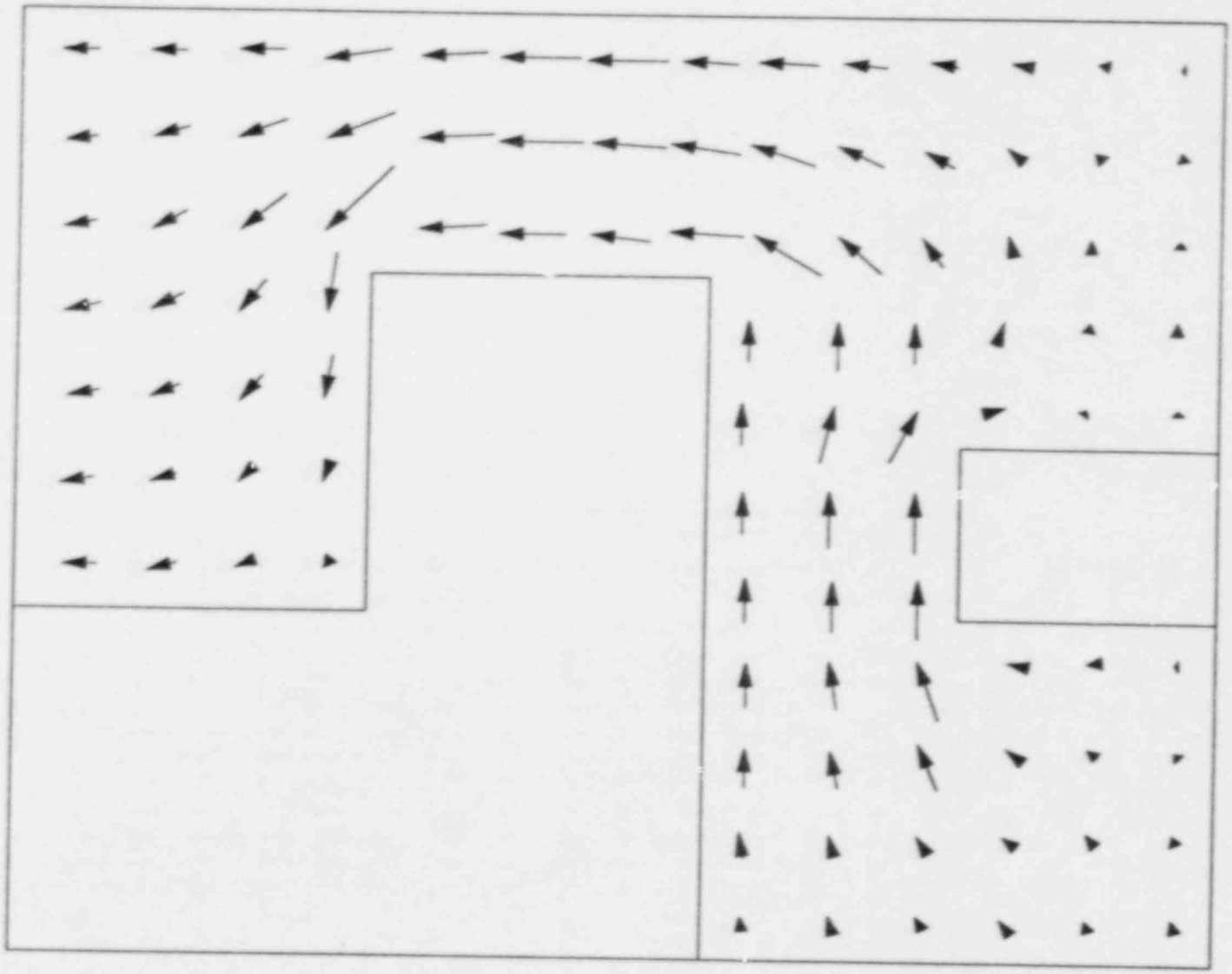

Figure C-3. Velocity vector plot for flow with blockage, from page 117 of Reference C-11.

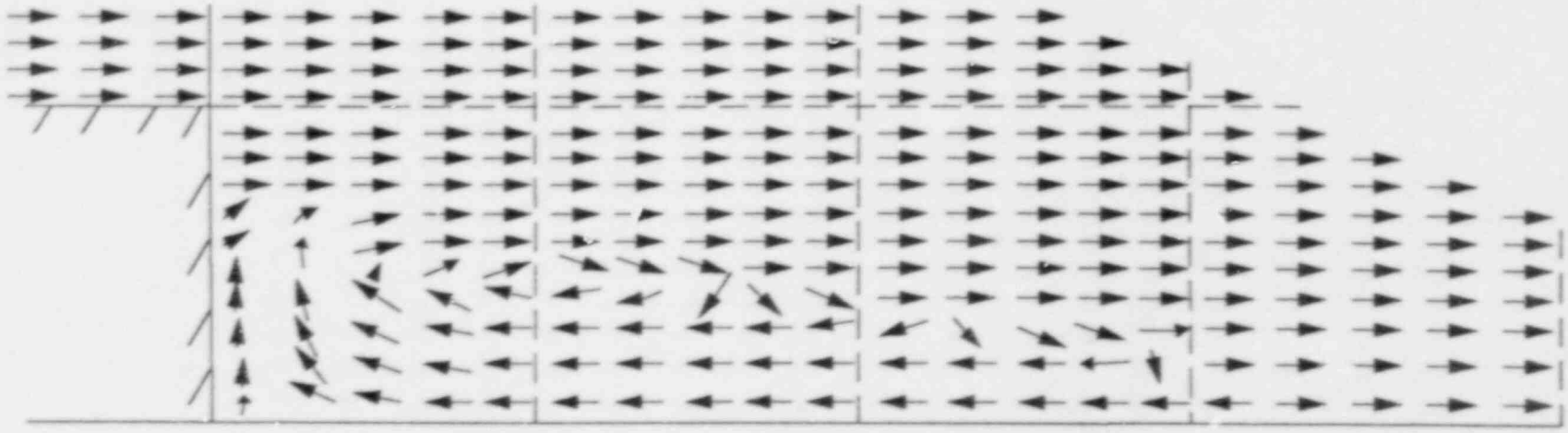

(c) flow direction for compressible flow in a base region, $M_0 = 2.24$, $Re = 300$, $\gamma = 1.4$.

Figure C-4. Calculated viscous flow over a backstep, from page 337 of Reference C-13.

REFERENCES

C-1. G. A. Berna, C. M. Allison, and L. J. Siefken, *SCDAP/MOD1/VO: A Computer Code for the Analysis of LWR Vessel Behavior During Severe Accident Transients*, IS-SAAM-83-002, Rev. 1, July 1984.

C-2. D. R. Liles et al., *TRAC-PD2, An Advanced Best-Estimate Computer Program for Pressurized Water Reactor Loss-of-Coolant Accident Analysis*, NUREG/CR-2054, 1981.

C-3. D. D. Taylor et al., *TRAC-BD1/MOD1: An Advanced Best Estimate Computer Program for Boiling Water Reactor Transient Analysis, Volume 1: Model Description*, NUREG/CR-3633, EGG-2294, April 1984.

C-4. V. H. Ransom et al., *RELAP5/MOD2 Code Manual, Volume 1: Code Structure, System Models, and Solution Methods*, NUREG/CR-4312, EGG-2396, August 1985.

C-5. H. Jordan, J. A. Gieseke, and P. Baybutt, *TRAP-MELT User's Manual*, NUREG/CR-0632, BMI-2017, February 1979.

C-6. Memorandum for O. E. Basset from C. N. Kelber on subject, "Trip Report, SNL and LANL, April 9-12, 1984," dated April 19, 1984.

C-7. M. J. Thurgood et al., *COBRA/TRAC—A Thermal-Hydraulics Code for Transient Analysis of Nuclear Reactor Vessels and Primary Cooling Systems, Volume I, Equations and Constitutive Models*, Pacific Northwest Laboratory, NUREG/CR-3046, March 1983.

C-8. M. Ishii, *Thermo-Fluid Dynamic Theory of Two-Phase Flow*, Eyrolles (1975).

C-9. J. C. Slattery, *Momentum, Energy, and Mass Transfer in Continua*, McGraw-Hill (1972).

C-10. W. Rodi, *Turbulent Models and Their Application in Hydraulics*, IHR (1980).

C-11. C. R. Broadus et al., *BEACON/MOD3: A Computer Program for Thermal-Hydraulic Analysis of Nuclear Reactor Containments, Users Manual*, NUREG/CR-1148, April 1980.

C-12. D. D. Amsden and F. H. Harlow, *KACHINA: An Eulerian Computer Program for Multifield Fluid Flows*, LA-5680, (1974).

C-13. P. J. Roache, *Computational Fluid Dynamics*, Hermosa (1972).

NRC FORM 335 (2 84) NRCM 1102 3201 3202

U.S. NUCLEAR REGULATORY COMMISSION

BIBLIOGRAPHIC DATA SHEET

SEE INSTRUCTIONS ON THE REVERSE

1 REPORT NUMBER (Assigned by TIDC and Vol. No., if any)

NUREG/CR-5214
EGG-2547

2 TITLE AND SUBTITLE

Analyses of Natural Circulation During a Surry Station Blackout Using SCDAP/RELAP5

2 LEAVE BLANK

4 DATE REPORT COMPLETED

MONTH: September YEAR: 1988

5 AUTHOR(S)

P.D. Bayless

6 DATE REPORT ISSUED

MONTH: October YEAR: 1988

7 PERFORMING ORGANIZATION NAME AND MAILING ADDRESS (Include Zip Code)

Idaho National Engineering Laboratory
EG&G Idaho Inc.
P.O. Box 1625
Idaho Falls, Idaho 83415

8 PROJECT/TASK/WORK UNIT NUMBER

9 FIN OR GRANT NUMBER

A6360

10 SPONSORING ORGANIZATION NAME AND MAILING ADDRESS (Include Zip Code)

Division of Systems Research
Office of Nuclear Regulatory Research
U.S. Nuclear Regulatory Commission
Washington, DC 20555

11a TYPE OF REPORT

Technical

b PERIOD COVERED (Inclusive dates)

12 SUPPLEMENTARY NOTES

13 ABSTRACT (200 words or less)

The effects of reactor coolant system natural circulation on the response of the Surry nuclear power plant during a station blackout transient were investigated. A TMLB' sequence (loss of all ac power, immediate loss of auxiliary feedwater) was simulated from transient initiation until after fuel rod relocation had begun. Integral analyses of the system thermal-hydraulics and the core damage behavior were performed using the SCDAP/RELAP5 computer code and several different models of the plant. Three scoping calculations were performed in which the complexity of the plant model was progressively increased to determine the overall effects of in-vessel and hot leg natural circulation flows on the plant response. The natural circulation flows extended the transient, slowing the core heatup and delaying core damage by transferring energy from the core to structures in the upper plenum and coolant loops. Increased temperatures in the ex-core structures indicated that they may fail, however. Nine sensitivity calculations were then performed to investigate the effects of modeling uncertainties on the multidimensional natural circulation flows and the system response. Creep rupture failure of the pressurizer surge line was predicted to occur in eight of the calculations, with the hot leg failing in the ninth. The failure time was fairly insensitive to the parameters varied. The failures occurred near the time that fuel rod relocation began, well before failure of the reactor vessel would be expected. A calculation was also performed in which creep rupture failure of the surge line was modeled. The subsequent blowdown led to rapid accumulator injection and quenching of the entire core.

14 DOCUMENT ANALYSIS - a KEYWORDS/DESCRIPTORS

natural circulation
station blackout
Surry
SCDAP/RELAP5

b IDENTIFIERS/OPEN-ENDED TERMS

15 AVAILABILITY STATEMENT

Unlimited

16 SECURITY CLASSIFICATION

(This page) Unclassified

(This report) Unclassified

17 NUMBER OF PAGES

18 PRICE

U.S. GOVERNMENT PRINTING OFFICE: 1988-241-590:80215

UNITED STATES
NUCLEAR REGULATORY COMMISSION
WASHINGTON, D.C. 20555